



THÈSE

En vue de l'obtention du

DOCTORAT DE L'UNIVERSITÉ DE TOULOUSE

Délivré par l'Université Toulouse III - Paul Sabatier

Discipline ou spécialité : *Physique Théorique - physique de la matière condensée*

Présentée et soutenue par Yasir IQBAL

Le 24 septembre 2012

Titre :

Spin liquids in quantum antiferromagnetic models on two dimensional frustrated lattices.

JURY

M. Ulrich SCHOLLWÖCK	Rapporteur
M. Karlo PENC	Rapporteur
M. Sandro SORELLA	Examineur
M. Grégoire MISGUICH	Examineur
M. Fabrice BERT	Examineur
M. Federico BECCA	Examineur
M. Pierre PUJOL	Examineur
M. Didier POILBLANC	Directeur de thèse

Ecole doctorale : Sciences de la matière

Unité de recherche : Laboratoire de Physique Théorique de Toulouse

Directeur(s) de Thèse : Didier POILBLANC

Contents

1	Introduction	4
I	Preliminaries	7
2	Magnetic structures	8
2.1	Models for magnetic structures	9
2.1.1	The Hamiltonian for a ferromagnet	9
2.1.2	The Hamiltonian for an antiferromagnet	10
2.2	Destruction of magnetic orders	10
2.2.1	Frustration: the “spice” of modern condensed matter	11
2.2.2	Spin liquids and valence bond crystals: a qualitative discussion	13
2.2.3	Building blocks of quantum paramagnets	15
2.3	Spin liquids: a theoretical framework	15
2.3.1	Mean field theory for spin liquids	17
2.3.2	Classification of spin liquids: projective symmetry groups	25
3	Numerical methods	35
3.1	The quantum variational Monte Carlo method	35
3.1.1	The quantum Metropolis algorithm	35
3.1.2	The wave function optimization algorithm	37
3.1.3	Green function Monte Carlo	41
3.2	The Lanczos algorithm and its implementation within a Monte Carlo scheme	44
3.2.1	The Lanczos method	44
3.2.2	Improvement of variational wave functions by application of Lanczos steps within a Monte Carlo scheme	46
3.2.3	The method of variance extrapolation	47
II	The spin-1/2 Heisenberg antiferromagnet on the kagomé lattice	50
4	History and mystery associated to the kagomé Heisenberg model	51
4.1	The spin-1/2 Heisenberg antiferromagnetic model on two dimensional lattices	51
4.2	The spin-1/2 Heisenberg antiferromagnetic model on the kagomé lattice	52
5	Experimental realizations of the kagomé spin-1/2 Heisenberg antiferromagnet	58
5.1	Structure and interactions in Herbertsmithite	58

5.2	Structural defects in Herbertsmithite	60
5.3	Nature of the ground state of Herbertsmithite	60
5.4	Other spin-1/2 kagomé antiferromagnet compounds	61
III Research projects		62
6	On the stability of critical spin liquids towards dimerizing into valence-bond crystals for the spin-1/2 Heisenberg antiferromagnet	63
6.1	Parent spin liquid states	63
6.2	Symmetry classification and enumeration of VBCs	66
6.3	The “hot” VBC competitors	67
6.4	General remarks on the VBC classification	68
6.5	Numerical results	69
6.5.1	Results on the stability of gapless spin liquids towards VBC perturbations	69
6.6	Conclusions and discussions	72
6.7	Physical Review B 83, 100404 (2011): Rapid Comm.	73
6.8	<u>New Journal of Physics 14, (2012): Invited paper for special focus issue on Quantum spin liquids</u>	78
7	On the potential instabilities of critical spin liquids towards \mathbb{Z}_2 spin liquids on the kagomé lattice for the spin-1/2 Heisenberg antiferromagnet	94
7.1	The $\mathbb{Z}_2[0, \pi]\beta$ spin liquid: the most promising ground state candidate	94
7.1.1	Numerical results for the $\mathbb{Z}_2[0, \pi]\beta$ spin liquid	95
7.2	Other promising ground state candidate \mathbb{Z}_2 spin liquids	97
7.2.1	Numerical results for the other gapped \mathbb{Z}_2 spin liquids	99
7.2.2	The \mathbb{Z}_2 gapless spin liquids	99
7.3	Conclusions and discussions	99
7.4	<u>Physical Review B 84, 020407 (2011): Rapid Comm, <i>Editor’s suggestion</i></u>	100
8	Finite size extrapolation of the kagomé spin-1/2 Heisenberg antiferromagnet using combined Lanczos and variational schemes	105
8.1	Ground state energy on different cluster sizes	105
9	Conclusions and perspectives	110
10	List of publications	112

Chapter 1

Introduction

For a long time the backbone of traditional condensed matter theory was comprised of two pieces. The first to be formulated was Landau's symmetry breaking theory [1–3], to be supplemented later by the theory of renormalization group and the second was Landau's Fermi liquid theory [4]. For about half a century these two theories dominated condensed matter physics since people could not find a system that was not described by Landau's theories. The exceptional success of these theories lead to the belief that we understood in principle the structure and behavior of all forms of matter. The shock came in 1982 with the discovery of the fractional quantum Hall effect [5], wherein it was found that these fractional quantum Hall liquids exhibit non-Fermi liquid behavior. Furthermore, different fractional quantum Hall liquids have the same symmetries, and thus fall out of the realm of Landau's symmetry breaking theory. These discoveries marked a revolution in condensed matter theory and acted as a passage to a whole new world beyond Landau's theories.

The frustrated low dimensional quantum spin systems provide a very promising playground to catch a glimpse of this new world of exotic non-Fermi liquid phases. These systems are examples of strongly correlated many body systems and have been argued to host states which lack long range order and do not spontaneously break any symmetries. These quantum spin liquid states contain completely new types of orders which are “dynamic” in origin, i.e. related to symmetries of complex ground state wave functions, as opposed to “static” positional crystalline orders which are related to symmetries of classical probability distribution functions of atoms, thus these novel orders are called “quantum orders” . In some cases quantum spin liquids also feature topological orders [6–8]. One can alternatively view quantum orders as describing the pattern of quantum entanglement in the many-body ground state, in this picture the conventional crystalline phase lacks any non-trivial entanglement pattern [9]. To this effect, the spin-1/2 quantum Heisenberg antiferromagnetic model on the kagomé lattice has been shown to host such an exotic quantum paramagnetic state. This is made possible through the combination of low spin, low dimensionality, low coordination number and frustrating antiferromagnetic interactions of the Heisenberg type, all of which combine to amplify quantum fluctuations to an extent needed to stabilize a quantum paramagnet, even at $T = 0$. The near perfect realization of this model Hamiltonian is found in Herbertsmithite ($\text{ZnCu}_3(\text{OH})_6\text{Cl}_2$) [10] on which various probes have established a quantum spin liquid behavior down to temperatures of 20 mK ($\sim J/10^4$) [11]. However, the precise identification of this quantum paramagnetic phase is still an open problem experimentally and even more so theoretically where this question has and is being vigorously debated without any definitive conclusions, till date. Different approximate theoretical approaches have yielded myriad of different possible ground states,

which have been found to be competing within a very narrow spectrum of energy, and are extremely sensitive to small perturbations. This extensive quasi-degeneracy of the ground state manifold is what makes the problem of the ground state of the kagomé antiferromagnet an extremely challenging puzzle.

In my thesis, I will revisit this problem within the realm of slave-particle approaches, which form the traditional line of attack for studying spin systems featuring a magnetically disordered ground state. In particular, I shall work within the SU(2) slave boson (Schwinger fermion) approach. Within this formalism, it was argued in [12, 13] that a particular algebraic spin liquid with a U(1) low energy gauge structure (so called U(1) Dirac spin liquid) possesses the lowest energy and should occur as the ground state. In fact, all experimental studies till date back up such a claim for a long range resonating valence bond state to be stabilized [14]. However, such algebraic spin liquids are *marginally* stable and hence “critical” [15], thus lending support to the thought that at least for spin-1/2 models such spin liquids should destabilize into either the class of stable \mathbb{Z}_2 spin liquids or into valence-bond crystals, and it has not been appreciated that such delicate phases can in fact be robust, and exist as real physical spin liquids [8]. The existence of algebraic spin liquids is quite a remarkable and revolutionary phenomenon as it disproves conventional wisdom, and indirectly proves the existence of quantum orders which are in fact responsible for protecting the gapless nature of the spin liquid excitations [7, 8]. This is another reason which makes the kagomé Heisenberg model not only challenging but also exciting, since it involves a frontier issue. The broad aim and conclusion of the work contained in the thesis is to study and demonstrate the remarkable stability of the U(1) Dirac spin liquid with respect to a very large class of perturbations, including \mathbb{Z}_2 spin liquids, valence bonds crystals and chiral spin liquids, and thus to vouch for it as the ground state of the spin-1/2 quantum Heisenberg model on the kagomé lattice.

The relevant numerical framework for tackling the above mentioned problems and issues is provided by the fermionic variational quantum Monte Carlo methods. In practice, we compute the energy of optimized variational wave functions that are constructed by applying the Gutzwiller projector to different states obtained from mean-field Hamiltonians of Schwinger fermions. In this respect, by an exact treatment of the full projector that ensures the one fermion per site constraint, we go much beyond the simple mean-field approach. To carry out the optimization of wave functions representing these competing phases I have used a state-of-the-art implementation of the stochastic reconfiguration optimization algorithm [16, 17]. This method enables one to obtain an extremely accurate determination of variational parameters, since small energy differences are effectively computed by using a correlated sampling, which makes it possible to strongly reduce statistical fluctuations. This feature is indispensable when one wants to literally “hair split” phases which are clustered together in a narrow energy width, as is the case with the kagomé spin-1/2 Heisenberg antiferromagnet problem. We also did an extension of the above scheme, by implementing the Lanczos algorithm within a variational Monte Carlo framework [18], since, this is necessary to improve the variational wave functions and also to extract the true ground state properties.

The thesis is structured in the following manner: In Part I, I will set up the theoretical framework and the numerical machinery, this part thus lays the necessary foundation for the rest of the manuscript. In particular, chapter 2 is devoted to introducing frustration and quantum paramagnetic phases in a qualitative manner and subsequently moves on to describe the SU(2) slave boson formalism and the consequent classification of spin liquids using projective symmetry groups, among other things. In chapter 3, the numerical methods,

namely the fermionic variational Monte Carlo scheme, Green function Monte Carlo, the wave function optimization algorithm and also the implementation of Lanczos algorithm within a Monte Carlo framework are described.

In Part II, I will trace through the history and the current scenario of the problem of finding the ground state of the kagomé Heisenberg antiferromagnet from both theoretical and experimental side. In particular, chapter 4 is devoted to a survey of the various ground states that have been proposed using different numerical techniques, and setting up the problem of the kagomé antiferromagnet within the current scenario. In chapter 5, a brief survey of the recent experimental developments on Herbertsmithite is given, the nature of the ground state vouched by experiments is discussed, and other promising kagomé compounds hosting a quantum spin liquid ground state are also discussed.

In Part III, I will present my PhD research projects. Chapter 6, deals with the complete symmetry classification of valence bond crystals on the kagomé lattice and results are given concerning the stability of the two critical spin liquids, the U(1) Dirac and uniform RVB spin liquid towards dimerizing into these crystals. It is shown that the U(1) Dirac spin liquid is robust to these perturbations and has the lowest energy for the spin-1/2 Heisenberg antiferromagnet. However, upon addition of a small second nearest neighbor ferromagnetic exchange coupling to the Hamiltonian, it is demonstrated that a non-trivial 36 site unit cell valence bond crystal is stabilized [19]. In chapter 7, I present the study concerning the stability of U(1) Dirac and uniform RVB spin liquids towards destabilizing into the class of \mathbb{Z}_2 spin liquids. It is shown that for the spin-1/2 Heisenberg antiferromagnet, both these gapless spin liquids are robust towards destabilizing into gapped \mathbb{Z}_2 spin liquids, one of which was recently conjectured to be the ground state that has been found in recent DMRG studies [20, 21]. The stability of these gapless spin liquids is also preserved on addition of an exchange coupling of both ferromagnetic and antiferromagnetic type to the Hamiltonian [22]. Finally, chapter 8 is concerned with extracting the true ground state properties of the spin-1/2 Heisenberg antiferromagnet, by applying a few Lanczos steps to the energetically lowest variational wave functions such as the U(1) Dirac spin liquid and subsequently analyzing their properties using variational Monte Carlo and Green function Monte Carlo. The ground state estimates of energy on the 48 site cluster and also larger clusters are given. We also perform a finite size extrapolation and give the energy estimate in the thermodynamic limit.

Part I
Preliminaries

Chapter 2

Magnetic structures

It is well known that at low enough temperatures compared to energies of interaction between atoms, “conventional” condensed matter systems tend to freeze in some of their degrees of freedom. Furthermore, if these systems are in thermodynamic equilibrium they acquire *ordering* or *regularity* in those frozen degrees of freedom. A classic example is a solid, which in thermodynamic equilibrium is *crystalline*. The subsequent variety of electrical and magnetic structures that occur in crystals is a consequence of their time-reversal symmetry ($t \rightarrow -t$), applied to a particular state within the space of equilibrium states. Precisely speaking, the behavior under time-reversal of the time averaged microscopic charge density function $\bar{\rho}(x, y, z)$ and current density function $\bar{j}(x, y, z)$ determines the electric and magnetic structure of the crystal, respectively [23]. A large number of materials existing in nature are “dull”, in the sense that on time-reversal their state does not change, and since \bar{j} is *odd* under time-reversal, it implies that $\bar{j} = 0$ identically. Thus, such crystals do not have any magnetic structure, but they *must* have an “electrical” structure, since $\bar{\rho}$ is even under time-reversal. We shall only concentrate on crystals which *have* a magnetic structure. It is clear that for such crystals to exist ($\bar{j} \neq 0$) their state must change under time-reversal. A further bifurcation can be done by noticing that even when $\bar{j} \neq 0$ the mean atomic magnetic moment over a “magnetic” unit cell can be either non-zero or zero, in the former case we call such bodies as *ferromagnetic* crystals and in the latter case *antiferromagnetic* crystals.

The above considerations also imply the existence of at least two magnetic sub-lattices for an antiferromagnet, with equal and opposite mean atomic magnetic moments compensating each other (in the absence of an external magnetic field) [24–26]. Multiple sub-lattices may also exist for ferromagnets. We will use the term ferromagnet in a more restricted sense, whereby assuming that all the atomic magnetic moments are aligned parallel to each other. The simplest examples of ferromagnetically ordered crystals are Fe, Ni and Co; on the other hand for antiferromagnets, the prominent examples are the transition metal oxides and fluorides. These magnetic structures exist only as long as the temperature is lower than a certain critical value, called the Curie temperature for “ferromagnets” [27] and Néel temperature for “antiferromagnets” [24, 26, 28]. Above these temperatures, thermal fluctuations wash out the order leading to a paramagnetic state, through a second order phase transition [28]. Finally, we mention that it may happen that in a crystal the magnetic moments of different sub lattices remain uncompensated, this gives rise to another type of magnetic structure called “ferrimagnetic”, [29, 30] examples of which are salts like $\text{MnO} \cdot \text{Fe}_2\text{O}_3$ and magnetite, the oldest known magnetic substance.

Thus, the types of possible magnetic structures existing in nature are dictated by considerations of symmetry *only*. However, to explain why these magnetic structures arise one has

to delve into the microscopics and identify the forces which are purely quantum-mechanical and relativistic in origin. But before we setup the Hamiltonian for these magnetic systems, one can qualitatively identify the various interactions and their relative strengths as follows. Firstly we recollect that, wave functions with different spatial symmetries give rise to different values of the energies of the system, in general. Also, the magnitude of the total spin of the system depends on the spatial symmetry of the wave function due to the principle of indistinguishability of physically identical particles. Thus its evident that the energy of the system depends on the magnitude of the total spin. This mechanism or rather the peculiar dependence of the energy on the total spin, is what is mainly responsible for the correlation between the directions of the electron spins, thus giving rise to different magnetic structures. It is a purely quantum-mechanical effect and is called the *exchange* effect [31, 32]. Another interaction which exists in the system is the direct magnetic interaction between the electron magnetic moments and between the electron's magnetic moment and the lattice electric field, however these are purely *relativistic* effects. Hence, compared to the exchange interaction, these are weaker due to the presence of a factor of $1/c^2$, which also implies that the dependence of the energy of the crystal on the direction of the total magnetization is extremely weak [23]. From now on, we will neglect these interactions in our treatment, *only* because we will study phases in thermal equilibrium and not kinetic processes. However, it should be remembered that without the relativistic interactions, thermal equilibrium can never be established.

2.1 Models for magnetic structures

2.1.1 The Hamiltonian for a ferromagnet

We can at once write down the microscopic Hamiltonian for a ferromagnet (in the non-relativistic approximation) as consisting of the kinetic energy of the particles and the energies of electrical interactions between the electrons, and between electrons and nuclei. However, a direct solution to this Hamiltonian is too cumbersome in general cases. It so turns out that the *exchange* Hamiltonian does the job and reproduces the correct energy spectrum near the ground state, which is what we are interested in. On the other hand, it is clearly mathematically much simpler to handle. Its mathematical form can be written down from extremely general considerations of symmetry *only* [33]. In particular, if we demand *isotropy* of the Hamiltonian for the interaction between a pair of *identical* particles, then the only invariant is $\hat{\mathbf{S}}_i \cdot \hat{\mathbf{S}}_j$, where $\hat{\mathbf{S}}_i$ are the spin operators at each site i of the crystal lattice. Hence, the Hamiltonian is an arbitrary function of $\hat{\mathbf{S}}_i \cdot \hat{\mathbf{S}}_j$, written as,

$$\hat{\mathcal{H}} = f(\hat{\mathbf{S}}_i \cdot \hat{\mathbf{S}}_j) \quad (2.1)$$

Furthermore, when the spin of the particles is $1/2$ then any arbitrary function of $\hat{\mathbf{S}}_i \cdot \hat{\mathbf{S}}_j$ can be reduced to an expression linear in $\hat{\mathbf{S}}_i \cdot \hat{\mathbf{S}}_j$. Thus, the exchange Hamiltonian of a ferromagnetic crystal consisting of *identical* spin- $1/2$ particles takes the following form [34],

$$\hat{\mathcal{H}} = \sum_{ij} J(r_{ij}) \hat{\mathbf{S}}_i \cdot \hat{\mathbf{S}}_j \quad (2.2)$$

where ij denotes sums over all pairs of sites and the $\hat{\mathbf{S}}_i$ are spin- $1/2$ operators at each site i . The $J(r_{ij})$ is a function of the distance between two sites and is called the *exchange* integral. For a ferromagnet $J(r_{ij}) < 0$, in our notation. Thus, it is evident from 2.2 that

in the ferromagnetic ground state the spins of all atoms are aligned parallel [35–37] and the ground state is strongly correlated. The Hamiltonian in 2.2 is called the Heisenberg Hamiltonian.

2.1.2 The Hamiltonian for an antiferromagnet

If we “picture” an antiferromagnet as an arrangement of alternating up and down spins, then in principle there is no isotropic microscopic Hamiltonian analogous to the exchange Hamiltonian for a ferromagnet, of which this Néel state is an exact eigenstate. Thus, any physical theory of an antiferromagnet has to be macroscopic, whereby one associates a mean magnetic moment with each of the magnetic sublattices [33, 38]. It is worth mentioning that there is no exact proof, till date, which shows the existence of magnetic sublattices in the Heisenberg antiferromagnetic model in three dimensions [39]. However, by using the Hartree-Fock method we know that in the ground state of this model it is possible to identify magnetic “sublattices”, say two of them, with the spins “principally” pointing *up* in one sublattice and “principally” pointing down in the other [40]. Using this picture, one obtains an excellent agreement with experimental data on magnetic as well as thermal properties of antiferromagnetic crystals, and also for neutron diffraction data which is a key probe for such magnetic structures. The spin-1/2 Heisenberg antiferromagnetic model, i.e. eqn 2.2 with $J(r_{ij}) > 0$, also arises as a limit of the Hubbard model at *half* filling for *large* onsite Coulomb repulsion [41]. Thus, the spin-1/2 Heisenberg antiferromagnetic model serves as an effective model for the *Mott* insulator phase [42].

The Heisenberg model has had a long and distinguished career and is still a cherished model due to the fact that it leads to physically reasonable results for magnetic systems at low temperatures and is considerably simpler to handle as compared to an *ab initio* Hamiltonian for the system. However, despite its deceptive simplicity, it has required the most sophisticated techniques, even to yield approximate solutions.

2.2 Destruction of magnetic orders

The ferromagnetic, antiferromagnetic and ferrite magnetic orderings exist only at temperatures much lower compared to J . Upon turning on the “heat”, thermal fluctuations wash out these orderings and stabilize a *paramagnetic* state. The temperature at which this second order phase transition occurs is called, as previously mentioned, the Curie temperature for ferromagnets and the Néel temperature for antiferromagnets. The resulting paramagnetic phases have uncorrelated spins and are in some sense a “liquid” of spins. Using conventional wisdom they should not possess *any* physical “orders” enabling the distinguishing of these paramagnetic phases from each other. In other words, since there is no breaking of any physical symmetry such as space group symmetry or/and time-reversal, there is thus no *order* parameter in the sense of Landau [1–3, 43], that one can associate to these thermally driven ($T \neq 0$) paramagnetic phases, all such phases are the *same*. However, a natural question that comes to mind is that “how do we know that there is no *non-trivial internal symmetry* which can characterize ‘different’ paramagnetic phases?”. Well, for $T \neq 0$ paramagnets we are sure that there are *no* non-trivial internal symmetries which can enable us to distinguish the apparently ‘boring’ paramagnets. This can be understood if one keeps in mind that thermal fluctuations are *not* phase coherent.

But there is another mechanism by which magnetic ordering can be washed out, namely by turning on the “heat” of quantum fluctuations at *zero* temperature, see Fig. 2.1. If the

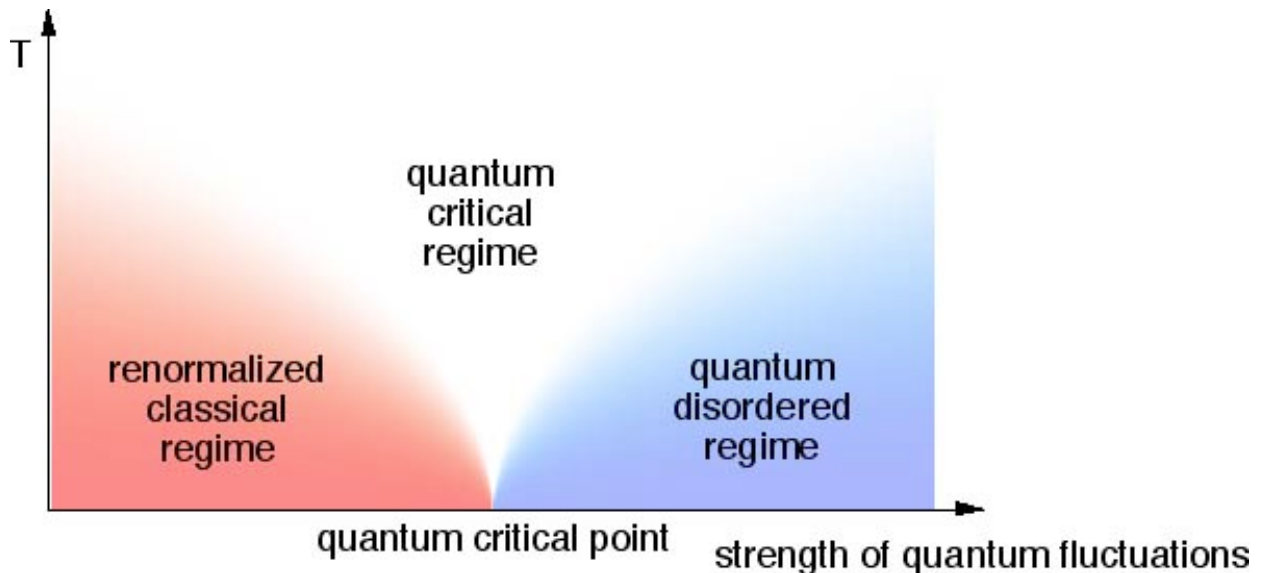


Figure 2.1: Adapted from [45]. A generic phase diagram of quantum antiferromagnets is shown w.r.t. to thermal and quantum fluctuation driven disorder. The nature of the phase transition, the critical point and the paramagnetic states are very different for a quantum fluctuation driver and a classical thermally driven transition.

system becomes hot enough at *zero* temperature, then one can have a *quantum paramagnetic* state which is again a “liquid” of spins, with the on-site magnetization $\langle \hat{S}_i \rangle$, and also more complex SU(2) breaking order parameters, being identically *zero*. As opposed to a classical ($T \neq 0$) paramagnet the quantum paramagnet is far more richer, due to the fact that quantum fluctuations can be phase coherent, as opposed to thermal fluctuations. A quantum spin liquid, thus possesses non-trivial internal symmetries/orders, non-trivial correlations and excitations and completely falls out of the grasp of the two monumental backbones of *traditional* condensed matter theory, i.e. the Landau’s theory of phase transitions [1–3] and the Landau’s Fermi liquid theory [4, 44]. In the next section I will describe the key ingredient which stabilizes such exotic phases, namely *frustration*.

2.2.1 Frustration: the “spice” of modern condensed matter

The key ingredient “spice” which helps, in part, to spoil long range magnetic order or magnetic freezing is *frustration* which results in an *accidental macroscopic* ground state degeneracy in the system at a classical level, this huge degeneracy is a defining characteristic of frustration and in part, is what prevents long range order from setting in. However, fluctuations about the classical state may select some preferred ground state out of the huge manifold, by a mechanism called ‘*order by disorder*’ [46, 47]. This is a consequence of the fact that the macroscopic ground state degeneracy is *not* related to any symmetries and is just *accidental*. This mechanism succeeds on the kagomé lattice (Fig. 2.2a) Heisenberg antiferromagnetic model [48], but fails for the three dimensional analogue, i.e. the pyrochlore lattice (Fig. 2.2b) [49, 50].

Frustration is achieved when there are interactions in the system which can never be simultaneously satisfied. On the one hand this can happen due to their competing nature, like in the $J_1 - J_2$ Heisenberg model on the square lattice [51], while on the other hand destruction of Néel order can also result from considerations of lattice geometry *only* [52, 53],

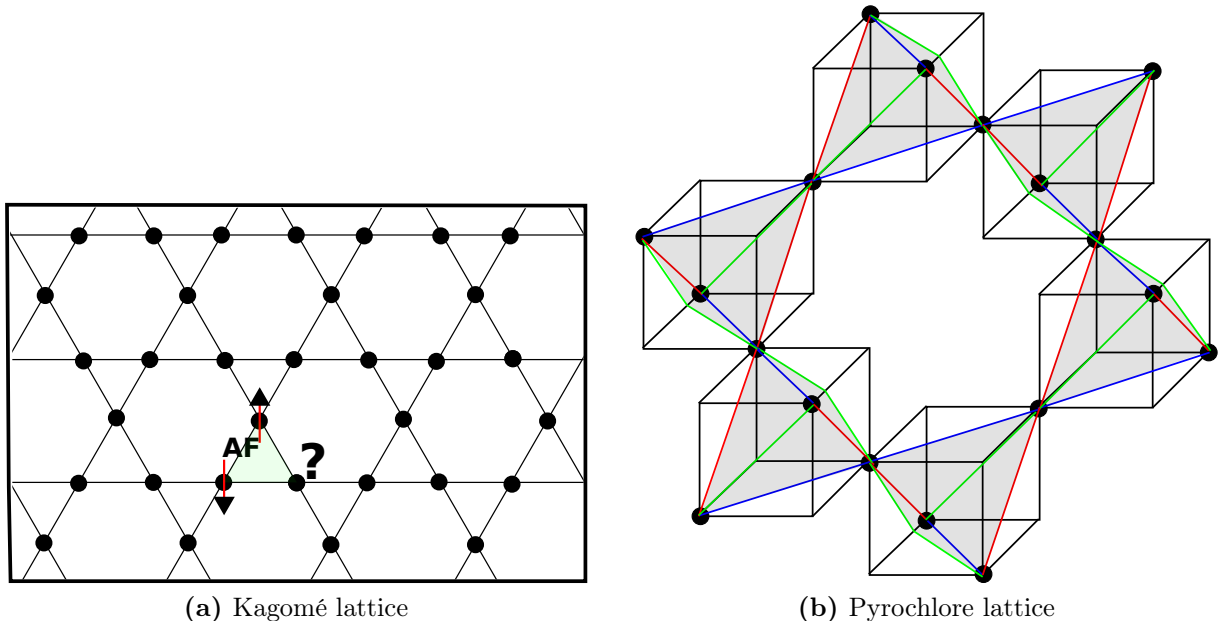


Figure 2.2: (a) The kagomé lattice is formed from corner-sharing triangles, hence its non-bipartite with a co-ordination number of 4. It is the most frustrated lattice in 2- d upon inclusion of nearest neighbor antiferromagnetic couplings. (b) The pyrochlore lattice is formed from corner sharing tetrahedra, and is in some sense the 3- d analogue of the kagomé lattice.

a dramatic example of this meltdown occurs on the kagomé lattice Heisenberg antiferromagnetic model, see Fig. 2.2a. In three dimensions the equivalent example is the pyrochlore lattice Heisenberg antiferromagnetic model, see Fig. 2.2b. This destruction of magnetic order is further aided by amplifying quantum fluctuations by having a low spin value on a lattice that is non-bipartite, with low dimensionality and a low coordination number. Furthermore, if the interactions are dominantly of Heisenberg type then the quantum fluctuations are stronger. Thus, if all these factors come together they can prevent magnetic freezing or ordering from setting in, thereby stabilizing the colorful exotic zoo of $T = 0$ quantum paramagnetic phases about which much remains to be understood. In this zoo, broadly speaking there are two species of quantum phases, namely “spin liquids” and “valence bond crystals”, the former preserve lattice translation symmetry and the latter break them, at the bare minimum level.

A “playground” where such phases can be stabilized is the spin-1/2 quantum Heisenberg antiferromagnet on the kagomé lattice. This is an example of pure geometric frustration inducing a spin disordered ground state, a fact which has been firmly established, both theoretically and experimentally, but the exact nature of the ground state is still elusive. The most promising candidate material to reproduce this environment is Herbertsmithite ($\text{ZnCu}_3(\text{OH})_6\text{Cl}_2$) and in general other materials of the paratacamite family. However, it is worth noting that in realistic systems there are other competing forces which try to align or freeze the system and thus work against the effects of frustration. In the simplest case, these can be interactions (of the same type) beyond nearest neighbor Heisenberg interaction, generally occurring at an energy scale smaller than nearest neighbor J , but below which order may set in, see [54, 55] for such a scenario on the pyrochlore lattice, and [56] for the kagomé lattice. If the crystal lacks a centre of inversion symmetry then Dzyaloshinskii-

Moriya interaction is also allowed and has been argued to play an important role in the low energy dynamics of Herbertsmithite. But on the pyrochlore lattice nearest neighbor Heisenberg antiferromagnet, its effect has been shown to be drastic at low temperature, whereby in [57] it was shown that it can drive the a phase transition to a long range ordered state at a temperature of the order of that corresponding to Dzyaloshinskii-Moriya interaction. Furthermore, all realistic systems suffer from some inter-site defects which also acutely affect the low energy dynamics [58, 59]. Finally, we mention that relativistic interactions of the dipolar type, despite their relative weakness can also induce long range order [60, 61].

2.2.2 Spin liquids and valence bond crystals: a qualitative discussion

Spin liquids and valence-bond crystals are examples of insulating phases. Till date, we lack a complete theory explaining the properties in general, of insulators, as opposed to metals where the Landau’s Fermi liquid theory [4] does a marvelous job at explaining the physical properties of the metallic state. This is simply due to the fact that a myriad of different insulators can exist depending on the fine tuning of the constants governing microscopic interactions. This situation is identical to what we have, if we compare ordinary gases and ordinary liquids. For the former phase we can construct a general theory and for the latter, no such general theory can be constructed due to precisely the same reason mentioned above [3]. In the case of those insulating phases which possess magnetic long range order, we have a much better understanding as opposed to those insulators which lack magnetic long range order. It is only in the recent decades that we have been making headway in a systematic manner to solve this long standing problem, namely that of constructing a general framework to understand magnetically disordered insulating phases, like spin liquids.

The existence of spin liquids, surprisingly enough was first conjectured way back in 1941 by Pomeranchuk, whereby in [62, 63] he argued that in a $S = 1/2$ Heisenberg antiferromagnetic model, quantum fluctuations can wash out long range order and stabilize a quantum paramagnet with gapless fermionic excitations, as opposed to magnon or gapped singlet excitations in a Néel state. Later in 1973, Anderson advocated these quantum phases as viable alternate ground states of highly frustrated quantum lattice antiferromagnetic models in two dimensions [64–66]. A common feature of both these *spin rotation invariant* Mott insulating (i.e. an insulator with an *odd* number of electrons per unit cell) quantum “disordered” phases, is that due to their paramagnetic nature, the two-spin correlation function $\langle \hat{\mathbf{S}}_i \cdot \hat{\mathbf{S}}_j \rangle$ goes to zero as the distance between the spins tends to infinity. However, what distinguishes these two phases is the behavior of the *four-spin* (dimer-dimer) correlation function, which for a VBC, *does not* go to zero at large distances, but shows long range order. On the other hand, for a spin liquid, the two, four and *all* higher order spin correlation functions go to zero at large distances. It is worth mentioning that we shall not put the constraint, as is usually done, that spin liquids *should not* spontaneously break *any* symmetry, this is unnecessary and restrictive. In one particular way of analyzing spin liquids, called the *projective* construction [7, 8], one can construct spin liquid wave functions which break point group and/or time reversal symmetry. Also, this constraint of *no* spontaneous symmetry breaking can be satisfied by phases like the Haldane phase, which are not quantum spin liquids, but are rather “valence bond solids”, this subtle distinction has its roots in the Lieb-Schultz-Mattis-Hastings theorem and its generalizations [6, 67–70]. In this work, when we talk about spin liquids, we shall mean a phase with an *odd* number of electrons

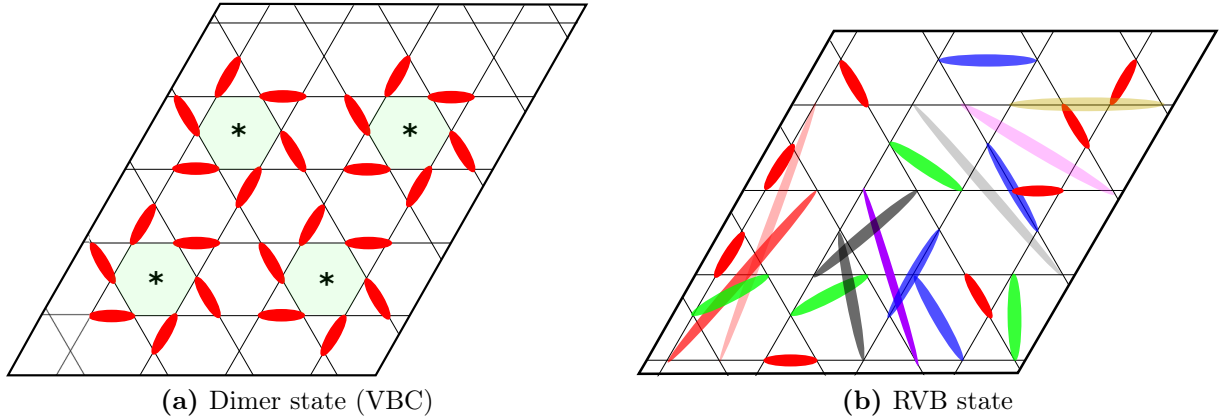


Figure 2.3: (a) A prototype of a VBC state: The solid red ovals represent spin singlets (valence bonds), which are frozen into a specific regular pattern. The singlets in a VBC are short ranged, here its nearest neighbor. Such a state in which the singlets form a crystalline order is also called a spin-Peierls state, it breaks the translation symmetry of the lattice. (b) A snapshot of a spin liquid RVB state. The spins are paired up into *randomly* distributed singlets of all possible lengths, denoted here by different colors. There is resonance between different configurations (ways of partitioning) spins into singlets. The total wave function is a superposition of each such snapshot.

per unit cell which preserves lattice translation symmetry along with spin rotation, if it also preserves lattice point group and time reversal symmetry, we shall refer to it as a *fully* symmetric spin liquid. A VBC on the other hand breaks the elementary lattice translational symmetry with unit cells of varying sizes.

It is also commonly mentioned that *fractionalization* is another hallmark of quantum spin liquids, this is not so, strictly speaking. Precisely speaking, fractionalization implies, firstly, that the elementary excitations (quasiparticles) carry quantum numbers which are a fraction of those corresponding to the local degrees of freedom and thus cannot be associated to collective modes in the sense of Landau; secondly, and more importantly it should be possible to separate these quasiparticles *infinitely* away from each other while expending only a *finite* amount of energy, the quasi-particles are then said to be deconfined. If we focus on spin-charge separation as a particular case of fractionalization, then e.g., the so called “critical” or “algebraic” spin liquids do not satisfy the second condition for fractionalization mentioned above, while \mathbb{Z}_2 and chiral spin liquids do so [7, 8]. Those phases of spin liquids that do admit *proper* fractionalization, also then contain topological orders and not just “internal” patterns (quantum orders). These states of matter are thus rightly called topologically ordered phases. We also mention, that in one dimension a VBC phase may sustain fractionalization, although this is, in general impossible in higher dimensions for ordered states (conventional or otherwise). These exotic fractional excitations are well established in one-dimensional systems where they occur as solitons, kinks or domain walls. However, in two dimensions, the experimental search is still going on for a *smoking gun* signature of fractionalization. For a recent review on these phases and their experimental search, see [71]. When dealing with these quantum phases, I will concentrate solely on quantum spin liquids and valence bond crystals in two dimensions arising in purely spin-1/2 models which are $SU(2)$ invariant, of the Heisenberg type.

2.2.3 Building blocks of quantum paramagnets

From the above discussion it is evident that spin liquids and valence bond crystals are *non-magnetic* in nature, so the wave function representing these phases should have spin-0. The wave function for the simplest building block of such a phase should obviously then be an anti-symmetrical spinor of rank two, i.e. $\gamma_{\alpha\beta}$, one index for each of the two electron spins at two different lattice sites. However, an anti-symmetrical spinor is just a scalar and thus corresponds to a system with total spin-0. Thus, we can picture the quantum spin liquid state as being built out of *singlets* in which the two electron spins are anti-parallel, due to antiferromagnetic interactions. This object is a valence bond [72, 73]. An additional requirement is that the spins should be partitioned in such a way that each spin is part of some specific singlet. This picture and requirement clearly leads to the *full* wave function for the phase which is also spin-0 and thus non-magnetic, as it should be. The *full* wave function, mathematically, will thus be a direct product of these singlets, this is of course an approximation. However, this is not the complete picture, see Fig. 2.3a. We know, that a valence bond is a highly quantum object and will therefore undergo strong quantum fluctuations between different configurations of valence bonds, i.e. different ways of partitioning the spins into valence bonds. There will thus be a *resonance* between different valence bond partitions and the wave function will be a superposition of differently partitioned valence bond configurations, see Fig. 2.3b. This is precisely the picture that was suggested by Anderson for describing these quantum phases and he appropriately (for reasons mentioned above) called them resonating valence bond (RVB) states [64, 65]. He further showed that the electrons which bind into the valence bonds are also *paired*, thus there is “potential” for superconductivity in such a RVB state. Thus, Anderson proposed a link between the physics of a hole doped RVB state and high temperature superconductivity, since the introduction of holes washes out Néel ordering and the spins then form a RVB state [66, 74].

It is worth mentioning that the RVB wave function should contain valence bonds of *all* possible lengths and not necessarily nearest neighbor or short range, except for a VBC. Depending on the distribution of weights on valence bond configurations of short or long lengths, one may get either short range RVBs (e.g. gapped \mathbb{Z}_2 spin liquids) or long range RVBs (e.g. algebraic spin liquids). Even among short range or long range RVBs, there can be many different states. Depending on the lattice geometry and more so on the gauge structure, the number of possible spin liquids may run from a few to *infinite* in number. This problem of classifying spin liquids for spin-1/2 quantum Heisenberg models has been pioneered by Wen [7]. A review of this technique will form the topic of section 2.3.

2.3 Spin liquids: a theoretical framework

In giving a brief qualitative account of the exotic quantum paramagnetic phases of matter such as spin liquids, one may get the impression, that a completely new and radical framework will be needed to understand these phases. This is to quite a good extent true, in some sense. However, there are many general traits or observations of traditional condensed matter theory which are also true for these exotic phases, when applied in a generalized manner. The first and foremost issue to be addressed, is on the prescription to be used in characterizing these phases, or, in other words what is the distinguishing feature of phases. This question was answered most comprehensively by Landau in 1937, when he pointed out in [1, 2] that *all* phases of matter are characterized and distinguished by symmetries, or more precisely, by the *set* of symmetries of some *mathematical* object (function) which

contains complete information about that particular phase or rather the “structure” of that phase. Thus, the *set* of symmetries of a function representing the phase reveals information about the structure/pattern of that phase, whence, we can distinguish the different phases. From the above description it is also evident that transition between phases involves the appearance or disappearance of some elements of symmetry. For conventional phases of matter at *finite* temperature, these structures/patterns in phases pertain to spatial symmetries and are thus tangible, e.g. crystallographic structures or magnetic structures. These phases then have *physical* order parameters. As opposed to this, exotic *zero* temperature phases only have “internal” structures.

For *classical* (neglecting quantum effects) conventional phases at *finite* temperature, the relevant mathematical object should be some function which determines the distribution of atoms in the body¹. This can, for example, be the time averaged microscopic charge density function $\bar{\rho}(x, y, z)$. The set of coordinate transformations with respect to which $\bar{\rho}(x, y, z)$ is invariant, i.e., its symmetry group, then naturally determines the pattern of distribution of atoms in the phase and hence its crystallographic structure. We know now, that there are in all 230 different types of symmetry groups (space groups) for $\bar{\rho}(x, y, z)$ possible, thus giving rise to 230 different crystallographic structures [3]. The key observation to make here is that we have studied the symmetry of a probability distribution function which is of course *positive*. This is a generic feature for all types of *classical* orders, i.e. where quantum effects are neglected.

However, by a naive extension we can attempt to describe the structure in phases where quantum effects cannot be neglected at all, i.e. phases at *zero* temperature, by simply taking $\bar{\rho}$ to its quantum version. However, by doing so we immediately land into the following difficulty; we know from theory and experiment that we can have “myriad” of *different* quantum phases with all of these phases having the *same* lattice space group symmetry. In other words, external tangible symmetries, structures and patterns that are visible to the human eye are not enough to distinguish the different quantum phases, “we need something more”. Thus, we can already intuitively see that quantum phases should possess deeper “internal” structures, which enable us to distinguish these phases. These “internal” structures are in fact the symmetries of the ground state wave function which is in general *complex*. A particular *set* of such symmetries correspond to a particular quantum order for a given phase. Here in lies the essential difference between classical orders and quantum orders, the former are described by symmetries of a *positive* definite function corresponding to static orders and the latter by symmetries of a *complex* wave function corresponding to motion to electrons and are thus dynamic in nature [7, 8]. This, automatically implies that quantum orders must be richer and varied than classical orders. It also enables us to clearly see the limitations of Landau’s theory on phases and their transitions, namely that it holds only for classical orders where there are *physical* spatial symmetries being broken and giving rise to *physical* order parameters. However, the essence of the principal commandments laid out by Landau on phases and phase transition in [1, 2] still hold true for quantum phases, the only difference being that the inclusion of “internal” symmetries used to describe “internal” orders along with the usual space group symmetries, will make the symmetry group more intricate. The consequent mathematical framework used to study these phases is called “projective symmetry group” (PSG), which is just an extension of the lattice symmetry group. But, still quantum orders will correspond to some “broken” PSG symmetries and phase transitions between quantum ordered states will involve appearance or disappearance

¹If one wants to study magnetic orders then the relevant object should give the distribution of magnetic moments in a body, this is the $\bar{j}(x, y, z)$ function.

of some PSG symmetry elements, in this sense the essence of Landau’s idea’s still holds in the quantum regime. For a certain class of quantum ordered states, there also exists another type of order called topological order, this has no analogue within the Landau scheme and requires a radically new formalism to study.

2.3.1 Mean field theory for spin liquids

At the onset we should mention that we shall focus only on developing the theory of spin liquids (and valence bond crystals) arising in purely Heisenberg spin systems with spin-1/2. The effective model for these Mott insulating phases is given by the spin-1/2 Heisenberg antiferromagnetic model,

$$\hat{\mathcal{H}} = \sum_{ij} J_{ij} \hat{\mathbf{S}}_i \cdot \hat{\mathbf{S}}_j, \quad (2.3)$$

the corresponding mean field Hamiltonian is one in which each spin couples to the mean value of the other in the given state, and is written as,

$$\hat{\mathcal{H}}_{\text{MF}} = \sum_{ij} J_{ij} (\hat{\mathbf{S}}_i \cdot \langle \hat{\mathbf{S}}_j \rangle + \langle \hat{\mathbf{S}}_i \rangle \cdot \hat{\mathbf{S}}_j - \langle \hat{\mathbf{S}}_i \rangle \cdot \langle \hat{\mathbf{S}}_j \rangle) \quad (2.4)$$

However, since spin liquids are spin disordered and thus have an *absence* of on-site magnetization, $\langle \hat{\mathbf{S}}_i \rangle = 0$, this implies that the conventional mean field procedure for spin systems fails for these spin rotation invariant phases. The way out of this problem will be guided by two factors, firstly, by allowing the possibility for *spin-charge* separation in spin liquids and secondly, by incorporating some internal (gauge) symmetries which will allow *different* quantum phases to be constructed with given lattice symmetries, these additional gauge symmetries are the “something more” that we mentioned before are needed to distinguish these phases. The procedure to be described below will enable us to construct mean-field wave functions for a large class of quantum spin liquids with different gauge structures and also for valence bond crystals.

SU(2) Slave boson (Schwinger fermion) formalism

The first step is to express or rather decompose the operators of spin-1/2 at every site i in terms of pseudo-quasiparticle creation (c_i^\dagger) and annihilation operators (c_i) representing spin-1/2 charge (electrical) neutral excitations (spinons), [6–8, 75–84]

$$\hat{\mathbf{S}}_i = \frac{1}{2} c_{i,\alpha}^\dagger \hat{\boldsymbol{\sigma}}^{\alpha\beta} c_{i,\beta} \quad (2.5)$$

where $\alpha, \beta = \uparrow, \downarrow$ and $\hat{\boldsymbol{\sigma}}$ is the Pauli matrix vector operator. Intuitively speaking, we have “cut” the spin operator into two halves, i.e. into a product of two spinon operators². In doing so, we are, at this stage, *not* tacitly implying that spin liquids harbor *free* spin-1/2 charge neutral excitations, since as we will see a generic feature of slave particle theories is that they are *strongly coupled*, implying that the spinons most probably remain *confined* and are then not well defined quasiparticles, they do not have a “life” of their own. In other cases, by invoking special mechanisms the interaction between spinons can be made short ranged and then the spin liquids will harbor true spin-1/2 excitations! [8]. Which of the above two cases actually occurs is difficult to predict at the mean field level, since the actual

²From a mathematical perspective this is just a trick enabling us to do mean field on such systems.

interactions between the spinons are mediated by a fluctuating dynamical gauge field, which appears only beyond the mean field level. It should also be noticed that, till now we have also not made any mention of the statistics obeyed by spinons, they may be either fermionic or bosonic, the choice is to some extent arbitrary. From now on, with a view of obtaining gapped as well as *gapless* quantum spin liquids, we will assume the spinons to be fermionic. This translates into,

$$\begin{aligned}\{c_{i,\alpha}^\dagger, c_{j,\beta}\} &= \delta_{i,j}\delta_{\alpha,\beta} \\ \{c_{i,\alpha}, c_{j,\beta}\} &= 0 \\ \{c_{i,\alpha}^\dagger, c_{j,\beta}^\dagger\} &= 0\end{aligned}\tag{2.6}$$

It is clear that the first requirement of the phenomenon of potential spin-charge separation has been captured in the fermionic picture, but it is not apparent at first sight if any additional structure or symmetry has been introduced in this picture. To see this, we first write eqn. 2.5 for each component explicitly, as follows.

$$\begin{aligned}\hat{S}_i^x &= \frac{1}{2}(c_{i,\uparrow}^\dagger c_{i,\downarrow} + c_{i,\downarrow}^\dagger c_{i,\uparrow}) \\ \hat{S}_i^y &= \frac{1}{2}i(c_{i,\downarrow}^\dagger c_{i,\uparrow} - c_{i,\uparrow}^\dagger c_{i,\downarrow}) \\ \hat{S}_i^z &= \frac{1}{2}(c_{i,\uparrow}^\dagger c_{i,\uparrow} - c_{i,\downarrow}^\dagger c_{i,\downarrow})\end{aligned}\tag{2.7}$$

Since $c_{i,\uparrow}$ and $c_{i,\downarrow}$ form a SU(2) doublet, and so do $c_{i,\downarrow}^\dagger$ and $-c_{i,\uparrow}^\dagger$; it implies that we can merge these two doublets into a 2×2 matrix, Φ_i , which is expressed below as, [80]

$$\Phi_i = \begin{pmatrix} c_{i,\uparrow} & c_{i,\downarrow} \\ c_{i,\downarrow}^\dagger & -c_{i,\uparrow}^\dagger \end{pmatrix}$$

Now, the key step en route to making the additional internal symmetry transparent, lies in recasting each component of the spin operator given in eqn. 2.7 in terms of Φ_i . This takes the following form,

$$\hat{S}_i^\alpha = \frac{1}{4}Tr[\Phi_i^\dagger \Phi_i (\hat{\sigma}^\alpha)^T]\tag{2.8}$$

where, $\alpha = x, y, z$. It is trivial to verify that eqn. 2.8 is equivalent to eqn. 2.7. Also, Φ_i transforms under SU(2) transformations as $\Phi_i \rightarrow W_i \Phi_i$, where $W_i \in \text{SU}(2)$. Thus, it is now evident from eqn. 2.8 that, at *every* site, each spin component operator remains *invariant* under a SU(2) transformation. Thus, we see that the fermionic representation of spin is endowed with a *local* (site-dependent) SU(2) symmetry under which the physical spin operator at that site remains invariant, i.e. $\hat{S}_i \rightarrow \hat{S}_i$ [66, 78–80, 85, 86]. Now, the feature is that since the Hamiltonian is a function of only the spin operators, this *local* SU(2) symmetry becomes a *gauge* symmetry. It was precisely this additional ‘‘internal’’ gauge symmetry that we sought after. This together with global spin rotations, the usual lattice space group and time-reversal symmetries of the Heisenberg model are the ingredients which enable one to distinguish different spin liquid phases [7, 8, 87].

It is worth mentioning that the SU(2) nature of the local gauge symmetry arose simply because we chose to write the original spin Hamiltonian in a particular way, in this sense

this SU(2) gauge group is the *full* “high energy” gauge group [7, 8, 84]. On the other hand, we could have also chosen to express the spin operators in a way, so as to have a U(1) or a \mathbb{Z}_2 local gauge symmetry. Depending on the choice of the high energy gauge group, this fermionic approach is called the SU(2), U(1) or \mathbb{Z}_2 [88] slave-boson approach, all three are completely equivalent descriptions of the Heisenberg model and lead to the same spin liquids, working in one or the other gauge structure is purely a matter of convenience, to a great extent [84]. This can be physically understood if we keep in mind that, *in part* the role of the gauge fluctuations is to restore back the Hilbert space of the original Heisenberg model. So, if the fluctuations of the SU(2), U(1) or \mathbb{Z}_2 lattice gauge fields in the SU(2), U(1) or \mathbb{Z}_2 slave boson approaches, respectively, are taken into account exactly, we get the same result. We shall work only within the SU(2) slave boson approach. It is worth mentioning, that the high energy gauge group can be made even more complicated as per our choice, all we need to do is to “cut” the physical spin operator $\hat{\mathbf{S}}_i$ into an *even* number of fermions.

Another artifact of the fermionic representation is that it *enlarges* the Hilbert space from two states per site to four states per site, which now include *doubly* occupied and *empty* sites. Hence, to have a faithful equivalence between the original Heisenberg model and its fermionic representation, we need to impose the constraint of *one* fermion per site. That is,

$$c_{i,\uparrow}^\dagger c_{i,\uparrow} + c_{i,\downarrow}^\dagger c_{i,\downarrow} = 1 \quad (2.9)$$

this constraint automatically implies that there are no doubly occupied and empty sites, these constraints are respectively written as,

$$\begin{aligned} c_{i,\downarrow} c_{i,\uparrow} &= 0 \\ c_{i,\downarrow}^\dagger c_{i,\uparrow}^\dagger &= 0 \end{aligned} \quad (2.10)$$

We can tidily write up all the three constraints using the Φ_i matrix as,

$$\frac{1}{2} \text{Tr}[\Phi_i^\dagger \hat{\sigma}^\alpha \Phi_i] = 0 \quad (2.11)$$

with $\alpha = x, y, z$. The $\alpha = z$ gives the constraint of eqn. 2.9 and $\alpha = x, y$ give the constraints of eqn. 2.10. These constraints are *not* gauge invariant, as can be seen.

Fermionic representation of the Heisenberg model

To obtain the fermionic representation of the spin-1/2 Heisenberg model, we simply substitute the form of $\hat{\mathbf{S}}_i$ from eqn. 2.8 into 2.3. Upon doing so, we get the following expression of the Heisenberg Hamiltonian,

$$\begin{aligned} \hat{\mathcal{H}} &= \sum_{ij} \frac{J_{ij}}{16} (\text{Tr}[\Phi_i^\dagger \Phi_i (\hat{\boldsymbol{\sigma}})^\text{T}]) \cdot (\text{Tr}[\Phi_j^\dagger \Phi_j (\hat{\boldsymbol{\sigma}})^\text{T}]) \\ &= -\frac{1}{8} \sum_{ij} J_{ij} \text{Tr}[\Phi_i \Phi_j^\dagger \Phi_j \Phi_i^\dagger] \end{aligned} \quad (2.12)$$

Thus, the two-spin Heisenberg interaction Hamiltonian in eqn. 2.3 has been mapped into a Hamiltonian composed of *four-fermion* interaction terms. Now, we observe that, since Φ_i transforms by a right SU(2) multiplication ($\Phi_i \rightarrow \Phi_i V$, where $V \in \text{SU}(2)$) under *global*

SU(2) spin rotations, it is manifest that the object “ $\Phi_i\Phi_j^\dagger$ ” is SU(2) spin-rotation invariant. We shall call this object, which is a “link” operator, as U_{ij} from now on. Its explicit form is given below,

$$U_{ij} = \Phi_i\Phi_j^\dagger = \begin{pmatrix} c_{i,\uparrow}c_{j,\uparrow}^\dagger + c_{i,\downarrow}c_{j,\downarrow}^\dagger & c_{i,\uparrow}c_{j,\downarrow} - c_{i,\downarrow}c_{j,\uparrow} \\ c_{i,\downarrow}c_{j,\uparrow}^\dagger - c_{i,\uparrow}c_{j,\downarrow}^\dagger & c_{i,\downarrow}c_{j,\downarrow}^\dagger + c_{i,\uparrow}c_{j,\uparrow}^\dagger \end{pmatrix}$$

From the above structure of U_{ij} it is also evident that it is in fact composed of *two* SU(2) spin rotation invariant operators defined between pairs of sites, these are namely,

$$\chi_{ij} = c_{i,\uparrow}^\dagger c_{j,\uparrow} + c_{i,\downarrow}^\dagger c_{j,\downarrow} \quad (2.13)$$

$$\Delta_{ij} = c_{i,\uparrow}^\dagger c_{j,\downarrow}^\dagger - c_{i,\downarrow}^\dagger c_{j,\uparrow}^\dagger \quad (2.14)$$

In terms of these operators, the U_{ij} matrix can be compactly written as,

$$U_{ij} = \begin{pmatrix} -\chi_{ij}^\dagger & -\Delta_{ij}^\dagger \\ -\Delta_{ij} & \chi_{ij} \end{pmatrix}$$

From the definition of U_{ij} , we see that under *local* SU(2) gauge transformations, it transforms as $U_{ij} \rightarrow W_i U_{ij} W_j^\dagger$. Now, finally in terms of the U_{ij} matrix operator, the Heisenberg Hamiltonian in the fermionic representation can be concisely cast as,

$$\hat{\mathcal{H}} = -\frac{1}{8} \sum_{ij} J_{ij} \text{Tr}[U_{ij} U_{ij}^\dagger] \quad (2.15)$$

The advantage of working explicitly with the Φ_i matrix representation of all operators, rather than with a two-component spinor is now obvious. First and foremost is that the invariance of the theory under *global* SU(2) spin rotations and *local* SU(2) gauge transformations, is manifest. Secondly, it enables one to figure out the transformation properties of any object/operator at once, under both the above symmetry operations, since, *global* SU(2) spin rotations are effected by a right SU(2) multiplication of Φ_i , i.e. $\Phi_i \rightarrow \Phi_i V$ and *local* SU(2) gauge transformations are effected by a left SU(2) multiplication of Φ_i , i.e. $\Phi_i \rightarrow W_i \Phi_i$. Thus, $\Phi_i \rightarrow W_i \Phi_i V$ and $\Phi_i^\dagger \rightarrow V^\dagger \Phi_i^\dagger W_i^\dagger$. It is also apparent that, *global* SU(2) spin-rotations and *local* SU(2) gauge transformations commute with each other.

We are now faced with the task of solving a *strongly coupled* problem between fermions, represented by eqn. 2.15 with *four-fermion* interactions. This is a generic feature of all slave particle constructions. However, this implies that the fields which mediate the interactions between the spinons (in our case) fluctuate extremely rapidly, hence, any picture provided by just a mean field type approximation cannot be trusted, in general. We would have to go beyond mean field and include some type of fluctuations, to get a physically and quantitatively reasonable picture [8]. In passing, we would like to mention that working in the fermionic representation has the advantage that Wick’s theorem can be exploited, this considerably simplifies the use of perturbation theory, when needed in handling certain types of “marginally” stable spin liquids.

Hubbard-Stratonovich transformation and the mean field approximation

As we saw that the fermionic formulation of the spin-1/2 Heisenberg model leads to a Hamiltonian which involves *many body* interaction terms (four fermion interactions), which

in general represent strong coupling, as they should since the Heisenberg spin model has no *small* parameters. The key step now is to re-express *exactly*, the Hamiltonian of eqn. 2.15 in a form on which the nature of mean field approximation becomes clear and the approximation can be transparently applied, this is the role of the Hubbard-Stratonovich transformation. The basic philosophy of the Hubbard-Stratonovich transformation, which is a purely formal technique, albeit exact, is to map the problem of a system of particles interacting “directly” with each other via many body interaction potentials *into* a system of *free* particles interacting with a fluctuating field which mediates the interactions between the particles. The degree of fluctuations of this “auxiliary” *scalar* (in general complex) field introduced in the transformation, depends on the strength of the “direct” interaction between the particles. Thus, in summary the Hubbard-Stratonovich transformation maps a particle theory into a field theory. The mean field approximation can thus be applied on the field variables. After the transformation, the fermionic Heisenberg model reads as,

$$\hat{\mathcal{H}}_{\text{HS}} = \sum_{ij} Tr[\Phi_i^\dagger \tilde{U}_{ij} \Phi_j + \text{h.c.}] + \sum_{ij} \frac{8}{J_{ij}} Tr[\tilde{U}_{ij}^\dagger \tilde{U}_{ij}] \quad (2.16)$$

Here, \tilde{U}_{ij} is the “auxiliary” field introduced by the Hubbard-Stratonovich transformation and is defined between every pair of sites. These “link” fields are 2×2 , in general complex matrices, which are *time dependent*. This implies, that w.r.t. *local* $SU(2)$ gauge symmetry, the \tilde{U}_{ij} must now transform under *time dependent* local $SU(2)$ gauge transformations, $\tilde{U}_{ij}(t) \rightarrow W_i(t) \tilde{U}_{ij}(t) W_j^\dagger(t)$.

It should be recalled that the above Hamiltonian of eqn. 2.16 is still not equivalent to the original Heisenberg model of eqn. 2.3, it is an incomplete representation, since, as we know, the fermionic representation enlarges the Hilbert space, and we need to impose the constraints of eqns. 2.9 and 2.10. This can be trivially done, by introducing three Lagrange multiplier terms, which impose the three constraints. Each such term at a given site i is, $a_i^\alpha (\frac{1}{2} Tr[\Phi_i^\dagger \hat{\sigma}^\alpha \Phi_i])$, where $\alpha = x, y, z$ and a_i^α are the three Lagrange multipliers. After, absorbing the factor of 1/2 in a_i^α , and including the three constraint terms at every site, one lands up with the following Hamiltonian,

$$\hat{\mathcal{H}}_{\text{HS}}^{\text{Heisenberg}} = \sum_{ij} Tr[\Phi_i^\dagger \tilde{U}_{ij} \Phi_j + \text{h.c.}] + \sum_{ij} \frac{8}{J_{ij}} Tr[\tilde{U}_{ij}^\dagger \tilde{U}_{ij}] + \sum_i Tr[\Phi_i^\dagger (\mathbf{a}_i \cdot \boldsymbol{\sigma}) \Phi_i] \quad (2.17)$$

The \mathbf{a}_i 's are *time dependent*, i.e. $\mathbf{a}_i(t)$. It is also worth noting that the $\tilde{U}_{ij}(t)$ and $\mathbf{a}_i(t)$ transform as the spatial and temporal components of a lattice $SU(2)$ gauge field, respectively, under time dependent *local* $SU(2)$ gauge transformations.³

We shall now apply the mean field approximation on eqn. 2.17 [6–8]. The *zeroth* order mean field approximation consists of completely neglecting *all* the fluctuations of the $SU(2)$ lattice gauge field, i.e. neglecting the time dependence of $\tilde{U}_{ij}(t)$ and $\mathbf{a}_i(t)$. This physically implies taking the non-interacting limit wherein the fermions (spinons) are *free* quasiparticles on a lattice, i.e. spinon gas. Mathematically, we implement it by replacing the oscillating fields $\tilde{U}_{ij}(t)$ and $\mathbf{a}_i(t)$ by their ground state expectation values, denoted by $\bar{U}_{ij} (= \langle U_{ij} \rangle =$

³The coupling of the gauge field (which mediates the interaction between spinons) to the spinons is *strong* (infinite), this implies that the coupling constant $g \rightarrow \infty$ in $(1/8\pi g) F_{\mu\nu} F^{\mu\nu}$ term in the Lagrangian ($F_{\mu\nu}$ is the field strength tensor). This limit corresponds formally to the Heisenberg model limit in which the fluctuations of the gauge field are large, and there is thus *no* “small” parameter in which we can expand, as we mentioned before.

$\langle \Phi_i \Phi_j^\dagger \rangle$). The \bar{U}_{ij} are time-independent matrices of complex numbers and the $\bar{\mathbf{a}}_i$ are now simply time independent. Implementing this prescription, we arrive at the following zeroth order mean field Hamiltonian,

$$\hat{\mathcal{H}}_{\text{MF}}^0 = \sum_{ij} Tr[\Phi_i^\dagger \bar{U}_{ij} \Phi_j + \text{h.c.}] + \sum_{ij} \frac{8}{J_{ij}} Tr[\bar{U}_{ij}^\dagger \bar{U}_{ij}] + \sum_i Tr[\Phi_i^\dagger (\bar{\mathbf{a}}_i \cdot \boldsymbol{\sigma}) \Phi_i] \quad (2.18)$$

We see now, that mathematically the above Hamiltonian is soluble, since it is quadratic in the fermion operators and hence, represents a system of free spinons. Thus, the mathematical obstruction to the solution of Heisenberg model in the fermionic representation has been cured by taking the above mean field approximation. However, on the other hand, it of course cannot be even a vaguely true representation of the physics of the Heisenberg model, since there are no correlations present in a free spinon systems, while the Heisenberg model is an interacting model with strong correlations. The inconsistency at this mean field level lies in the fact that in the beginning when giving the fermionic expression for spin operators in eqn. 2.7 we split the physical spin operator into a product of spinon operators and the zeroth order mean field approximation clearly forgot to “glue” the spinons back together to get back the spin operator. The absence of the “glue” implies that excitations around the mean field state described by eqn. 2.18 are free spinons, a conclusion which is clearly an artifact of the slave boson approach at the zeroth order mean field level [7, 8].

Also, if we diagonalize the above Hamiltonian and obtain the mean field ground state $|\Psi_{\text{MF}}^0(\bar{U}_{ij}, \bar{\mathbf{a}}_i)\rangle$ then it will contain sites which are empty and some which are doubly occupied, because the constraint of one-fermion per site is satisfied *only* on an average, i.e. $\langle \frac{1}{2} Tr[\Phi_i^\dagger \hat{\sigma}^z \Phi_i] \rangle = 0$. Thus the mean field ground state is not even a legitimate wave function for the original Heisenberg spin model. If we compare the situation here, or in general for slave particle approaches with that of ordinary mean field theory, we see a striking difference, namely that the Hilbert space is changed in mean field approximation within slave particle approaches, this doesn't happen in ordinary mean field theory.

From the above considerations it is clear, that we *must* go beyond mean field theory *at all costs*, not only to improve quantitative estimates but also to obtain a physically sound and logically consistent picture. The most important type of fluctuations that are absolutely needed and should be incorporated first, are those which recover back the original Hilbert space of one-fermion per site of the Heisenberg model. The fluctuations, i.e. time dependence of \mathbf{a}_i^z , precisely perform this one-fermion per site constraint enforcing job. What one can do numerically, is to take the mean field Slater determinant $|\Psi_{\text{MF}}^0(\bar{U}_{ij}, \bar{\mathbf{a}}_i)\rangle$ and to remove empty and doubly occupied sites, this procedure is called Gutzwiller projection and can be implemented in a Monte Carlo scheme [89, 90], since implementation of the projection operation is extremely complicated by analytical means. The resulting state that one obtains, is then at least a legitimate trial wave function for the original spin Heisenberg model of eqn. 2.3, and can be expressed as $|\Psi_{\text{trial}}(\bar{U}_{ij}, \bar{\mathbf{a}}_i)\rangle = \mathcal{P}_{\mathcal{G}} |\Psi_{\text{MF}}^0(\bar{U}_{ij}, \bar{\mathbf{a}}_i)\rangle$, where $\mathcal{P}_{\mathcal{G}}$ is the *full* Gutzwiller projector which removes empty and doubly occupied sites. In other words, this Gutzwiller projected state has incorporated in itself exactly, the fluctuations of the \mathbf{a}_i^z , i.e. the oscillations of the temporal component of the SU(2) lattice gauge field⁴. Thus, the fact that after projection the one-fermion per site constraint is satisfied exactly at *all* times implies, that the Gutzwiller projected wave function has *in built* strong correlations.

⁴Thus, Gutzwiller projection amounts to integrating over *exactly* the temporal component of the gauge field, or in other words taking the Heisenberg limit of $g \rightarrow \infty$. This naturally amounts to incorporating strong correlations in the spinon system.

We mention that this projection leaves out the fluctuations of U_{ij} , i.e. the spatial component of the $SU(2)$ lattice gauge field; in principle if we include them then we would of course solve the original Heisenberg spin model exactly.

Now we would like to address the very important question of, “how good a starting point is provided by the zeroth order mean field state?”. In other words, we wish to understand to what degree and in what manner the mean field state is altered when one includes fluctuations. To answer this question we have to study the behavior of the ratio of interaction strength between spinons with that of the energy of the system, in the low energy limit. We recall that the strength of interaction between spinons scales directly with the strength of fluctuations about the mean field state. So, the behavior of this ratio is the relevant quantity to look it. In the simplest case, if this ratio goes to *zero*, then of course the interactions between spinons at low energies are *irrelevant* operators in the RG sense. This implies that the fluctuations of the gauge field are weak and thus will not drive the system into a quantum phase transition, so we can get a qualitatively relevant picture for the physical spin liquid phase, by just studying the zeroth order approximated mean field state. However, on the quantitative level the critical exponents for various quantities will change after inclusion of fluctuations. Such type of spin liquids are called “stable” spin liquids. Examples of which are gapped and gapless \mathbb{Z}_2 spin liquids, and *chiral* spin liquids [6–8]. These spin liquids can harbor free spin-1/2 excitations because the gauge field is only able to mediate short range interactions due to its gapped nature, and the spinons can thus be deconfined. So, the business of formally “cutting” the spin operator into two halves, has actually produced two independent spinons.

In the opposite case this ratio can diverge in the low energy limit. Then of course the interactions between the spinons are *relevant* operators. This implies that the fluctuations of the gauge field are strong and will definitely drive the system into a quantum phase transition. In such cases, even qualitative estimates from mean field theory will not carry over to the real physical spin liquid phase. Such spin liquids are thus called, “unstable” spin liquids. Examples are spin liquids with in general, $U(1)$ or $SU(2)$ low energy gauge structures. A third situation occurs, if in the low energy limit the ratio approaches a finite constant. This implies that the interactions between the spinons are *marginal* operators. Analyzing the stability of such states is a tricky business in general. If this finite ratio is small, then the situation can be studied by perturbation theory. On the other hand, if this ratio is of the order of unity, then the question of stability of such spin liquids is extremely hard [15]. There exists till now, no general field theoretical framework within which one can address such a question. One then has to analyze the effect of various perturbations one by one, which is a tedious task. An example of such a “marginal” spin liquid is given by the $U(1)$ Dirac spin liquid on the kagomé lattice. In such a spin liquid, the the gauge field is confining and the business of cutting the spin operator into two halves is just a formal picture. We shall be addressing the issue of its stability in great detail in this thesis.

It is worth mentioning that there is a small but important caveat regarding what we have mentioned above. Up to now, we only emphasized the role of fluctuations in the low energy, i.e. large distance limit. However, if the short distance fluctuations are strong enough, then they may also drive the system into a quantum phase transition [8]. Therefore, for zeroth order mean field theory to give a physically reliable picture, it is necessary that, firstly, the mean field states must be either “stable” or at most “marginal”, and furthermore the short distance fluctuations should be weak⁵. However, we should not give a message of despair

⁵This is precisely a catch-22 situation, in reality these fluctuations are never weak because the Heisenberg spin model has no “natural” small parameters in it.

since by invoking special mechanisms the fluctuations of the gauge field can be suppressed. We shall see how this is done later in the text.

Now, finally we would like to recast the zeroth order mean field Hamiltonian of eqn. 2.18 into a convenient form, which we will use throughout. First, we notice that the second term of eqn. 2.18 is a constant and we shall drop it henceforth. This leaves us with the following expression,

$$\hat{\mathcal{H}}_{\text{MF}}^0 = \sum_{ij} \text{Tr}[\Phi_i^\dagger \bar{U}_{ij} \Phi_j + \text{h.c.}] + \sum_i \text{Tr}[\Phi_i^\dagger (\bar{\mathbf{a}}_i \cdot \boldsymbol{\sigma}) \Phi_i] \quad (2.19)$$

The time-independent, 2×2 complex matrices \bar{U}_{ij} are explicitly written as,

$$\bar{U}_{ij} = \begin{pmatrix} -\bar{\chi}_{ij}^* & -\bar{\Delta}_{ij}^* \\ -\bar{\Delta}_{ij} & \bar{\chi}_{ij} \end{pmatrix}$$

where,

$$\bar{\chi}_{ij} = \langle \chi_{ij} \rangle = \langle c_{i,\uparrow}^\dagger c_{j,\uparrow} + c_{i,\downarrow}^\dagger c_{j,\downarrow} \rangle \quad (2.20)$$

$$\bar{\Delta}_{ij} = \langle \Delta_{ij} \rangle = \langle c_{i,\uparrow}^\dagger c_{j,\downarrow}^\dagger - c_{i,\downarrow}^\dagger c_{j,\uparrow}^\dagger \rangle \quad (2.21)$$

In terms of these amplitudes the above Hamiltonian of eqn. 2.19 can be recast into the following convenient and transparent form,

$$\begin{aligned} \hat{\mathcal{H}}_{\text{MF}}^0 &= \sum_{ij} [\bar{\chi}_{ij} c_{j,\alpha}^\dagger c_{i,\alpha} + \bar{\Delta}_{ij} (c_{i,\uparrow} c_{j,\downarrow} - c_{i,\downarrow} c_{j,\uparrow}) + \text{h.c.}] \\ &+ \sum_i \bar{a}_i^z (c_{i,\alpha}^\dagger c_{i,\alpha} - 1) + [(\bar{a}_i^x + i\bar{a}_i^y) (c_{i,\downarrow} c_{i,\uparrow} - c_{i,\uparrow} c_{i,\downarrow}) + \text{h.c.}] \end{aligned} \quad (2.22)$$

We see, that the mean field Hamiltonian consists of the following parts, (i) a spinon hopping term, with amplitude $\bar{\chi}_{ij}$, (ii) a spinon pairing term, with amplitude $\bar{\Delta}_{ij}$, (iii) an onsite chemical potential \bar{a}_i^z , (iv) real and imaginary onsite pairing terms, \bar{a}_i^x and \bar{a}_i^y respectively. From now on, we shall denote the chemical potential \bar{a}_i^z as μ_i and the complex imaginary pairing $\bar{a}_i^x + i\bar{a}_i^y$ as ζ_i . The zeroth order mean field Hamiltonian can then be finally written as [7, 8],

$$\begin{aligned} \hat{\mathcal{H}}_{\text{MF}}^0 &= \sum_{ij} [\bar{\chi}_{ij} c_{j,\alpha}^\dagger c_{i,\alpha} + \bar{\Delta}_{ij} (c_{i,\uparrow} c_{j,\downarrow} - c_{i,\downarrow} c_{j,\uparrow}) + \text{h.c.}] \\ &+ \sum_i \mu_i (c_{i,\alpha}^\dagger c_{i,\alpha} - 1) + [\zeta_i (c_{i,\downarrow} c_{i,\uparrow} - c_{i,\uparrow} c_{i,\downarrow}) + \text{h.c.}] \end{aligned} \quad (2.23)$$

The above Hamiltonian is clearly isotropic in spin space, and therefore leads to a spin singlet ground state. Thus, the slave boson approach is biased towards capturing spin disordered ground states. The complementary approach using slave fermions is also able to capture magnetic long range order. In retrospect, we see that $\bar{\chi}_{ij}$ and $\bar{\Delta}_{ij}$ arise from the two ways we can represent that Heisenberg exchange term in the fermionic representation, after a mean field decoupling.

A specification of $\bar{\chi}_{ij}$, $\bar{\Delta}_{ij}$, μ_i and ζ_i is called a mean field Ansatz [6–8]. By definition these quantities are *not* gauge invariant and therefore, e.g. $\bar{\chi}_{ij}$ cannot serve as a local order

parameter in the conventional sense of the word. It is also useful to note that the \bar{U}_{ij} matrix given above can be expanded as,

$$\bar{U}_{ij} = \begin{pmatrix} -\bar{\chi}_{ij}^* & -\bar{\Delta}_{ij}^* \\ -\bar{\Delta}_{ij} & \bar{\chi}_{ij} \end{pmatrix} = \bar{\chi}_{ij}^R \sigma_3 + i \bar{\chi}_{ij}^I \sigma_0 + \bar{\Delta}_{ij}^R \sigma_1 + \bar{\Delta}_{ij}^I \sigma_2$$

where, σ_1, σ_2 and σ_3 are the three Pauli matrices and σ_0 is the identity matrix. The $\bar{\chi}_{ij}^R$ and $\bar{\chi}_{ij}^I$ denote the real and imaginary hoppings, respectively; the $\bar{\Delta}_{ij}^R$ and $\bar{\Delta}_{ij}^I$ denote real and imaginary pairings, respectively. The \bar{U}_{ij} matrix is clearly seen to be *not* Hermitian. The mean field Ansatz labels the mean field ground state wave function, $|\Psi_{\text{MF}}^0(\bar{\chi}_{ij}, \bar{\Delta}_{ij}, \mu, \zeta)\rangle$. Due to the gauge non-uniqueness in the choice of the Ansatz, the labeling is not one-to-one, but rather many-to-one. This has non-trivial consequences, among them being the fact that two mean field Ansätze connected by a SU(2) gauge transformation but being “apparently” unrelated, will after projection, actually give rise to the *same* physical spin wave function, hence representing the same quantum phase. This observation highlights the physical meaning of the SU(2) local gauge symmetry in the fermionic representation.

However, one *should not* get the impression that this *local* SU(2) gauge symmetry is just a “junk” redundancy acquired in dealing with the SU(2) slave boson approach, and of no use, and in fact complicating the problem by introducing many labels for the same quantum phase. This gauge redundancy was powerfully exploited by Wen in [7], whereby he showed that different spin liquids can in fact be distinguished by these different gauge symmetries, when compounded with lattice space group and time reversal symmetries. The relevant mathematical framework to do so is called “Projective symmetry groups”, the review of which, will form the topic of our next section.

2.3.2 Classification of spin liquids: projective symmetry groups

If one considers the class of *fully symmetric* spin liquids, then as the name suggests, the projected physical spin wave functions corresponding to each and every one of these “different” spin liquids, have *all* the space-time symmetries of the Heisenberg model. Thus, all these “different” quantum phases are invariant under the same symmetry group, namely the lattice space group and time reversal, and hence can not be distinguished *only* on the basis of the symmetries present in the original spin model. The fermionic representation, adds to our arsenal another symmetry, namely the *local* SU(2) gauge symmetry. So, the symmetries we now have in our hand are the following, (i) lattice space group, (ii) time-reversal, and (iii) *local* SU(2) gauge. If we apply a *particular* lattice space group and/or time-reversal operation on a mean field Ansatz for a given spin liquid, then of course the Ansatz will change. We are permitting the Ansatz to change *only* because we are now armed with a *local* SU(2) gauge symmetry also. So, the only key reservation is that the change should be such that there exists a *local* SU(2) gauge transformation which can “undo” this change and restore back the original Ansatz. It is also obvious, that, in general, the change of mean field Ansatz due to different lattice space group operations, will be “restored” by *different* SU(2) gauge transformations. Now, if we apply a *particular* lattice symmetry and/or time-reversal operation simultaneously on the different Ansätze for the n different fully symmetric spin liquids, all the Ansätze will change, *but* the gauge transformation (corresponding to this lattice symmetry operation) which restores/undoes this change is actually *different* for the “different” spin liquids. This statement applies, in general, to all lattice symmetry operations. Thus, the difference in the “restoring” gauge transformations (for each and every lattice symmetry) enable us to distinguish the n different *fully symmetric* spin liquids, de-

spite them all having the same space-time symmetries. This implies, in particular, as we mentioned before, that classical orders are not sufficient to distinguish different spin liquids, and that the internal quantum orders that are present, need to be revealed, this is the role of gauge symmetries, as explained above. It was this extremely important observation that was made by Wen [7, 8] and forms the basis for the mathematical framework of projective symmetry groups which enables us to distinguish and classify different spin liquids. We shall now present the formal mathematical framework for it,

Let \mathcal{R} be a lattice space group symmetry operation which maps a site $i \rightarrow \mathcal{R}(i)$. Then the operation \mathcal{R} maps \bar{U}_{ij} to \bar{U}'_{ij} in the following manner,

$$\bar{U}'_{ij} = \mathcal{R}(\bar{U}_{ij}) = \bar{U}_{\mathcal{R}(i)\mathcal{R}(j)} \quad (2.24)$$

Now, we introduce a site-dependent (time-independent) $SU(2)$ gauge transformation corresponding to \mathcal{R} which undoes the change in the Ansatz, we call it $W_i^{\mathcal{R}}$. Now, the sequential operation of \mathcal{R} and $W_i^{\mathcal{R}}$ acting on \bar{U}_{ij} is expressed as,

$$\bar{U}_{ij} = (W_i^{\mathcal{R}})\bar{U}_{\mathcal{R}(i)\mathcal{R}(j)}(W_j^{\mathcal{R}})^\dagger \quad (2.25)$$

similarly the same relation can be written for the onsite components $\bar{\mathbf{a}}_i$ of the mean field Ansatz as follows,

$$\bar{\mathbf{a}}_i \cdot \hat{\boldsymbol{\sigma}} = (W_i^{\mathcal{R}})\bar{\mathbf{a}}_{\mathcal{R}(i)} \cdot \hat{\boldsymbol{\sigma}}(W_i^{\mathcal{R}})^\dagger \quad (2.26)$$

Thus, the PSG consists of all symmetry transformations (lattice space group, time-reversal and local $SU(2)$ gauge) that keep the mean field Ansatz invariant. From the above two mathematical relations, it is clear that the lattice symmetries act ‘‘projectively’’ on the fermions. Hence, for a *given* mean field Ansatz $\{\bar{U}_{ij}, \bar{\mathbf{a}}_i\}$, the set of *all* possible lattice symmetry operations (and time-reversal) $\{\mathcal{R}\}$ taken together *pairwise* with the corresponding gauge transformations $W_i^{\mathcal{R}}$, which satisfy eqn. 2.25 and 2.26 form a group called the ‘‘projective symmetry group’’ (PSG), $\{\mathcal{R}, W_i^{\mathcal{R}}\}$ of that particular mean field Ansatz $\{\bar{U}_{ij}, \bar{\mathbf{a}}_i\}$. From the qualitative arguments above, it follows that different spin liquids will have different PSGs and can thus be distinguished from each other. So, just as classical orders are classified by crystal and magnetic space groups, we see that quantum orders are classified by projective symmetry groups (at the mean field level), which are just extensions of the ordinary lattice symmetry groups. Since, there are many different extensions possible of the ordinary symmetry group, these different extensions each correspond to a particular quantum order. This is another way of seeing why PSG is needed to classify quantum orders.

We also know that two Ansatz connected by a *local* $SU(2)$ gauge transformation actually describe the same physical spin liquid, i.e. the same quantum ordering. Thus, their PSG’s should also be the same up to a local $SU(2)$ gauge transformation. We will show this explicitly below,

From eqn. 2.25 we have,

$$\bar{U}_{ij} = (W_i^{\mathcal{R}})\bar{U}_{\mathcal{R}(i)\mathcal{R}(j)}(W_j^{\mathcal{R}})^\dagger \quad (2.27)$$

Let G_i be the local $SU(2)$ gauge transformation on the Ansatz \bar{U}_{ij} . Then on applying this transformation to the above equation and rearranging, we get,

$$\begin{aligned}
G_i \bar{U}_{ij} G_j^\dagger &= G_i [(W_i^{\mathcal{R}}) \bar{U}_{\mathcal{R}(i)\mathcal{R}(j)} (W_j^{\mathcal{R}})^\dagger] G_j^\dagger \\
&= G_i [(W_i^{\mathcal{R}}) \mathcal{R} \bar{U}_{ij} (W_j^{\mathcal{R}})^\dagger] G_j^\dagger \\
&= G_i [(W_i^{\mathcal{R}}) \mathcal{R} G_i^\dagger (G_i \bar{U}_{ij} G_j^\dagger) G_j (W_j^{\mathcal{R}})^\dagger] G_j^\dagger \\
&= [G_i (W_i^{\mathcal{R}}) \mathcal{R} G_i^\dagger \mathcal{R}^{-1}] \mathcal{R} (G_i \bar{U}_{ij} G_j^\dagger) [G_j (W_j^{\mathcal{R}})^\dagger G_j^\dagger] \\
&= [G_i (W_i^{\mathcal{R}}) G_{\mathcal{R}(i)}^\dagger] \mathcal{R} (G_i \bar{U}_{ij} G_j^\dagger) [G_j (W_j^{\mathcal{R}})^\dagger G_j^\dagger]
\end{aligned} \tag{2.28}$$

Thus, we see that when the mean field Ansatz is gauge transformed from $\{\bar{U}_{ij}, \bar{\mathbf{a}}_i\} \rightarrow \{G_i \bar{U}_{ij} G_j^\dagger, G_i(\bar{\mathbf{a}}_i \cdot \hat{\boldsymbol{\sigma}}) G_i^\dagger\}$, then the corresponding change in PSG is $\{\mathcal{R}, W_i^{\mathcal{R}}\} \rightarrow \{\mathcal{R}, G_i(W_i^{\mathcal{R}}) G_{\mathcal{R}(i)}^\dagger\}$. This, implies that the ‘‘restoring’’ SU(2) gauge transformations $W_i^{\mathcal{R}}$ have been transformed under SU(2) gauge transformation G_i in the following manner, $W_i^{\mathcal{R}} \rightarrow G_i W_i^{\mathcal{R}} G_{\mathcal{R}(i)}^\dagger$. We thus see clearly, that the gauge restoring transformations $W_i^{\mathcal{R}}$ for the two Ansatz are the same up to an SU(2) gauge transformation and thus the two PSGs describe the same spin liquid.

The Invariant Gauge Group and Low energy dynamics

The PSG of an Ansatz has an extremely important subgroup which determines the nature of the low energy effective theory of the spin liquid and is called the invariant gauge group (IGG) [7, 8]. It is defined as the set of all *local* SU(2) gauge transformations which keep the Ansatz invariant, i.e., the set of all $W_i \in \text{SU}(2)$ such that,

$$\bar{U}_{ij} = W_i \bar{U}_{ij} W_j^\dagger \tag{2.29}$$

The above equation is clearly seen to be a special case of eqn. 2.27 when the lattice symmetry operation \mathcal{R} is just the identity \mathbb{I} . So, the subset of transformations of the full PSG satisfying eqn. 2.29 is $\{\mathbb{I}, W_i^{\mathbb{I}}\}$, which constitutes the IGG, and is a *normal* subgroup of the full PSG for the Ansatz \bar{U}_{ij} . We shall denote the IGG subgroup as \mathbb{W} and its elements as $W^{\mathbb{I}}$. From the way the IGG is defined above one will get the impression that its *just* a property of the mean field ground state and that it does not have any influence on what happens beyond mean field. On the contrary, the IGG completely determines the nature of the low energy effective theory of the spin liquid and hence enables us to answer all the key questions related to stability of spin liquids, symmetry group of the gauge field, deconfinement among others. We shall now elucidate precisely how this comes about. In the mean field Hamiltonian of eqn. 2.19, we can do two types of fluctuations about the mean field Ansatz \bar{U}_{ij} , the first are amplitude fluctuations (δU_{ij}) which are *massive* and cost an energy proportional to $\text{Tr}[\delta U_{ij}^\dagger \delta U_{ij}]$, hence we do not consider them. The other type of fluctuations are the pure phase fluctuations about \bar{U}_{ij} parameterized by a *real* ‘‘link’’ field A_{ij} , these are the important low energy fluctuations that we shall incorporate in going beyond mean field.

Let us first choose a mean field Ansatz \bar{U}_{ij} such that its IGG is the U(1) group, for the sake of simplicity in exposition. This means,

$$\bar{U}_{ij} = W_i^{\mathbb{I}} \bar{U}_{ij} W_j^{\mathbb{I}\dagger}, \quad \text{where } W_i^{\mathbb{I}} \in \text{U}(1) \tag{2.30}$$

henceforth, we shall drop the superscript \mathbb{I} in $W_i^{\mathbb{I}}$. A generic IGG element at site i is given by,

$$W_i = e^{i\theta_i \hat{\mathbf{n}}_i \cdot \hat{\boldsymbol{\sigma}}} \quad (2.31)$$

where, in general, at every site the axis about which the U(1) rotation by angle θ_i is done, points in different directions $\hat{\mathbf{n}}_i$. This unnecessary complicacy can always be removed by exploiting a SU(2) transformation, say Q_i which rotates the $\hat{\mathbf{n}}_i$ vectors at each site to the $\hat{\mathbf{z}}$ direction. That is, at every site we have,

$$Q_i W_i Q_i^\dagger = e^{i\theta_i \hat{\sigma}_3}, \quad \text{where } Q_i \in \text{SU}(2) \quad (2.32)$$

it is obvious that we must simultaneously change the mean field Ansatz \bar{U}_{ij} to account for the change in gauge. The new gauge rotated mean field Ansatz is,

$$\bar{U}'_{ij} = Q_i \bar{U}_{ij} Q_j^\dagger \quad (2.33)$$

we now do a phase fluctuation about the mean field Ansatz in the new gauge, this gives,

$$\tilde{U}'_{ij} = \bar{U}'_{ij} e^{iA_{ij} \hat{\sigma}_3} \quad (2.34)$$

where, the \tilde{U}'_{ij} is the fluctuated Ansatz. We shall now determine how the fluctuated Ansatz transforms under the IGG, effecting the gauge transformation we get,

$$\begin{aligned} e^{i\theta_i \hat{\sigma}_3} \tilde{U}'_{ij} e^{-i\theta_j \hat{\sigma}_3} &= e^{i\theta_i \hat{\sigma}_3} \bar{U}'_{ij} e^{iA_{ij} \hat{\sigma}_3} e^{-i\theta_j \hat{\sigma}_3} \\ &= e^{i\theta_i \hat{\sigma}_3} Q_i \bar{U}_{ij} Q_j^\dagger e^{iA_{ij} \hat{\sigma}_3} e^{-i\theta_j \hat{\sigma}_3} \\ &= Q_i e^{i\theta_i \hat{\sigma}_3} \bar{U}_{ij} Q_j^\dagger e^{iA_{ij} \hat{\sigma}_3} e^{-i\theta_j \hat{\sigma}_3} \\ &= Q_i \bar{U}_{ij} e^{i\theta_i \hat{\sigma}_3} Q_j^\dagger e^{iA_{ij} \hat{\sigma}_3} e^{-i\theta_j \hat{\sigma}_3} \\ &= Q_i \bar{U}_{ij} Q_j^\dagger e^{i\theta_i \hat{\sigma}_3} e^{iA_{ij} \hat{\sigma}_3} e^{-i\theta_j \hat{\sigma}_3} \\ &= \bar{U}'_{ij} e^{i\theta_i \hat{\sigma}_3} e^{iA_{ij} \hat{\sigma}_3} e^{-i\theta_j \hat{\sigma}_3} \\ &= \bar{U}'_{ij} e^{i(A_{ij} + \theta_i - \theta_j) \hat{\sigma}_3} \\ &= \bar{U}'_{ij} e^{i(A'_{ij}) \hat{\sigma}_3} \end{aligned} \quad (2.35)$$

where $A'_{ij} = A_{ij} + \theta_i - \theta_j$. Whence, we see that under an IGG transformation, the fluctuated Ansatz \tilde{U}'_{ij} just undergoes a phase shift, $\Delta\theta = \theta_i - \theta_j$. Thus, both describe the same physical spin liquid, and so the A_{ij} actually describes the gauge fluctuations.

Now, if we incorporate the phase (gauge) fluctuations in the zeroth order mean field Hamiltonian, eqn. 2.19, then it becomes,

$$\hat{\mathcal{H}}_{\text{MF}}^1 = \sum_{ij} \text{Tr}[\Phi_i^\dagger \bar{U}'_{ij} e^{iA_{ij} \hat{\sigma}_3} \Phi_j + \text{h.c.}] + \sum_i \text{Tr}[\Phi_i^\dagger (\bar{\mathbf{a}}_i \cdot \boldsymbol{\sigma}) \Phi_i] \quad (2.36)$$

under the action of the IGG, the $A_{ij} \rightarrow A_{ij} + \theta_i - \theta_j$. On the other hand, we also know that being in the low energy sector (much below the Mott-Hubbard gap), we have another *local* gauge symmetry, namely that of rotating the spinon operators at every site i , i.e., $\Phi_i \rightarrow e^{i\theta_i} \Phi_i$, this symmetry is a consequence of the constraint/conservation of one fermion per site [79]. Thus, we see that the Hamiltonian describing the low energy fluctuations is invariant under following combined gauge transformations,

$$A_{ij} \rightarrow A_{ij} + \theta_i - \theta_j, \quad \text{and} \quad \Phi_i \rightarrow e^{i\theta_i} \Phi_i \quad (2.37)$$

But, the above transformations are precisely those which keep invariant the Hamiltonian of a U(1) lattice gauge theory, and in fact eqn. 2.36 is precisely the Hamiltonian of a U(1) lattice gauge theory [7, 8, 79]. This implies, that the fluctuations of A_{ij} and \mathbf{a}_i are simply the fluctuations in the spatial and temporal components, respectively, of a U(1) lattice gauge field. Since, the fluctuations of a gauge field mediate the interactions between spinons, we see clearly that in first order beyond mean field the spinons are coupled via a fluctuating *compact* U(1) lattice gauge field.⁶ If we had chosen an Ansatz with a \mathbb{Z}_2 or SU(2) IGG, then beyond mean field the spinons would have been coupled by a fluctuating \mathbb{Z}_2 or SU(2) gauge field respectively, since we would have then obtained a \mathbb{Z}_2 or SU(2) lattice gauge theory Hamiltonian, by a similar construction as for U(1). In the above example, the fact that the interaction between the elementary particles (spinons) is described by a gauge theory automatically implies that the interaction takes place by the exchange of gauge bosons, which are the quanta of the fluctuations of the gauge field. In this case, since the gauge group is simply U(1), there is just one type of gauge boson, which is furthermore uncharged in contrast to SU(2) gauge bosons, in all three, all of which have a non-zero gauge charge. Furthermore, since considerations of gauge invariance require the gauge bosons to be massless, it implies that the interactions mediated by them between spinons are long ranged. Whence, the U(1) and SU(2) spin liquids are always in the confined phase⁷, and are marginally stable or unstable. The key to obtaining stable spin liquids with deconfined spinons is to give mass to the gauge boson via the Anderson-Higgs mechanism, i.e. with or even without using the Higgs boson. We shall discuss how this works, later in the text.

The reason why the IGG occupies a special status is now manifest. Although it is defined purely to be a property of a mean field Ansatz by eqn. 2.29, it remarkably turns out that the low energy effective theory controlling the dynamics of excitations has the same gauge group/structure, namely that of the IGG. Thus, the IGG can rightly be called as the “low energy” gauge group. One should contrast this with the high energy gauge group which we introduced earlier as being the gauge group of the fermionic partons⁸. The two gauge groups/structures have *absolutely nothing* to do with each other and should never be mixed up [7, 8]. For e.g. when we use the term, \mathbb{Z}_2 spin liquid, the “ \mathbb{Z}_2 ” here means the “low energy” gauge group (IGG). On the other hand, when we say \mathbb{Z}_2 slave boson approach, the \mathbb{Z}_2 here means the “high energy” gauge group. Similar interpretations hold when for the usage of U(1) and SU(2) gauge structures. It is *wrong* to think that a \mathbb{Z}_2 spin liquid is constructed from a \mathbb{Z}_2 slave boson approach. Any slave boson approach, be it \mathbb{Z}_2 , U(1), or SU(2) can be used to construct spin liquids with *any* low energy gauge structure⁹. For e.g., later we shall study the U(1) and \mathbb{Z}_2 spin liquids within a SU(2) slave boson formalism. In summary, the physical difference between the two gauge structures that are present can be put as follows;

⁶Strictly speaking, the lattice gauge field is *compact*, i.e. $A_{ij} \equiv A_{ij} + 2\pi$, this is the case in our treatment as seen from the way we have defined the link field as a phase. For a non-compact gauge field we would have an extra symmetry being introduced in the problem, which was not originally present [87]. The compactness of a gauge field is also intimately connected to problem of confinement [84].

⁷Mathematically speaking, the invariance of the energy (and action) under $A_{ij} \rightarrow A_{ij} + \theta_i - \theta_j$, i.e. $E(A_{ij}) = E(A_{ij} + \theta_i - \theta_j)$ is what is responsible for making the fluctuations of A_{ij} behave as gauge bosons [84].

⁸Precisely, the most general transformations between the partons which keeps the physical spin operator invariant.

⁹The low energy gauge structure can also be larger than the high energy gauge structure. This happens when the low energy excitations occur with several different finite crystal momenta. For each momenta we have a gauge field, the IGG for which contains site independent gauge transformations if one is at $\mathbf{q} = 0$, and site dependent gauge transformations if one is at $\mathbf{q} \neq 0$. e.g. SU(2)×SU(2) spin liquids in SU(2) slave boson approach [7, 8].

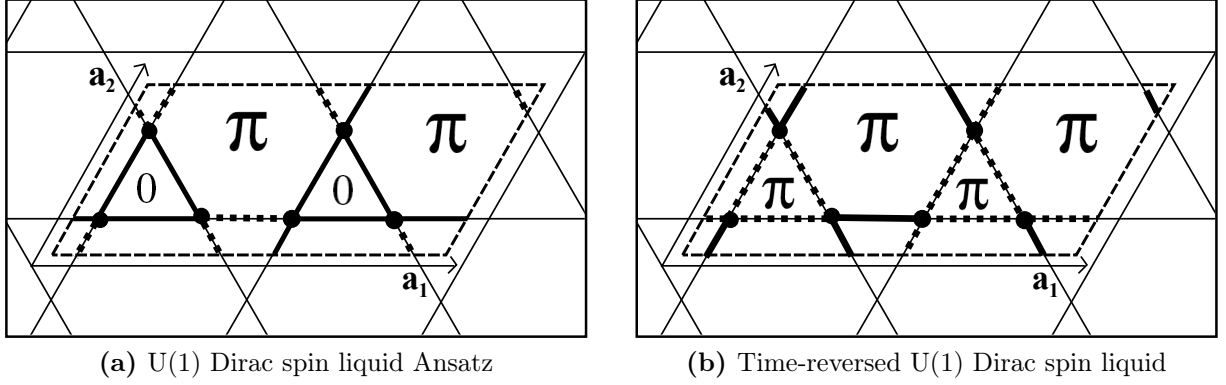


Figure 2.4: (a) The mean field Ansatz of the U(1) Dirac spin liquid in a particular gauge. The solid lines denote positive hoppings ($s_{ij} = +1$) and the dashed lines denote negative hoppings ($s_{ij} = -1$). The U(1) flux φ ($e^{i\varphi} = \prod_{\text{plaquette}} \chi_{ij}$) is zero through all triangles and π through all hexagons. Hence, the original geometrical 3 site unit cell has to be doubled to accommodate the fluxes. (b) The sign structure of hoppings and the corresponding flux pattern is shown for the time-reversed Ansatz of the U(1) Dirac spin liquid with respect to its (a) version.

the “low energy” gauge group/structure (IGG) reveal the internal quantum orders in the mean field ground state. On the other hand, the “high energy” gauge structure tells the way in which the spin Hamiltonian is expressed.

An example of a mean field Ansatz

To illustrate the concept of IGG and also the equivalence of two Ansätze upto a SU(2) gauge transformation, we shall take a concrete example, namely that of an algebraic spin liquid on the kagome lattice, called the U(1) Dirac spin liquid. At the mean field level, its defined to be the ground state of the following Hamiltonian [13],

$$\hat{\mathcal{H}}_{\text{MF}}^0 = \bar{\chi} \sum_{\langle ij \rangle} s_{ij} c_{j,\alpha}^\dagger c_{i,\alpha} + \text{h.c.} \quad (2.38)$$

here, $\langle ij \rangle$ denotes nearest neighbor bonds, we shall fix $\bar{\chi} = 1$ as the unit of hopping, and s_{ij} is ± 1 is distributed in the manner shown in Fig. 2.4a. The mean field Ansatz of such a spin liquid is conveniently expressed as $U_{ij} = \pm \sigma_3$. In Fig. 2.4b we have given another Ansatz which on the face of it looks different. A careful observation reveals that it is in fact obtained by simply flipping the sign of the Ansatz of Fig. 2.4a globally, i.e. $U_{ij} \rightarrow -U_{ij}$. Furthermore, this flip in sign turns out to be effected by a SU(2) gauge transformation, i.e. $(i\sigma_2)U_{ij}(-i\sigma_2) = -U_{ij}$. Hence, the gauge transformation is $W_i = i\sigma_2$, thus both Ansätze of Fig. 2.4 describe the same same spin liquid. It is worth noting that $U_{ij} \rightarrow -U_{ij}$ is in fact the time-reversal operation in the SU(2) slave-boson approach [7, 8]. Hence, the two Ansätze in Fig. 2.4 are related by a time-reversal symmetry, and since the U(1) Dirac spin liquid is time reversal invariant, they describe the same physical state, as they should.

From the form of the Ansatz, $U_{ij} = \pm \sigma_3$ we can explicitly obtain its IGG in the following manner. Plugging $U_{ij} = \pm \sigma_3$ into $U_{ij} = W_i U_{ij} W_j^\dagger$ and re-arranging we get, $W_j = \sigma_3 W_i \sigma_3$. If we now focus on say, a triangle on the kagome lattice and imagine its sites to be numbered 1, 2 and 3 counterclockwise, then $W_2 = \sigma_3 W_1 \sigma_3$ and then $W_3 = \sigma_3 W_2 \sigma_3$, implying that

$W_3 = W_1$. Finally, circulating once more, we get $W_1 = \sigma_3 W_3 \sigma_3$, implying $W_1 = \sigma_3 W_1 \sigma_3$, leading to $[W_1, \sigma_3] = 0$. Hence, $W \in U(1)$, and is the same for all i . This is why this spin liquid is called a “U(1)” algebraic spin liquid. For its *full* PSG, please see Ref. [91]. In the later chapters we shall be dealing extensively with the nature of this rather exotic spin liquid.

Mean field phase transitions between spin liquids

We will now give a general qualitative discussion of phase transitions between different spin liquids/quantum orders at the mean field level. First we recall some generic features of phase transitions of the second kind between classical orders. Such phase transitions always involve some *definite* change in symmetry of the body, so that at every moment the body has either one symmetry or the other, so we can always assign the body to one of the phases. Another extremely important and general feature is that the symmetry group of either one of the two phases should be a subset of the symmetry group of the other phase, this is a necessary condition for a phase transition to take place, but by no means is it sufficient. For e.g. if one is studying phase transitions between different crystal modifications, then a transition between a *rhombohedral* class to *tetragonal* class is forbidden. Also, at the transition point itself, the symmetry group of the body contains all the symmetry elements from both the phases on either side [3].

The mean field phase transitions between different *fully symmetric* spin liquids share the same generic features of classical transitions mentioned above. The symmetry group of the spin liquid is just its PSG. A phase transition between spin liquids thus involves a *definite* change in the PSG. Thus, at every moment we have one quantum order or the other, so that we can always associate the phase to one spin liquid or the other. A phase transition between two spin liquids will only take place, if the PSG of one spin liquid is a subgroup of the PSG of the other spin liquid¹⁰. For, e.g. a spin liquid with PSG_1 can undergo a phase transition to a spin liquid with PSG_2 if and only if, $PSG_1 \subset PSG_2$ or $PSG_2 \subset PSG_1$. Since, both PSG_1 and PSG_2 are the extensions of the *same* (lattice) symmetry group SG with different IGG 's, namely IGG_1 and IGG_2 , it automatically implies that these phase transitions *do not* change any physical symmetry, in that sense they are continuous in the lattice symmetry sector. Such exotic phase transitions are also present in the classical regime, the Berezinskii-Kosterlitz-Thouless transition [92–94] presents such a case where no symmetry breaking takes place across the transition point and the transition is thus continuous.

PSG beyond the mean field level

It is clear from the way we have introduced PSG's, that they describe quantum orders at the mean field level *only*, since PSG are mathematically defined to be the group of transformations that keep the mean field Ansatz unchanged. Based on PSG, the Ansatz can be grouped together into *classes* such that the Ansatz within each class have the same physical properties. Since, the PSG is a universal property these classes of Ansatz are just the universality classes, where each class corresponds to a particular quantum order. However, one may ask as to why we didn't directly classify (group into universality classes) the *projected* physical spin many body wave functions which represent the real quantum

¹⁰To study these mean field phase transitions one can construct Landau-Ginzburg free energy functionals, just as we do for classical phases, but now these functionals should be invariant under the full PSG, and not just the lattice symmetry group as is done for studying classical phase transitions

phases?. The answer to this question is very simple and honest, we simply don't know till present *any* way/property/structure on the basis of which we can group together projected wave function into classes such that when going from a wave function of one class to another we encounter a singularity in the ground state energy [7, 8]. Intuitively this is because in general correlated many body wave functions are a complete “mess” and trying to group them together into classes by simply “looking” at them is near impossible¹¹.

That is why we are only able to classify those many body (projected real physical spin) wave functions which can be obtained from an Ansatz¹². Then, we simply classify the Ansatz, which we know how to do based on PSG. The important link still missing is, how are we sure that the PSG would also hold beyond mean field or in other words would the PSG still classify the real quantum spin phases after quantum fluctuations (which are in general strong) have been incorporated?. The thumb rule is that if the mean field state is stable against quantum fluctuations, i.e. there is no phase transition, then the PSG classification can safely be extended beyond mean field, and it will classify the real spin liquids¹³ [7, 8]. This is a consequence of the fact that fluctuations ($\delta\bar{U}_{ij}$) in the Ansatz (\bar{U}_{ij}) at the perturbative level have the same PSG as the Ansatz itself, and hence cannot change the symmetries and the low energy gauge structure of the spin liquid. For, e.g. they cannot drive a phase transition from a *fully symmetric* spin liquid into a *chiral* spin liquid, and similarly cannot drive a *fully symmetric* U(1) gapless spin liquid into a *fully symmetric* gapped \mathbb{Z}_2 spin liquid, the former would involve breaking of time-reversal symmetry and parity, and the latter would involve breaking the IGG from U(1) to \mathbb{Z}_2 . This symmetry preserving property under perturbations is what makes the PSG a property also of a real quantum spin liquid. This property can sometimes lead to dramatic consequences, whereby certain *mass* terms are actually generated by these perturbative fluctuations, but none of them is invariant under the PSG and thus are forbidden, and the system remains gapless. Such spin liquids are thus very delicately balanced, and owe their existence to the PSG (quantum orders) which “protects” them, examples of which are algebraic spin liquids. Thus, we see that PSG of a particular quantum order protects gapless excitations (both gauge bosons and fermions) even in the absence of any symmetry breaking![7, 8]. Thus, the very existence of algebraic spin liquids points towards the fact that quantum orders do “really” exist.

Recipe for obtaining stable spin liquids and the concept of SU(2) flux

We know that beyond the mean field approximation, the interactions between spinons is mediated via *massless* gauge bosons which implies that that the interactions are long ranged and that the spinons are confined, this gives rise to either marginally stable or unstable spin liquids. The corresponding gauge group of such gauge bosons is either U(1) or SU(2), which is in fact the IGG for the mean field Ansatz. In order to obtain stable spin liquids we need to find those mean field Ansatz, whose fluctuations (gauge bosons) are *massive*. In such

¹¹A possible way out will be provided by performing some mathematical transform on the real space spin wave function, so that some universal property becomes visible. e.g. This is precisely how one groups free-fermion wave functions into classes, by performing a Fourier transform on the real space Slater determinant and then observing that the Fermi surface topology provides a universal basis on which to group free fermion wave functions. Well, for spin wave function we still don't know the appropriate transform.

¹²There exist many spin liquids for which the projected physical spin wave function *cannot* be obtained from an Ansatz, these correspond to some “algebraic” PSG's. We are restricting ourselves only to the subgroup of algebraic PSG called as “invariant” PSGs.

¹³The PSG classification can also hold for some marginally stable spin liquids, but then it depends case to case and one cannot make such sweeping statements.

spin liquids, the gapped nature of the gauge bosons will ensure that they mediate only short range interactions between the spinons, which implies free or deconfined spinons, and thus such spin liquids are bound to be stable. In other words, such spin liquids will “survive” Gutzwiller projection. However, the procedure to construct such stable Ansätze depends on whether the one wants to give mass to U(1) gauge bosons or SU(2) gauge bosons. We shall now take up the first case, namely of U(1) gauge bosons.

If the mean field Ansatz of the spin liquid has an IGG which is U(1), then the low energy effective theory is given by a compact U(1) lattice gauge theory with gapless U(1) gauge bosons which *do not* carry any gauge charge. However, in order to make the U(1) gauge bosons massive we have to invoke the Anderson-Higgs mechanism which in fact requires charged bosons, which we don’t have. But, on the other hand we do have charged fermions (spinons), so we can cook charged bosons by pairing up the spinons. This is achieved by the fermion pair condensation term ($\bar{\Delta}_{ij}$) in the mean field Hamiltonian of eqn. 2.23 [7, 8]. The U(1) chargeless gauge bosons then couple to these charged bosons (condensed) and become massive, and are thus able to mediate only short range interactions between the spinons. So, we see that if an Ansatz contains only spinon hopping amplitudes ($\bar{\chi}_{ij}$) then the gauge bosons are gapless and if the Ansatz is made to include $\bar{\Delta}_{ij}$ pairing term then there will be *no* gapless gauge bosons, and we expect that such an Ansatz will describe a stable spin liquid.

If the mean field Ansatz of the spin liquid has an IGG which is SU(2), then the low energy effective theory is given by a SU(2) lattice gauge theory with three species of gapless SU(2) gauge bosons, which in contrast to U(1) gauge bosons, are charged. So, we do not need to cook up additional charged bosons in order to invoke the Anderson-Higgs mechanism, which can surprisingly enough be realized without Higgs boson, and just requires the condensation of non-abelian gauge fluxes. We shall only give some qualitative analysis and important conclusions. The relevant quantity we need to look at, is the SU(2) flux for a given mean field Ansatz, which is defined for a closed loop on the lattice, with a given fixed base point i . It is defined in the following manner[7, 8],

$$P(C_i) = \bar{U}_{ij}\bar{U}_{jk}\bar{U}_{kl}\dots\bar{U}_{li} \quad (2.39)$$

from the above definition we see that the SU(2) can always be written as a linear combination of the Pauli matrices and the identity, in the following manner,

$$P(C_i) = m_0\sigma_0 + \sum_{\alpha} m_{\alpha}\sigma_{\alpha} \quad (2.40)$$

whence, we can always associate a sense of direction to the SU(2) flux, except in the trivial case when all $m_{\alpha} = 0$. Also, under local SU(2) gauge transformations the flux transforms as,

$$P(C_i) \rightarrow W_i P(C_i) W_i^{\dagger} \quad (2.41)$$

from the above observation it follows that it is meaningless to compare directions of SU(2) fluxes for loops with different base points, since the local SU(2) gauge transformations can be used to change the directions of SU(2) fluxes for loops with different base points, independently. On the other hand, comparison of SU(2) flux directions for loops with the *same* base point is quite useful. Broadly we can divide the Ansätze into three classes, (i) Those with SU(2) fluxes through all loops being proportional to the identity, (ii) Those with *collinear* SU(2) fluxes through all loops, and (iii) Those with *non-collinear* SU(2) fluxes.

In case (i), one has SU(2) gapless spin liquids which are marginally stable or unstable and the SU(2) gauge structure remains intact. In case (ii), one has U(1) gapless spin liquids which are again either marginally stable or unstable and the SU(2) gauge structure is broken down to U(1)¹⁴. In case (iii), one obtains \mathbb{Z}_2 spin liquids which are always stable, this is because for non-collinear fluxes all three SU(2) gauge bosons become massive and the gauge field is thus *fully* gapped. The SU(2) gauge structure in this case, is directly broken down from SU(2) to \mathbb{Z}_2 , since the ansatz for such a spin liquid is invariant only under the trivial transformation $W_i = \pm\mathbb{I}$ because of the presence of off-diagonal $\bar{\Delta}_{ij}$ terms in the mean field Ansatz \bar{U}_{ij} . Thus, we finally see that the key to obtaining stable spin liquids is to construct Ansatz with IGG being \mathbb{Z}_2 so that we have non-commuting SU(2) fluxes for different plaquettes corresponding to the same base point¹⁵, see Ref. [7, 8] for details.

¹⁴Two out of the three gauge bosons acquire mass terms and the third (A_{ij}^z) remains gapless, thus, giving rise to a U(1) gapless spin liquid.

¹⁵The \mathbb{Z}_2 lattice gauge field is always gapped, thus even if the spinons are gapless, the corresponding spin liquid is a stable one. Thus both gapped (spinon) and gapless (spinon) \mathbb{Z}_2 spin liquids are stable and can thus occur as real physical spin liquids.

Chapter 3

Numerical methods

3.1 The quantum variational Monte Carlo method

One of the fundamental tasks of quantum mechanics is the calculation of average/expectation values of operators, and also equally important is the calculation of matrix elements. If the quantum system is a *many-body* one then the above mentioned quantities can not be computed by hand. This is because of the impossibility of factorizing a strongly correlated quantum many body wave function into a single particle wave functions. Therefore, the task of computing such quantities in quantum many body systems is the job of Monte Carlo methods which exploit stochastic sampling to evaluate these quantities which are integrals over a multi-dimensional space.

As is well known that a Monte Carlo method is based on the Metropolis algorithm which generates a random walk in the configuration space, this chain of configurations is called a Markov chain. The sampling of configurations during the random walk is done according to a given time-independent probability distribution, and upon equilibration after a certain number of steps, the configurations are distributed according to the same probability distribution. The Variational quantum Monte Carlo approach simply applies this methodology to probability distributions which are the square of the modulus of quantum many body trial wave functions. Thus, by computing different observables of such wave functions one can finally extract out the nature of the quantum state. It is also worth mentioning that within this scheme it is also possible to optimize trial wave functions in order to obtain the lowest variational energy. The various intricacies of implementing these schemes so as to have an efficient algorithm are presented in the ensuing text.

3.1.1 The quantum Metropolis algorithm

We take as our wave function, the Gutzwiller projected state (Ψ) whose squared modulus serves as a probability distribution function in the sampling. We shall now describe how to compute expectation values, which, as is known, involve integrals bilinear in Ψ and Ψ^* .

In the variational quantum Monte Carlo method, the first step is to choose the starting point configuration of the *to be* random walk. This amounts to randomly choosing for $t = 0$, the coordinates x_i for all the particles $i = 1, 2, 3, \dots N$ on the lattice. We have to of course avoid choosing those configurations of electrons, for which $|\Psi(x)|^2 = 0$. We denote this configuration as $\{x_i\}_0$. We then propose a new trial configuration $\{x_i\}_0^T$ by permuting two electrons. Based on the Metropolis algorithm the Markov chain is constructed in the following manner. Generically, if we are at the n th point (configuration) $\{x_i\}_n$ of the

Markov chain and we propose a move to a new trial configuration $\{x_i\}_n^T$. Then, this new configuration is accepted (i.e., $\{x_i\}_{n+1} = \{x_i\}_n^T$) with a probability which is equal to,

$$\mathcal{P} = \text{Min}[1, \mathcal{R}] \quad \text{where} \quad \mathcal{R} = \left| \frac{\Psi(\{x_i\}_n^T)}{\Psi(\{x_i\}_n)} \right|^2 \quad (3.1)$$

subsequently we generate a random number ϵ such that $0 < \epsilon \leq 1$. If it turns out that $\mathcal{R} \geq \epsilon$ then we accept the move that was proposed, i.e., $\{x_i\}_{n+1} = \{x_i\}_n^T$ otherwise we reject it, i.e. $\{x_i\}_{n+1} = \{x_i\}_n$, and stay where we were. In order to compute \mathcal{R} we need to evaluate two Slater determinants, if one deals with a fermionic system. The ratio of two determinants can be computed with $\mathcal{O}(1)$ cost. The cost of updating scales as $\mathcal{O}(N^2)$, this fact is made possible because the new configuration differs from the old one by just a single permutation of particles and thus, the computation of the ratio of two determinants can be reduced to just computing a single matrix element. It is worth noting that we do not need to have a knowledge of the normalization constant of the wave functions, since only the ratio's of the wave functions enter into the computations. Also, we mention that the configurations $\{x_i\}_n$ in the Markov chain are independent of the starting point $\{x_i\}_0$ if thermalization has been achieved, i.e. after a ‘‘sufficient’’ number of steps and are distributed according to $|\Psi(\{x_i\})|^2$, upto a normalization factor.

The construction of the Markov chain with a given probability distribution enables one to calculate the expectation values of any operator \hat{A} in that state. This is effected by simply taking the average over the values taken by \hat{A} along the Markov chain configurations, and for a sufficiently large Markov chain the central limit theorem ensures that the average over the chain tends to the true expectation value of the observable. That is,

$$\langle \hat{A} \rangle = \lim_{L \rightarrow \infty} \frac{1}{L} \sum_{n=1}^L \hat{A}(\{x_i\}_n) \quad (3.2)$$

where $\hat{A}(\{x_i\}_n)$ is the value of the observable \hat{A} corresponding to the configuration $\{x_i\}_n$. However, since in any finite time we can sample only a finite number of configurations leads to the appearance of a statistical error which is computed from the variance,

$$\sigma^2(\bar{\hat{A}}) = \langle (\bar{\hat{A}} - \langle \hat{A} \rangle)^2 \rangle \quad (3.3)$$

then from statistical considerations it is easy to show that the statistical error $\sqrt{(\sigma^2(\bar{\hat{A}}))}$ scales inversely with the square root of the length L of the Markov chain, and directly with the *auto-correlation* time, i.e., the number of steps in the Markov chain which separate two statistically independent configurations. Thus, it is better to compute expectation values over uncorrelated samplings, which is done using the ‘‘binning’’ technique, as described below. Whence, the average values obtained from the Monte Carlo are extremely good estimates of the true expectation values for a large number of samplings.

In the ‘‘binning’’ technique, one first takes the average of the operator \hat{A} over some fixed number of configurations L_{bin} where $L_{\text{bin}} = L/N_{\text{bins}}$. Thus, we compute the average of eqn. 3.2 for a bin, as follows

$$\bar{\hat{A}}_{\text{bin}} = \frac{1}{L_{\text{bin}}} \sum_{n=1}^{L_{\text{bin}}} \hat{A}(\{x_i\}_n) \quad (3.4)$$

subsequently we average over the *binned* expectation values, as follows,

$$\bar{\hat{A}} = \frac{1}{N_{\text{bins}}} \sum_{n=1}^{N_{\text{bins}}} (\bar{\hat{A}}_{\text{bin}})_n \quad (3.5)$$

thus, we see manifestly the advantage of the binning procedure. Firstly, the autocorrelation time is now of the order of unity and thus $\bar{\hat{A}} = \langle \hat{A} \rangle$ which simply illustrates the fact that $\bar{\hat{A}}_{\text{bin}}$ are less correlated compared to $\hat{A}(\{x_i\}_n)$. The expression for the variance then takes the following form,

$$\sigma^2(\hat{A}) = \frac{1}{(N_{\text{bins}} - 1)} \sum_{n=1}^{N_{\text{bins}}} ((\bar{\hat{A}}_{\text{bin}})_n - \langle \hat{A} \rangle)^2 \quad (3.6)$$

3.1.2 The wave function optimization algorithm

The task of the algorithm is to tune the variational wave function $\Psi_{\{\alpha_k\}}(x)$ in a manner which minimizes the expectation value of the energy, given by,

$$E(\Psi) = \frac{\langle \Psi | \hat{\mathcal{H}} | \Psi \rangle}{\langle \Psi | \Psi \rangle} \quad (3.7)$$

for later use it is worth re-casting the above expression for the energy into the following form,

$$\begin{aligned} E(\Psi) &= \frac{\langle \Psi | \hat{\mathcal{H}} | \Psi \rangle}{\langle \Psi | \Psi \rangle} \\ &= \frac{\sum_x \langle \Psi | x \rangle \langle x | \hat{\mathcal{H}} | \Psi \rangle}{\sum_x \langle \Psi | x \rangle \langle x | \Psi \rangle} \\ &= \frac{\sum_x |\Psi(x)|^2 \frac{\langle x | \hat{\mathcal{H}} | \Psi \rangle}{\langle x | \Psi \rangle}}{\sum_x |\Psi(x)|^2} \\ &= \frac{\sum_x |\Psi(x)|^2 e_L(x)}{\sum_x |\Psi(x)|^2} \geq E_0 \end{aligned} \quad (3.8)$$

where E_0 is the ground state energy. The object $e_L(x)$ is called the *local* energy of the given configuration $\{x_i\}$ (henceforth denoted as $|x\rangle$ for convenience of exposition). The above last relation is extremely important and shows that the expectation value of the Hamiltonian in a given state can be evaluated as the weighted average of the local energy $e_L(x)$ computed over all possible configurations $|x\rangle$, with the weights given by the squared modulus of the wave function. This can be implemented stochastically by averaging the local energy over the Markov chain points, generated according to $|\Psi(x)|^2$.

$$E(\Psi) = \lim_{L \rightarrow \infty} \frac{1}{L} \sum_{n=1}^L e_L(x_n) \quad (3.9)$$

The way in which the variational parameters $\{\alpha_k\}$ in the wave function will be tuned so as to reach an energy minima in a stable and optimum way will now be described, as given in [16, 17]. It is worth noting that these variational parameters can also belong to the *correlation* terms in the wave function, in addition to the Slater determinant.

If we do an infinitesimal change in the variational parameters, then $\{\alpha_k\} \rightarrow \{\alpha'_k\} = \{\alpha_k\} + \{\delta\alpha_k\}$. To linear order, the corresponding change in the wave function reads as,

$$\Psi_{\{\alpha'_k\}}(x) = \Psi_{\{\alpha_k\}}(x) \left[1 + \sum_{k=1}^p O_k(x) \delta\alpha_k \right] \quad (3.10)$$

where $O_k(x)$ is the logarithmic derivative of the wave function $\Psi_{\{\alpha_k\}}(x)$, given by,

$$O_k(x) = \frac{\partial}{\partial\alpha_k} \ln \Psi_{\{\alpha_k\}}(x) \quad (3.11)$$

this derivative has to be evaluated numerically for each of the variational parameters α_k ($k = 1, 2, 3 \dots, p$) and for each of the configurations $|x\rangle$ of the Markov chain¹. One can further simplify the writing of eqn. 3.10 by formally introducing an operator \hat{O}_k corresponding to $O_k(x)$ defined in the following manner,

$$\langle x | \hat{O}_k | x' \rangle = O_k(x) \delta_{xx'} \quad (3.12)$$

in terms of this operator eqn. 3.10 takes the following form,

$$|\Psi_{\{\alpha'_k\}}\rangle = \left[1 + \sum_{k=1}^p \delta\alpha_k \hat{O}_k \right] |\Psi_{\{\alpha_k\}}\rangle \quad (3.13)$$

The usefulness of computing $O_k(x)$ and $e_L(x)$ is that the derivatives of the energy w.r.t the variational parameters (called *generalized forces*) are completely determined in terms of $O_k(x)$ and $e_L(x)$. These generalized forces determine how the variational parameters change iteratively in such a manner so as to minimize the variational energy. We shall now show this explicitly. The generalized forces f_k are expressed as,

$$\begin{aligned} f_k &= -\frac{\partial E(\Psi_{\{\alpha_k\}})}{\partial\alpha_k} \\ &= -\frac{\langle \Psi_{\{\alpha_k\}} | [\hat{O}_k \hat{\mathcal{H}} + \hat{\mathcal{H}} \hat{O}_k] | \Psi_{\{\alpha_k\}} \rangle}{\langle \Psi_{\{\alpha_k\}} | \Psi_{\{\alpha_k\}} \rangle} + 2E(\Psi_{\{\alpha_k\}}) \frac{\langle \Psi_{\{\alpha_k\}} | \hat{O}_k | \Psi_{\{\alpha_k\}} \rangle}{\langle \Psi_{\{\alpha_k\}} | \Psi_{\{\alpha_k\}} \rangle} \\ &= -\frac{2}{L} \sum_{n=1}^L \hat{O}_k(x_n) e_L(x_n) + 2\bar{\bar{O}}_k \bar{e}_L \end{aligned} \quad (3.14)$$

where \bar{e}_L and $\bar{\bar{O}}_k$ are given by,

$$\begin{aligned} \bar{e}_L &= \frac{1}{L} \sum_{n=1}^L e_L(x_n) \\ \bar{\bar{O}}_k &= \frac{1}{L} \sum_{n=1}^L \hat{O}_k(x_n) \end{aligned} \quad (3.15)$$

¹To evaluate $O_k(x)$, one first needs to calculate $|\Psi_{\{\alpha_k + \delta\alpha_k\}}\rangle$ using perturbation theory on $\hat{\mathcal{H}}_{\text{MF}}$. Subsequently, we determine $\Psi_{\{\alpha_k + \delta\alpha_k\}}(x)$ from which $O_k(x)$ can be computed. Such a route is required because the variational parameters $\{\alpha_k\}$ are explicitly defined in the Hamiltonian but only implicitly present in the variational wave function

thus we see explicitly that once we stochastically compute $e_L(x)$ and $O_k(x)$ for a Markov chain, then we can compute f_k in a straightforward manner. Now, all we need to show is that convergence to an energy minimum is achieved upon iteratively changing the variational parameters $\{\alpha_k\}$. The difference in the energy $E(\Psi)$ to linear order is expressed as follows,

$$\begin{aligned}\Delta E &= E(\Psi_{\{\alpha'_k\}}) - E(\Psi_{\{\alpha_k\}}) \\ &= - \sum_{k=1}^p f_k \delta \alpha_k\end{aligned}\quad (3.16)$$

now if $\delta \alpha_k$ is small enough it can be written as $f_k \delta t$, where $\delta t > 0$ and is determined within the minimization method at each iteration step. Thus, the above expression can be re-cast as,

$$\Delta E = - \sum_{k=1}^p f_k^2 \delta t \quad (3.17)$$

thus, we see transparently that the change in energy is negative at each iteration and convergence to the energy minimum is achieved when all $f_k = 0$. This forms the content of the method of steepest descent. An important point to note is that the ‘‘distance’’ between the two sets of variational parameters, $\{\alpha_k\}$ and $\{\alpha'_k\}$ is measured via their squared Cartesian distance in the parameter space of p dimensions. That is,

$$\Delta \alpha^{\text{SD}} = \sum_{k=1}^p (\alpha'_k - \alpha_k)^2 \quad (3.18)$$

however, this way of measuring distance between iterations is not the only choice possible. In fact, there are various other better choices possible which lead to convergence to an energy minima in a much more controlled manner compared to the standard steepest descent method. We describe below one such possibility.

The small change in variational parameters $\delta \alpha_k$ can, in general be written as,

$$\delta \alpha_k = \sum_{m=1}^p s_{km}^{-1} f_m \delta t \quad (3.19)$$

the matrix s_{km} should be positive definite, with this condition satisfied it is trivial to show that convergence to an energy minimum will be achieved, since the change in energy at each iteration can now be expressed as,

$$\Delta E = - \sum_{k=1}^p \sum_{m=1}^p s_{km}^{-1} f_k f_m \delta t \quad (3.20)$$

where δt is positive constant at each iteration. Whence, ΔE is always negative, until the energy minima is reached, i.e. all $f_k = 0$. From the above considerations it is also clear that the steepest descent method forms a special case when the matrix $s = \mathbb{I}$, the unit matrix. Our choice of the matrix s is the following,

$$s_{mk} = \frac{\langle \Psi_{\{\alpha_k\}} | \hat{O}_m \hat{O}_k | \Psi_{\{\alpha_k\}} \rangle}{\langle \Psi_{\{\alpha_k\}} | \Psi_{\{\alpha_k\}} \rangle} - \frac{\langle \Psi_{\{\alpha_k\}} | \hat{O}_m | \Psi_{\{\alpha_k\}} \rangle \langle \Psi_{\{\alpha_k\}} | \hat{O}_k | \Psi_{\{\alpha_k\}} \rangle}{\langle \Psi_{\{\alpha_k\}} | \Psi_{\{\alpha_k\}} \rangle \langle \Psi_{\{\alpha_k\}} | \Psi_{\{\alpha_k\}} \rangle} \quad (3.21)$$

thus, we see that once we have computed stochastically the $O_k(x)$ for the set of configurations along the Markov chain (as described before), the matrix s_{mk} can be computed at once in an efficient manner. This is also transparently seen if one re-casts the above expression for s_{mk} in the following manner,

$$s_{mk} = \frac{1}{L} \sum_{n=1}^L [O_m(x_n) - \bar{O}_m][O_k(x_n) - \bar{O}_k] \quad (3.22)$$

the above expression for s_{mk} also shows that if we associate $O_m(x_n) - \bar{O}_m$ to a vector in the L dimensional space, then the matrix s_{mk} is just an overlap matrix and is always positive regardless of the nature of the Markov chain. When one uses the above choice of the matrix for optimization, then the method is called ‘‘stochastic reconfiguration optimization’’ method.

Within the stochastic reconfiguration optimization method, the squared distance between the variational parameters $\{\alpha_k\}$ and $\{\alpha'_k\}$ for two consecutive iterations is measured via the corresponding normalized wave functions, instead being directly measured in the variational parameter space as in eqn. 3.18 for the steepest descent method. Thus we have,

$$\Delta\alpha^{\text{SR}} = 2 - 2 \frac{\langle \Psi_{\{\alpha_k\}} | \Psi_{\{\alpha'_k\}} \rangle}{\sqrt{\langle \Psi_{\{\alpha_k\}} | \Psi_{\{\alpha_k\}} \rangle \langle \Psi_{\{\alpha'_k\}} | \Psi_{\{\alpha'_k\}} \rangle}} \quad (3.23)$$

such a scheme of distance measurement has the obvious advantage that it captures the cases when during optimization a small change in the variational parameters leads to a large change in the wave function and vice versa when a large change in the variational parameters only leads to a small change in the wave function. Thus, this new definition of distance is more sensitive and leads to a more accurate determination of the variational parameters². Also, it is interesting to note that $\Delta\alpha^{\text{SR}}$ can be expressed in terms of the s matrix elements in the following manner,

$$\Delta\alpha^{\text{SR}} = \sum_{k=1}^p \sum_{m=1}^p s_{km} (\alpha'_k - \alpha_k) (\alpha'_m - \alpha_m) \quad (3.24)$$

hence, once we have computed the s matrix as mentioned before, the $\Delta\alpha^{\text{SR}}$ can be determined. All the results on optimization, in the current thesis have been obtained using this stochastic reconfiguration optimization method.

To highlight the advantage of this scheme over the steepest descent, we shall now present the results of a case study on the spin-1/2 quantum Heisenberg antiferromagnet on the kagomé lattice of 432 sites, using stochastic reconfiguration optimization. The variational wave function is chosen to be that of a particular \mathbb{Z}_2 spin liquid on the kagomé lattice, and is labelled by five *real* variational parameters. These are the 1st NN real hopping (χ_1), 2nd NN real hopping (χ_2), 2nd NN real spinon pairing (Δ_2), and two onsite terms, one for the chemical potential μ and the other for the real onsite pairing ζ_{R} . After fixing $\chi_1 = 1$, the variational wave functions can symbolically be written as $|\Psi_{\text{VMC}}(\chi_2, \Delta_2, \mu, \zeta_{\text{R}})\rangle$. For a generic unbiased starting point in the four-dimensional variational space, the variation of parameters and energy in the stochastic reconfiguration optimization is shown in Fig. 3.1.

²In other words, this feature is possible because the changes in parameters $\{\delta\alpha_k\}$ are related not only to energy differences and generalized forces but also on the s matrix.

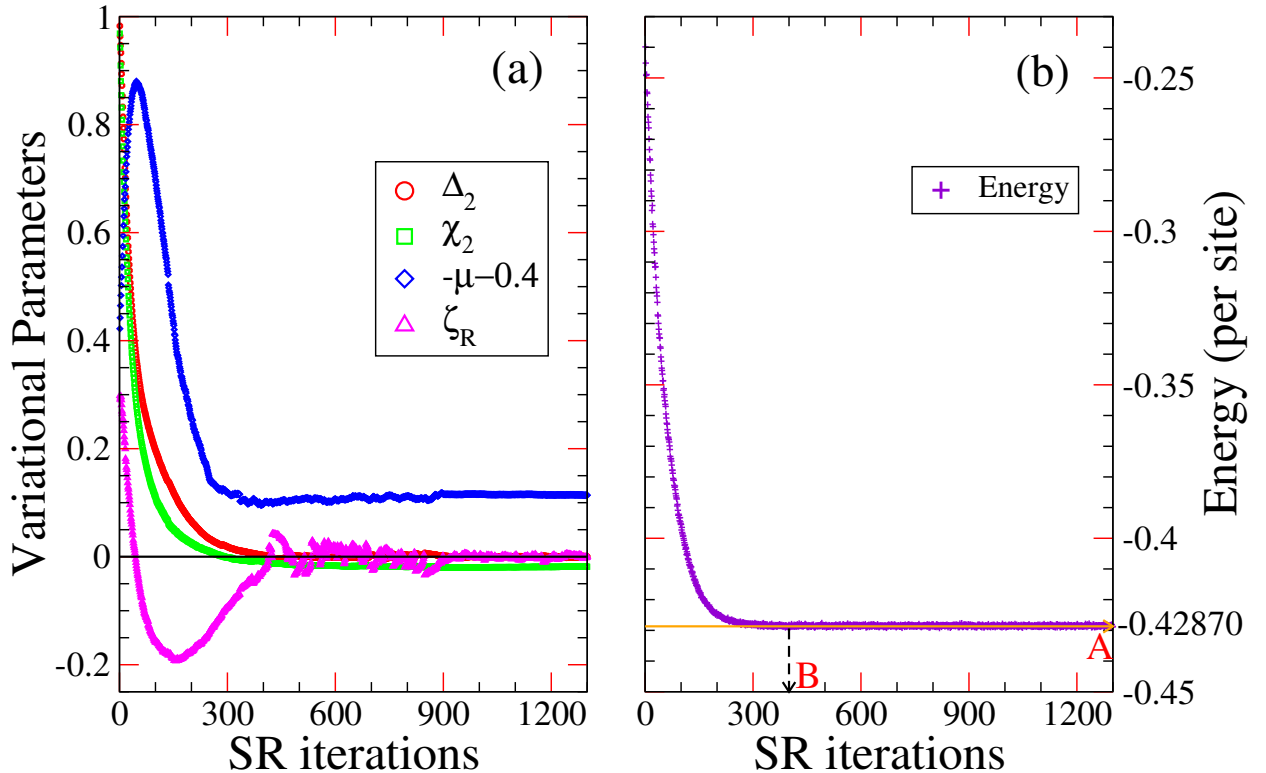


Figure 3.1: A typical variational Monte Carlo stochastic reconfiguration optimization run for the \mathbb{Z}_2 spin liquid wave function: (a) variational parameters Δ_2 , χ_2 , μ , and ζ_R and (b) energy, as a function of stochastic reconfiguration iterations. In (a), the initialized parameter values are: $\Delta_2 = \chi_2 = 1$, $\mu = -0.8$, and $\zeta_R = 0.3$. The \mathbb{Z}_2 spin liquid wave function optimizes to that of the U(1) 2nd NN Dirac spin liquid which corresponds to $\Delta_2 = 0$, $\chi_2 = -0.0186(2)$, $\zeta_R = 0$. The final optimized parameter values are then obtained by averaging over a much larger number of converged iterations than shown above.

Here, we bring attention to the important fact that, despite the energy having converged after about 400 iterations (see point B in Fig. 3.1(b)), the parameters did not converge and were still varying, converging to their final values much later than the energy. This fact is possible because, as we mentioned before, in the energy minimization forces are calculated through correlated sampling and not just by energy differences. Thus, in general whenever the energy landscape is relatively flat and many competing phases occur in a narrow width of energy, the optimization using stochastic reconfiguration becomes indispensable in order to arrive at unambiguous conclusions.

3.1.3 Green function Monte Carlo

A problem of utmost importance is that of extracting the ground state $|\Phi_0\rangle$ of a particular Hamiltonian \mathcal{H} , from a variational trial wave function $|\Psi_{\text{trial}}\rangle$, provided these two have a finite overlap, i.e., $\langle\Phi_0|\Psi_{\text{trial}}\rangle \neq 0$. This can be achieved by using the power method, which consists of iteratively applying the operator $G = \Lambda - \mathcal{H}$ to the trial wave function, in the following manner,

$$G^n|\Psi_{\text{trial}}\rangle = (\Lambda - E_0)^n \left\{ a_0|\Phi_0\rangle + \sum_{i \neq 0} \left(\frac{\Lambda - E_i}{\Lambda - E_0} \right)^n a_i|\Phi_i\rangle \right\} \quad (3.25)$$

here, the E_i and $|\Phi_i\rangle$ are the eigenvalues and eigenvectors of \mathcal{H} respectively, and the $a_i = \langle \Phi_i | \Psi_{\text{trial}} \rangle$. Λ is a constant chosen in a way so as to allow convergence to the ground state. Whence, it follows from the above definition that,

$$\lim_{n \rightarrow \infty} G^n |\Psi_{\text{trial}}\rangle \approx |\Phi_0\rangle \quad (3.26)$$

thus, the convergence to the true ground state of the Hamiltonian \mathcal{H} is guaranteed by this procedure, when $n \rightarrow \infty$. However, an *exact* brute force evaluation of these iterative recursion relations proves to be impossible, especially on large clusters. This is because the application of G generates transitions to a very large number of different states even after just a few applications, thus costing a huge amount of memory. The way to go about is to use a stochastic technique to implement the power method, this is the essence of the Green function Monte Carlo method [95].

We first define the electron spin configuration on the lattice, i.e., the basis $|x\rangle$ and then iteratively apply the operator $G_{x'x}$, for which a single iteration on $\Psi_n(x)$ yields,

$$\Psi_{n+1}(x') = \sum_x G_{x'x} \Psi_n(x). \quad (3.27)$$

The key step is to stochastically evaluate using Markov process, the matrix vector product in eqn. 3.27.

It so turns out that for an efficient implementation it is convenient to deal not with the original symmetric matrix G , but rather with the following non-symmetric one [96],

$$\bar{G}_{x'x} = \frac{\Psi_G(x')}{\Psi_G(x)} G_{x'x} \quad (3.28)$$

where, $\Psi_G(x)$ is called the *guiding* wave function which should be chosen such that it can be implemented efficiently in the calculation of matrix elements in eqn. 3.27, and should be as close as possible to the ground state of G . The simplest wave function satisfying these criteria should be chosen. Furthermore, if $\Phi_i(x)$ is an eigenvector of G with eigenvalue E_i , then it is easy to show that $\Psi_G(x)\Phi_i(x)$ is an eigenvector of \bar{G} with the same eigenvalue. Thus, G and \bar{G} are iso-spectral. The advantage of using \bar{G} instead of G is seen if we write the expression of the local energy E_x ,

$$E_x = \sum_{x'} \frac{\Psi_G(x')}{\Psi_G(x)} \mathcal{H}_{x'x} = \sum_{x'} \bar{\mathcal{H}}_{x'x} \quad (3.29)$$

thus we see clearly that if $\Psi_G(x)$ is exactly equal to the ground state of \mathcal{H} then $E_x = E_0$ and hence the LHS of the above expression is independent of x . Herein lies the power of the method, namely that, if the guiding wave function approaches an exact eigenstate of \mathcal{H} , the method is essentially free of statistical fluctuations, this is called as the *zero-variance* property. Finally, after having expounded the advantage of working with \bar{G} , we can write the recursion relation of eqn. 3.27 in terms of \bar{G} as,

$$\Psi_{n+1}(x') \Psi_G(x') = \sum_x \bar{G}_{x'x} \Psi_n(x) \Psi_G(x) \quad (3.30)$$

The fixed-node approximation

We mentioned previously that the recursive relation in eqn. 3.27 has to be evaluated stochastically, and that the operator G generates transitions to a number of states which scale as

$\mathcal{O}(N)$. A feature of this calculation is that there are always some walkers whose weights are *not* positive, although this does not hinder the determination of the transition probability of the stochastic process it nevertheless leads to an instability in the calculations due to wild cancellations between positive and negative weights. It is worth mentioning that the Markov process may still converge to a probability distribution corresponding to the ground state wave function. Thus, to cure this instability one needs to make some kind of approximation. The fixed-node approximation [97] does the job, wherein one defines an effective Hamiltonian $\bar{\mathcal{H}}^{\text{eff}}$ from the original Hamiltonian $\bar{\mathcal{H}}$, by setting to zero the positive off-diagonal elements of $\bar{\mathcal{H}}$. Thus, the $\bar{\mathcal{H}}^{\text{eff}}$ reads as,

$$\bar{\mathcal{H}}_{x'x}^{\text{eff}} = \begin{cases} \bar{\mathcal{H}}_{x'x}, & \text{if } \bar{\mathcal{H}}_{x'x} \leq 0 \\ 0, & \text{if } \bar{\mathcal{H}}_{x'x} > 0 \end{cases}$$

however, in order to have variational results for the energies, it is in addition necessary that the diagonal terms undergo a sign flip, i.e.,

$$\bar{\mathcal{H}}_{xx}^{\text{eff}} = \bar{\mathcal{H}}_{xx} + \mathcal{V}(x) \quad (3.31)$$

where,

$$\mathcal{V}(x) = \sum_{\bar{\mathcal{H}}_{x'x} > 0, x' \neq x} \bar{\mathcal{H}}_{x'x} \quad (3.32)$$

this redefined effective Hamiltonian constitutes the essence of the fixed-node approximation.

It is interesting and important to note that the fixed-node approximation actually gives us an upper bound of the ground state energy. If we consider any variational state $|\Psi_{\text{trial}}\rangle$ and we compute and compare its energy for \mathcal{H} and \mathcal{H}^{eff} , we get,

$$\begin{aligned} \Delta E &= \langle \Psi_{\text{trial}} | (\mathcal{H}^{\text{eff}} - \mathcal{H}) | \Psi_{\text{trial}} \rangle \\ &= \sum_{\bar{\mathcal{H}}_{xx'} > 0, x' \neq x} |\mathcal{H}_{xx'}| \left| \Psi_{\text{trial}}(x) \sqrt{\left| \frac{\Psi_G(x')}{\Psi_G(x)} \right|} - \Psi_{\text{trial}}(x') \sqrt{\left| \frac{\Psi_G(x)}{\Psi_G(x')} \right|} \text{sgn}(\mathcal{H}_{xx'}) \right|^2 \end{aligned} \quad (3.33)$$

thus, we see that $\Delta E > 0$ for any wave function. Hence, it follows at once that the ground state energy E_0^{eff} of \mathcal{H}^{eff} serves as an upper bound of the ground state energy E_0 of \mathcal{H} . Thus, if Ψ^{eff} is the ground state wave function, we can write down the following extremely important inequality,

$$E_0^{\text{eff}} \geq \frac{\langle \Psi^{\text{eff}} | \mathcal{H} | \Psi^{\text{eff}} \rangle}{\langle \Psi^{\text{eff}} | \Psi^{\text{eff}} \rangle} \geq E_0 \quad (3.34)$$

Hence, it is now manifest that the fixed-node energy serves as an upper bound to the true ground state energy. Also, the fixed-node approximation improves the energy of the guiding wave function, expressed in the following inequality,

$$E_0^{\text{eff}} \leq \frac{\langle \Psi_G | \mathcal{H}^{\text{eff}} | \Psi_G \rangle}{\langle \Psi_G | \Psi_G \rangle} = \frac{\langle \Psi_G | \mathcal{H} | \Psi_G \rangle}{\langle \Psi_G | \Psi_G \rangle} \quad (3.35)$$

3.2 The Lanczos algorithm and its implementation within a Monte Carlo scheme

3.2.1 The Lanczos method

The Lanczos method is an iterative procedure used to determine the eigenspectrum of Hermitian matrices. It is much better than the power method because of the manner in which the ground state is reconstructed. In the power method, the ground state is approximated by a single state, $|\Psi_0\rangle \approx G^n |\Psi_{\text{trial}}\rangle$, in contrast the Lanczos method uses the information contained in all powers $G^i |\Psi_{\text{trial}}\rangle$, with $i = 1, 2, \dots, n$ to reconstruct the ground state which is then approximated as,

$$|\Psi_0\rangle \approx \sum_{i=1}^n \alpha_i \mathcal{H}^i |\Psi_{\text{trial}}\rangle \quad (3.36)$$

The starting point is chosen to be an arbitrary vector $|\Psi_1\rangle$ in the Hilbert space, satisfying $\langle \Psi_0 | \Psi_1 \rangle \neq 0$. If there is no a priori information about the ground state, then a prescription is to choose random coefficients in the wave function, for the given basis vectors. In some cases, from general considerations, there is information about the ground state available, like its momentum, or total spin, or its transformation properties under point group symmetry operations. In these cases it is better to choose the starting vector $|\Psi_1\rangle$ in the relevant subspace having the right quantum numbers.

The Lanczos iterations generate a set of orthogonal vectors, in the following manner; we first normalize the initial random state $|\Psi_1\rangle$ and define a new vector obtained by applying the Hamiltonian \mathcal{H} to $|\Psi_1\rangle$, and finally subtract the projection over $|\Psi_1\rangle$, this gives,

$$\beta_2 |\Psi_2\rangle = \mathcal{H} |\Psi_1\rangle - \alpha_1 |\Psi_1\rangle \quad (3.37)$$

where α_1 and β_2 are such that $\langle \Psi_2 | \Psi_2 \rangle = 1$ and $\langle \Psi_1 | \Psi_2 \rangle = 0$, this gives for the coefficients the following expression,

$$\begin{aligned} \alpha_1 &= \langle \Psi_1 | \mathcal{H} | \Psi_1 \rangle \\ \beta_2 &= \langle \Psi_2 | \mathcal{H} | \Psi_1 \rangle \end{aligned} \quad (3.38)$$

we can subsequently construct a new state which is orthogonal to the previous ones, in the following manner,

$$\beta_3 |\Psi_3\rangle = \mathcal{H} |\Psi_2\rangle - \alpha_2 |\Psi_2\rangle - \beta_2 |\Psi_1\rangle \quad (3.39)$$

with,

$$\begin{aligned} \alpha_2 &= \langle \Psi_2 | \mathcal{H} | \Psi_2 \rangle \\ \beta_3 &= \langle \Psi_3 | \mathcal{H} | \Psi_2 \rangle \end{aligned} \quad (3.40)$$

Thus, we see that a general iteration takes the following form,

$$\beta_{n+1} |\Psi_{n+1}\rangle = \mathcal{H} |\Psi_n\rangle - \alpha_n |\Psi_n\rangle - \beta_n |\Psi_{n-1}\rangle \quad (3.41)$$

with,

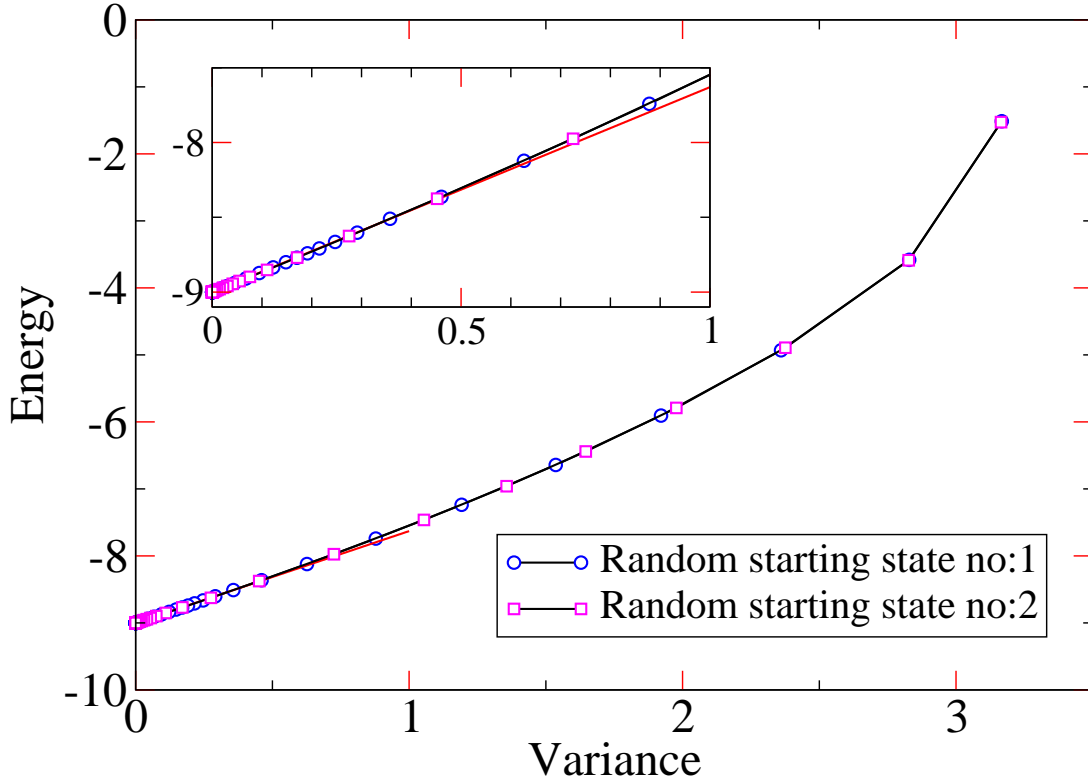


Figure 3.2: Plot of Energy vs Variance for the Lanczos iterative convergence to the ground state starting from two random state vectors. As one gets closer to the ground state the relation between the energy and variance becomes essentially linear (marked by red line), see inset for magnification near the ground state region. This implies that to extract the ground state energy it is sufficient to choose (if possible) a “good” enough starting wave function and perform only a few Lanczos steps followed by a zero variance extrapolation. This extrapolation scheme will be used extensively when performing Lanczos within a Monte Carlo scheme, since within the scheme it is only possible to perform a few Lanczos steps.

$$\begin{aligned}
 \alpha_n &= \langle \Psi_n | \mathcal{H} | \Psi_n \rangle \\
 \beta_{n+1} &= \langle \Psi_{n+1} | \mathcal{H} | \Psi_n \rangle
 \end{aligned}
 \tag{3.42}$$

It is worth noting that, by construction, the vector $|\Psi_n\rangle$ are orthogonal to all the previous ones, despite the fact that we subtract only the projections of the previous two vectors. It is also transparent that, in the Lanczos basis, the Hamiltonian acquires a tridiagonal form,

$$\mathcal{H} = \begin{pmatrix}
 \alpha_1 & \beta_2 & 0 & 0 & \cdots \\
 \beta_2 & \alpha_2 & \beta_3 & 0 & \cdots \\
 0 & \beta_3 & \alpha_3 & \beta_4 & \cdots \\
 0 & 0 & \beta_4 & \alpha_4 & \cdots \\
 \cdots & \cdots & \cdots & \cdots & \cdots
 \end{pmatrix}$$

In this form, the Hamiltonian can be easily diagonalized using standard routines. In order, to obtain the exact ground state of a given Hamiltonian, it is necessary to perform a number of iterations equal to the dimension of the Hilbert space. However, in practice an extremely accurate approximation of the ground state is obtained after only a few iterations (≈ 100),

this is the greatest advantage of the of the Lanczos method. The ground state can then be expressed as,

$$|\Psi_0\rangle \approx \sum_{n=1}^{\sim 100} c_n |\Psi_n\rangle \quad (3.43)$$

The limitation due to the exponential growth of the Hilbert space can be controlled by exploiting the symmetries of the Hamiltonian, e.g. in the case of periodic boundary conditions on a chain, there is translational invariance and the momentum is thus a conserved quantity.

The results of a case study for the spin-1/2 $J_1 - J_2$ XXZ chain of 24 sites are given in Fig. 3.2, wherein we start from two random states and show the manner in which the convergence to the ground state is reached, within very few iterations, by plotting the energy ($\langle \mathcal{H} \rangle$) versus variance ($\sigma^2 = \langle \mathcal{H}^2 \rangle - \langle \mathcal{H} \rangle^2$) of the iterated states. As can be seen the relation between the energy and variance becomes essentially linear as one approaches near the ground state. This is discussed in more detail in sec. 3.2.3.

3.2.2 Improvement of variational wave functions by application of Lanczos steps within a Monte Carlo scheme

After one has “guessed” (of course by using some prescription) a trial wave function $|\Psi_{\text{trial}}\rangle$ for a given Hamiltonian, then the question arises as to how should one “improve” it so as to get closer to the true ground state. This improvement can be systematically carried out by applying the Hamiltonian operator a given number, say p times on the trial wave function and then constructing a linear combination of all the p terms [18]. That is,

$$|\Psi_{\alpha_1, \dots, \alpha_p}\rangle = \sum_{i=1, \dots, p} \alpha_i \mathcal{H}^i |\Psi_{\text{trial}}\rangle \quad (3.44)$$

the resulting variational wave function $|\Psi_{\alpha_1, \dots, \alpha_p}\rangle$ contains p variational parameters (the coefficients α_i) in addition to its internal ones.

We shall first take up the case of $p = 1$, i.e. one Lanczos step wave function and show how to go about calculating the expectation value of the Hamiltonian for the following state,

$$|\Psi_\alpha\rangle = (1 + \alpha \mathcal{H}) |\Psi_{\text{trial}}\rangle \quad (3.45)$$

assuming that the value of α is already fixed and determined in a way so as to yield the minimum energy. The energy of the one Lanczos step wave function reads as,

$$\begin{aligned} E(\alpha) &= \frac{\langle \Psi_\alpha | \mathcal{H} | \Psi_\alpha \rangle}{\langle \Psi_\alpha | \Psi_\alpha \rangle} \\ &= \frac{\sum_{xx'} \Psi_\alpha(x') \mathcal{H}_{x'x} \Psi_\alpha(x)}{\sum_x |\Psi_\alpha(x)|^2} \\ &= \frac{\sum_x E_x(\alpha) |\Psi_\alpha(x)|^2}{\sum_x |\Psi_\alpha(x)|^2} \end{aligned} \quad (3.46)$$

where $E_x(\alpha)$ is the local energy, defined as,

$$E_x(\alpha) = \sum_{x'} \mathcal{H}_{x'x} \frac{\Psi_\alpha(x')}{\Psi_\alpha(x)} \quad (3.47)$$

The ratio $\Psi_\alpha(x')/\Psi_\alpha(x)$ is the central quantity entering the Metropolis algorithm can be expressed as,

$$\frac{\Psi_\alpha(x')}{\Psi_\alpha(x)} = \frac{\langle x' | (1 + \alpha \mathcal{H}) | \Psi_{\text{trial}} \rangle}{\langle x | (1 + \alpha \mathcal{H}) | \Psi_{\text{trial}} \rangle} = \frac{\Psi_{\text{trial}}(x')}{\Psi_{\text{trial}}(x)} \left(\frac{1 + \alpha E_{x'}}{1 + \alpha E_x} \right) \quad (3.48)$$

Therefore, at each Monte Carlo step, we have to compute the local energy of the trial wave function $|\Psi_{\text{trial}}\rangle$ on both the configurations $|x\rangle$ and $|x'\rangle$. This calculation involves computing *all* the matrix elements $\langle x' | \mathcal{H} | \Psi_{\text{trial}} \rangle$, whether or not the move from $|x\rangle \rightarrow |x'\rangle$ is accepted, and requires operations of the order of number of lattice sites. The exact computation for, say p Lanczos steps requires evaluating matrix elements $\langle x' | \mathcal{H}^i | \Psi_{\text{trial}} \rangle$ for $i = 1, \dots, 2p+1$, and the algorithm scales in time exponentially with the number of Lanczos steps, since one has to take into account *all* the possible configurations that arise when \mathcal{H}^i is applied to $|x'\rangle$. However, using the stochastic reconfiguration technique it proves feasible to perform a few Lanczos steps on a given trial wave function, within a reasonable amount of time. If one has a good enough trial wave function as the starting point, then *only* a couple of Lanczos steps are needed in order to have an energy quite close to the true value from exact diagonalization. Subsequently, one can perform a variance extrapolation to obtain the ground state energy to an extremely good degree of accuracy, even the exact one sometimes if the symmetry sectors of the trial wave function and the ground state wave function are the same.

3.2.3 The method of variance extrapolation

Any variational Monte Carlo calculation of an observable, e.g. the energy, of a trial wave function has statistical fluctuations, except if one is exactly at an eigenstate of the Hamiltonian, in which case the fluctuations vanish. Therefore, the extent to which $|\Psi_{\text{trial}}\rangle$ deviates or is away from the ground state is indicated by the width of the energy distribution of the trial wave function $|\Psi_{\text{trial}}\rangle$. The variance of the energy distribution is a quantitative estimate of this width and provides a criterion for determining how close a trial wave function is, to the true ground state. The variance is given by,

$$\begin{aligned} \sigma^2 &= \frac{1}{N^2} (\langle \mathcal{H}^2 \rangle - \langle \mathcal{H} \rangle^2) \\ &= \frac{1}{N^2} \left(\frac{\langle \Psi_{\text{trial}} | \mathcal{H}^2 | \Psi_{\text{trial}} \rangle}{\langle \Psi_{\text{trial}} | \Psi_{\text{trial}} \rangle} - \left(\frac{\langle \Psi_{\text{trial}} | \mathcal{H} | \Psi_{\text{trial}} \rangle}{\langle \Psi_{\text{trial}} | \Psi_{\text{trial}} \rangle} \right)^2 \right) \end{aligned} \quad (3.49)$$

the variance thus measures the “quality” of the trial wave function. A good variational state has an energy close to E_0 and *also* a small variance. This additional information provided about the quality of the variational state is one of the advantages of the variational approach.

The calculation of the variance can be done within the variational Monte Carlo scheme, as can be seen from the expression below,

$$\frac{\langle \Psi_{\text{trial}} | \mathcal{H}^2 | \Psi_{\text{trial}} \rangle}{\langle \Psi_{\text{trial}} | \Psi_{\text{trial}} \rangle} = \frac{\sum_x \langle \Psi_{\text{trial}} | \mathcal{H} | x \rangle \langle x | \mathcal{H} | \Psi_{\text{trial}} \rangle}{\sum_x |\Psi_{\text{trial}}(x)|^2} = \frac{\sum_x E_x^2 |\Psi_{\text{trial}}(x)|^2}{\sum_x |\Psi_{\text{trial}}(x)|^2} \quad (3.50)$$

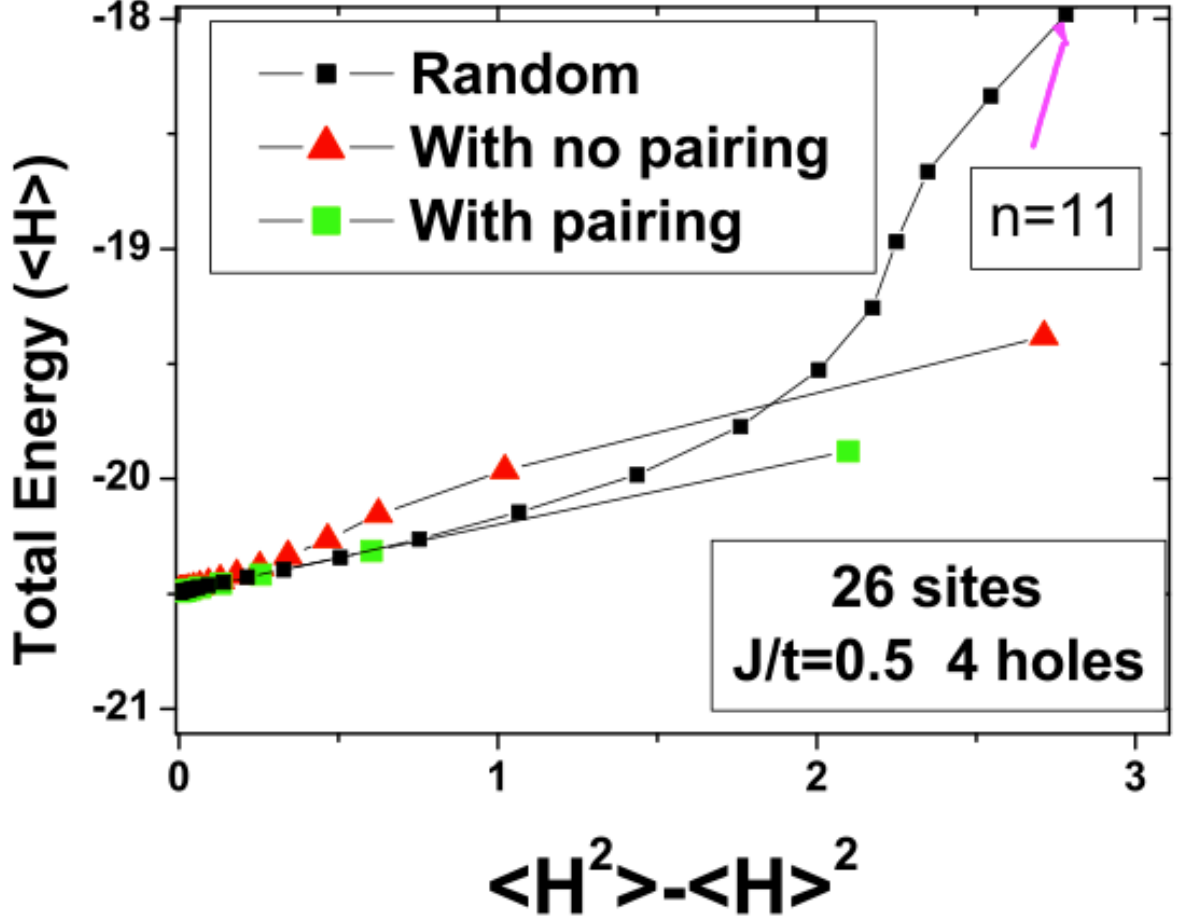


Figure 3.3: Adapted from Ref. [98]. The energy is plotted as a function of variance for various wave functions, for the t-J model. It shows that for good enough starting variational wave functions, only a few Lanczos steps are necessary to obtain an excellent estimate of the exact ground state energy. In the case of the state “with pairing” (the best one of the three), if one takes only the points for 0, 1 and 2 Lanczos steps and perform a quadratic fit extrapolation, we land up with an energy which is within error bars of that obtained by following all the Lanczos steps. Hence, given such good starting wave functions, the method of variance extrapolation after a couple of Lanczos steps forms an excellent and economical tool to extract the exact ground state energy.

where E_x is the local energy as previously defined. Therefore, the variance can be computed by sampling the square of the local energy, in addition to the local energy itself.

If the trial wave function $|\Psi_{\text{trial}}\rangle$ is close enough to the true ground state $|\Psi_0\rangle$. Then, $|\Psi_{\text{trial}}\rangle = |\Psi_0\rangle + \epsilon|\eta\rangle$, with $\langle\Psi_0|\eta\rangle = 0$ and $\langle\Psi_0|\Psi_0\rangle = \langle\eta|\eta\rangle = 1$. The energy per site can be expressed as,

$$\frac{E}{N} = \frac{1}{N} \left(\frac{E_0 + \epsilon^2 \langle\eta|\mathcal{H}|\eta\rangle}{1 + \epsilon^2} \right) \approx \frac{E_0}{N} + \frac{\epsilon^2}{N} (\langle\eta|\mathcal{H}|\eta\rangle - E_0) \quad (3.51)$$

thus we see that the difference between the variational and exact ground state energy vanishes linearly with ϵ^2 . Analogously the variance can be expressed as,

$$\sigma^2 = \frac{1}{N^2} \left(\frac{E_0^2 + \epsilon^2 \langle \eta | \mathcal{H}^2 | \eta \rangle}{1 + \epsilon^2} - \left(\frac{E_0 + \epsilon^2 \langle \eta | \mathcal{H} | \eta \rangle}{1 + \epsilon^2} \right)^2 \right) \quad (3.52)$$

to leading order in ϵ^2 the above expression reads as,

$$\sigma^2 \approx \frac{\epsilon^2}{N^2} \langle \eta | (\mathcal{H} - E_0)^2 | \eta \rangle \quad (3.53)$$

Whence, when the trial state is close enough to the ground state, the following relation holds between the energy and the variance,

$$\frac{E}{N} \approx \frac{E_0}{N} + \text{constant} \times N \times \sigma^2 \quad (3.54)$$

We have manifestly seen the validity of the above expression in Fig. 3.2, for a pure Lanczos calculation, and in Fig. 3.3 for the implementation of Lanczos algorithm within a Monte Carlo scheme. The above relation is extremely important and can be used to extract the ground state energy of a Hamiltonian on a given cluster size. For a given starting trial wave function and for the hierarchy of wave functions obtained by applying p Lanczos steps on it, we calculate the energies E and variances σ^2 for each one of them, and subsequently extrapolate to $\sigma^2 = 0$ to obtain an estimate of the ground state energy E_0 , see Fig. 3.3.³ In this hierarchy, each variational state descends from the previous one and has a lower energy and variance compared the previous one. It is worth mentioning that we can also compute the energies for each of these states using Green's function Monte Carlo and similarly extrapolate to $\sigma^2 = 0$ to obtain a possibly better estimate of the ground state energy of the Hamiltonian on a given cluster. Finally, it is worth mentioning that we can obtain these ground state energies E_0 for many different cluster sizes and perform a finite-size extrapolation to obtain an estimate of the ground state energy for the infinite system.

³As a proof of principle, it is necessary to validate the extrapolated energy by repeating this procedure starting from different wave functions and verifying that the extrapolations indeed match within error bars.

Part II

The spin-1/2 Heisenberg antiferromagnet on the kagomé lattice

Chapter 4

History and mystery associated to the kagomé Heisenberg model

4.1 The spin-1/2 Heisenberg antiferromagnetic model on two dimensional lattices

It is well known from the Mermin-Wagner theorem that in two (and one) dimensional isotropic Heisenberg spin systems at non-zero temperature, there can never be magnetic long range ordering as long as the range of exchange interactions is finite [99]. However, at zero temperature the presence of magnetic long range order is “permitted”, but its presence or absence depends on the strength of quantum fluctuations and no sweeping statements can be made. The extent to which quantum fluctuations are amplified depends on the lattice topology and geometry, and the manner in which it interplays with exchange interactions.

In two dimensions there are 11 possible uniform Archimedean tilings formed from different arrangements of regular polygons. Out of these 11 lattices only 3 are made of a single type of regular polygon which is periodically arranged, these are the triangular lattice, the square lattice and the hexagonal (honeycomb) lattice. The other 8 lattices are composed of periodic arrangement of two or more types of regular polygons with the same edge length, e.g. combining triangles and hexagons gives rise to the kagomé lattice or combining triangles, squares and hexagons gives rise to the bounce lattice. Only the square and triangular lattices have a primitive unit cell, rest all have at least two sites per unit cell. Among these 11 lattices, 4 of them are composed of only even sided polygons and are thus unfrustrated, these are termed as bipartite lattices. The rest 7 lattices are also composed of odd sided polygons, they are thus frustrated geometrically and are termed as non-bipartite lattices. Also, the triangular, square, hexagonal and kagomé lattices all have equivalent nearest neighbor bonds, the rest 7 lattices have non-equivalent bonds. These 11 lattices have coordination numbers ranging from $z = 3$ to $z = 6$. Thus, from the above considerations it is clear that these lattices differ in their topology and geometry, these geometrical properties in turn have a strong influence on the magnetic properties of the spin system on the respective lattices. Precisely speaking, the non-bipartite nature of a lattice and a low coordination number greatly enhance quantum fluctuations and thereby aid the stabilization of a quantum paramagnetic state. The kagomé lattice serves as the ideal playground to stabilize these exotic phases, since it has a coordination number on the lower side $z = 4$ and possesses the maximum geometric frustration [100–102].

4.2 The spin-1/2 Heisenberg antiferromagnetic model on the kagomé lattice

The spin-1/2 Heisenberg antiferromagnetic model on the kagomé lattice has had a decently long and a very distinguished career, both in terms of challenges it has posed and still poses to theoretical and numerical methods, and more recently in pushing developments in experimental techniques used to study these novel systems. The story began just after it was realized that the ground state of the spin-1/2 Heisenberg antiferromagnetic model on the triangular lattice is actually Néel ordered [103–113] contrary to the conjecture by Anderson and Fazekas that the ground state should be a rotationally invariant RVB spin liquid [64, 65]. Subsequently the limelight shifted to the kagomé lattice in search for an exotic quantum paramagnetic ground state since, despite being as frustrated as the triangular lattice, it has a lower coordination number $z = 4$. Indeed, all studies have pointed at a quantum paramagnetic ground state of the kagomé spin-1/2 Heisenberg antiferromagnetic model [56, 104, 113–127].

The geometrical unit cell of the kagomé lattice contains 3 sites and the Bravais lattice is a triangular one. The classical ground state of the Heisenberg antiferromagnetic model consists of neighboring spins pointing at an angle of 120° relative to each other, see Fig. 4.1. The energy per site comes out to be $E/\text{site} = -s^2 = -0.25$. The classical ground states on the kagomé lattice have a non-trivial *infinite* degeneracy [48, 128, 129] and this feature is responsible, in the quantum version of the model, for the unusually high number of singlet excitations below the triplet gap.

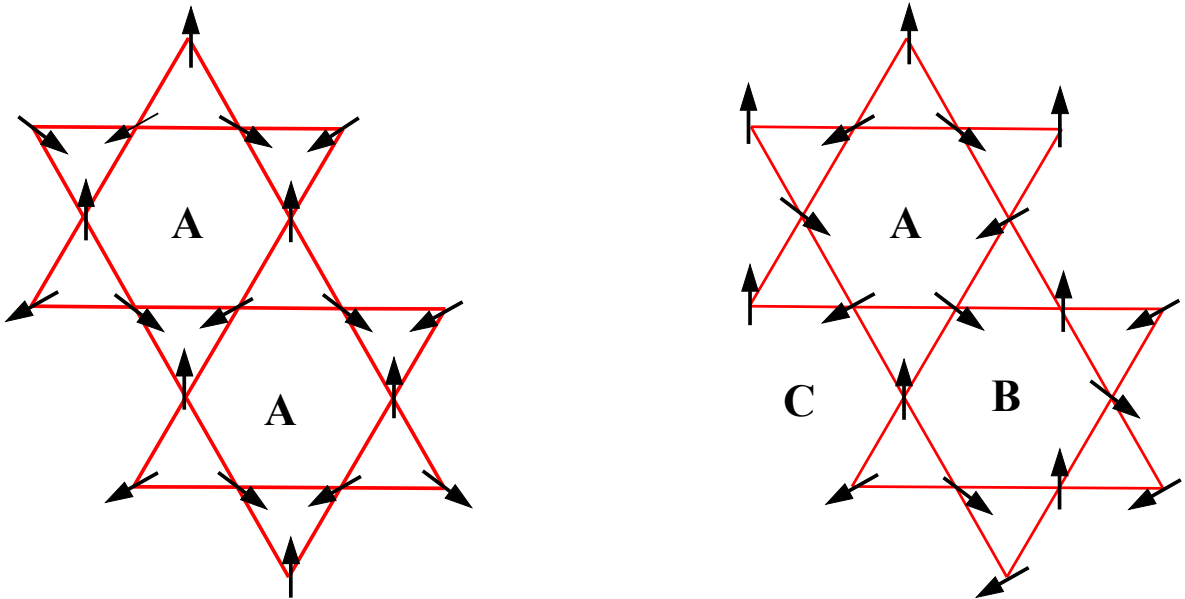


Figure 4.1: The two different ground states of the classical kagomé Heisenberg antiferromagnetic model. The state on the left is called the $q = 0$ state and it does not break the elementary (3-site unit cell) translational symmetry of the kagomé lattice. The state on the right is called the $\sqrt{3} \times \sqrt{3}$ state and it breaks the elementary translational symmetry of the kagomé lattice because its magnetic unit cell is three times larger compared to the underlying geometrical unit cell. The infinite degeneracy of both these states is reflected in the fact that we can freely rotate in a synchronized manner, the spins at every site.

The identification of the precise nature of the quantum paramagnetic ground state of the kagomé spin-1/2 quantum Heisenberg antiferromagnetic model is still a wide open, intensely debated and a controversial issue. This is because the ground state manifold is extensively quasi-degenerate with a stiff competition between myriad of different phases all concentrated within a very narrow energy range. The problem is further aggravated by the fact that the respective stability and nature of these phases can be changed upon minor perturbations. Some of these phases are extremely “delicate” while others are robust and occupy a finite region in phase space. The combined presence of such unique features have pushed the envelope of theoretical and numerical ideas, and techniques aimed at solving this delicately balanced Hamiltonian on the kagomé lattice. This delicate balancing in the vicinity of a quantum critical point has the effect that it is extremely difficult to even broadly claim if the ground state is a spin liquid or a valence bond crystal. This is because nearby a critical point the VBC may also have strong quantum fluctuations suppressing its order parameter leading to a very weak breaking of translational symmetry which cannot be unambiguously captured by all methods, and is very difficult to distinguish from signatures of a spin liquid behavior. Thus, it can safely be said in retrospect that any development towards a solution to this problem has also lead and will lead to progress in theoretical and numerical techniques. On the other hand, in order to extract thermodynamic properties one has to use approximate numerical techniques in the absence of an exact method of solution in $2d$ and also because exact diagonalization studies are restricted to relatively small system sizes, the current limit being 48 sites. Each technique is biased in some way or another towards capturing a particular type of quantum order, as a consequence many competing phases of very different nature’s have been vouched for as ground states. The claims of ground state made using one technique have not generally been backed up or verified by other techniques unanimously, which is an unpleasant situation and is a reflection of the difficulty of the problem at hand. We shall now present a survey of the kagomé ground state landscape within various approaches and also outline the current situation on this infamous lattice.

First, we survey the “hot” competitors which have been proposed within the framework of the SU(2) slave boson (Schwinger fermion) approach, where in particular the gapless/critical spin liquids with a U(1) low energy gauge structure have been argued to be a good approximation to the true ground state. The competing spin liquids within this approach are the following,

- An **algebraic spin liquid**, the so called U(1) Dirac spin liquid. Its mean field band structure consists of two Dirac cones (at the Fermi energy) at which the spectrum becomes relativistic (linear) with Dirac conical excitations described by 4 flavors of massless two component Dirac fermions coupled to a dynamical U(1) compact lattice gauge field. Its mean field Ansatz is given by nearest neighbor uniform hopping amplitudes ($|\chi_{ij}| = 1$) with phases such that 0 flux threads through the triangles and π through the hexagons, hence its also called the $[0, \pi]$ spin liquid. After projection, its energy per site on a 48 site cluster is computed (using variational Monte Carlo) to be $E/\text{site} = -0.4293510(4)$ which is within 2% of the exact diagonalization value on the 48 site cluster, which is quite remarkable keeping in mind the fact that the wave function has *no* variational parameters. The real space spin-spin correlations in the projected state decay as a power law, being proportional to $1/L^4$. It is an example of a *fully symmetric* long range RVB spin liquid and is *marginally* stable. For a detailed study of the properties of this spin liquid, see [12, 13, 130].

- **A uniform RVB spin liquid**, which is also a U(1) gapless spin liquid. Its mean field band structure consists of large circular spinon Fermi surfaces coupled to a compact U(1) lattice gauge field. Its mean field Ansatz is given by nearest neighbor uniform hopping amplitudes ($|\chi_{ij}| = 1$) with phases such that 0 flux threads through both triangles and hexagons, hence its also called as the $[0, 0]$ spin liquid. After projection, its energy per site on a 48 site cluster is computed (using variational Monte Carlo) to be $E/\text{site} = -0.4114624(8)$, which is higher compared to the U(1) Dirac spin liquid, and within 6% of the exact diagonalization value. This wave function also does not require any fine tuning of variational parameters. Upon addition of a small ferromagnetic exchange coupling (J_2) to the Hamiltonian this state becomes lower in energy than the U(1) Dirac spin liquid. The $[0, 0]$ spin liquid is also an example of a *fully symmetric* long range RVB spin liquid. For more details see [131].
- **Chiral spin liquids**: These spin liquids are *not* fully symmetric, specifically, they break time-reversal symmetry due to chiral mass terms acquired by the fermions, and hence these are gapped states and belong to the category of stable short range RVB spin liquids. In general, their mean field Ansatz are obtained by having a flux different from 0 and π through the triangles and hexagons, this is implemented by having complex hoppings (χ_{ij}). It is these spin liquids which host fractionalized excitations which are free spinons obeying fractional statistics, this is because the gauge field becomes gapped via the Chern-Simons mechanism [132, 133]. If we perturb the U(1) Dirac spin liquid by inserting a θ flux through the triangles and remove $\pi - 2\theta$ flux through the hexagons, one finds that the energy increases, and this increase is monotonic till the limit $[\pi/2, 0]$, see [12]. Thus, these class of chiral spin liquids are energetically unfavorable compared to the U(1) Dirac spin liquid. The energetics of two more chiral states was investigated in [12], these were the staggered flux state with $+\pi/2$ flux through up triangles and $-\pi/2$ flux through down triangles, and zero flux through hexagons, hence called the $[\pm\pi/2, 0]$ spin liquid. The other spin liquid has $\pi/2$ flux through the triangles and π flux through hexagons is called the $[\pi/2, \pi]$ spin liquid. Both these spin liquids were found to have higher energies compared to the U(1) Dirac spin liquid and also the $[0, 0]$ spin liquid. It is worth noting that at the mean field level (without projection), the $[\pi/2, 0]$ chiral state has the lowest energy [134], and the Dirac spin liquid has the lowest mean field energy among non-chiral spin liquids [130], albeit higher than the $[\pi/2, 0]$ spin liquid. However, upon incorporating fluctuations the scenario is reversed and the chiral $[\pi/2, 0]$ spin liquid becomes higher in energy compared to the U(1) Dirac spin liquid.
- **The \mathbb{Z}_2 spin liquids**: There are in all 20 fully symmetric \mathbb{Z}_2 spin liquids that can exist on the kagomé lattice [91]. Out of these, 5 spins liquids are gapped and the rest are gapless. Since, the \mathbb{Z}_2 gauge field is gapped all \mathbb{Z}_2 spin liquids are stable and hence more likely to occur as real physical spin liquids. Among these 20 spin liquids only 12 are likely to occur as ground states of a nearest neighbor Heisenberg Hamiltonian, and all of them are *continuously* connected to some U(1) gapless spin liquid. The energies of all these 12 \mathbb{Z}_2 spin liquids was found to be higher compared to the U(1) Dirac spin liquid for the nearest neighbor Heisenberg Hamiltonian [22].
- **Valence bond crystals**: The valence bond crystals break the elementary 3 site unit cell translational symmetry with different unit cell sizes. If one restricts to sizes upto 36 sites, then in all 20 symmetry distinct valence bond crystals can exist on the

kagomé lattice. Some of them, in particular a 12 site C_{6v} symmetric valence bond crystal was proposed as an instability of the U(1) Dirac spin liquid in Ref. [130], but a computation of the energy shows that in fact this Valence bond crystal is higher in energy compared to the U(1) Dirac spin liquid, and that even the $[0,0]$ spin liquid is stable against this perturbation [12, 19, 131]. The competing 18 site and 36 site unit cell valence bond crystal was also shown to be higher in energy compared to the U(1) Dirac spin liquid, see Ref. [19, 131]. In fact, in a recent study we showed that the U(1) Dirac spin liquid is robust (locally and globally) against destabilizing into all 20 valence bond crystals. It is worth mentioning that the valence bond crystal state is stabilized as the ground state upon addition of a very weak 2nd nearest neighbor ferromagnetic exchange coupling in the Hamiltonian.

Thus, in conclusion we can safely say that within the SU(2) slave boson (Schwinger fermion) formalism, the U(1) Dirac spin liquid has the lowest variational energy for the nearest neighbor spin-1/2 Heisenberg antiferromagnetic model on the kagomé lattice. We will now describe the scenario regarding the competing states proposed within the slave fermion (Schwinger boson) approach, all of which are hence gapped.

- **The \mathbb{Z}_2 spin liquids:** There are in all 8 fully symmetric \mathbb{Z}_2 spin liquids that can exist on the kagomé lattice [135]. Among these 8 spin liquids, only 4 of them are likely to be stabilized as ground states of a nearest neighbor Heisenberg Hamiltonian. In Ref. [136], the energies of these 4 spin liquids were computed and were found to be higher compared to the U(1) Dirac spin liquid for the nearest neighbor Hamiltonian. However, the study found that upon addition of a small 2nd nearest neighbor antiferromagnetic coupling to the Hamiltonian, the energy of a particular \mathbb{Z}_2 spin liquid, the so called $q = 0$ state [137] becomes lower than the U(1) Dirac spin liquid.
- **Chiral spin liquid:** A particular gapped chiral topological spin liquid called the *cuboc1* phase, was argued in Ref. [138] as the ground state of the spin-1/2 Heisenberg antiferromagnetic model. The claims were made purely at a mean field level, and the claim is partly supported by exact diagonalization results for dynamical and static spin structure factors. However, an energetic analysis using projected wave functions on e.g. the 48 site cluster would be needed to categorically comment on the viability of such a state being stabilized as the ground state.

Whence, we can safely conclude that, till date, within the slave particle formalisms, the best variational energy is given by the projected U(1) Dirac spin liquid, for the nearest neighbor spin-1/2 quantum Heisenberg antiferromagnet.

We now turn our focus to other formalisms and numerical techniques that have been used to attack this problem and survey the ground states that have been proposed using those techniques for the spin-1/2 Heisenberg antiferromagnet,

- **Density matrix renormalization group (DMRG):** An early DMRG study [139] pointed towards a spin liquid ground state of the short range RVB type which is fully symmetric, and is furthermore gapped in the spin-triplet channel but gapless in the spin-singlet channel. On a 48 site cluster using periodic boundary conditions its ground state energy per site was computed to be $E/\text{site} = -0.43663$, which is within 0.4% of the exact diagonalization value. It is worth noting that this energy estimate is lower than that for the U(1) Dirac spin liquid. A subsequent study using multi scale entanglement renormalization ansatz (MERA) [140], claimed that the best

approximation to the ground state of an infinite system is a 36 site unit cell valence bond crystal. But, this claim cannot be treated as conclusive since MERA is biased towards capturing low entanglement solutions as compared to relatively more entangled states such as algebraic spin liquids. Hence, a spin liquid ground state cannot be categorically excluded by using this technique alone.

On the other hand, relatively recent large scale and improved DMRG studies [20, 21] have made a strong claim for a fully gapped, fully symmetric \mathbb{Z}_2 spin liquid ground state of the spin-1/2 Heisenberg antiferromagnetic model, which has been further supported by computations of topological entanglement entropy using DMRG, finding a scaling of entanglement entropies consistent with a \mathbb{Z}_2 spin liquid.

- **Series expansion:** The series expansion studies carried out in Refs. [141, 142] have unanimously claimed the ground state to be a 36 site unit cell valence bond crystal. The energy of such a crystal is slightly lower than for the U(1) Dirac spin liquid.
- **Quantum dimer models:** The study of the kagomé Heisenberg antiferromagnet using an effective quantitative quantum dimer model have claimed the ground state to be a 36 site unit cell valence bond crystal. It also found a topological \mathbb{Z}_2 dimer liquid nearby, in an extended parameter space [143, 144]. A more recent generalized quantum dimer model study [145] found a new (possibly chiral) valence bond crystal of 12 site unit cell to be competing with the 36 site unit cell valence bond crystal. Also, a 6 site columnar valence bond crystal was found to be competing for the ground state.
- **Contractor renormalization (CORE):** On mapping the spin-1/2 Heisenberg antiferromagnet to an effective Hamiltonian using CORE, one finds a variational ground state which is a 6 site valence bond crystal possessing columnar dimer order [146]. This claim has also been backed up by a generalized quantum dimer model study mentioned above.

The “jungle” of proposed ground states and their corresponding frameworks are summarized in the table below.

1st Author	GS proposed	Energy/site	Method used
Ran	U(1) algebraic SL	$\approx -0.42866 J$	Proj. Schwinger fermion
Messio	Chiral topological gapped SL		Schwinger boson mean field
Singh	36 site HVBC	$\approx -0.433 J$	Dimer series expansion
Budnik	6 site CVBC		CORE
Poilblanc	6, 12 (chiral) & 36 site VBCs		Quantum dimer models
Evenbly	36 site HVBC	$\approx -0.43221 J$	MERA
Yan	\mathbb{Z}_2 fully gapped SL	$\approx -0.4379 J$	DMRG
Depenbrock	\mathbb{Z}_2 fully gapped non-chiral SL	$\approx -0.4386 J$	DMRG

Thus, even a brief survey of the manifold of possible ground states of the spin-1/2 Heisenberg antiferromagnet proposed using different approximate methods highlights the muddle that infects this difficult problem. We shall address this problem only within the SU(2) slave boson (Schwinger fermion) variational approach and confront the question of construction of variational wave functions for these myriad of different phases which have been proposed from different techniques. Since, within this formalism the best variational

wave function is that of a $U(1)$ Dirac spin liquid which is *critical* and hence marginally stable, we shall subsequently analyze the question of *local* and *global* stability of this critical phase towards destabilizing into other stable competing phases. To this effect, we will use the fermionic variational quantum Monte Carlo method. This issue is extremely exciting and important, since if this critical phase survives perturbations/fluctuations, it demonstrates that conventional wisdom is incorrect [8], and the existence of this algebraic spin liquid would be a truly remarkable and revolutionary phenomenon, it would also be an indirect evidence for the existence of quantum orders, which would then be responsible for protecting gapless excitations. The PhD research projects dealing with this problem form the content of Part III of this thesis.

Chapter 5

Experimental realizations of the kagomé spin-1/2 Heisenberg antiferromagnet

Ever since the story began on the kagomé network in the late eighties, with intriguing and novel ground states being proposed regularly for the spin-1/2 Heisenberg antiferromagnet, there has been a desire to have some experimental playgrounds so as to directly test the theoretical proposals. An experimental backing was desperately required for this problem, since the theoretical scenario regarding the nature of the ground state is in a complete “mess”. The long wait finally came to an end in 2005 when a structurally perfect kagomé compound called Herbertsmithite ($\text{ZnCu}_3(\text{OH})_6\text{Cl}_2$) was first synthesized at M. I. T [10]. This is also a naturally occurring rare mineral. In it the combination of low dimensionality, low coordination number, low spin value $S = 1/2$ and frustrating antiferromagnetic interactions lead to an amplification of quantum fluctuations to an extent needed to stabilize a quantum paramagnet [147, 148]. Indeed, no magnetic freezing or order has been detected in Herbertsmithite at temperatures well below J , from any experimental technique [149, 150].

5.1 Structure and interactions in Herbertsmithite

The in-plane structure of Herbertsmithite consists of Cu^{2+} ions, which are distributed on the vertices of a *perfect* kagomé lattice, with the (OH) group mediating an in-plane super exchange interaction of moderate strength between the Cu^{2+} ions. The non-magnetic Zn^{2+} ions occupy the positions in between two kagomé planes and are distributed on a triangular lattice, see Fig. 5.1. The magnetic coupling between the kagomé planes is virtually non-existent, thus the material is in essence a $2d$ kagomé network with spin-1/2 at each vertex. The dominant interactions are in-plane and isotropic of the Heisenberg type with antiferromagnetic couplings (J) between nearest neighbor Cu^{2+} spin-1/2's. The strength of $J \approx 180(10)$ K, and no sign of spin freezing has been observed down to 50 mK, i.e. $\approx J/4000$. Recent studies [11] on the Mg version of Herbertsmithite ($\text{MgCu}_3(\text{OH})_6\text{Cl}_2$) have pushed this limit to 20 mK, i.e. $\approx J/10000$ without observing any sign of magnetic ordering, i.e. a quantum paramagnetic behavior.

The absence of inversion symmetry implies that Dzyaloshinskii-Moriya (DM) interactions ($\mathbf{D}_{ij} \cdot \hat{\mathbf{S}}_i \times \hat{\mathbf{S}}_j$) are permitted in the Hamiltonian. The results from electron spin resonance (ESR) measurements tell us that there is a small in-plane DM interaction, $D_p \approx 0.01J$ and the out-of-plane DM interaction is considerably stronger $D_z \approx 0.04 - 0.08J$ [152–154], see Fig. 5.1. If the ground state of the spin-1/2 pure Heisenberg antiferromagnet is a spin liquid phase, then upon inclusion of DM interactions (as perturbations) the original spin liq-

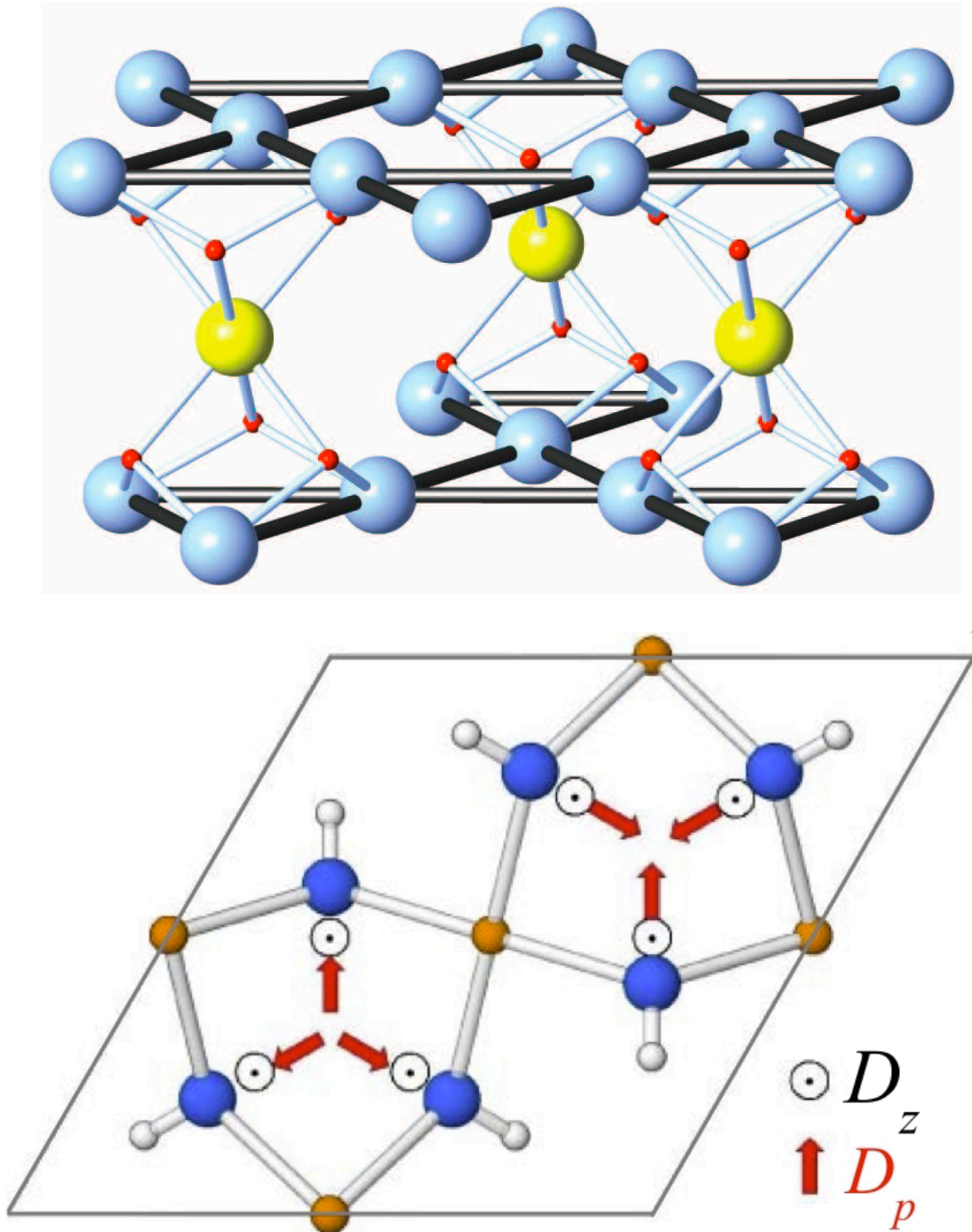


Figure 5.1: *Top:* Adapted from [151]. A simplified structure of ideal Herbertsmithite is shown. The blue balls depict the Cu^{2+} ions in the top and bottom kagomé layers, the small red balls are the (OH) group which bridge two Cu^{2+} ions and finally the yellow balls depict the Zn^{2+} ions which lie in between the planes. *Bottom:* The Dzyaloshinskii-Moriya vectors are given. The Cu^{2+} ions are marked by small and the O by large solid circles.

uid phase survives¹. In contrast, in the classical case even a small amount of DM interaction induces magnetic ordering [158].

¹Even for spin-1/2 a quantum critical point at $D/J \approx 0.1$ appears and separates the spin liquid and Néel phases [155–157].

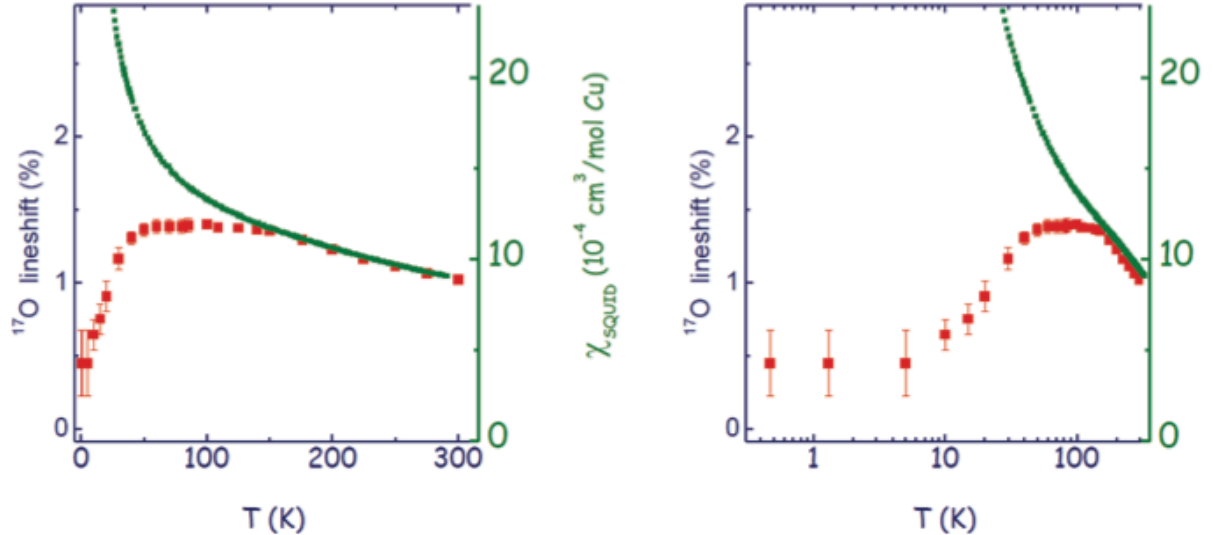


Figure 5.2: Adapted from [151]. Shown, is the variation with temperature, of the susceptibility of the kagomé planes, measured from the ^{17}O NMR shift (in red) and the susceptibility from macroscopic measurements (in green). The difference between the in-plane susceptibility and macroscopic susceptibility is significant, this is because the latter gets significant contributions at low temperature, from out-of-plane defects. The important observation to make is that $T = 0$ susceptibility is non-zero.

5.2 Structural defects in Herbertsmithite

The first class are the out-of-plane defects, where the magnetic Cu^{2+} ions occupy the Zn^{2+} ion positions in between the kagomé layers and therefore behave as quasi-free spin-1/2 moments. The extent of this substitution is estimated to be 15(2)% from X-ray scattering on single crystals [159]. But, it has been argued that these defects have negligible impact on the in-plane kagome physics till temperatures ≈ 1 K, below that temperature there is just an effective interaction between the spin moments.

The other class of defects are the in-plane vacancies, whereby the non-magnetic Zn^{2+} ions occupy the positions in the kagomé layers thereby creating spin vacancies. Their extent is estimated to be $\approx 5\%$ as determined from X-ray scattering [159] and NMR studies [160].

5.3 Nature of the ground state of Herbertsmithite

The physics of the kagomé planes, which is what we are interested in, is best and most reliably captured by local probes, in particular O-nuclei NMR, since oxygen is responsible for providing exchange pathways between two Cu^{2+} ions. The susceptibility measurements using ^{17}O NMR point to a *gapless* ground state of Herbertsmithite [160, 161]. Also, dynamical susceptibility measurements using NMR T_1 and inelastic neutron scattering strongly suggest a gapless ground state [150, 160, 162, 163]. It is also worth mentioning that using optical techniques, in particular Raman spectroscopy, a gapless (in the singlet channel) spin liquid behavior of the algebraic type, has been claimed [14].

From some theoretical studies, it is known that the energy of a particular \mathbb{Z}_2 fully gapped spin liquid [20, 21] and also a 36 site valence bond crystal [141, 142] are lower compared

to the energy of the best gapless spin liquid state, a fact which is in direct contradiction to the experimental findings. The theoretical winner is thus a *gapped* spin liquid ground state, *pro tem*. In *all* experiments carried out on Herbertsmithite, no singlet gap has been observed even way below $J/100$, this fact is inconsistent with the relatively large singlet gap $\approx J/20$ predicted from DMRG studies [20]. Regarding the 36 site valence bond crystal, there is absolutely no signature in the data accumulated on Herbertsmithite to suggest the formation of localized singlets (dimers) being formed in a pattern consistent with the 36 site valence bond crystal. However, it is worth emphasizing that a valence bond crystal may have strong quantum fluctuations which suppress the order parameter, hence such crystals are near the critical point and only *weakly* break translational symmetry, which is extremely difficult to detect and distinguish from spin liquid signals. The possibility of such a valence bond crystal being stabilized cannot thus be categorically ruled out. Exact diagonalization studies, which have now reached cluster sizes of 48 sites, also provide support to the claim that in the thermodynamic limit the ground state can be gapless. So, all in all, the conclusion from the experimental side is that Herbertsmithite is a **gapless spin liquid**. The duty of theory is now to better understand in what manner and how much the ground state of the pure Heisenberg model is affected by the presence of in- and out-of-plane defects and Dzyaloshinskii-Moriya anisotropy.

5.4 Other spin-1/2 kagomé antiferromagnet compounds

Finally, we would like to briefly mention about other spin-1/2 kagomé antiferromagnetic compounds, one is volborthite ($\text{Cu}_3\text{V}_2\text{O}_7(\text{OH})_2 \cdot 2\text{H}_2\text{O}$) featuring a distorted kagomé lattice, but its ground state is magnetic [164–166]. The other compound is vesignieite $\text{Cu}_3\text{Ba}(\text{VO}_5\text{H})_2$ with a nearly ideal kagomé geometry, and nearest neighbor $J' \approx J = 53$ K. A freezing of some percentage of spins has been observed at $T \approx 9\text{K}$, but to categorically establish the nature of the dynamic component exhibiting quantum spin liquid behavior further investigations are needed [167–170]. Another promising and recently proposed candidate is kapellasite ($\text{Cu}_3\text{Zn}(\text{OH})_6\text{Cl}_2$), which is polymorphous to Herbertsmithite and has been shown to exhibit quantum spin liquid behavior of gapless nature down to 20 mK, using inelastic neutron scattering and muon spin relaxation [171–173]. The nearest neighbor exchange couplings in kapellasite are ferromagnetic while further neighbor are antiferromagnetic.

Part III

Research projects

Chapter 6

On the stability of critical spin liquids towards dimerizing into valence-bond crystals for the spin-1/2 Heisenberg antiferromagnet

6.1 Parent spin liquid states

We shall focus on the two energetically lowest, *critical* spin liquids on the kagomé lattice for the spin-1/2 quantum Heisenberg antiferromagnet, these states will be called as parent spin liquids. They are the U(1) Dirac spin liquid ($[0, \pi]$ state) and the uniform RVB spin liquid ($[0, 0]$ state). They belong to the class of non-chiral, space-group symmetric, U(1) gapless spin liquids. The projective symmetry group of the Ansätze (see Fig. 6.1(a)) of both these states permits us to add 2nd nearest neighbor mean field hopping amplitudes ($\chi_{\text{n.n.n.}}$) without changing any of their above mentioned properties, including the Dirac spectrum and the large spinon Fermi surface for the U(1) Dirac spin liquid and the uniform RVB spin liquid, respectively. This extension has the advantage that it leads to considerably lower energies when one adds further neighbor exchange couplings to the Heisenberg antiferromagnetic Hamiltonian.

The addition of 2nd nearest neighbor hopping amplitudes leads to the appearance of two new plaquettes (triangles abc and acd), see Fig. 6.1. Space group symmetric, non-chiral spin liquids may now be labelled by four fluxes, but only three are independent (i.e. by $[\alpha, \beta; \gamma, \delta]$, α and β are fluxes through the original triangles and hexagons, respectively; γ and δ instead are the fluxes through the new triangles abc and acd , respectively). The only possible states built upon the $[0, \pi]$ state are the $[0, \pi; \pi, 0]$ or the $[0, \pi; 0, \pi]$ states, and those built upon the $[0, 0]$ state are the $[0, 0; \pi, \pi]$ or the $[0, 0; 0, 0]$ states, see Fig. 6.1. It is worth noting that for both the Dirac spin liquid and the uniform RVB spin liquid, the two possible extended states with different γ and δ fluxes are related by a change of sign in $\chi_{\text{n.n.n.}}$. Which of the two extended states is energetically lower and is stabilized will depend on the actual value of the ratio J_2/J_1 , at which the “free” variational parameter $\chi_{\text{n.n.n.}}$ is optimized. We purposely restrict our calculations to small enough J_2/J_1 , since for larger 2nd nearest neighbor couplings (of both antiferromagnetic and ferromagnetic type), it is probable that Néel states are energetically favorable, and consequently our treatment using Schwinger fermions becomes insufficient.

The variation of optimized $\chi_{\text{n.n.n.}}$ with J_2 is shown in Fig. 6.2(a). Point D in Figs. 6.2(b)

and 6.3 marks a transition between the $[0, 0; 0, 0]$ and $[0, 0; \pi, \pi]$ states, and point E, the transition between $[0, \pi; 0, \pi]$ and $[0, \pi; \pi, 0]$ states, both occurring at $J_2 \neq 0$. Therefore, we find a finite $\chi_{\text{n.n.n.}}$ even for the nearest neighbor Heisenberg model (see points F and G in Fig. 6.2(b)). Due to negative next nearest neighbor spin-spin correlations of the $[0, \pi]$ state and positive correlations for the $[0, 0]$ state, a level crossing occurs at $J_2/J_1 \approx -0.16$ (see point B in Fig. 6.3) [131]. However, the addition of the next nearest neighbor hopping shifts the level crossing between the two spin liquids, the $[0, 0; 0, 0]$ and $[0, \pi; 0, \pi]$ states to $J_2/J_1 \approx -0.335$ (see point A in Fig. 6.3).

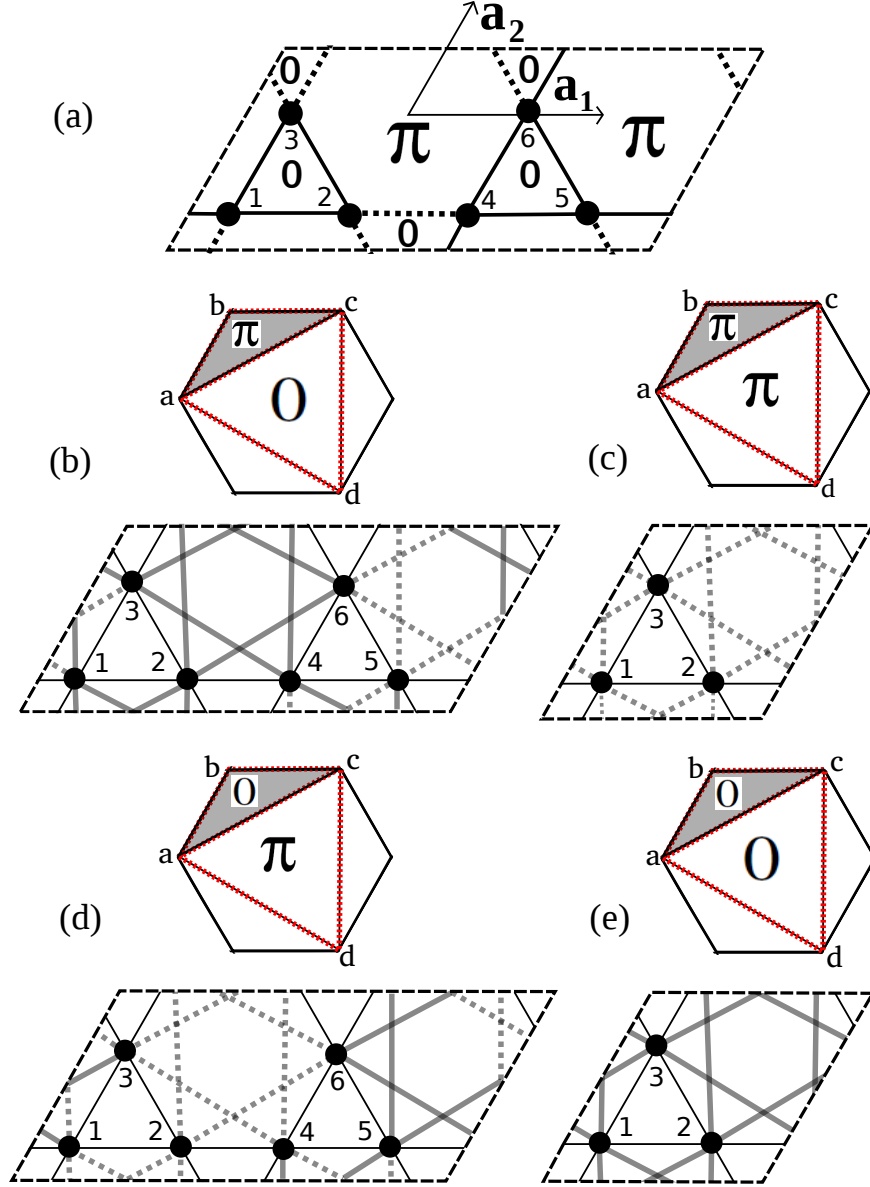


Figure 6.1: (a) The U(1) Dirac spin liquid Ansatz, solid (dashed) bonds denote positive (negative) hoppings. The unit cell is doubled to accommodate the π -flux. The $[0, 0]$ spin liquid Ansatz has all bonds with positive hoppings, and requires only a 3 site cell to be constructed. Cases with next nearest neighbor hoppings are also reported; the only possible non-chiral, space group symmetric states built upon the $[0, \pi]$ state are the $[0, \pi; \pi, 0]$ (b) or the $[0, \pi; 0, \pi]$ (d) spin liquids and those built upon the $[0, 0]$ state are the $[0, 0; \pi, \pi]$ (c) or the $[0, 0; 0, 0]$ (e) spin liquids. The sign convention is the same as in (a).

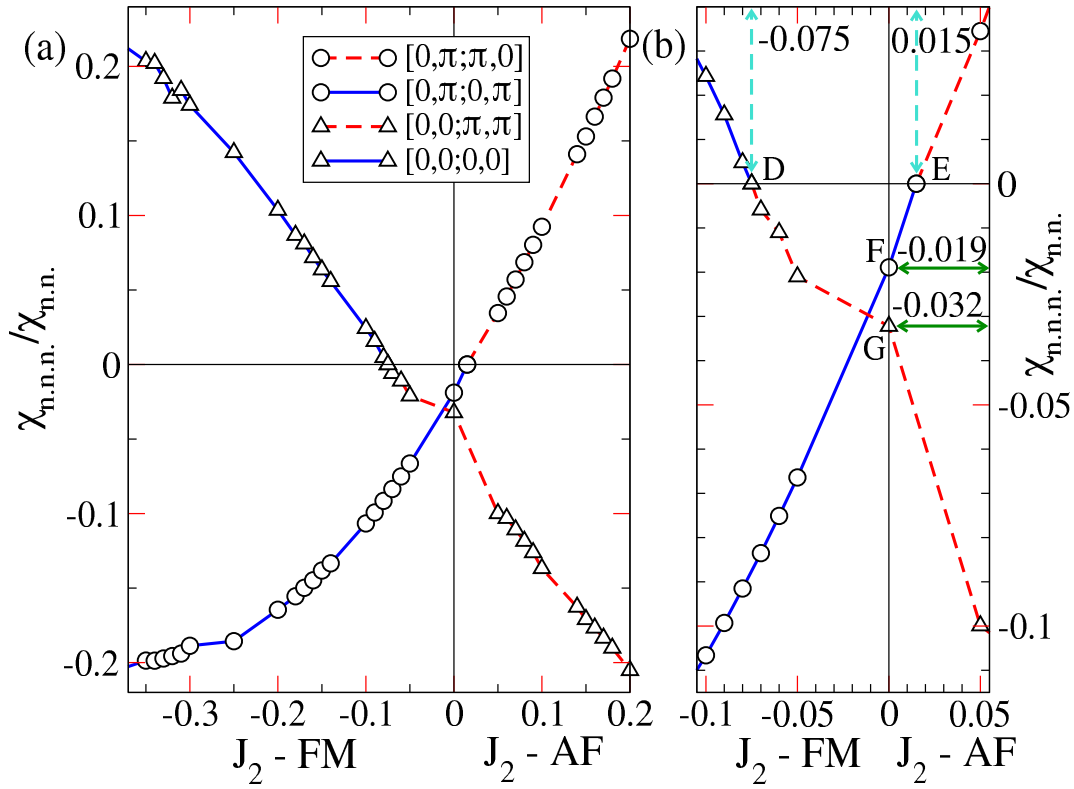


Figure 6.2: (a) Optimized $\chi_{n.n.n.}/\chi_{n.n.}$ versus J_2 for the extended $[0, \pi]$ and $[0, 0]$ states of Fig. 6.1. A zoom around $J_2 = 0$ is shown in (b).

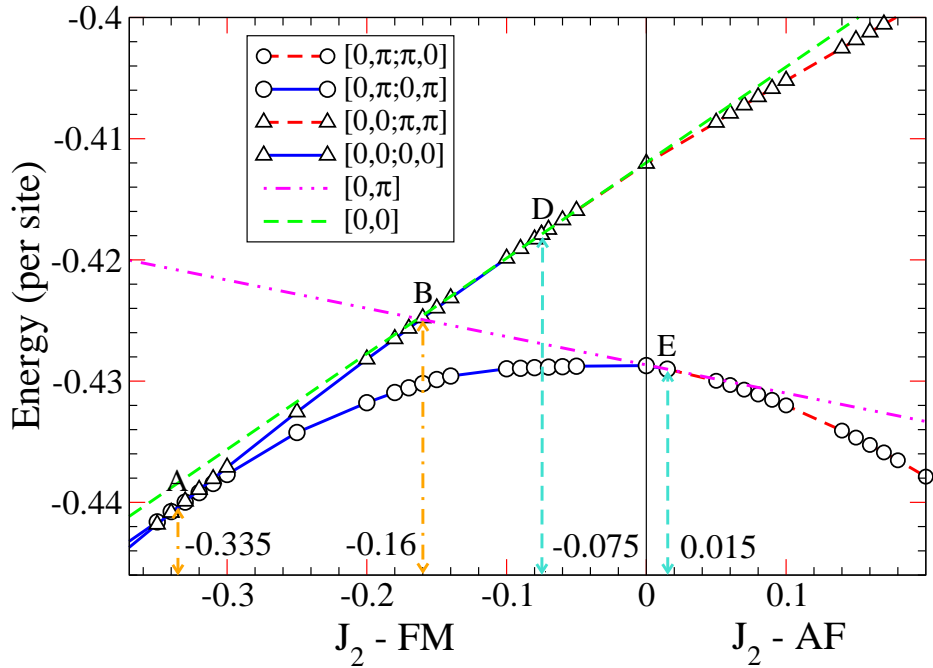


Figure 6.3: Energy versus J_2 for spin liquid states of Fig. 6.1.

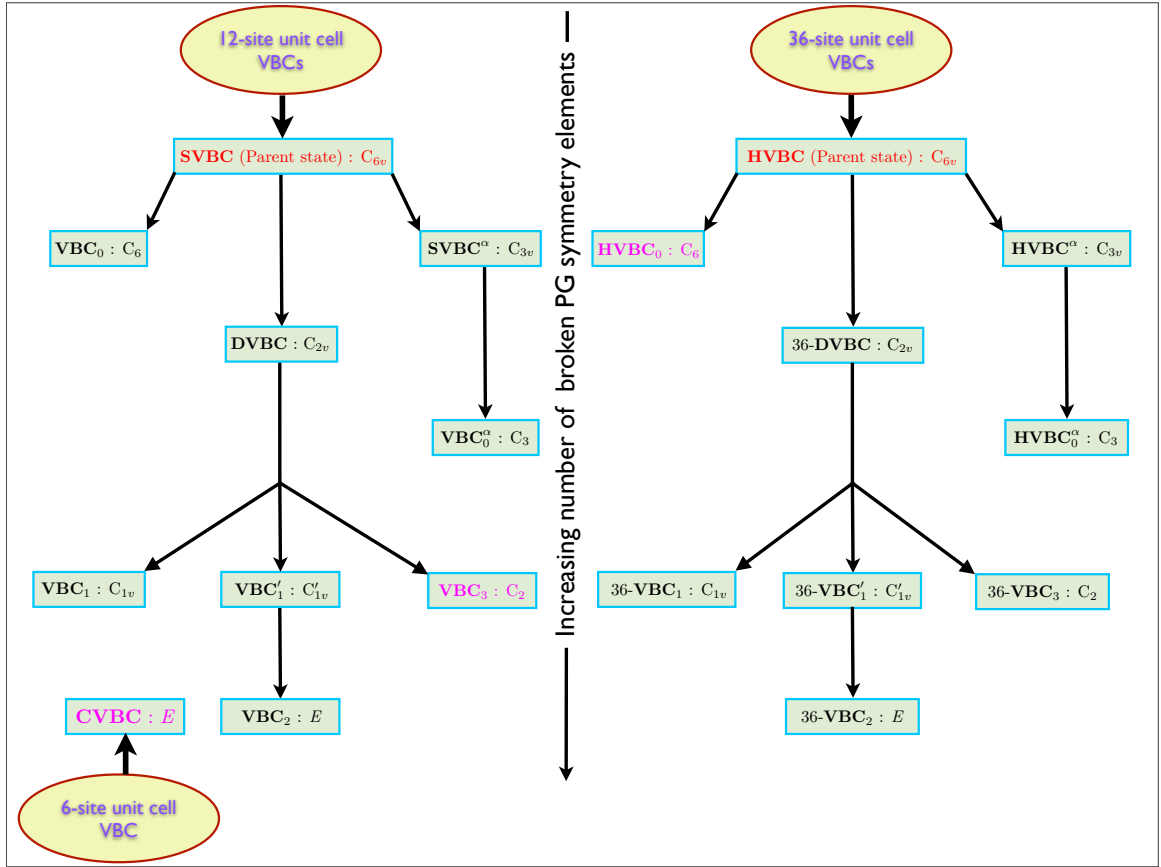


Figure 6.4: A hierarchical flowchart sorting out the myriad of different 6-, 12- and 36-site unit cell VBCs in order of increasing (from top to bottom) number of broken point group (PG) symmetry elements. The square boxes contain the VBC names followed by their respective symmetry point group. The ‘parent’ (maximally symmetric) VBCs are marked in red and those which have been found as competing ground states in studies using quantum dimer models are marked in pink [143–145]. The corresponding VBC patterns and their discussion is given in the text and attached papers (at the end of the chapter). As much as possible, we use labeling for the VBCs which is similar to that used in [145].

6.2 Symmetry classification and enumeration of VBCs

The valence bond crystal states on the kagomé lattice break its elementary (3-site) unit cell translation symmetry with different unit cell sizes which describe their modulation. In previous studies [126, 130, 134, 140, 141, 143–146, 174], using different methods, valence bond crystals with 6-, 12-, 18- and 36-site unit cells were identified as possible ground states of the spin-1/2 quantum Heisenberg antiferromagnet. In this work, we will restrict our analysis to valence bond crystals with 6-, 12- and 36-site unit cells. For each unit cell size with a given center of symmetry, we enumerate valence bond crystals starting from the maximally symmetric (C_{6v}) ‘parent’ valence bond crystal and systematically break point group symmetry elements, right down to the valence bond crystal with no symmetry at all. This results in an enumeration of 19 valence bond crystals in total, 9 valence bond crystals each for the 12 and 36 site unit cells and 1 valence bond crystal for the 6 site unit cell (see Fig. 6.4). Only 6 out of the 19 valence bond crystals have been studied previously. In this chapter, we will study the possibility of any of these valence bond crystals to occur as the ground state.

6.3 The “hot” VBC competitors

A generalized quantum dimer model study [145] found a 6 site unit cell columnar-VBC, a 12 site unit cell VBC, the so called VBC_3 state and a 36 site unit cell VBC called HVBC_0 , to be competing ground states (marked in pink in Fig. 6.4). Also, the DMRG study in Ref. [20] concluded that the 12 site diamond-VBC state is close by in a generalized parameter space. Their symmetry patterns, restricted to nearest neighbor amplitudes are given below and the patterns of rest of the VBCs are given in the papers attached.

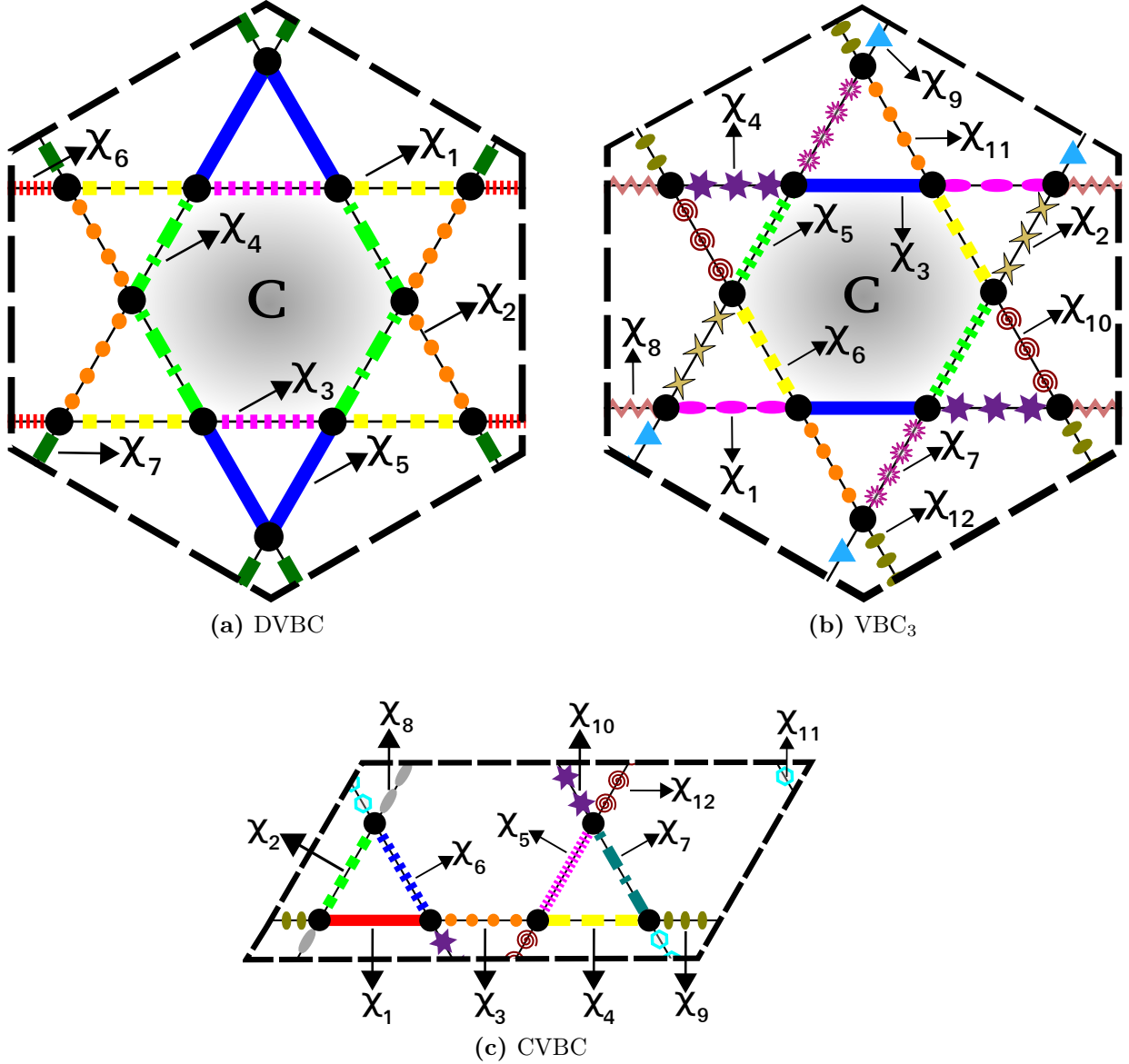


Figure 6.5: Competing VBCs: the center of symmetry is marked ‘C’ (the center of the shaded hexagon), around which bonds connected by the given point group symmetry operations are marked with the same color and style of the line. We will henceforth refer to these bonds as being in the same *class*. (a) The diamond-VBC has two perpendicular axes of reflection symmetry, thus giving rise to C_{2v} symmetry, with 7 classes of bonds. (b) The VBC_3 has only π rotation symmetry, thus its symmetry group is C_2 . It has 12 classes of bonds. (c) The columnar-VBC has no point group symmetries at all, hence all its 12 bonds are different. Its symmetry point group is thus, the identity E .

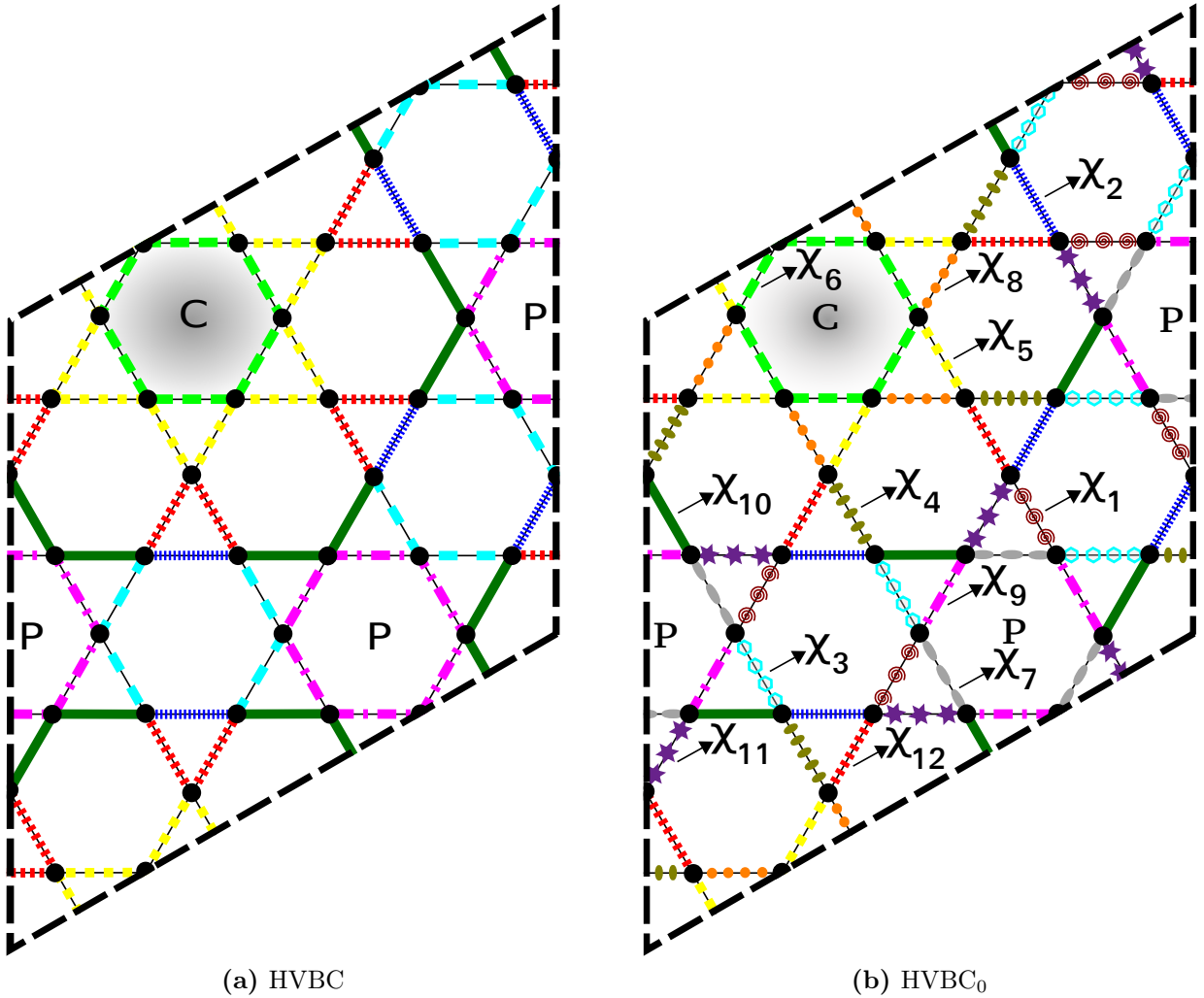


Figure 6.6: The center of symmetry is marked ‘C’ (the center of the shaded hexagon). The *perfect* hexagons, marked at their centers by ‘P’ form a honeycomb lattice at the center of which lie the shaded hexagons. (a) The hexagonal-VBC has the maximal point group symmetry, C_{6v} , hence it acts as a ‘parent’ VBC. Its bonds breakup into 7 distinct classes. (b) The hexagonal-VBC₀, in contrast to the HVBC, lacks reflection symmetries about crystallographic axes, thus its symmetry group is reduced to C_6 . It has 12 classes of bonds.

6.4 General remarks on the VBC classification

It is worth mentioning that this VBC classification (for a given unit cell) is based on very general considerations of symmetry *only* and hence is *not* dependent on the formalism in which one studies these phases. In principle, it is possible to translate its construction from one language (e.g. QDM) to another (e.g. Schwinger fermions or bosons) for a VBC with a given symmetry, as has been done for the above given VBCs. Moreover, within a given framework there can be different ways of constructing wave functions for a given VBC, consistent with its symmetry group. Firstly, one can add amplitudes beyond NN, consistent with the VBC symmetry group. Since we will study these phases within a slave particle approach, one can construct at the naive level simple mean-field wave functions or go much

beyond mean-field and include the effects of full projection. At a next level, it is possible to improve the wave function by applying the Hamiltonian operator on it a given number of times and considering an optimized linear superposition of these wave functions with the original projected wave function. It is also worth noting that this hierarchical sorting of VBCs in each fixed symmetry sector also greatly eases the numerical search for a possible VBC stabilization as the ground state of the spin-1/2 QHAF.

6.5 Numerical results

We studied the relative energetics of the parent spin liquid and *all* VBC phases for the spin-1/2 Heisenberg antiferromagnet using Gutzwiller projected fermionic wave functions with variational quantum Monte Carlo technique. Our variational calculations are done on clusters with 432 (i.e. $3 \times 12 \times 12$) or 576 (i.e. $36 \times 4 \times 4$) sites and mixed periodic-antiperiodic boundary conditions which ensures non-degenerate mean-field wave functions at half filling. The large size of the cluster ensures that the spatial modulations induced in the observables by breaking of rotational symmetry (due to mixed boundary conditions) remain smaller than the uncertainty in the Monte Carlo simulations.

The energy of the nearest neighbor U(1) Dirac spin liquid for the spin-1/2 Heisenberg antiferromagnet, on a 432-site cluster is, energy per site $E/J_1 = -0.42863(2)$ and that of the nearest neighbor uniform RVB spin liquid is slightly higher at, energy per site $E/J_1 = -0.41216(1)$ [12]. For the 576-site cluster these values are $E/J_1 = -0.42866(1)$ for the U(1) Dirac spin liquid and $E/J_1 = -0.41197(1)$ for the uniform RVB spin liquid [19]. The energies of the extended U(1) Dirac and the uniform RVB spin liquid are only slightly lower for the spin-1/2 Heisenberg antiferromagnet, but are considerably lower for the $J_1 - J_2$ spin-1/2 Heisenberg model, for both antiferromagnetic and ferromagnetic 2nd nearest neighbor exchange couplings.

6.5.1 Results on the stability of gapless spin liquids towards VBC perturbations

We carried out an extensive numerical study of the *local* and *global* stability of the nearest neighbor U(1) Dirac and uniform RVB spin liquid towards dimerizing into *all* 6-, 12- and 36-site unit cell VBCs. Our main focus was on the “hot” competitors, that is, the DVBC (Fig. 6.5a), VBC₃ (Fig. 6.5b), CVBC (Fig. 6.5c) and HVBC₀ (Fig. 6.6b) states. We perform our analysis by first fixing a background flux corresponding to the spin liquid whose stability we wish to study. Then, we introduce an amplitude modulation of χ_{ij} consistent with the point group symmetries of the VBC, i.e. bonds belonging to the same *class* (color/line marking in Figs. 6.5 and 6.6) have the same amplitude (χ_λ), which is set to different values for different classes. Starting from an arbitrary unbiased point ($\{\chi_\lambda\}$) in the variational space we perform an optimization of the wave function to obtain the lowest energy state [16, 17].

The case of the U(1) Dirac spin liquid

For the spin-1/2 Heisenberg antiferromagnet, the variation of parameters and energy in the Monte Carlo optimization for the four competing VBCs (regarded as a dimerization of the U(1) Dirac spin liquid) mentioned above is given in figure 6.7. As one can clearly see, the energy converges neatly to the reference value of the nearest neighbor U(1) Dirac spin

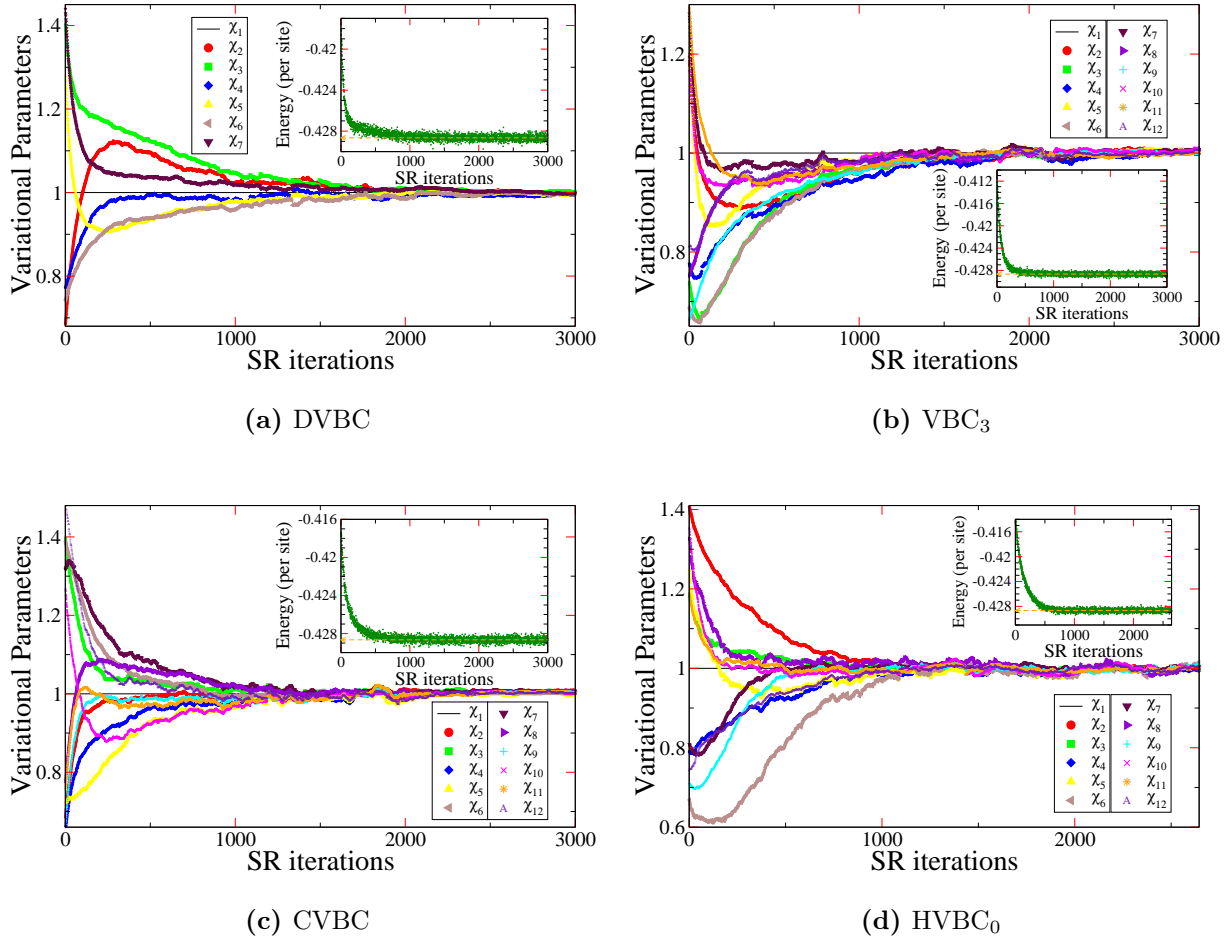


Figure 6.7: A typical variational Monte Carlo optimization run for the DVBC (a), VBC₃ (b), CVBC (c) and HVBC₀ (d) wave functions, for the $S = 1/2$ Heisenberg antiferromagnet. The variational parameters χ_λ and energy (insets) are shown as a function of Monte Carlo iterations. The nearest neighbor U(1) Dirac spin liquid corresponds to $|\chi_\lambda| = 1$. On starting from different sets of initialized parameter values we return back (within error bars) to the U(1) spin liquid. The optimized parameter values are obtained by averaging over a much larger number of converged Monte Carlo iterations than shown above.

liquid, and all the parameters converge to $\chi_\lambda = 1$ (within error bars) after averaging over a sufficient number of converged Monte Carlo steps, thus the translation symmetry associated with the spin liquid state is restored. In fact, we carried out these calculations for all 6-, 12- and 36-site VBCs and found that in each case the U(1) Dirac spin liquid is stable towards opening a gap and destabilizing into any of these VBCs¹. This remarkable stability (for all VBCs) is also preserved upon addition of a 2nd nearest neighbor (J_2) super-exchange coupling in the Hamiltonian of both antiferromagnetic and ferromagnetic type. We verified these results by doing many optimization runs starting from different initial values of the parameters in the respective variational spaces. Thus, we can safely conclude that the U(1) Dirac spin liquid has the lowest variational energy among all proposed competing VBC states, at least within the Schwinger fermion representation of the spin model for J_2 greater than a certain critical value $J_{2,c}$, which is given and discussed in the ensuing text.

¹The SVBC and HVBC states were already ruled out as potential instabilities in earlier studies [12, 19, 131].

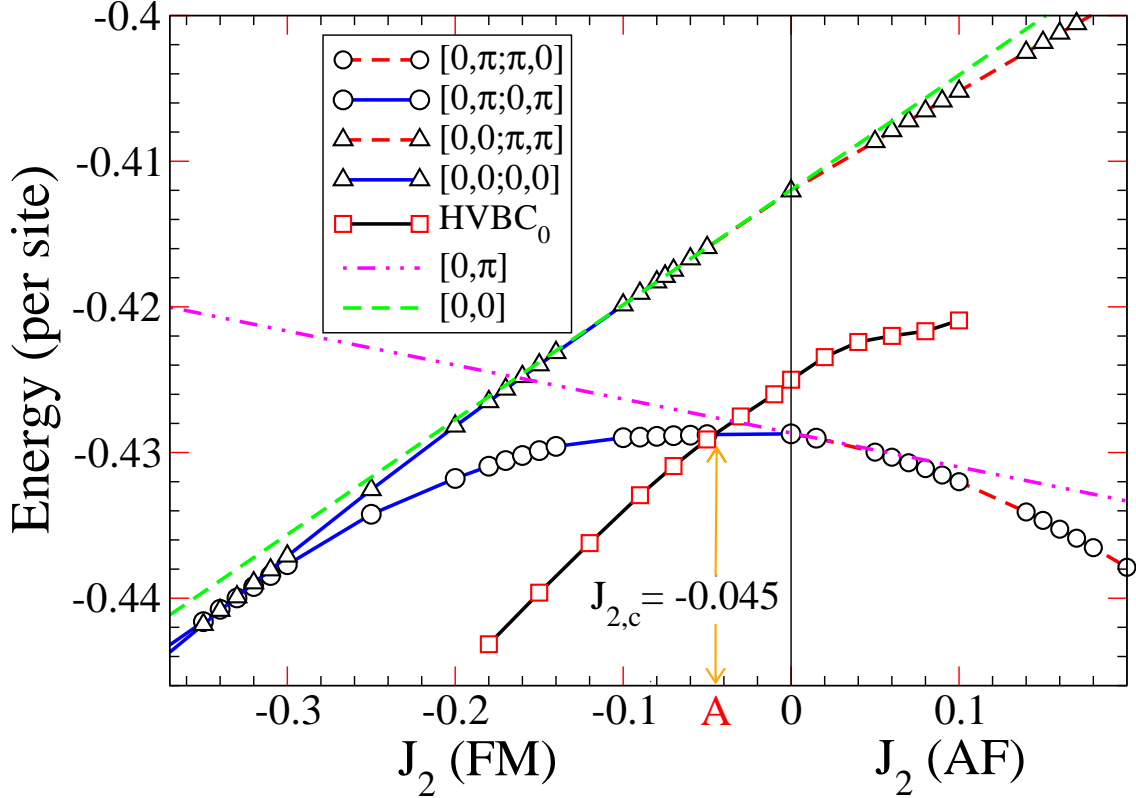


Figure 6.8: Energy versus J_2 for spin liquids of Fig. 6.1 and the HVBC₀ state (Fig. 6.6b). The HVBC₀ state becomes the lowest in energy for $J_2 \lesssim -0.045$. Error bars are smaller than the symbol sizes.

The case of the uniform RVB spin liquid

We now shift our focus to the uniform RVB spin liquid and address the question of its stability. For the spin-1/2 Heisenberg antiferromagnet, including the case in which we have 2nd nearest neighbor exchange couplings (antiferromagnetic and ferromagnetic), we find that *all* 6 and 12 site unit cell VBCs have a higher energy compared to the uniform RVB spin liquid. However, interestingly enough, for the spin-1/2 Heisenberg antiferromagnet, the nearest neighbor uniform RVB spin liquid opens up a gap and destabilizes into a 36 site unit cell VBC, namely the HVBC₀ state (see Fig. 6.6b). The gain in energy due to dimerization becomes more pronounced on addition of 2nd nearest neighbor hopping amplitudes to the wave function which are consistent with C_6 symmetry. On adding a 2nd nearest neighbor exchange coupling of the ferromagnetic type to the Hamiltonian and following this 2nd nearest neighbor HVBC₀ state (now, a dimerization of the extended uniform RVB spin liquid), one finds that it becomes the lowest in energy for $J_2 \lesssim -0.045$ (see point A in Fig. 6.8), consistent with the findings in Ref. [19, 175]. It is worth noting that the symmetry of this VBC is precisely that of the VBC identified in the quantum dimer model study [143–145] and has a lower symmetry compared to the HVBC state that was previously studied by us with similar qualitative conclusions[19]². The flux pattern of this

²The HVBC state has a higher symmetry (C_{6v}) and consequently lesser number of variational parameters compared to the HVBC₀ state (C_6) and hence the level crossing (point A in Fig. 6.8) marking the onset of VBC order was estimated to be higher at $J_{2,c} \approx -0.09$ in our earlier work (see Fig. 3 of [19]).

VBC consists of 0 flux through all elementary triangles and hexagons, and a π -flux through the abc plaquettes (see Fig. 6.1) inside the *perfect* hexagons *only*. Thus, our results still point to a gapless ground state for $J_2 \gtrsim -0.045$, which is along the lines of our previous work [19, 22].

6.6 Conclusions and discussions

We enumerated *all* 6-, 12- and 36-site unit cell VBCs based on symmetry considerations alone and subsequently investigated the possibility of stabilizing any of these VBCs in the spin-1/2 quantum Heisenberg antiferromagnet in the presence of 2nd nearest neighbor exchange couplings of both ferromagnetic and antiferromagnetic type. We found that the U(1) Dirac spin liquid is remarkably robust towards dimerizing into any of these VBCs, for the Heisenberg model, even in the presence of 2nd nearest neighbor ferromagnetic and antiferromagnet exchange couplings. However, the uniform RVB spin liquid dimerized into a 36 site unit cell VBC, which becomes the lowest in energy on addition of a very weak 2nd nearest neighbor ferromagnetic coupling, $J_{2,c} \approx -0.045$. Our systematic and thorough numerical investigation brings us to the conclusion that, at least within the Schwinger fermion approach to the spin model, the U(1) Dirac SL has the best variational energy for $J_2 \gtrsim -0.045$. The conflict of our results, which point towards a gapless ground state in this region and the ones by exact diagonalizations and DMRG calculations, which instead suggested the presence of a fully gapped spectrum remain open and deserve further investigation. One possible direction would be to include *vison* dynamics in the projected wave functions [176], which may be necessary to capture topological order faithfully. Another step would be to improve our variational wave functions based upon the application of a few Lanczos steps [18] and then perform an approximate fixed-node projection technique. The possibility that an unconventional VBC breaking time-reversal symmetry is stabilized as the ground state cannot be ruled out [145]. Finally we mention that VBC order might also set in via confinement transitions of the \mathbb{Z}_2 SLs [177], this remains to be investigated numerically.

6.7 Physical Review B 83, 100404 (2011): Rapid Comm.

Valence-bond crystal in the extended kagome spin-1/2 quantum Heisenberg antiferromagnet: A variational Monte Carlo approach.

Yasir Iqbal, Federico Becca, and Didier Poilblanc

see next page

Valence-bond crystal in the extended kagome spin- $\frac{1}{2}$ quantum Heisenberg antiferromagnet: A variational Monte Carlo approach

Yasir Iqbal,¹ Federico Becca,² and Didier Poilblanc¹

¹*Laboratoire de Physique Théorique UMR-5152, CNRS and Université de Toulouse, F-31062, France*

²*Democritos National Simulation Center, Istituto Officina dei Materiali del CNR and Scuola Internazionale Superiore di Studi Avanzati (SISSA), Via Bonomea 265, I-34136 Trieste, Italy*

(Received 19 November 2010; published 7 March 2011)

The highly frustrated spin- $\frac{1}{2}$ quantum Heisenberg model with both nearest (J_1) and next-nearest (J_2) neighbor exchange interactions is revisited by using an extended variational space of projected wave functions that are optimized with state-of-the-art methods. Competition between modulated valence-bond crystals (VBCs) proposed in the literature and the Dirac spin liquid (DSL) is investigated. We find that the addition of a *small* ferromagnetic next-nearest-neighbor exchange coupling $|J_2| > 0.09J_1$ leads to stabilization of a 36-site unit cell VBC, although the DSL remains a local minimum of the variational parameter landscape. This implies that the VBC is not trivially connected to the DSL; instead it possesses a nontrivial flux pattern and large dimerization.

DOI: 10.1103/PhysRevB.83.100404

PACS number(s): 75.10.Kt, 75.10.Jm, 75.40.Mg

Introduction. It is well known that, on the nonbipartite two-dimensional Kagomé lattice, the combination of low spin ($S = 1/2$), low coordination number ($z = 4$), and frustrating antiferromagnetic (AF) exchange interactions lead to extremely strong quantum fluctuations. It is, however, a widely debated and long-standing theoretical issue whether the ground state of the nearest-neighbor (n.n.) spin- $1/2$ quantum Heisenberg antiferromagnet (QHAF) on the Kagomé lattice is a spin disordered state (quantum spin liquid),^{1,2} which preserves spin rotation and lattice space group symmetry, or instead a valence bond crystal (VBC),³⁻⁷ which breaks lattice symmetries. On the experimental side, studies on a nearly perfect spin- $1/2$ Kagomé compound, Herbertsmithite $\text{ZnCu}_3(\text{OH})_6\text{Cl}_2$,⁸⁻¹⁵ reveal the absence of any spin ordering down to 50 mK despite a sizable n.n. AF exchange coupling ($J \approx 180$ K) between spin- $1/2$ moments of Cu^{2+} . In particular, Raman spectroscopic data on Herbertsmithite points towards a gapless, algebraic spin liquid state.¹⁶ This lends support to the view that the ground state of the n.n. spin- $1/2$ QHAF model on the Kagomé lattice is a long-range resonating-valence bond state. Within a class of variational projected wave functions, a particular gapless spin liquid belonging to the class of algebraic spin liquids, the $U(1)$ Dirac state, has been claimed to possess the lowest energy.^{17,18} In such a state, the (mean-field) Fermi surface collapses to two points, where the spectrum becomes relativistic with Dirac conical excitations. On the contrary, a recent study of the n.n. spin- $1/2$ QHAF model using density-matrix renormalization group (DMRG),¹⁹ establishes the ground state to be a singlet-gapped spin liquid, supposedly with a Z_2 low-energy gauge structure.

From the experimental point of view, the weak ferromagnetism observed in Herbertsmithite has been attributed to the ferromagnetic (FM) nature of the next-nearest-neighbor (n.n.n.) coupling between Cu^{2+} ions in the Kagomé layers. This model was investigated in Ref. 20 by using projected wave functions and it has been found that, above a certain critical n.n.n. FM coupling, a gapless spin liquid with a large circular spinon Fermi surface, named here as uniform projected Fermi sea (PFS), is stabilized as opposed to the $U(1)$ Dirac state. Furthermore, this state undergoes a small dimerization, which

lowers slightly its energy. The same n.n.n. FM model was also recently investigated using a quantum dimer model approach in Ref. 21, showing consistently that a 36-site cell VBC order is favored.

In this Rapid Communication, we revisit the spin- $1/2$ QHAF with the inclusion of n.n.n. exchange interactions using a more extended variational space of projected wave functions that may be optimized by using the technique of Ref. 22. In the following, we will limit to nonmagnetic variational states and, therefore, we will not consider possible instabilities toward magnetically ordered states.²³ Our main result is that the addition of ferromagnetic n.n.n. exchange coupling leads to the stabilization of a 36-site unit cell VBC (in agreement with the results of Ref. 21) over an extended ferromagnetic region which starts from a very weak coupling. Although being a dimerization of the uniform PFS, our VBC does not arise from a local instability of the latter. In other words, it is not trivially connected to it in the variational parameter landscape; instead it possesses a nontrivial flux pattern and dimerization. Moreover, we find that the level crossing between the PFS and the $U(1)$ Dirac state (once suitably extended with n.n.n. hopping) occurs at nearly twice the value previously reported.²⁰ For AF n.n.n. exchange coupling, the inclusion of n.n.n. hoppings in the $U(1)$ Dirac state leads to a considerable lowering in energy, which becomes more pronounced with increasing the AF coupling. Moreover, no VBC order is found in the AF n.n.n. coupling region.

Model and wave function. The Hamiltonian for spin- $1/2$ quantum Heisenberg $J_1 - J_2$ model is

$$\hat{\mathcal{H}} = J_1 \sum_{\langle ij \rangle} \hat{\mathbf{S}}_i \cdot \hat{\mathbf{S}}_j + J_2 \sum_{\langle\langle ij \rangle\rangle} \hat{\mathbf{S}}_i \cdot \hat{\mathbf{S}}_j, \quad (1)$$

where $\langle ij \rangle$ and $\langle\langle ij \rangle\rangle$ denote sums over n.n. and n.n.n. neighbor sites, respectively. In the following, we will consider $J_1 > 0$ and both FM and AF superexchange J_2 ; all energies will be given in units of J_1 .

The variational wave functions are defined by projecting noncorrelated fermionic states:

$$|\Psi_{\text{VMC}}(\chi_{ij}, \Delta_{ij}, \mu)\rangle = \mathcal{P}_G |\Psi_{\text{MF}}(\chi_{ij}, \Delta_{ij}, \mu)\rangle, \quad (2)$$

where $\mathcal{P}_G = \prod_i (1 - n_{i,\uparrow} n_{i,\downarrow})$ is the full Gutzwiller projector enforcing the one fermion per site constraint. Here, $|\Psi_{\text{MF}}(\chi_{ij}, \Delta_{ij}, \mu)\rangle$ is the ground state of mean-field Hamiltonian containing chemical potential, hopping, and pairing terms:

$$\mathcal{H}_{\text{MF}} = \sum_{i,j,\alpha} (-\chi_{ij} + \mu\delta_{ij}) c_{i,\alpha}^\dagger c_{j,\alpha} + \Delta_{ij} c_{i,\alpha}^\dagger c_{j,-\alpha}^\dagger + \text{h.c.} \quad (3)$$

In this work, all states that we consider include hopping terms only (i.e., χ_{ij} up to second neighbors). The effect of including BCS pairing terms is discussed at the end of this Rapid Communication. Cases in which the translational symmetry is explicitly broken will also be considered, so as to include VBC states.

Different spin liquid and VBC phases correspond to different patterns of distribution of χ_{ij} and Δ_{ij} on the lattice bonds; they are the *ansatz* of a given state and serve as the variational parameters that are optimized within the variational Monte Carlo scheme to find the energetically best state.²² It is worth mentioning that this method allows us to obtain an extremely accurate determination of variational parameters. All parameters belonging to one class (i.e., with the same magnitude) are generically labeled as χ_λ .

Results. We have performed our variational calculations on a 576-site (i.e., $36 \times 4 \times 4$) cluster with mixed periodic-antiperiodic boundary conditions. Such a cluster accommodates all possible VBC supercells proposed in the literature. In addition, it ensures nondegenerate wave functions at half-filling.

For n.n. spin-1/2 QHAF, among the class of n.n. translationally symmetric, nonchiral, gapless spin liquids, the $U(1)$ Dirac state is given by the *ansatz* in Fig. 1(a). Due to flux φ being 0 and π [$\exp(i\varphi) = \prod_{\text{plaquette}} \chi_\lambda$] through the triangles and hexagons, respectively, it is denoted as $[0, \pi]$. Its energy per site is $E/J_1 = -0.42866(1)$. The n.n. uniform PFS state has no flux through any plaquette and is therefore denoted as $[0, 0]$; its energy per site is $E/J_1 = -0.41197(1)$.^{17,18} In this work we study only gapless states in particular those with a $U(1)$ low energy gauge structure. However, we believe that by performing a case by case projected wave function study of all possible (a few hundred) Z_2 spin liquids on the Kagomé lattice, one can identify variationally the state found in Ref. 19 using DMRG.

With the aim of investigating the effect of an additional n.n.n. exchange coupling (of both AF and FM type), we first extend the $[0, \pi]$ and $[0, 0]$ states. While previous studies,²⁰ considered wave functions with n.n. couplings only, here we include in addition n.n.n. couplings in the mean-field Hamiltonian (3), which also leads to space group symmetric, nonchiral, gapless spin liquids (see Fig. 1). Two new plaquettes (triangles abc and acd in Fig. 1) appear upon the inclusion of n.n.n. couplings. Space group symmetric, nonchiral spin liquids may now be labeled by four fluxes (but only three are independent) (i.e., by $[\alpha, \beta; \gamma, \delta]$, α and β are fluxes through original triangles and hexagons, respectively; γ and δ instead are fluxes through triangles abc and acd , respectively). The only possible states built upon the $[0, \pi]$ state are $[0, \pi; \pi, 0]$ or $[0, \pi; 0, \pi]$ and those upon the $[0, 0]$ state are $[0, 0; \pi, \pi]$ or $[0, 0; 0, 0]$ (see Fig. 1). Notice that for both DSL and PFS, the two states with different γ and δ fluxes are related by

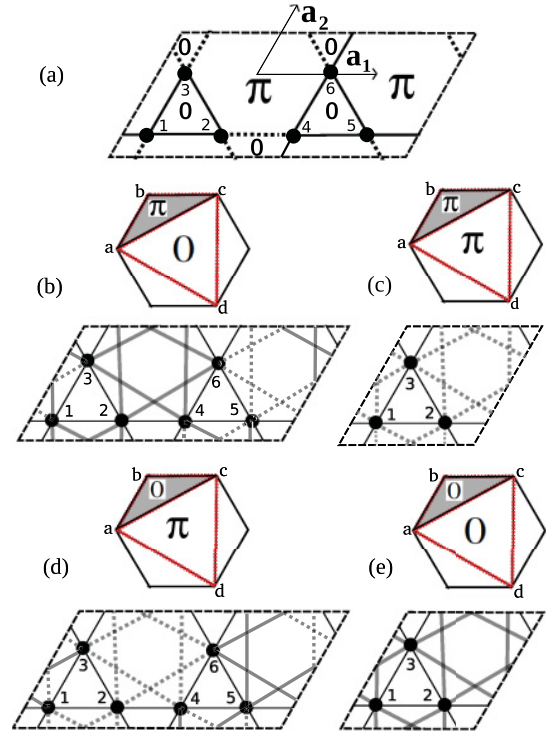


FIG. 1. (Color online) The $U(1)$ DSL *ansatz*, solid (dashed) bonds denote positive (negative) hoppings (a). The unit cell is doubled to accommodate $[0, \pi]$ flux. Cases with n.n.n. hopping are also reported; the only possible (nonchiral) space group symmetric states built upon $[0, \pi]$ state are $[0, \pi; \pi, 0]$ (b) or $[0, \pi; 0, \pi]$ (d) and those upon the uniform $[0, 0]$ state (i.e., PFS) are $[0, 0; \pi, \pi]$ (c) or $[0, 0; 0, 0]$ (e).

a change of sign in $\chi_{\text{n.n.n.}}$. The energetically lower states will depend upon the actual value of the ratio J_2/J_1 . This extension does not modify the topological properties associated with the wave functions, such as the Dirac spectrum and the large spinon Fermi surface. Most importantly, the inclusion of n.n.n. hopping parameters leads to lowering of the variational energies, via an optimal tuning of $\chi_{\text{n.n.n.}}$ as a function of J_2 [see Fig. 2(a)]. It is important to note that we purposely restrict our calculations to small enough J_2/J_1 , since for larger n.n.n. couplings (of both AF and FM type), it is probable that Néel states are energetically favored, and consequently our treatment becomes insufficient.

Point D in Figs. 2(b) and 3 marks a transition between the $[0, 0; 0, 0]$ and $[0, 0; \pi, \pi]$ states, and point E the transition between $[0, \pi; 0, \pi]$ and $[0, \pi; \pi, 0]$ states, both occurring at $J_2 \neq 0$. Therefore, we find a finite $\chi_{\text{n.n.n.}}$ even for the n.n. spin-1/2 QHAF [see points F and G in Fig. 2(b)]. We mention that these extended wave functions with n.n.n. hoppings lead to slightly lower energies, namely $E/J_1 = -0.42872(1)$ for the $[0, \pi; 0, \pi]$ state and $E/J_1 = -0.41209(1)$ for the $[0, 0; \pi, \pi]$ state.

Due to negative n.n.n. spin-spin correlations of $[0, \pi]$ state and positive for the $[0, 0]$ state, a level crossing occurs at $J_2/J_1 \approx -0.16$ ²⁰ (see point B in Fig. 3). However, the addition of the n.n.n. hopping shifts the level crossing between the reference spin liquids, the $[0, 0; 0, 0]$ and $[0, \pi; 0, \pi]$ states to $J_2/J_1 \approx -0.335$ (see point A in Fig. 3).

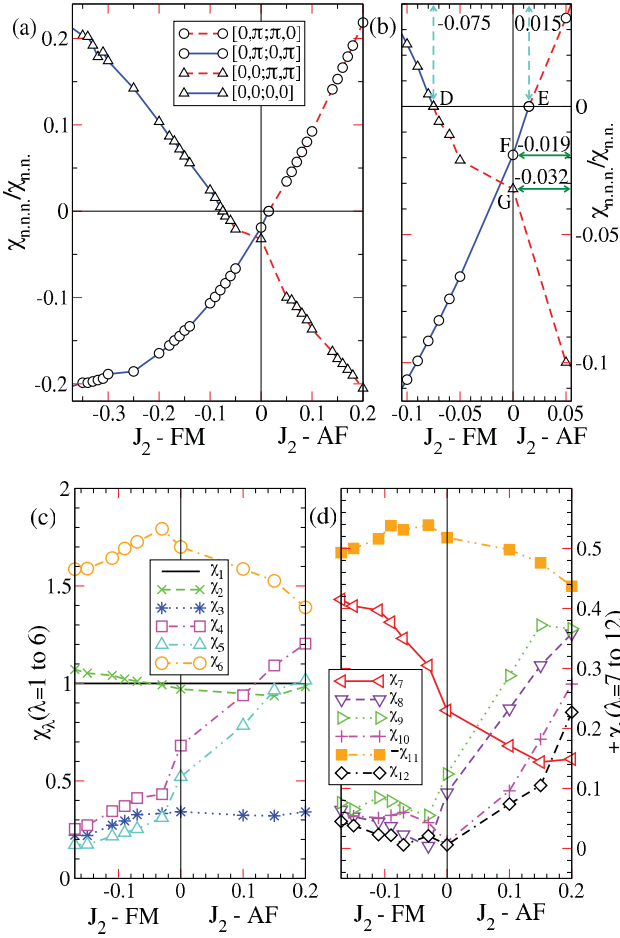


FIG. 2. (Color online) (a) Optimized $\chi_{n.n.n.}/\chi_{n.n.}$ versus J_2 for the extended PFs and DSL states of Fig. 1. A zoom around $J_2 = 0$ is shown in (b). The optimized n.n. (c) and n.n.n. (d) hopping parameters versus J_2 for the 36-site supercell VBC are also reported. $\chi_1 = 1$ is the reference bond. Only $\chi_{11} < 0$, which implies $[0,0;\pi,\pi]$ flux in the P hexagons of Fig. 4.

The question of global and local instability of these spin-liquid states toward a VBC ordering is now thoroughly addressed. In contrast to previous studies,^{17,20} which aimed

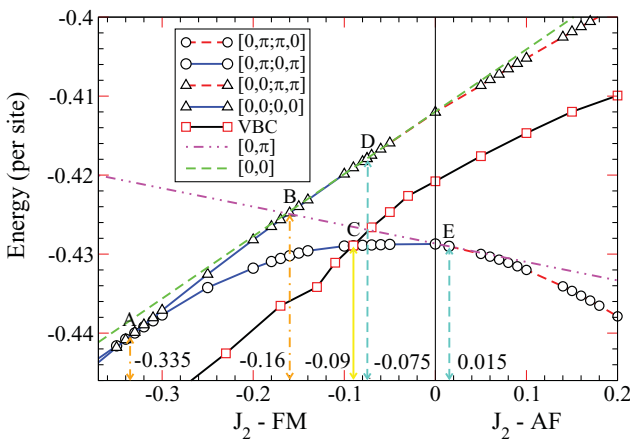


FIG. 3. (Color online) Energy versus J_2 for spin liquid (see Fig. 1) and VBC states [see Figs. 4(c) and 4(d)].

at checking only the local instabilities of spin liquids toward various dimerization patterns via the imposition of a small bond amplitude modulation (5%–10%) of χ_λ , we make a complete optimization of the parameters to detect a possible stabilization of VBC states.

In the 12-site supercell, all bonds connected by D_6 operations have the same magnitude [see Fig. 4(a)], leading to three classes of different bonds. In the 18-site supercell [see Fig. 4(b)], there are only two classes of bonds. In the 36-site supercell with n.n. couplings [see Fig. 4(c)], there are six classes, given the D_6 symmetry about the hexagon C. By adding n.n.n. bonds and preserving this symmetry, we obtain six more independent bonds [see Fig. 4(d)].

In our analysis, we start from a large number of arbitrary different points (amplitude modulation of χ_λ) in the variational space and thoroughly scan the landscape. As a consequence we find that for the n.n. spin-1/2 QHAF, the $[0,\pi]$ and $[0,0]$ states are locally and globally stable with respect to 12-site,⁴ 18-site,^{3,20} and 36-site^{3,5-7} supercell dimerizations. Indeed, the optimization procedure always gives back the uniform $|\chi_\lambda| = 1$ state. We bring attention to the fact that the 36-site supercell considered by us has a much larger variational space

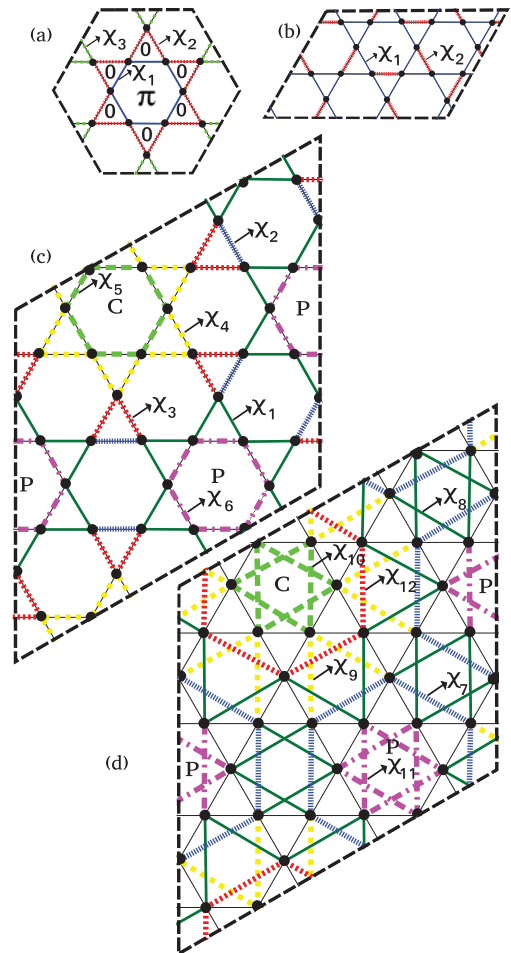


FIG. 4. (Color online) Twelve-site supercell (a) with three different parameters for the hopping; 18-site supercell with two different parameters; 36-site supercell with six n.n. parameters (c), and with six n.n.n. parameters (d).

(six different hoppings) as compared to the ones studied in literature, which considered a dimerization only along the hexagon P in Fig. 4(c).

Upon the inclusion of a finite FM J_2 , we detect the appearance of another competing state with broken symmetries which is stabilized and is the lowest in energy for $J_2 < -0.09$ (see point C in Fig. 3). This state is found to be a 36-site supercell VBC, shown in Figs. 4(c) and 4(d). It breaks translational symmetry in the magnitude of the n.n. and n.n.n. order parameters and the $[\gamma, \delta]$ fluxes but preserves the rotation and reflection symmetry in both magnitude of χ_λ and $[\alpha, \beta; \gamma, \delta]$ fluxes. The corresponding state has 12 different hopping parameters. Although we obtain this VBC as a dimerization of the $[0, 0; 0, 0]$ state, it is not a local instability of it. Instead, it possesses a large bond amplitude modulation in the extended variational space of n.n. and n.n.n. order parameters and selects a flux pattern with $[\gamma, \delta]$ fluxes being $[\pi, \pi]$ in the P hexagons which form a honeycomb lattice [see Fig. 4(d)]. On the contrary, all other hexagons have $[0, 0]$ fluxes. The optimized χ_λ as a function of J_2 are shown in Figs. 2(c) and 2(d). In a previous work, which investigated the effect of a J_2 FM exchange coupling using projected variational wave functions,²⁰ it was found that a dimer modulation leads to an energy minimum at $J_2/J_1 \approx -0.16$, for approximately 4% bond amplitude modulation. In contrast, we

find a different VBC wave function, which is stabilized starting from a very weak FM n.n.n. coupling. As mentioned above, this state possesses a very large 36-site modulation, leading to a significant large gain in energy.

We finish by considering the case of an AF J_2 coupling. Our study reveals the absence of symmetry breaking; instead we find a gapless state with Dirac fermions, the $[0, \pi; \pi, 0]$ state. Upon optimizing $\chi_{n.n.n.}/\chi_{n.n.}$, this state gets a significantly lower energy than the n.n. $[0, \pi]$ state, this gain becoming more pronounced for larger J_2 (see Fig. 3). Finally, the addition of a BCS pairing term of the s -wave type in the $[0, \pi; \pi, 0]$ wave function for J_2 AF is also studied, and our calculations show that such an inclusion always increases the energy. However, the effect of including other forms of pairing terms which might stabilize a gapped spin liquid or a VBC in the J_2 AF model is left as a direction of future research. This might provide a reconciliation with the exact diagonalization results of Ref. 24, which point toward an opening of a gap upon addition of a small AF J_2 coupling.

In summary, we investigated the spin-1/2 QHAF on the Kagomé lattice by using improved variational wave functions. We found that a VBC is stabilized when an n.n.n. ferromagnetic superexchange coupling is considered. This state possesses a nontrivial distribution of hopping parameters and flux pattern.

-
- ¹P. W. Anderson, *Mater. Res. Bull.* **8**, 153 (1973).
²P. W. Anderson, *Science* **235**, 1196 (1987).
³J. B. Marston and C. Zeng, *J. Appl. Phys.* **69**, 5962 (1991).
⁴M. B. Hastings, *Phys. Rev. B* **63**, 014413 (2000).
⁵P. Nikolic and T. Senthil, *Phys. Rev. B* **68**, 214415 (2003).
⁶R. R. P. Singh and D. A. Huse, *Phys. Rev. B* **76**, 180407(R) (2007).
⁷D. Poilblanc, M. Mambrini, and D. Schwandt, *Phys. Rev. B* **81**, 180402(R) (2010); D. Schwandt, M. Mambrini, and D. Poilblanc, *ibid.* **81**, 214413 (2010).
⁸A. Olariu, P. Mendels, F. Bert, F. Duc, J. C. Trombe, M. A. de Vries, and A. Harrison, *Phys. Rev. Lett.* **100**, 087202 (2008).
⁹F. Bert, S. Nakamae, F. Ladieu, D. L'Hôte, P. Bonville, F. Duc, J.-C. Trombe, and P. Mendels, *Phys. Rev. B* **76**, 132411 (2007).
¹⁰P. Mendels, F. Bert, M. A. de Vries, A. Olariu, A. Harrison, F. Duc, J. C. Trombe, J. S. Lord, A. Amato, and C. Baines, *Phys. Rev. Lett.* **98**, 077204 (2007).
¹¹T. Imai, E. A. Nytko, B. M. Bartlett, M. P. Shores, and D. G. Nocera, *Phys. Rev. Lett.* **100**, 077203 (2008).
¹²O. Ofer, A. Keren, E. A. Nytko, M. P. Shores, B. M. Bartlett, D. G. Nocera, C. Baines, and A. Amato, e-print [arXiv:cond-mat/0610540](https://arxiv.org/abs/cond-mat/0610540) (2006).
¹³J. S. Helton, K. Matan, M. P. Shores, E. A. Nytko, B. M. Bartlett, Y. Yoshida, Y. Takano, A. Suslov, Y. Qiu, J.-H. Chung, D. G. Nocera, and Y. S. Lee, *Phys. Rev. Lett.* **98**, 107204 (2007).
¹⁴S.-H. Lee, H. Kikuchi, Y. Qiu, B. Lake, Q. Huang, K. Habicht, and K. Kiefer, *Nat. Mater.* **6**, 853 (2007).
¹⁵M. A. de Vries, K. V. Kamenev, W. A. Kockelmann, J. Sanchez-Benitez, and A. Harrison, *Phys. Rev. Lett.* **100**, 157205 (2008).
¹⁶D. Wulferding, P. Lemmens, P. Scheib, J. Röder, P. Mendels, S. Chu, T. Han, and Y. S. Lee, *Phys. Rev. B* **82**, 144412 (2010).
¹⁷Y. Ran, M. Hermele, P. A. Lee, and X.-G. Wen, *Phys. Rev. Lett.* **98**, 117205 (2007).
¹⁸M. Hermele, Y. Ran, P. A. Lee, and X.-G. Wen, *Phys. Rev. B* **77**, 224413 (2008).
¹⁹S. Yan, D. A. Huse, and S. R. White, e-print [arXiv:1011.6114](https://arxiv.org/abs/1011.6114) (2010).
²⁰O. Ma and J. B. Marston, *Phys. Rev. Lett.* **101**, 027204 (2008).
²¹D. Poilblanc and A. Ralko, *Phys. Rev. B* **82**, 174424 (2010).
²²S. Yunoki and S. Sorella, *Phys. Rev. B* **74**, 014408 (2006).
²³P. Lecheminant, B. Bernu, C. Lhuillier, L. Pierre, and P. Sindzingre, *Phys. Rev. B* **56**, 2521 (1997).
²⁴P. Sindzingre and C. Lhuillier, *Euro. Phys. Lett.* **88**, 27009 (2009).

6.8 New Journal of Physics 14, (2012): Invited paper for special focus issue on Quantum spin liquids

Valence-bond crystals in the kagomé spin-1/2 Heisenberg antiferromagnet: a symmetry classification and projected wave function study.

Yasir Iqbal, Federico Becca, and Didier Poilblanc

see next page

Valence-bond crystals in the kagomé spin-1/2 Heisenberg antiferromagnet: a symmetry classification and projected wave function study

Yasir Iqbal¹, Federico Becca² and Didier Poilblanc¹

¹ Laboratoire de Physique Théorique UMR-5152, CNRS and Université de Toulouse, F-31062 Toulouse, France

² Democritos National Simulation Center, Istituto Officina dei Materiali del CNR, Via Bonomea 265, I-34136 Trieste, Italy

E-mail: iqbal@irsamc.ups-tlse.fr, becca@sissa.it and didier@irsamc.ups-tlse.fr

New Journal of Physics **14** (2012) 000000 (15pp)

Received 19 March 2012

Published xxx

Online at <http://www.njp.org/>

doi:10.1088/1367-2630/14/6/000000

Abstract. In this paper, we do a complete classification of valence-bond crystals (VBCs) on the kagomé lattice based on general arguments of symmetry only and thus identify many new VBCs for different unit cell sizes. For the spin-1/2 Heisenberg antiferromagnet, we study the relative energetics of competing gapless spin liquids (SLs) and VBC phases within the class of Gutzwiller-projected fermionic wave functions using variational Monte Carlo techniques, hence implementing exactly the constraint of one fermion per site. By using a state-of-the-art optimization method, we conclusively show that the U(1) Dirac SL is remarkably stable towards dimerizing into all 6-, 12- and 36-site unit cell VBCs. This stability is also preserved on addition of a next-nearest-neighbor super-exchange coupling of both antiferromagnetic and ferromagnetic (FM) type. However, we find that a 36-site unit cell VBC is stabilized on addition of a very small next-nearest-neighbor FM super-exchange coupling, i.e. $|J_2| \approx 0.045$, and this VBC is the same in terms of space-group symmetry as that obtained in an effective quantum dimer model study. It breaks reflection symmetry, has a nontrivial flux pattern and is a strong dimerization of the uniform RVB SL.

Contents

1. Introduction	2
1.1. The model, wave functions and the numerical technique	3
1.2. Parent spin liquid (SL) states	4
2. Symmetry classification and enumeration of valence-bond crystals (VBCs)	5
2.1. The 12-site unit cell VBCs	5
2.2. The 36-site unit cell VBCs	6
2.3. General remarks on the VBC classification	7
3. Numerical results	9
3.1. Results on the stability of gapless SLs toward VBC perturbations	10
4. Conclusions and discussions	13
Acknowledgments	14
References	14

1. Introduction

For many decades, physicists have been actively searching for playgrounds that are ‘hot’ enough to melt magnetic freezing at temperatures well below the characteristic interaction energy scales in the system. This melting being fueled by quantum fluctuations leads to stabilization of exotic quantum paramagnetic phases of matter [1]. Representatives of such phases are spin liquids (SLs) and valence-bond crystals (VBCs); the former preserve lattice symmetries and the latter break them, according to a generally accepted definition. Long before any experimental hints, theoreticians such as Pomeranchuk already conjectured the existence of SLs [2], which were later advocated by Anderson to be possible appropriate ground states for the spin-1/2 Heisenberg antiferromagnet [3, 4]. On the experimental side, the drought in the search for SLs ended with the discovery of Herbertsmithite ($\text{ZnCu}_3(\text{OH})_6\text{Cl}_2$), a compound with perfect kagomé lattice geometry, belonging to the paratacamite family [5–13]. In it, the combination of low spin value ($S = 1/2$), low dimensionality ($d = 2$) and coordination number ($z = 4$) and frustrating nearest-neighbor (NN) antiferromagnetic (AF) super-exchange interactions on a non-bipartite lattice leads to the amplification of quantum fluctuations that stabilize a quantum paramagnet. Indeed, all experimental probes on Herbertsmithite point to a SL behavior down to 20 mK ($\sim J/10^4$), which was established on the magnesium version of Herbertsmithite (i.e. $\text{MgCu}_3(\text{OH})_6\text{Cl}_2$) [14–16]. Furthermore, Raman spectroscopic studies on Herbertsmithite hint at a gapless (algebraic) SL [17].

On the theoretical side however, the nature of the ground state of the NN spin-1/2 quantum Heisenberg antiferromagnet (QHAF) on the kagomé lattice is still elusive and intensively debated. Exact diagonalization studies have revealed a magnetically disordered ground state and a huge number of singlet excitations below the triplet gap [18–31]. Using approximate numerical techniques various claims as to the nature of the ground state have been made. These have included, among SL phases, a gapless (algebraic) U(1) Dirac SL using projected fermionic variational Monte Carlo [32–36], a gapped \mathbb{Z}_2 SL [37–39] using density matrix renormalization group (DMRG) [40, 41] and a chiral topological SL using Schwinger boson mean field theory [42]. Among the VBC phases, the proposals have included a 36-site unit cell VBC [43, 44] numerically studied using series expansion [45, 46], multi-scale entanglement

renormalization ansatz (MERA) [47] and also using quantum dimer models (QDM) [48–50]. Furthermore, VBCs with smaller unit cells of 6 sites [51], 12 sites [52–54] and 18 sites [43] were also argued to be viable ground states of the spin-1/2 QHAF. A more recent generalized QDM study found a new (possibly chiral) VBC of a 12-site unit cell to be competing with the 36-site unit cell VBC. It also established an extensive quasi-degeneracy of the ground state manifold of the kagomé $S = 1/2$ QHAF with a stiff competition between several phases [55].

In this work, we will study these non-magnetic phases within a Schwinger fermion formulation of the spin model. Within this approach, the *projected* gapless (algebraic) U(1) Dirac SL has the best variational energy [32]; despite being a marginally stable phase, it was argued in [33] to be stable against a certain class of perturbations. Explicit numerical calculations using projected wave functions have in fact shown it to be stable (*locally* and *globally*) w.r.t. dimerizing into all known VBC perturbations [32, 34, 35]. Furthermore, it was shown that within this class of Gutzwiller projected wave functions, all the fully symmetric gapped \mathbb{Z}_2 SLs have a higher energy compared to the U(1) Dirac SL [36]. Similar conclusions were also reached within the Schwinger boson approach to the spin model [56, 57]. Note that a simple tensor network (PEPS) representation of such a projected bosonic RVB ansatz can be constructed and has been studied in [58].

In this paper, in section 2 we first perform a systematic symmetry classification of VBC patterns on the kagomé lattice and thus identify and enumerate many new VBCs, independent of the formalism used to study them. In section 3, we address the question of relative energetics of SL and VBC phases. In particular, in section 3.1.1 we show that the U(1) Dirac SL is remarkably stable w.r.t. dimerizing into any of these new VBCs. This stability is also preserved upon addition of a finite next-nearest-neighbor (NNN) super-exchange coupling of both AF and ferromagnetic (FM) type. Such an NNN coupling might be a possible perturbation in Herbertsmithite. In section 3.1.2, we show that a broken symmetry phase is stabilized on addition of a small NNN FM coupling, which is consistent with the findings in [59]. This VBC has a 36-site unit cell with a non-trivial flux pattern threading its plaquettes and it is found to be a strong dimerization of another competing U(1) gapless SL, the so-called uniform RVB SL [32]. This 36-site unit cell VBC has a lower symmetry as compared to that studied in our previous work [35] and has precisely the same symmetry as that identified in QDM studies [49, 50, 55]. Thus, here we mainly establish the stability of the U(1) Dirac SL w.r.t. an extremely large class of potential VBC instabilities and detect a non-trivial 36-site unit cell VBC instability of the uniform RVB SL which is stabilized on addition of a very weak NNN FM super-exchange coupling to the Hamiltonian.

1.1. The model, wave functions and the numerical technique

The Hamiltonian for the spin-1/2 quantum Heisenberg $J_1 - J_2$ model is

$$\hat{\mathcal{H}} = J_1 \sum_{\langle ij \rangle} \hat{\mathbf{S}}_i \cdot \hat{\mathbf{S}}_j + J_2 \sum_{\langle\langle ij \rangle\rangle} \hat{\mathbf{S}}_i \cdot \hat{\mathbf{S}}_j, \quad (1)$$

where $\langle ij \rangle$ and $\langle\langle ij \rangle\rangle$ denote sums over NN and NNN pairs of sites, respectively. The $\hat{\mathbf{S}}_i$ are spin-1/2 operators at each site i . In the following, we will consider $J_1 > 0$ (AF) and both FM and AF super-exchange J_2 ; all energies will be given in units of J_1 .

The physical variational wave functions are defined by projecting noncorrelated fermionic states:

$$|\Psi_{\text{VMC}}(\chi_{ij}, \Delta_{ij}, \mu, \zeta)\rangle = \mathcal{P}_{\text{G}}|\Psi_{\text{MF}}(\chi_{ij}, \Delta_{ij}, \mu, \zeta)\rangle, \quad (2)$$

where $\mathcal{P}_{\text{G}} = \prod_i (1 - n_{i,\uparrow} n_{i,\downarrow})$ is the full Gutzwiller projector enforcing the one fermion per site constraint. Here, $|\Psi_{\text{MF}}(\chi_{ij}, \Delta_{ij}, \mu, \zeta)\rangle$ is the ground state of a mean-field Hamiltonian constructed out of Schwinger fermions and containing hopping, chemical potential and singlet pairing terms:

$$\mathcal{H}_{\text{MF}} = \sum_{i,j,\alpha} (\chi_{ij} + \mu \delta_{ij}) c_{i,\alpha}^\dagger c_{j,\alpha} + \sum_{i,j} \{(\Delta_{ij} + \zeta \delta_{ij}) c_{i,\uparrow}^\dagger c_{j,\downarrow}^\dagger + h.c.\}, \quad (3)$$

where $\chi_{ij} = \chi_{ji}^*$ and $\Delta_{ij} = \Delta_{ji}$. Besides the chemical potential μ , we will also consider real and imaginary components of on-site pairing, which are absorbed in ζ .

The SL phases are characterized by different patterns of distribution of underlying SU(2) gauge fluxes through the plaquettes which are implemented by a certain distribution of the phases of χ_{ij} and Δ_{ij} on the lattice links. Since in a SL state $|\chi_{ij}|^2 + |\Delta_{ij}|^2$ is constant for each geometrical distance, a complete specification of a SL state up to n th NN amounts to specifying, in addition to the SU(2) fluxes, the optimized magnitude of hopping and pairing parameters at each geometrical distance and the specification of the on-site terms μ and ζ [60, 61]. On the other hand, in a VBC state $|\chi_{ij}|^2 + |\Delta_{ij}|^2$ may be different from bond to bond and, therefore, the specification of VBCs amounts to giving the pattern of amplitudes of χ_{ij} and Δ_{ij} at each geometrical distance, in addition to specifying the SU(2) fluxes through the plaquettes. These parameters are the ansätze of a given state and serve as the variational parameters in the physical wave function that are optimized within the variational Monte Carlo scheme to find the energetically best state. It is worth mentioning that we use a sophisticated implementation of the stochastic reconfiguration (SR) optimization method which allows us to obtain an extremely accurate determination of variational parameters [62, 63]. Indeed, small energy differences are effectively computed by using a correlated sampling, which makes it possible to strongly reduce statistical fluctuations. This feature is especially important for the spin-1/2 QHAF since the energies of all the competing phases are rather close.

1.2. Parent spin liquid (SL) states

The ansatz for the energetically best variational state, the U(1) Dirac SL, is given in figure 1(a). Due to the U(1) flux φ being 0 and π [$\exp(i\varphi) = \prod_{\text{plaquette}} \chi_{ij}$] through triangles and hexagons, respectively, it is denoted as $[0, \pi]$ SL. In its mean-field band structure the Fermi surface collapses to two points at which the spectrum becomes relativistic with Dirac conical excitations [32]. Another energetically competing state, the uniform RVB SL, has zero flux through all plaquettes and is therefore denoted as $[0, 0]$ SL. Its mean-field band structure consists of large circular spinon Fermi surfaces [34]. Both these states are fully symmetric, U(1) gapless SLs and can be extended to include second NN hoppings, leading to a gain in energy without changing their nature [35]. It is worth noting that the effect of projection on these mean-field states can be drastic.

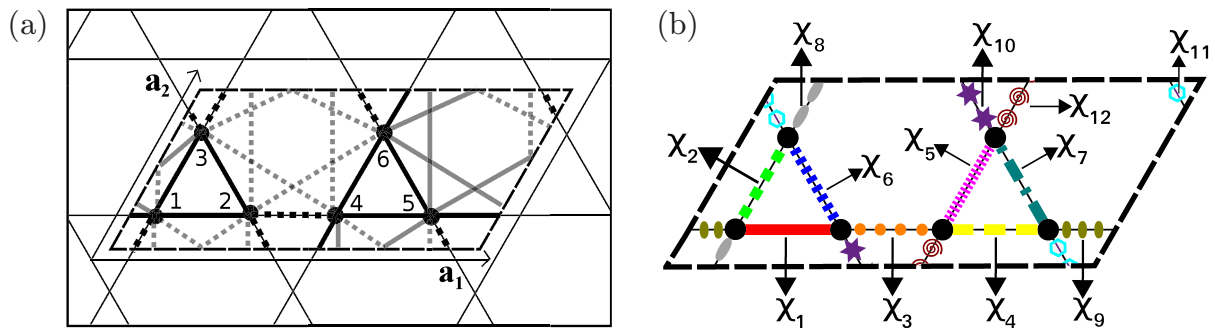


Figure 1. (a) The U(1) Dirac SL ansatz given up to second NN bonds. The unit cell has to be doubled to accommodate the π -flux. The black (gray) bonds denote first NN real hopping (second NN real hopping) terms. The solid (dashed) bonds denote positive (negative) hoppings. (b) The columnar VBC has no (point group) symmetries at all; hence all its 12 bonds are different, which are thus marked with different colors and line styles. Consequently, its symmetry (point) group is the identity E .

2. Symmetry classification and enumeration of valence-bond crystals (VBCs)

The VBC states on the kagomé lattice break its elementary (three-site) unit cell translation symmetry with different unit cell sizes, which describe their modulation. In previous studies [43–45, 47, 49–55], using different methods, VBCs with 6-, 12-, 18- and 36-site unit cells were identified as possible ground states of the spin-1/2 QHAF. In this work, we will restrict our analysis to VBCs with 6-, 12- and 36-site unit cells. For each unit cell size with a given center of symmetry, we enumerate VBCs starting from the maximally symmetric (C_{6v}) ‘parent’ VBC and systematically break point group symmetry elements, right down to the VBC with no symmetry at all. This results in an enumeration of 19 VBCs in total, 9 VBCs each for 12- and 36-site unit cells and 1 VBC for the 6-site unit cell (see figure 2). Only 6 out of the 19 VBCs have been studied previously. In this paper, we will study the possibility of any of these VBCs to occur as the ground state.

2.1. The 12-site unit cell VBCs

The kagomé lattice can be viewed as a triangular lattice of 12-site blocks shaped in the form of ‘stars’. Within this picture, it was argued in [53, 54] that the ground state of the spin-1/2 QHAF has possible long-range singlet order that settles in this triangular star arrangement. This lends support to the picture that the ground state can be a VBC with a 12-site unit cell capturing some modulation. In total, nine symmetry distinct VBCs with a 12-site unit cell can occur; see figures 3 and 4 for their NN patterns. In particular, the SVBC state (figure 3(a)) was argued in [52] to occur as an instability of the U(1) Dirac SL and to be consequently stabilized as the ground state of the NN spin-1/2 QHAF. Numerical studies using projected wave functions have shown this proposal to be incorrect and have also established the stability of the uniform RVB SL w.r.t. dimerizing into the SVBC state [32, 34, 35]. Furthermore, a recent QDM study [55] found the VBC₃ state (figure 4(c)) to be a competing ground state and a DMRG study [41] concluded that the DVBC state (figure 4(b)) is closeby in a generalized parameter space. In

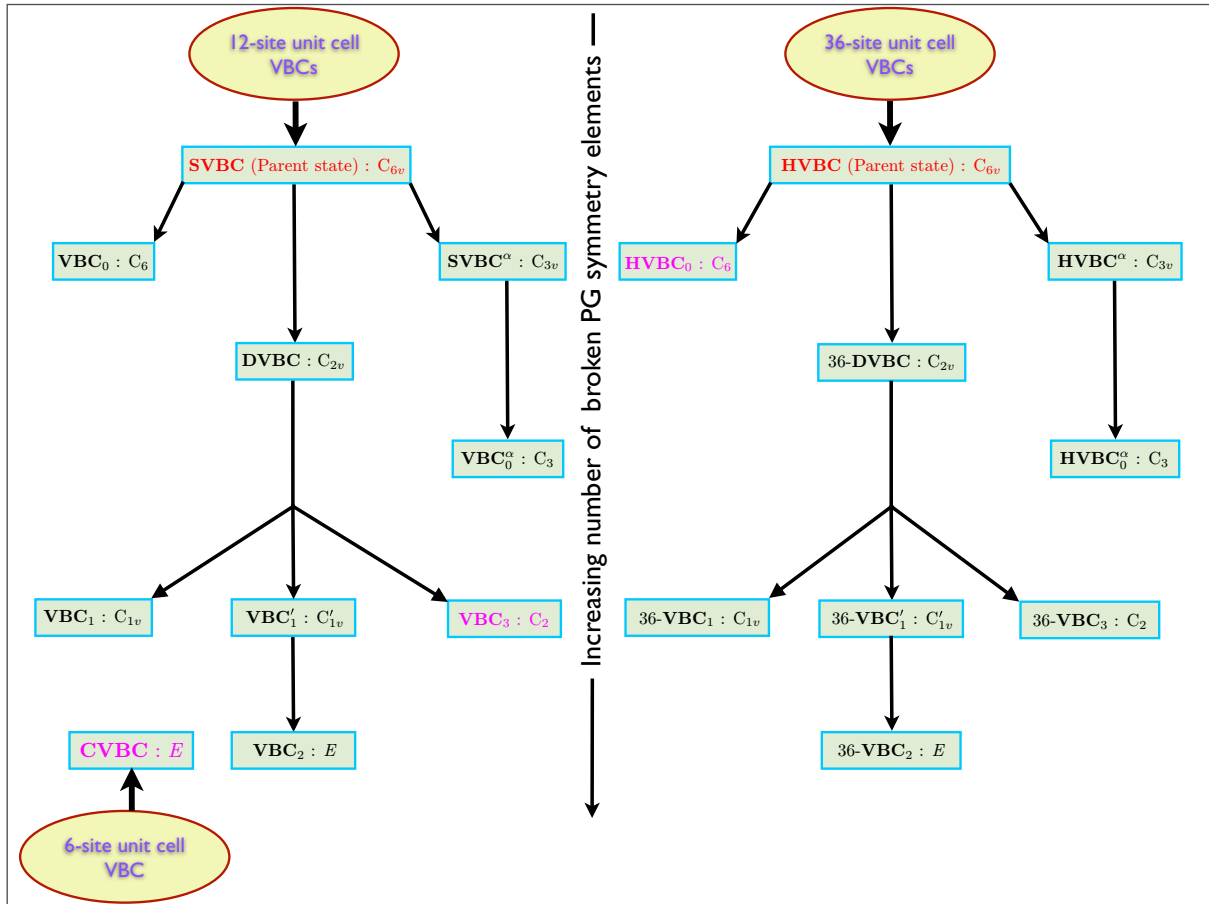


Figure 2. A hierarchical flowchart sorting out the myriad of different 6-, 12- and 36-site unit cell VBCs in order of increasing (from top to bottom) number of broken point group (PG) symmetry elements. The square boxes contain the VBC names followed by their respective symmetry PG. The ‘parent’ (maximally symmetric) VBCs are marked in red and those which have been found as competing ground states in studies using quantum dimer models are marked in pink [49, 50, 55]. The corresponding VBC patterns, and their discussion, are given in the text. As much as possible, we use labeling for the VBCs which is similar to that used in [55].

section 3, we study the possibility of a ground state realization of VBC_3 and DVBC states numerically, within the framework of projected wave functions. In fact, we perform this study for all 12-site unit cell VBCs.

2.2. The 36-site unit cell VBCs

The building blocks of the kagomé lattice can take nontrivial forms such as a $2\sqrt{3} \times 2\sqrt{3}$ expansion of the elementary 3-site unit cell, thus giving rise to a tilted 36-site unit cell. It was shown in [43, 44] that such a construction maximizes the density of hexagons on which dimer resonances occur, thereby lowering the energy. This 36-site unit cell VBC was studied numerically using series expansion [45, 46] and MERA [47], which found it to be a good

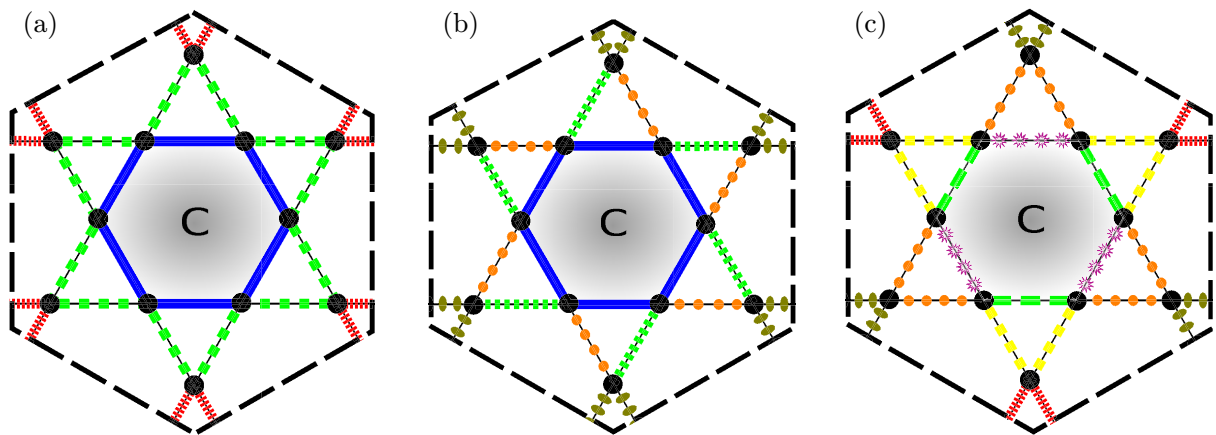


Figure 3. The most symmetric 12-site unit cell VBCs: the center of symmetry is marked ‘C’ (the center of the shaded hexagon), around which bonds connected by the given PG symmetry operations are marked with the same color and style of the line. We will henceforth refer to these bonds as being in the same class. (a) The Star-VBC has the maximal PG symmetry, C_{6v} ; hence it acts as a ‘parent’ VBC. Its bonds break up into three distinct classes. (b) The VBC_0 lacks crystallographic axes reflection symmetries in contrast to the SVBC; thus its symmetry group is reduced to C_6 . It has four classes of bonds. (c) The $Star-VBC^\alpha$ has reduced ($2\pi/3$) rotation symmetry but preserves reflection symmetry; thus its symmetry group is C_{3v} . It has six classes of bonds.

approximation to the ground state of the NN spin-1/2 QHAF. Similar conclusions were also obtained from a QDM study [49, 50, 55]. Motivated by these findings we classify all 36-site unit cell VBC patterns on the kagomé lattice, which leads to the identification of nine symmetry distinct VBCs; see figures 5–7 for their NN patterns.

In our previous work [35] we studied the HVBC state (see figure 5(a)) by using projected wave functions and found it to be higher in energy compared to the gapless SLs. However, the symmetry of the VBC identified in QDM studies [49, 50, 55] is that of the $HVBC_0$ state (see figure 5(b)), which has a lower symmetry compared to the HVBC state. In section 3, we study the possibility of a ground state realization of the $HVBC_0$ state for the NN and NNN spin-1/2 QHAF.

2.3. General remarks on the VBC classification

It is worth mentioning that this VBC classification (for a given unit cell) is based on very general considerations of symmetry *only* and hence is *not* dependent on the formalism in which one studies these phases. In principle, it is possible to translate its construction from one language (e.g. QDM) into another (e.g. Schwinger fermions or bosons) for a VBC with a given symmetry. Moreover, within a given framework there can be different ways of constructing wave functions for a given VBC, consistent with its symmetry group. Firstly, one can add amplitudes beyond NN, consistent with the VBC symmetry group. Since we will study these phases within a slave particle approach, one can construct at the naive level simple mean-field wave functions or go much beyond mean-field and include the effects of full projection. At a next level, it is

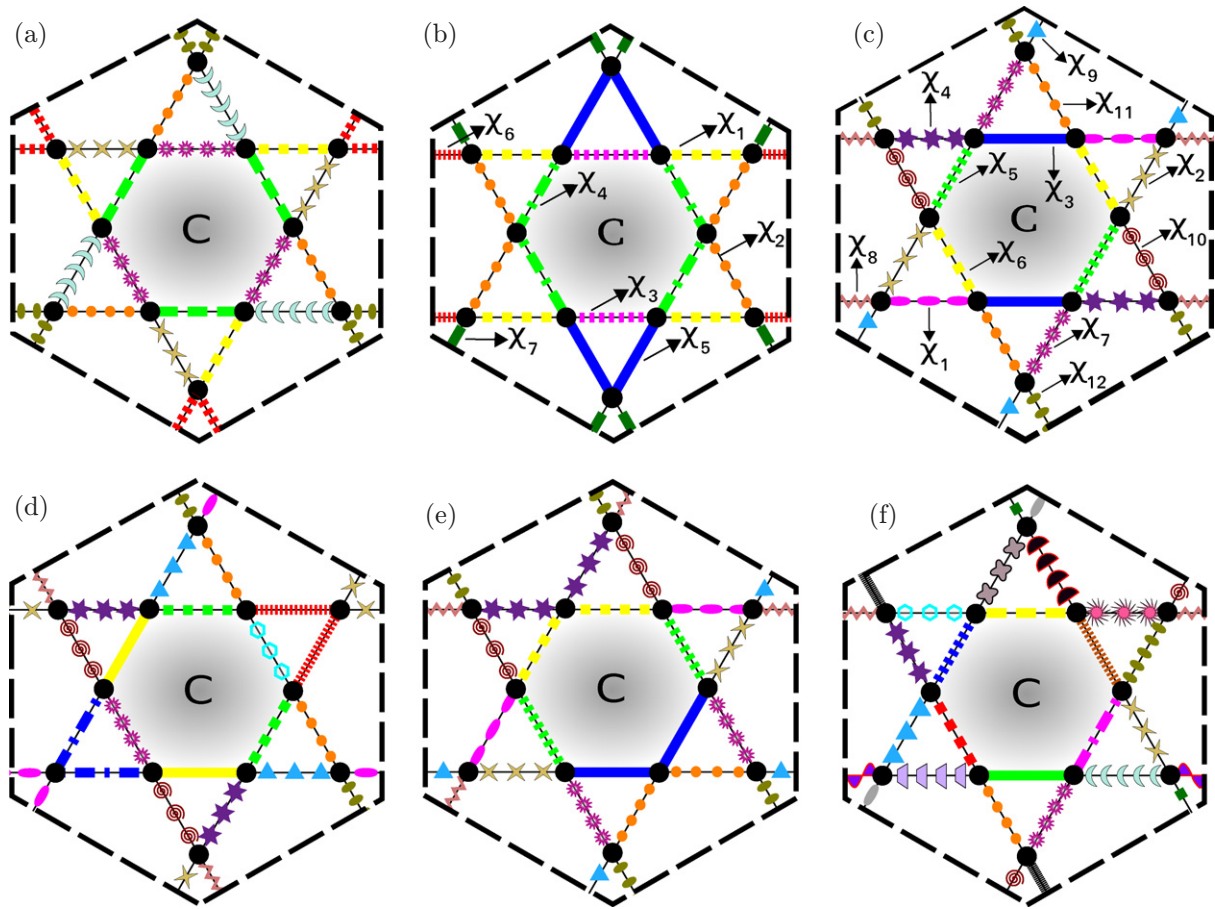


Figure 4. Other 12-site unit cell VBCs: (a) the VBC_0^α has only reduced rotation symmetry ($2\pi/3$); thus in contrast to $SVBC^\alpha$ its symmetry group is reduced to C_3 . It has eight classes of bonds. (b) The diamond-VBC has two perpendicular axes of reflection symmetry, thus giving rise to C_{2v} symmetry, with seven classes of bonds. (c) The VBC_3 has only π -rotation symmetry; thus its symmetry group is C_2 . It has 12 classes of bonds. (d) The VBC_1 possesses only a single axis of reflection symmetry which bisects the sides of the shaded hexagon; consequently, its symmetry group is C_{1v} . It has 14 classes of bonds. (e) The VBC'_1 has the same symmetry as VBC_1 , but its reflection symmetry axis passes through a vertex of the shaded hexagon; we shall denote the symmetry group as C'_{1v} to distinguish it from that of VBC_1 . It has 12 classes of bonds. (f) The VBC_2 has no symmetry whatsoever; hence its symmetry group is just the identity, denoted here as E . Consequently, it has 24 distinct classes of bonds.

possible to improve the wave function by applying the Hamiltonian operator on it a given number of times and considering an optimized linear superposition of these wave functions with the original projected wave function. It is also worth noting that this hierarchical sorting of VBCs in each fixed symmetry sector also greatly eases the numerical search for a possible VBC stabilization as the ground state of the spin-1/2 QHAF.

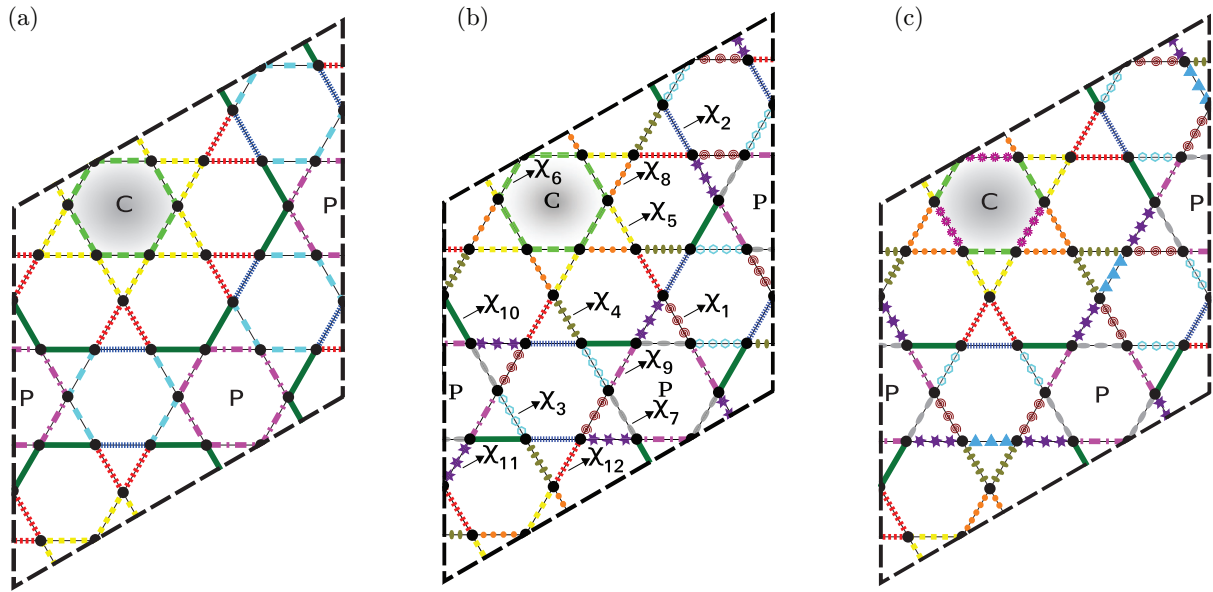


Figure 5. The 36-site unit cell VBCs: the center of symmetry is marked ‘C’ (the center of the shaded hexagon). The perfect hexagons, marked at their centers by ‘P’, form a honeycomb lattice at the center of which lie the shaded hexagons³. (a) The hexagonal-VBC has the maximal PG symmetry, C_{6v} ; hence it acts as a ‘parent’ VBC. Its bonds break up into seven distinct classes. (b) The hexagonal-VBC₀, in contrast to the HVBC, lacks reflection symmetries about crystallographic axes; thus its symmetry group is reduced to C_6 . It has 12 classes of bonds. (c) The HVBC ^{α} has reduced ($2\pi/3$) rotation symmetry but preserves reflection symmetry; thus its symmetry group is C_{3v} . It has 14 classes of bonds.

3. Numerical results

We study the energetics of SL and VBC phases for the spin-1/2 QHAF using Gutzwiller projected fermionic wave functions with the variational quantum Monte Carlo technique. Our variational calculations are performed on clusters with 432 (i.e. $3 \times 12 \times 12$) or 576 (i.e. $36 \times 4 \times 4$) sites and mixed periodic–antiperiodic boundary conditions which ensure non-degenerate mean-field wave functions at half filling. The large size of the cluster ensures that the spatial modulations induced in the observables by breaking of rotational symmetry (due to mixed boundary conditions) remain smaller than the uncertainty in the Monte Carlo simulations.

Among the class of NN fully symmetric and gapless SLs, the U(1) Dirac SL ($[0, \pi]$ SL) has the lowest energy for the NN spin-1/2 QHAF. On a 432-site cluster its energy per site is $E/J_1 = -0.428\,63(2)$ and the uniform RVB SL ($[0, 0]$ SL) has a slightly higher energy per site, $E/J_1 = -0.412\,16(1)$ [32]. For the 576-site cluster these values are $E/J_1 = -0.428\,66(1)$ for the U(1) Dirac SL and $E/J_1 = -0.411\,97(1)$ for the uniform RVB SL [35]. Upon inclusion of NNN hopping amplitudes, one gets the extended U(1) Dirac SL or the extended uniform RVB SL, which are labeled by one additional flux through a plaquette of the type ‘234’ in figure 1(a);

³ The points P are *not* centers of inversion (π -rotation) symmetry, as has been mismarked in figure 1(a) of [55], which corresponds to the HVBC₀ state in this work.

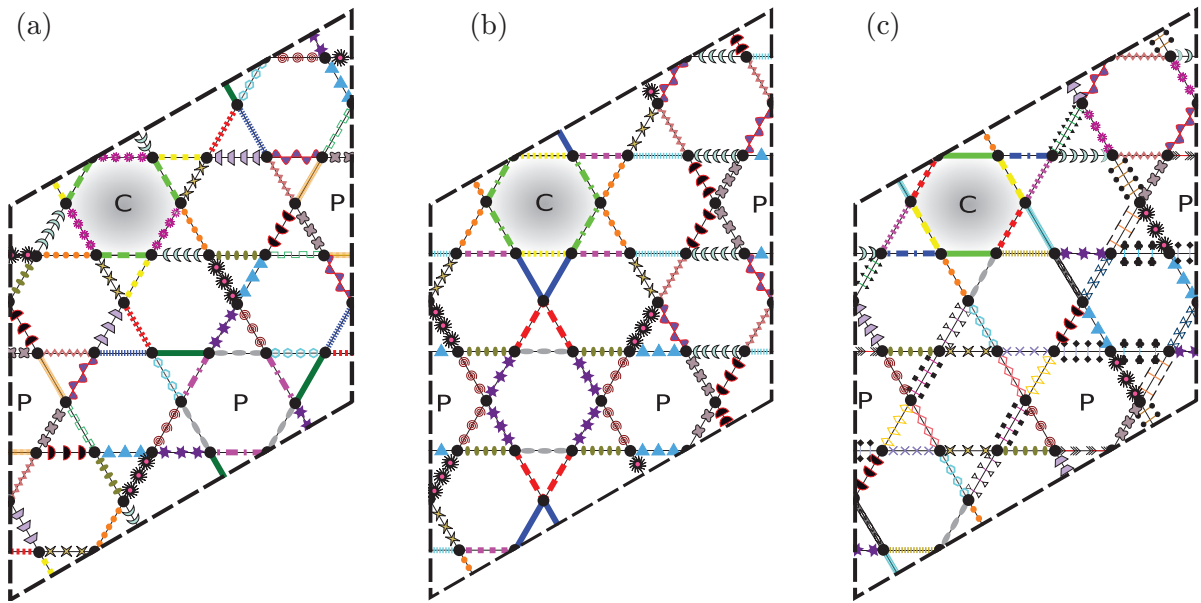


Figure 6. (a) The HVBC_0^α has only a reduced rotation symmetry ($2\pi/3$); thus in contrast to HVBC^α its symmetry group is reduced to C_3 . It has 24 classes of bonds. (b) The 36-diamond-VBC has two perpendicular axes of reflection symmetry, thus giving rise to C_{2v} symmetry, with 19 classes of bonds. (c) The 36-VBC₃ has only π rotation symmetry; thus its symmetry group is C_2 . It has 36 classes of bonds.

the flux through the other triangular plaquette formed by NNN bonds only is then fixed. Hence, the extended Dirac SL can be either the $[0, \pi; \pi, 0]$ or the $[0, \pi; 0, \pi]$ SL and analogously the extended uniform RVB SL can be either the $[0, 0; \pi, \pi]$ or the $[0, 0; 0, 0]$ SL [35]. For the NN spin-1/2 QHAF these extended SLs have a slightly lower energy, but they perform much better for the $J_1 - J_2$ spin-1/2 QHAF, see figure 9.

3.1. Results on the stability of gapless SLs toward VBC perturbations

We carried out an extensive numerical study of the local and global stability of the NN U(1) Dirac and uniform RVB SL toward dimerizing into all 6-, 12- and 36-site unit cell VBCs. In cases where we did find dimerization with NN bond amplitudes, we added second NN bond amplitudes to the SL and VBC ansatz (consistent with symmetries), since this led to a significant gain in energy. Our main focus was on the CVBC (figure 1(b)), DVBC (figure 4(b)), VBC₃ (figure 4(c)) and HVBC_0 (figure 5(b)) states, since these have been identified as ground states of the spin-1/2 QHAF in other studies. We perform our analysis by first fixing a background flux corresponding to the SL liquid whose stability we wish to study. Then, we introduce an amplitude modulation of χ_{ij} consistent with the symmetries of the VBC, i.e. bonds belonging to the same class (color/line marking in figures 1(b) and 3–7) have the same amplitude (χ_λ), which is set to different values for different classes. Starting from an arbitrary unbiased point (χ_λ 's) in the variational space we perform an optimization of the wave function to obtain the lowest energy state [62, 63].

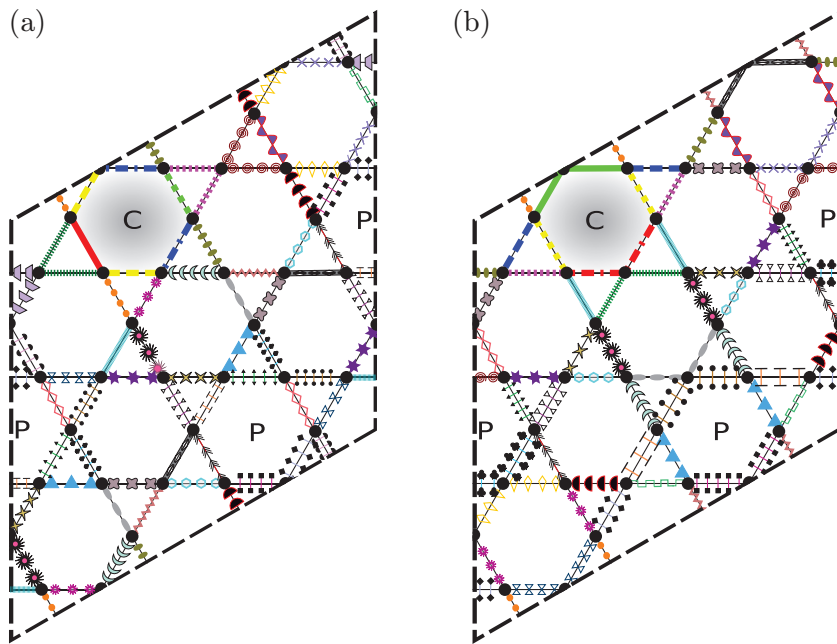


Figure 7. (a) The 36-VBC_1 possesses only a single axis of reflection symmetry, which bisects the sides of the shaded hexagon; consequently, its symmetry group is C_{1v} . It has 38 classes of bonds. (b) The $36\text{-VBC}'_1$ has the same symmetry as 36-VBC_1 , but its reflection symmetry axis passes through a vertex of the shaded hexagon; we shall denote its symmetry group as C'_{1v} to distinguish it from that of 36-VBC_1 . It has 36 classes of bonds. Note that the 36-VBC_2 (which has no symmetry at all) has not been drawn. Its symmetry group is just the identity E . Consequently, it has 72 distinct classes of bonds.

3.1.1. The case of the $U(1)$ Dirac SL. For the NN spin-1/2 QHAF, the variation of parameters and energy in the Monte Carlo optimization for the four competing VBCs (regarded as a dimerization of the $U(1)$ Dirac SL) mentioned above is given in figure 8. As can be clearly seen, the energy converges neatly to the reference value of the $U(1)$ Dirac SL, and all the parameters converge to $\chi_\lambda = 1$ (within error bars) after averaging over a sufficient number of converged Monte Carlo steps; thus the translation symmetry associated with the SL is restored. In fact, we performed these calculations for all 6-, 12- and 36-site VBCs and found that in each case the $U(1)$ Dirac SL is stable towards opening a gap and destabilizing into any of these VBCs. This remarkable stability (for all VBCs) is also preserved upon addition of an NNN (J_2) super-exchange coupling in the Hamiltonian of both AF and FM type. We verified these results by doing many optimization runs starting from different initial values of the parameters in the respective variational spaces. Thus, we can safely conclude that the $U(1)$ Dirac SL has the lowest variational energy among all proposed competing VBC states, at least within the Schwinger fermion representation of the spin model for J_2 greater than a certain critical value $J_{2,c}$, which is given and discussed in the ensuing text.

3.1.2. The case of the uniform RVB SL. We now shift our focus to the uniform RVB SL and address the question of its stability. For the NN and NNN (AF and FM) spin-1/2 QHAF, we find

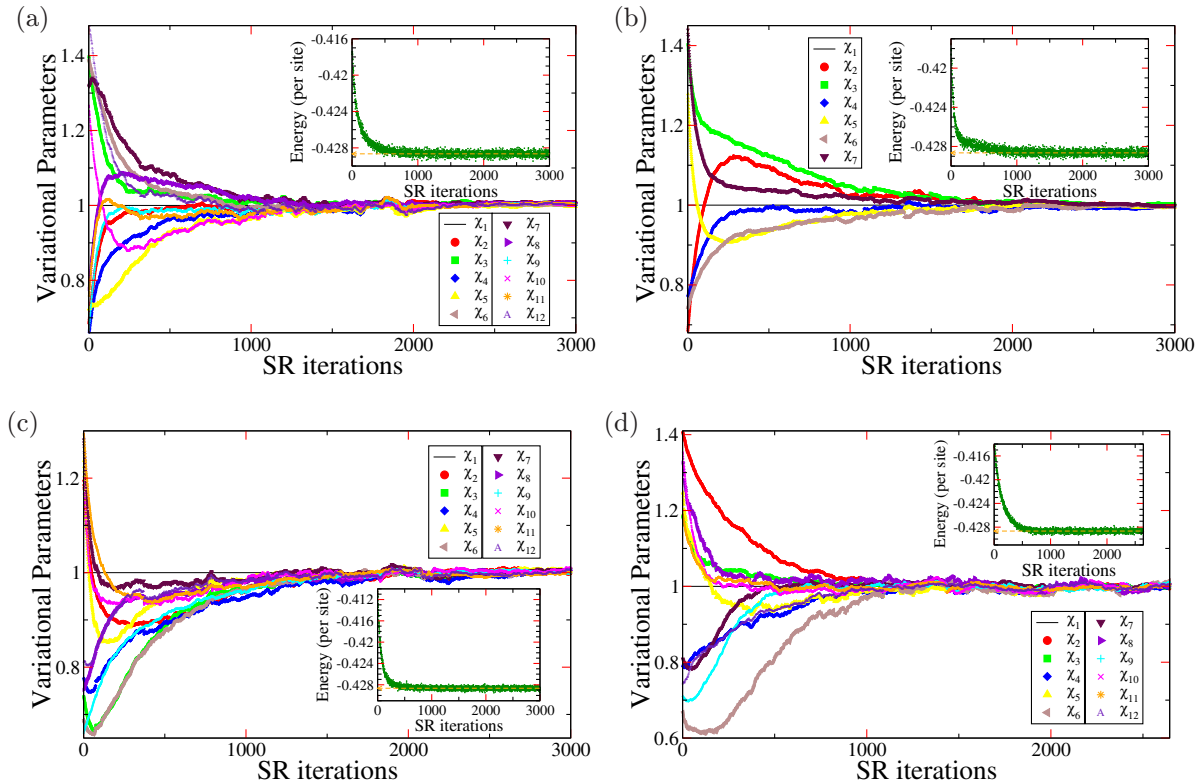


Figure 8. A typical variational Monte Carlo optimization run for the CVBC (a), DVBC (b), VBC₃ (c) and HVBC₀ (d) wave functions, for the NN $S = 1/2$ QHAF. The variational parameters χ_λ and energy (insets) are shown as a function of Monte Carlo iterations. The NN U(1) Dirac SL corresponds to $|\chi_\lambda| = 1$. On starting from different sets of initialized parameter values, we return (within error bars) to the U(1) SL. The optimized parameter values are obtained by averaging over a much larger number of converged Monte Carlo iterations than that shown above.

that *all* 6- and 12-site unit cell VBCs have a higher energy compared to the uniform RVB SL. However, interestingly enough, for the NN spin-1/2 QHAF, this NN uniform RVB SL opens up a gap and destabilizes into a 36-site unit cell VBC, namely the HVBC₀ state (see figure 5(b)). The gain in energy due to dimerization becomes more pronounced on addition of second NN hopping amplitudes to the wave function which are consistent with C₆ symmetry. On adding an NNN super-exchange coupling of FM type to the Hamiltonian and following this second NN HVBC₀ state (now, a dimerization of the extended uniform RVB SL), one finds that it becomes the lowest in energy for $J_2 \lesssim -0.045$ (see point A in figure 9), consistent with the findings in [59]. It is worth noting that the symmetry of this VBC is precisely that of the VBC identified in the QDM study [49, 50, 55] and has a lower symmetry compared to the HVBC state that was previously studied by us with similar conclusions [35]. The flux pattern of this VBC consists of 0 flux through all elementary triangles, hexagons and a π flux through the ‘234’ plaquettes (see figure 1(a)) inside the perfect hexagons only. The lower symmetry of the HVBC₀ compared to the HVBC implies a larger variational space of hopping amplitudes and consequently a lower

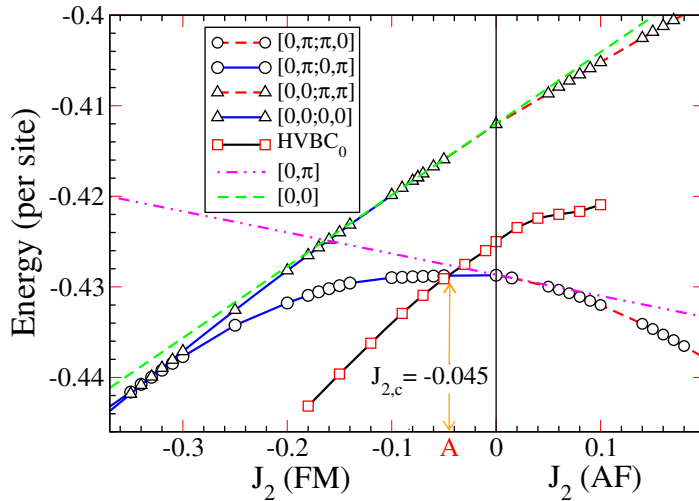


Figure 9. Energy versus J_2 for SLs and the HVBC₀ state (see figure 5(b)). The HVBC₀ state becomes the lowest in energy for $J_2 \lesssim -0.045$. Error bars are smaller than the symbol sizes.

energy that is seen from the fact that the level crossing or the onset of VBC order is shifted from $J_2 \approx -0.09$ [35] for HVBC to $J_{2,c} \approx -0.045$ for HVBC₀ state. Thus our results still point to a gapless ground state for $J_2 \gtrsim -0.045$, which is along the lines of our previous work [35, 36].

4. Conclusions and discussions

In this paper, we enumerated all 6-, 12- and 36-site unit cell VBCs based on symmetry considerations alone and subsequently investigated the possibility of stabilizing any of these VBCs in the NN and NNN spin-1/2 QHAF on a kagomé lattice. We found that the U(1) Dirac SL is remarkably robust toward dimerizing into any of these VBCs, for both the NN and NNN spin-1/2 QHAF. However, the uniform RVB SL dimerizes into a 36-site unit cell VBC, which becomes the lowest in energy on addition of a very weak FM coupling, $J_{2,c} \approx -0.045$. Our systematic and thorough numerical investigation brings us to the conclusion that, at least within the Schwinger fermion approach to the spin model, the U(1) Dirac SL has the best variational energy for $J_2 \gtrsim -0.045$. The conflict between our results, which point to a gapless ground state in this region, and those obtained by exact diagonalizations and DMRG calculations, which instead suggested the presence of a fully gapped spectrum, remains open and deserves further investigation. One possible direction would be to include vision dynamics in the projected wave functions [64], which may be necessary to capture topological order faithfully. Another step would be to improve our variational wave functions based on the application of a few Lanczos steps [65] and then perform an approximate fixed-node projection technique. The possibility that an unconventional VBC breaking time-reversal symmetry is stabilized as the ground state cannot be ruled out [55]. Finally, we mention that VBC order might also set in via confinement transitions of the \mathbb{Z}_2 SLs [66]; this remains to be investigated numerically.

Acknowledgments

YI and DP acknowledge support from the ‘Agence Nationale de la Recherche’ under grant no. ANR 2010 BLANC 0406-0. We are grateful for the permission granted to access the HPC resources of CALMIP under the allocation 2012-P1231.

References

- [1] Balents L 2010 *Nature* **464** 199–208
- [2] Pomeranchuk I 1941 *Zh. Eksp. Teor. Fiz.* **11** 226
- [3] Anderson P W 1973 *Mater. Res. Bull.* **8** 153
- [4] Anderson P W 1987 *Science* **235** 1196–8
- [5] Shores M P, Nytko E A, Bartlett B M and Nocera D G 2005 *J. Am. Chem. Soc.* **127** 13462
- [6] Bert F, Nakamae S, Ladiou F, L’Hôte D, Bonville P, Duc F, Trombe J C and Mendels P 2007 *Phys. Rev. B* **76** 132411
- [7] Lee S H, Kikuchi H, Qiu Y, Lake B, Huang Q, Habicht K and Kiefer K 2007 *Nature Mater.* **6** 853–7
- [8] Lee P A 2008 *Sci., Perspect.* **321** 1306
- [9] de Vries M A, Kamenev K V, Kockelmann W A, Sanchez-Benitez J and Harrison A 2008 *Phys. Rev. Lett.* **100** 157205
- [10] Imai T, Nytko E A, Bartlett B M, Shores M P and Nocera D G 2008 *Phys. Rev. Lett.* **100** 077203
- [11] Olariu A, Mendels P, Bert F, Duc F, Trombe J C, de Vries M A and Harrison A 2008 *Phys. Rev. Lett.* **100** 087202
- [12] Mendels P and Bert F 2010 *J. Phys. Soc. Japan* **79** 011001
- [13] Han T H, Helton J S, Chu S, Prodi A, Singh D K, Mazzoli C, Müller P, Nocera D G and Lee Y S 2011 *Phys. Rev. B* **83** 100402
- [14] Mendels P, Bert F, de Vries M A, Olariu A, Harrison A, Duc F, Trombe J C, Lord J S, Amato A and Baines C 2007 *Phys. Rev. Lett.* **98** 077204
- [15] Helton J S *et al* 2007 *Phys. Rev. Lett.* **98** 107204
- [16] Kermarrec E, Mendels P, Bert F, Colman R H, Wills A S, Strobel P, Bonville P, Hillier A and Amato A 2011 *Phys. Rev. B* **84** 100401
- [17] Wulferding D, Lemmens P, Scheib P, Röder J, Mendels P, Chu S, Han T and Lee Y S 2010 *Phys. Rev. B* **82** 144412
- [18] Elser V 1989 *Phys. Rev. Lett.* **62** 2405
- [19] Zeng C and Elser V 1990 *Phys. Rev. B* **42** 8436
- [20] Chalker J T and Eastmond J F 1992 *Phys. Rev. B* **46** 14201
- [21] Leung P W and Elser V 1993 *Phys. Rev. B* **47** 5459
- [22] Elstner N and Young A P 1994 *Phys. Rev. B* **50** 6871
- [23] Lecheminant P, Bernu B, Lhuillier C, Pierre L and Sindzingre P 1997 *Phys. Rev. B* **56** 2521
- [24] Waldtmann C, Everts H U, Bernu B, Lhuillier C, Sindzingre P, Lecheminant P and Pierre L 1998 *Eur. Phys. J. B* **2** 501
- [25] Sindzingre P, Misguich G, Lhuillier C, Bernu B, Pierre L, Waldtmann Ch and Everts H U 2000 *Phys. Rev. Lett.* **84** 2953
- [26] Waldtmann Ch, Kreutzmann H, Schollwöck U, Maisinger K and Everts H U 2000 *Phys. Rev. B* **62** 9472
- [27] Richter J, Schulenburg J and Honecker A 2004 *Quantum Magnetism (Lecture Notes in Physics vol 645)* (Berlin: Springer) p 85
- [28] Sørensen E S, Lawler M J and Kim Y B 2009 *Phys. Rev. B* **79** 174403
- [29] Sindzingre P and Lhuillier C 2009 *Europhys. Lett.* **88** 27009
- [30] Nakano H and Sakai T 2011 *J. Phys. Soc. Japan* **80** 053704
- [31] Läuchli A M, Sudan J and Sørensen E S 2011 *Phys. Rev. B* **83** 212401

- [32] Ran Y, Hermele M, Lee P A and Wen X G 2007 *Phys. Rev. Lett.* **98** 117205
- [33] Hermele M, Ran Y, Lee P A and Wen X G 2008 *Phys. Rev. B* **77** 224413
- [34] Ma O and Marston J B 2008 *Phys. Rev. Lett.* **101** 027204
- [35] Iqbal Y, Becca F and Poilblanc D 2011 *Phys. Rev. B* **83** 100404
- [36] Iqbal Y, Becca F and Poilblanc D 2011 *Phys. Rev. B* **84** 020407
- [37] Sachdev S 1992 *Phys. Rev. B* **45** 12377
- [38] Wang F and Vishwanath A 2006 *Phys. Rev. B* **74** 174423
- [39] Lu Y M, Ran Y and Lee P A 2011 *Phys. Rev. B* **83** 224413
- [40] Jiang H C, Weng Z Y and Sheng D N 2008 *Phys. Rev. Lett.* **101** 117203
- [41] Yan S, Huse D A and White S R 2011 *Science* **332** 1173–6
- [42] Messio L, Bernu B and Lhuillier C 2012 Kagome antiferromagnet: a chiral topological spin liquid? *Phys. Rev. Lett.* **108** 207204
- [43] Marston J B and Zeng C 1991 *J. Appl. Phys.* **69** 5962
- [44] Nikolic P and Senthil T 2003 *Phys. Rev. B* **68** 214415
- [45] Singh R R P and Huse D A 2007 *Phys. Rev. B* **76** 180407
- [46] Singh R R P and Huse D A 2008 *Phys. Rev. B* **77** 144415
- [47] Evenbly G and Vidal G 2010 *Phys. Rev. Lett.* **104** 187203
- [48] Zeng C and Elser V 1995 *Phys. Rev. B* **51** 8318
- [49] Poilblanc D, Mambrini M and Schwandt D 2010 *Phys. Rev. B* **81** 180402
- [50] Schwandt D, Mambrini M and Poilblanc D 2010 *Phys. Rev. B* **81** 214413
- [51] Budnik R and Auerbach A 2004 *Phys. Rev. Lett.* **93** 187205
- [52] Hastings M B 2000 *Phys. Rev. B* **63** 014413
- [53] Syromyatnikov A V and Maleyev S V 2002 *Phys. Rev. B* **66** 132408
- [54] Syromyatnikov A V and Maleyev S V 2004 *J. Exp. Theor. Phys.* **98** 538–45
- [55] Poilblanc D and Misguich G 2011 *Phys. Rev. B* **84** 214401
- [56] Tay T and Motrunich O I 2011 *Phys. Rev. B* **84** 020404
- [57] Yang F and Yao H 2012 Frustrated RVB states in 2D: classifications and short-range correlations arXiv:1204.6381v1 [cond.mat]
- [58] Poilblanc D, Schuch N, Perez-Garcia D and Ignacio Cirac J 2012 Entanglement and boundary theories of resonating valence bond wave functions arXiv:1202.0947v3 [cond.mat]
- [59] Poilblanc D and Ralko A 2010 *Phys. Rev. B* **82** 174424
- [60] Wen X G 1991 *Phys. Rev. B* **44** 2664
- [61] Wen X G 2002 *Phys. Rev. B* **65** 165113
- [62] Sorella S 2005 *Phys. Rev. B* **71** 241103
- [63] Yunoki S and Sorella S 2006 *Phys. Rev. B* **74** 014408
- [64] Tay T and Motrunich O I 2011 *Phys. Rev. B* **84** 193102
- [65] Sorella S 2001 *Phys. Rev. B* **64** 024512
- [66] Huh Y, Punk M and Sachdev S 2011 *Phys. Rev. B* **84** 094419

Chapter 7

On the potential instabilities of critical spin liquids towards \mathbb{Z}_2 spin liquids on the kagomé lattice for the spin-1/2 Heisenberg antiferromagnet

The large scale DMRG studies in Refs. [20, 21] have claimed the ground state to be a fully gapped, fully symmetric, topological spin liquid with a \mathbb{Z}_2 low energy gauge structure. The energies obtained in these studies are some of the closest to exact diagonalization, thereby giving strong support to the nature of the ground state claimed in these works. Within the SU(2) slave boson (Schwinger fermion) formalism, a *complete* classification of fully symmetric \mathbb{Z}_2 spin liquids on the kagomé lattice results in an enumeration of a total of 20 \mathbb{Z}_2 spin liquids, and no more [91]. Out of these 20, *only* 5 \mathbb{Z}_2 spin liquids are fully gapped and hence contain topological orders [8], thereby these 5 states possess all the features of the spin liquid discovered in the DMRG studies. Another common feature of all these 5 \mathbb{Z}_2 spin liquids is that they are in the neighborhood of either the U(1) Dirac or the uniform RVB spin liquid¹. Whence, their Ansätze can be obtained from the U(1) Dirac or uniform RVB spin liquid Ansatz by continuously tuning a variational parameter which breaks the U(1) gauge structure to \mathbb{Z}_2 and also opens up a gap via the Higgs mechanism.

7.1 The $\mathbb{Z}_2[0, \pi]\beta$ spin liquid: the most promising ground state candidate

Out of these 5 fully gapped, fully symmetric, topological \mathbb{Z}_2 spin liquids, only 1 of them is continuously connected to the U(1) Dirac spin liquid. Since, the U(1) Dirac spin liquid has the lowest variational energy among the class of U(1) gapless spin liquids, it has been conjectured in [91] that this spin liquid, the $\mathbb{Z}_2[0, \pi]\beta$ state may describe the ground state that has been numerically observed in the DMRG studies [20, 21].

The Ansatz of the $\mathbb{Z}_2[0, \pi]\beta$ spin liquid is given in Fig. 7.1. In a suitable gauge, its mean-field Ansatz is specified by five real parameters. These parameters are the 1st nearest neighbor real hopping (χ_1), 2nd nearest neighbor real hopping (χ_2), 2nd nearest neighbor real spinon pairing (Δ_2), and two onsite terms, one for the chemical potential μ and the

¹Mathematically speaking, “neighborhood” means that the PSGs of these 5 \mathbb{Z}_2 spin liquids are subgroups of either the U(1) Dirac spin liquid PSG or the uniform RVB spin liquid PSG.

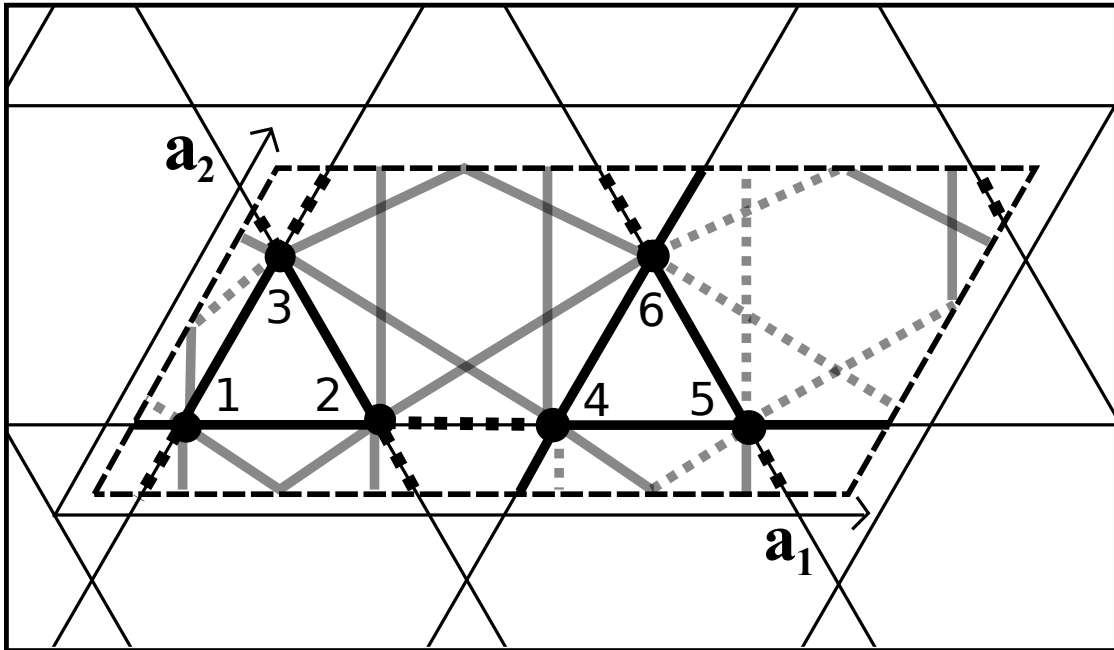


Figure 7.1: The $\mathbb{Z}_2[0, \pi]\beta$ spin liquid Ansatz; black (grey) bonds denote 1st nearest neighbor real hopping (2nd nearest neighbor real hopping and real spinon pairing) terms; solid (dashed) black bonds have $s_{ij} = 1$ (-1), solid (dashed) grey bonds have $\nu_{ij} = 1$ (-1), see Eq. (7.1). The 1st nearest neighbor (2nd nearest neighbor) mean field Ansatz is written as $U_{\langle ij \rangle} = \pm\sigma_3$ ($U_{\langle\langle ij \rangle\rangle} = \pm(\chi_2\sigma_3 + \Delta_2\sigma_1)$). The SU(2) flux (P), through elementary triangles (e.g., 123) is $P_{123} = \sigma_3$, and that through triangles formed by two 1st nearest neighbor and one 2nd nearest neighbor bonds (e.g., 234) is $P_{234} = -(\chi_2\sigma_3 + \Delta_2\sigma_1)$. Their commutator is non-zero, $[P_{123}, P_{234}] = (-2i\sigma_2)\Delta_2$. Hence, a finite Δ_2 breaks the U(1) gauge structure down to \mathbb{Z}_2 , and opens up an energy gap via the Anderson-Higgs mechanism [6, 7].

other for the real on-site pairing ζ_R . The mean field Hamiltonian can be then conveniently cast in the following form:

$$\begin{aligned}
\mathcal{H}_{\text{MF}}\{\mathbb{Z}_2[0, \pi]\beta\} &= \chi_1 \sum_{\langle ij \rangle, \alpha} s_{ij} c_{i, \alpha}^\dagger c_{j, \alpha} \\
&+ \sum_{\langle\langle ij \rangle\rangle} \nu_{ij} \left\{ \chi_2 \sum_{\alpha} c_{i, \alpha}^\dagger c_{j, \alpha} + \Delta_2 (c_{i, \uparrow}^\dagger c_{j, \downarrow}^\dagger + h.c.) \right\} \\
&+ \sum_i \left\{ \mu \sum_{\alpha} c_{i, \alpha}^\dagger c_{i, \alpha} + \zeta_R (c_{i, \uparrow}^\dagger c_{i, \downarrow}^\dagger + h.c.) \right\}, \tag{7.1}
\end{aligned}$$

where $\langle ij \rangle$ and $\langle\langle ij \rangle\rangle$ denote sums over 1st and 2nd nearest neighbor sites, respectively. s_{ij} and ν_{ij} encode the sign structure of the 1st and 2nd nearest neighbor bonds, respectively, as shown in Fig. 7.1. The 1st nearest neighbor real hopping (χ_1) will be taken as a reference, and hence set to unity hereafter. The physical variational wave function of this spin liquid state then depends on four variational parameters, $|\Psi_{\text{VMC}}(\chi_2, \Delta_2, \mu, \zeta_R)\rangle = \mathcal{P}_G |\Psi_{\text{MF}}(\chi_2, \Delta_2, \mu, \zeta_R)\rangle$.

7.1.1 Numerical results for the $\mathbb{Z}_2[0, \pi]\beta$ spin liquid

We performed our variational calculations on a 432-site cluster with mixed periodic-antiperiodic boundary conditions which ensures non-degenerate mean-field wave functions at half filling.

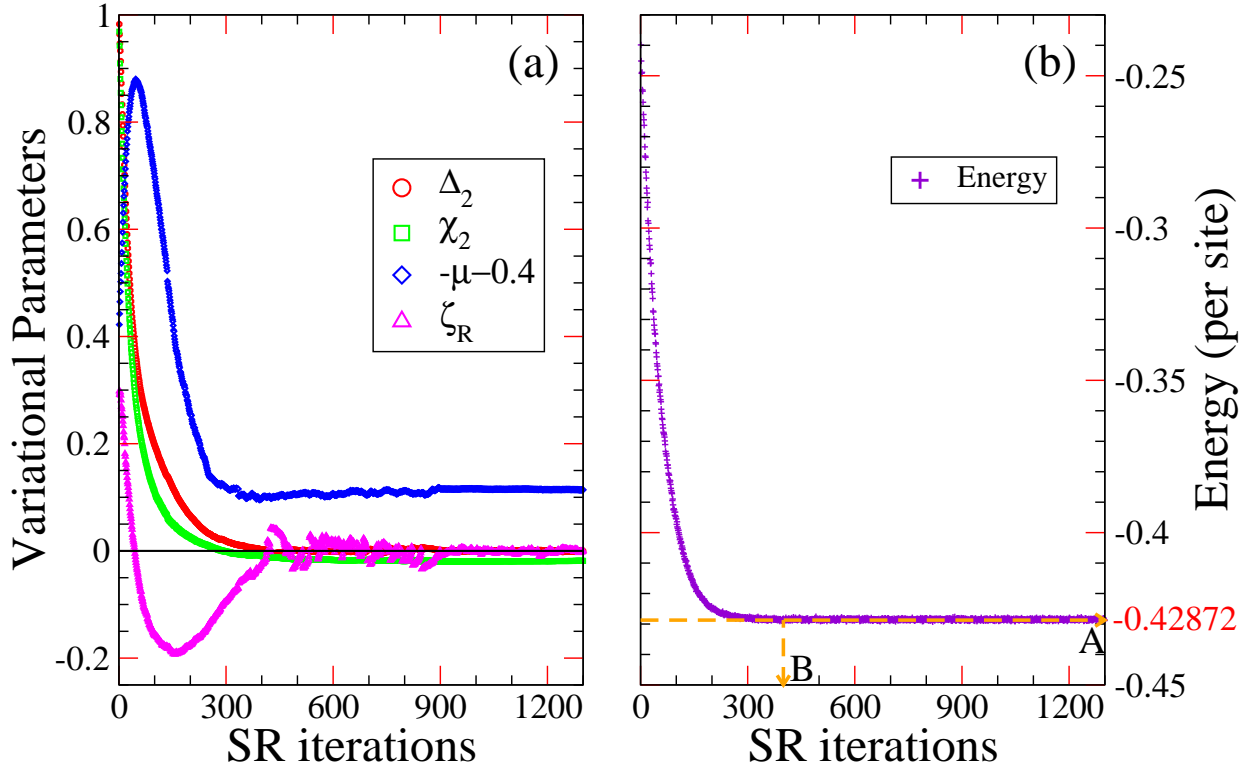


Figure 7.2: A typical variational Monte Carlo optimization run for the $\mathbb{Z}_2[0, \pi]\beta$ wave function: (a) variational parameters Δ_2 , χ_2 , μ , and ζ_R and (b) energy, as a function of stochastic reconfiguration (SR) iterations. In (a), the initialized parameter values are: $\Delta_2 = \chi_2 = 1$, $\mu = -0.8$, and $\zeta_R = 0.3$. The U(1) 2nd nearest neighbor $[0, \pi; 0, \pi]$ Dirac spin liquid corresponds to $\Delta_2 = 0$, $\chi_2 = -0.0186(2)$, $\zeta_R = 0$, as found in Ref. [19]. The optimized parameter values are obtained by averaging over a much larger number of converged SR iterations than shown above.

The large size of the cluster ensures that the spatial modulations induced in the observables by breaking of rotational symmetry (due to mixed boundary conditions) remain smaller than the uncertainty in the Monte Carlo simulations. On this cluster the energy per site of the U(1) Dirac spin liquid is $E/J = -0.42863(2)$ [12, 19].

For a generic unbiased starting point in the four-dimensional variational space, the variation of parameters and energy in the SR optimization is shown in Fig. 7.2. As one can clearly see, the energy converges neatly [see point B in Fig. 7.2(b)] to the reference value of the suitably extended 2nd nearest neighbor U(1) Dirac spin liquid, the $[0, \pi; 0, \pi]$ state [see point A in Fig. 7.2(b)], with small but finite χ_2 [see Fig. 7.2(a)] previously computed by us [19]. For the present cluster, these values are $E/J = -0.42872(1)$ per site, and $\chi_2 = -0.0186(2)$, $\mu = -0.5124(5)$. Also, it is manifest that $(\Delta_2, \zeta_R) \rightarrow 0$, becoming exactly zero (within the error bars) after averaging over a sufficient number of converged Monte Carlo steps. Here, we bring attention to the important fact that, despite the energy having converged after ≈ 400 iterations, the parameters did not converge and were still varying, converging to their final values much later than the energy (see Fig. 7.2). This fact is possible because, in the energy minimization, forces are calculated through the correlated sampling and not by energy differences [16]. Our result shows that the energy landscape

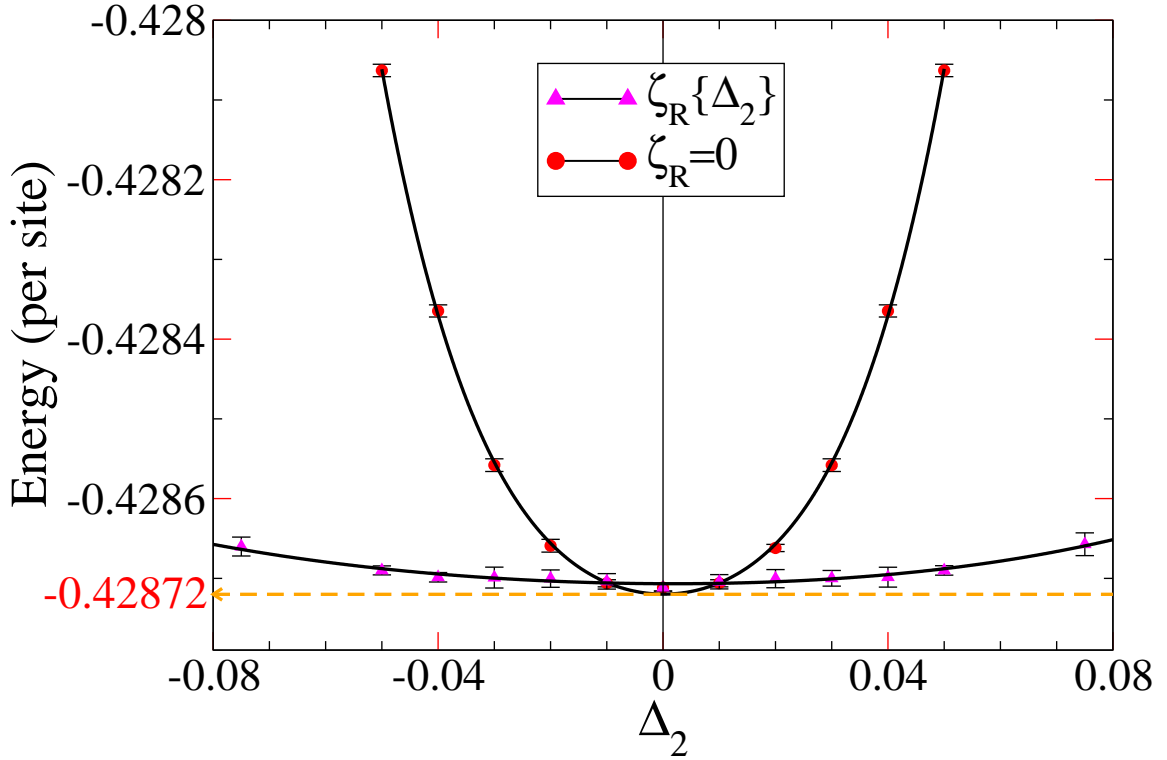


Figure 7.3: The variation in energy on addition of a small Δ_2 (both for $\zeta_R = 0$, and optimized ζ_R for each value of Δ_2) upon the $[0, \pi; 0, \pi]$ Dirac spin liquid is shown, the increase in energy is apparent. The gapless point, $\Delta_2 = 0$ is the energy minima.

along the manifold connecting the U(1) Dirac spin liquid to the $\mathbb{Z}_2[0, \pi]\beta$ spin liquid is *very* flat close to the U(1) Dirac spin liquid [see Fig. 7.3 for the case $\zeta_R\{\Delta_2\}$]. Consequently, a small perturbation around the U(1) Dirac spin liquid, e.g., by setting $\Delta_2 = 0.05$ along with the corresponding optimized value of $\zeta_R = 0.1780(2)$ will not lead to any detectable change in energy. Hence, one cannot unambiguously conclude anything about the stability of the U(1) Dirac spin liquid by solely computing the energy of the perturbed wave function with fixed parameters, point by point locally. Only by performing an accurate SR optimization method [16] can one successfully optimize the parameters and transparently show that $\Delta_2 = 0$ corresponds to the actual minimum of the variational energy. This fact implies that the U(1) gauge structure is kept intact and the Dirac spin liquid state is *locally* and *globally* stable with respect to destabilizing into the $\mathbb{Z}_2[0, \pi]\beta$ state. We verified this result by doing many optimization runs starting from different random initial values of the parameters in the four-dimensional variational space. Finally, we would like to mention that the $\mathbb{Z}_2[0, \pi]\beta$ spin liquid *is not* stabilized even in the presence of a 2nd nearest neighbor exchange coupling term in the Hamiltonian, of both the ferromagnetic and antiferromagnetic type and we still recover the gapless extended U(1) Dirac spin liquid ground state upon optimization.

7.2 Other promising ground state candidate \mathbb{Z}_2 spin liquids

The other 4 fully gapped, fully symmetric, topological \mathbb{Z}_2 spin liquids are continuously connected to the uniform RVB spin liquid via tuning of a gauge breaking (and gap opening)

$State$	Λ_{onsite}	$U_{\text{n.n.}}$	$U_{2\text{ndn.n.}}$	$U_{3\text{rdn.n.}}$	$\tilde{U}_{3\text{rdn.n.}}$
$\mathbb{Z}_2[0, \pi]\beta$	μ, ζ_R	χ_R	χ_R, Δ_R	0	0
$\mathbb{Z}_2[0, 0]A$	μ, ζ_R	χ_R	χ_R, Δ_R	0	0
$\mathbb{Z}_2[0, 0]B$	μ	χ_R, Δ_I	0	0	0
$\mathbb{Z}_2[0, 0]C$	μ	χ_R	χ_R	χ_R, Δ_I	χ_R
$\mathbb{Z}_2[0, 0]D$	μ	χ_R	χ_R, Δ_I	0	0

Table 7.1: The mean field Ansatz of the five gapped \mathbb{Z}_2 spin liquids investigated by us, given only up to the neighbor (geometrical distance) at which the gauge symmetry is broken, in a form used by us in numerical simulations. The parameters highlighted in red are responsible for opening a gap by breaking the $U(1)$ gauge symmetry down to \mathbb{Z}_2 . The $U_{3\text{rdn.n.}}$ denotes bonds of length 2 connecting two sites and passing through a third site (such as the bond $1 \rightarrow 4$ in Fig. 7.1); instead, $\tilde{U}_{3\text{rdn.n.}}$ denotes bonds of length 2 which do not pass through any site.

variational parameter occurring at different geometrical distances for these four distinct spin liquids, see Table 7.1. Although the uniform RVB spin liquid has a slightly higher energy (compared to the $U(1)$ Dirac spin liquid), there is nevertheless a chance that opening a gap in one of these 4 spin liquids might lead to a large gain in energy so as to make one of these states go lower than the $U(1)$ Dirac spin liquid, near to the DMRG value of $E/J = -0.4386(5)$ [21].

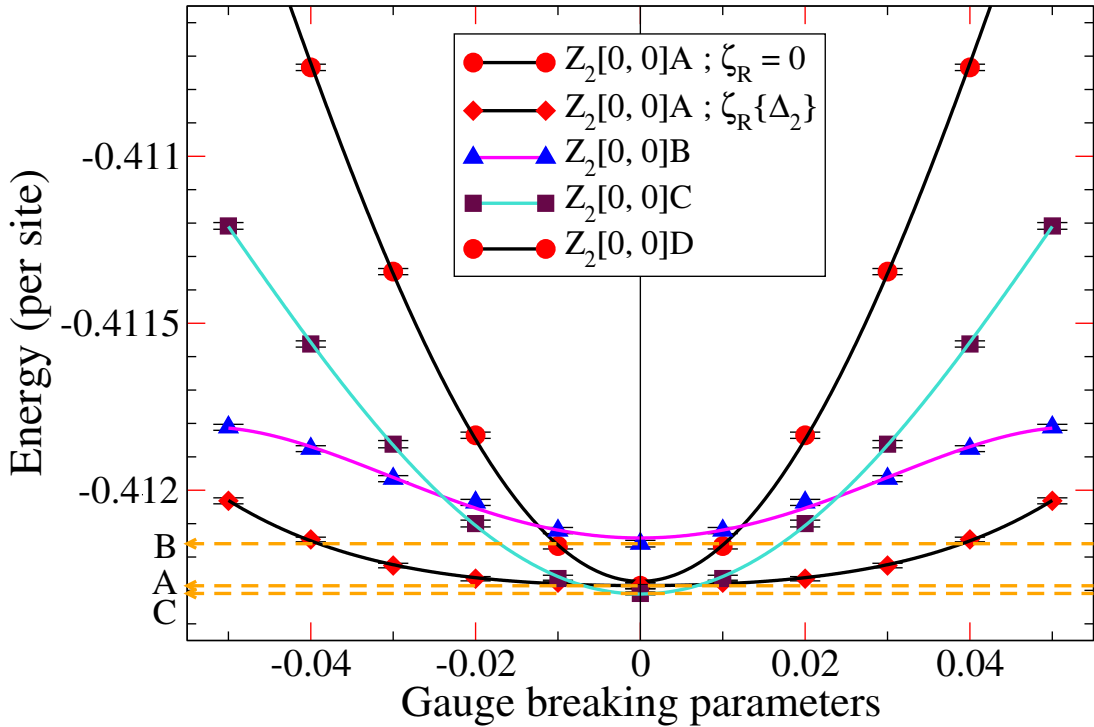


Figure 7.4: For the four gapped \mathbb{Z}_2 spin liquids in the neighborhood of the uniform RVB spin liquid: the manner of variation of energy as the gauge breaking parameter (shown in red in Table 7.1) is tuned on from zero to a small finite value, is shown. The parameters in black in Table 7.1 are fixed to their optimized values, and correspond to a suitably extended n^{th} nearest neighbor gapless uniform RVB spin liquid. The increase in energy upon opening a gap is apparent. For all four cases the minima of energy is situated at $\Delta_n = 0$.

7.2.1 Numerical results for the other gapped \mathbb{Z}_2 spin liquids

The energy of the nearest neighbor uniform RVB spin liquid is $E/J = -0.41216(1)$ on a 432 site cluster implemented with mixed periodic-antiperiodic boundary conditions. The results of our simulations show that all four of these spin liquids return upon optimization to the extended gapless uniform RVB spin liquid, with optimized hopping (χ_n) upto n th nearest neighbor. The results showing how the energies of these extended gapless uniform RVB spin liquids increase as the $U(1) \rightarrow \mathbb{Z}_2$ gauge breaking parameter is tuned on from zero to a small finite value are shown in Fig. 7.4. The points B, A, C in Fig. 7.4 correspond to the energies of the nearest neighbor, extended 2nd nearest neighbor and 3rd nearest neighbor uniform RVB spin liquids, respectively. These fully gapped \mathbb{Z}_2 spin liquids *are not* stabilized even in the presence of 2nd nearest neighbor exchange couplings in the Hamiltonian, of both the ferromagnetic and antiferromagnetic type.

7.2.2 The \mathbb{Z}_2 gapless spin liquids

There are 7 other gapless \mathbb{Z}_2 spin liquids which can potentially occur as the ground state of the nearest neighbor Heisenberg Hamiltonian, although a claim for such a ground state has not been made from any other numerical study. We investigated the energetics for three of these spin liquids which lie in the neighborhood of the $U(1)$ Dirac spin liquid. In all cases, we found negative results, namely that upon optimization the $U(1) \rightarrow \mathbb{Z}_2$ gauge breaking parameter goes to zero. The remaining four gapless spin liquids are continuously connected to two types of $U(1)$ gapless spin liquids, both of which suffer from a *macroscopic* degeneracy at half-filling, which leads to an open shell, and hence we did not carry out an investigation of the energetics of these four spin liquids. Please see the attached paper at the end of this chapter, for more details.

7.3 Conclusions and discussions

We investigated the possibility of stabilizing gapped \mathbb{Z}_2 spin liquids in the nearest neighbor and next-nearest-neighbor spin-1/2 Heisenberg antiferromagnet on the kagomé lattice. We found that *none* of the five gapped, topological \mathbb{Z}_2 spin liquids [one connected to the $U(1)$ Dirac state and the other four connected to the uniform RVB state] can occur as ground states. In particular, the most promising gapped spin liquid conjectured to describe the ground state, the $\mathbb{Z}_2[0, \pi]\beta$ state, is always higher in energy compared to the $U(1)$ Dirac spin liquid. Our systematic numerical results bring us to the conclusion that, at least within the Schwinger fermion approach of the spin model, the $U(1)$ Dirac spin liquid has the best variational energy for the nearest neighbor and next nearest neighbor spin-1/2 Heisenberg antiferromagnet on the kagomé lattice. The conflict of our results, which point towards a gapless ground state, and the ones by recent DMRG calculations [20, 21], which instead suggested the presence of a fully gapped spectrum, remain open and deserves further investigations. One possible direction would be to consider further improvements of our variational wave functions, based upon the application of few Lanczos steps or an approximated (fixed-node) projection technique. Another possible direction would be to explore the energetics of gapped \mathbb{Z}_2 spin liquids which break some symmetries such as point group and/or time-reversal. The possibility that the fully gapped spin liquid found by the DMRG study possesses a different low energy gauge structure other than \mathbb{Z}_2 also remains open.

7.4 Physical Review B 84, 020407 (2011): Rapid Comm,
Editor's suggestion

Projected wave function study of \mathbb{Z}_2 spin liquids on the kagome lattice for the spin-1/2 quantum Heisenberg antiferromagnet.

Yasir Iqbal, Federico Becca, and Didier Poilblanc

see next page



Projected wave function study of \mathbb{Z}_2 spin liquids on the kagome lattice for the spin- $\frac{1}{2}$ quantum Heisenberg antiferromagnet

Yasir Iqbal,¹ Federico Becca,² and Didier Poilblanc¹

¹Laboratoire de Physique Théorique UMR-5152, CNRS and Université de Toulouse, F-31062 France

²Democritos National Simulation Center, Istituto Officina dei Materiali del CNR and Scuola Internazionale Superiore di Studi Avanzati (SISSA), Via Bonomea 265, I-34136 Trieste, Italy

(Received 6 May 2011; revised manuscript received 7 June 2011; published 20 July 2011)

Motivated by recent density-matrix renormalization group (DMRG) calculations [Yan, Huse, and White, *Science* **332**, 1173 (2011)], which claimed that the ground state of the nearest-neighbor spin-1/2 Heisenberg antiferromagnet on the kagome lattice geometry is a fully gapped spin liquid with numerical signatures of \mathbb{Z}_2 gauge structure, and a further theoretical work [Lu, Ran, and Lee, *Phys. Rev. B* **83**, 224413 (2011)], which gave a classification of all Schwinger-fermion mean-field fully symmetric \mathbb{Z}_2 spin liquids on the kagome lattice, we have thoroughly studied Gutzwiller-projected fermionic wave functions by using quantum variational Monte Carlo techniques, hence implementing exactly the constraint of one fermion per site. In particular, we investigated the energetics of all \mathbb{Z}_2 candidates (gapped and gapless) that lie in the neighborhood of the energetically competitive U(1) gapless spin liquids. By using a state-of-the-art optimization method, we were able to conclusively show that the U(1) Dirac state is remarkably stable with respect to all \mathbb{Z}_2 spin liquids in its neighborhood, and in particular for opening a gap toward the so-called $\mathbb{Z}_2[0,\pi]\beta$ state, which was conjectured to describe the ground state obtained by the DMRG method. Finally, we also considered the addition of a small second nearest-neighbor exchange coupling of both antiferromagnetic and ferromagnetic type, and obtained similar results, namely, a U(1) Dirac spin-liquid ground state.

DOI: [10.1103/PhysRevB.84.020407](https://doi.org/10.1103/PhysRevB.84.020407)

PACS number(s): 75.10.Kt, 75.10.Jm, 75.40.Mg

Introduction. The nearest-neighbor (NN) spin-1/2 quantum Heisenberg antiferromagnet (QHAF) on the kagome lattice provides ideal conditions for the amplification of quantum fluctuations and a consequent stabilization of an exotic magnetically disordered ground state, which may be a valence-bond crystal (VBC)¹⁻⁵ or a spin liquid (SL) with fractionalized excitations.⁶⁻⁸ Recent experiments have unanimously pointed toward a SL behavior;⁹⁻¹⁶ in particular, Raman spectroscopic data on a nearly perfect spin-1/2 kagome compound with Heisenberg couplings (the so-called Herbertsmithite) suggested a gapless (algebraic) SL.¹⁷ On the theoretical side, the question is still wide open and intensely debated. On the one hand, series expansion provided evidence that a VBC with a 36-site unit cell has lower energy than other proposed competing states.⁴ On the other hand, it was shown that within the class of Gutzwiller-projected fermionic wave functions, a particular algebraic SL, the so-called U(1) Dirac state, has a competing energy.¹⁸ Its properties were studied in detail in Ref. 19 and it was argued that it can be a stable SL state. However, a recent DMRG study⁸ has challenged the above results, and proposed that the ground state can be a fully gapped \mathbb{Z}_2 SL with a substantially lower energy as compared to both the above estimates.

The \mathbb{Z}_2 SLs have the nice property that they are stable mean-field states and can survive quantum fluctuations. Hence, they are more likely to occur as real physical SLs, and one can safely use the projective symmetry group classification of \mathbb{Z}_2 SLs beyond mean-field level.²⁰ This complete classification of fully symmetric \mathbb{Z}_2 SLs on the kagome lattice was recently done in Ref. 21 within the Schwinger-fermion mean-field theory, resulting in an enumeration of a total of 20 \mathbb{Z}_2 mean-field states. Their main result was the identification of a *unique* gapped \mathbb{Z}_2 SL (called the $\mathbb{Z}_2[0,\pi]\beta$ state) in the neighborhood of the U(1) Dirac state. Since the U(1) Dirac SL state has the best

variational energy among the class of U(1) gapless SLs, in Ref. 21, it has been conjectured that the $\mathbb{Z}_2[0,\pi]\beta$ state may describe the ground state that has been numerically observed in the DMRG study.⁸

In this paper, we thoroughly investigate the possibility of any of these \mathbb{Z}_2 SLs being stabilized as the ground state of the NN spin-1/2 QHAF, with a particular emphasis on the $\mathbb{Z}_2[0,\pi]\beta$ state. In practice, we compute the energy of optimized variational wave functions that are constructed by applying the Gutzwiller projector to different states obtained from mean-field Hamiltonians of Schwinger fermions. In this respect, by an exact treatment of the full projector that ensures the one fermion per site constraint, we go much beyond the simple mean-field approach of Ref. 21. We calculate the energies of all \mathbb{Z}_2 SLs which can be realized up to 3rd NN in mean-field *Ansatz* and have a nonvanishing 1st NN mean-field bond. Only 12 of the 20 \mathbb{Z}_2 SLs satisfy these criteria, and all of them are continuously connected to some U(1) gapless SL.²¹ Our main result is that, contrary to what has been proposed in Ref. 21, the $\mathbb{Z}_2[0,\pi]\beta$ state has a higher energy than the gapless U(1) Dirac SL, or in other words, the U(1) Dirac SL is remarkably stable with respect to opening of a gap and consequently destabilizing into the $\mathbb{Z}_2[0,\pi]\beta$ state. We also find that all gapped \mathbb{Z}_2 SLs in the neighborhood of another competing gapless state, the uniform resonating-valence bond (RVB) state, have higher energies. Moreover, we find that all \mathbb{Z}_2 SLs have higher energy than the gapless SL states in whose neighborhoods they lie.

Model and wave function. The Hamiltonian for the NN spin-1/2 Heisenberg model is

$$\hat{H} = J \sum_{\langle ij \rangle} \hat{\mathbf{S}}_i \cdot \hat{\mathbf{S}}_j, \quad (1)$$

where $\langle ij \rangle$ denote sums over NN sites and \hat{S}_i is the spin-1/2 operator at site i . All energies will be given in units of J .

The variational wave functions are defined by projecting noncorrelated fermionic states:

$$|\Psi_{\text{VMC}}(\chi_{ij}, \Delta_{ij}, \mu, \zeta)\rangle = \mathcal{P}_G |\Psi_{\text{MF}}(\chi_{ij}, \Delta_{ij}, \mu, \zeta)\rangle, \quad (2)$$

where $\mathcal{P}_G = \prod_i (1 - n_{i,\uparrow} n_{i,\downarrow})$ is the full Gutzwiller projector enforcing the one fermion per site constraint. Here, $|\Psi_{\text{MF}}(\chi_{ij}, \Delta_{ij}, \mu, \zeta)\rangle$ is the ground state of mean-field Hamiltonian containing chemical potential, hopping, and *singlet* pairing terms:

$$\begin{aligned} \mathcal{H}_{\text{MF}} = & \sum_{i,j,\alpha} (\chi_{ij} + \mu \delta_{ij}) c_{i,\alpha}^\dagger c_{j,\alpha} \\ & + \sum_{i,j} \{ (\Delta_{ij} + \zeta \delta_{ij}) c_{i,\uparrow}^\dagger c_{j,\downarrow}^\dagger + \text{H.c.} \}, \end{aligned} \quad (3)$$

where $\chi_{ij} = \chi_{ji}^*$ and $\Delta_{ij} = \Delta_{ji}$. Besides the chemical potential μ , we will also consider real and imaginary components of on-site pairing, which are absorbed in ζ . We briefly mention that a somewhat similar approach, based upon a bosonic representation of the spin operators (i.e., through Schwinger bosons), has been also used recently.²² In the latter case, however, the bosonic nature of quasiparticle operators implies that one has to deal with permanents instead of determinants, which makes the numerical calculations much heavier than in our fermionic case.

Different SL phases correspond to different patterns of distribution of χ_{ij} and Δ_{ij} on the lattice links, along with the specification of the on-site terms μ and ζ . Then, a complete specification of a SL state up to n th NN amounts to specifying the SU(2) flux through closed loops along with the optimized hopping and pairing parameters at each geometrical distance.^{20,23} These parameters are the *Ansätze* of a given state and serve as the variational parameters in the physical wave function that are optimized within the variational Monte Carlo scheme to find the energetically best state. It is worth mentioning that we use a sophisticated implementation of the stochastic reconfiguration (SR) optimization method,^{24,25} which allows us to obtain an extremely accurate determination of variational parameters. Indeed, small energy differences are effectively computed by using a correlated sampling, which makes it possible to strongly reduce statistical fluctuations. The current problem of the study of the instability of a U(1) Dirac SL state toward the $\mathbb{Z}_2[0, \pi]\beta$ state will clearly demonstrate the power of this method to capture the essential subtleties.

Results. We performed our variational calculations on a 432-site cluster with mixed periodic-antiperiodic boundary conditions which ensures nondegenerate wave functions at half-filling. The large size of the cluster ensures that the spatial modulations induced in the observables by breaking of rotational symmetry (due to mixed boundary conditions) remain smaller than the uncertainty in the Monte Carlo simulations.

Among the class of NN fully symmetric and gapless SLs, the U(1) Dirac state has the lowest energy. Its energy per site is $E/J = -0.42863(2)$, and its *Ansatz* is given by the sign convention for NN bonds in Fig. 1. Due to the U(1) flux φ being 0 and π [$\exp(i\varphi) = \prod_{\text{plaquette}} \chi_{ij}$] through triangles and hexagons, respectively, it is denoted as $[0, \pi]$. Another

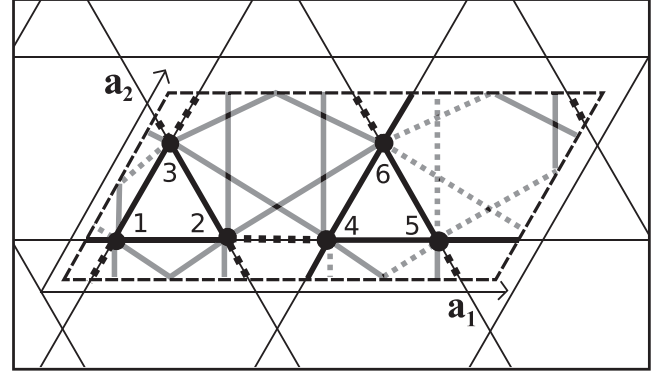


FIG. 1. The $\mathbb{Z}_2[0, \pi]\beta$ SL *Ansatz*; black (grey) bonds denote 1st NN real hopping (2nd NN real hopping and real spinon pairing) terms; solid (dashed) black bonds have $s_{ij} = 1$ (-1), solid (dashed) grey bonds have $v_{ij} = 1$ (-1), see Eq. (4). The 1st NN (2nd NN) mean-field *Ansatz* is written as $U_{\langle ij \rangle} = \pm \sigma_3 [U_{\langle ij \rangle}] = \pm (\chi_2 \sigma_3 + \Delta_2 \sigma_1)$. The SU(2) flux P , through elementary triangles (e.g., 123) is $P_{123} = \sigma_3$, and that through triangles formed by two 1st NN and one 2nd NN bonds (e.g., 234) is $P_{234} = -(\chi_2 \sigma_3 + \Delta_2 \sigma_1)$. Their commutator is nonzero, $[P_{123}, P_{234}] = (-2i\sigma_2)\Delta_2$. Hence, a finite Δ_2 breaks the U(1) gauge structure down to \mathbb{Z}_2 , and opens up an energy gap via the Anderson-Higgs mechanism.^{20,23}

competing state, the NN uniform RVB state has zero flux through any plaquette and is therefore denoted as $[0, 0]$; its energy per site is $E/J = -0.41216(1)$.^{18,19}

The study in Ref. 21 identified four \mathbb{Z}_2 SLs in the neighborhood of the $[0, \pi]$ state; only one of them, the $\mathbb{Z}_2[0, \pi]\beta$ state, was found to be gapped (via the 2nd NN spinon pairing term). Its *Ansatz* up to 2nd NN mean-field bond is reproduced in Fig. 1.²¹ In a suitable gauge, its mean-field *Ansatz* is specified by five real parameters. These parameters are the 1st NN real hopping (χ_1), 2nd NN real hopping (χ_2), 2nd NN real spinon pairing (Δ_2), and two onsite terms, one for the chemical potential μ and the other for the real on-site pairing ζ_R . The mean-field Hamiltonian can be then conveniently cast in the following form:

$$\begin{aligned} \mathcal{H}_{\text{MF}}\{\mathbb{Z}_2[0, \pi]\beta\} = & \chi_1 \sum_{\langle ij \rangle, \alpha} s_{ij} c_{i,\alpha}^\dagger c_{j,\alpha} + \sum_{\langle\langle ij \rangle\rangle} v_{ij} \left\{ \chi_2 \sum_{\alpha} c_{i,\alpha}^\dagger c_{j,\alpha} \right. \\ & \left. + \Delta_2 (c_{i,\uparrow}^\dagger c_{j,\downarrow}^\dagger + \text{H.c.}) \right\} + \sum_i \left\{ \mu \sum_{\alpha} c_{i,\alpha}^\dagger c_{i,\alpha} \right. \\ & \left. + \zeta_R (c_{i,\uparrow}^\dagger c_{i,\downarrow}^\dagger + \text{H.c.}) \right\}, \end{aligned} \quad (4)$$

where $\langle ij \rangle$ and $\langle\langle ij \rangle\rangle$ denote sums over 1st and 2nd NN sites, respectively. s_{ij} and v_{ij} encode the sign structure of the 1st and 2nd NN bonds, respectively, as shown in Fig. 1. The 1st NN real hopping (χ_1) will be taken as a reference, and hence set to unity hereafter. The physical variational wave function of this SL state then depends on four variational parameters, $|\Psi_{\text{VMC}}(\chi_2, \Delta_2, \mu, \zeta_R)\rangle = \mathcal{P}_G |\Psi_{\text{MF}}(\chi_2, \Delta_2, \mu, \zeta_R)\rangle$.

For a generic unbiased starting point in the four-dimensional variational space, the variation of parameters and energy in the SR optimization is shown in Fig. 2. As one can clearly see, the energy converges neatly [see point B in Fig. 2(b)] to the reference value of the suitably extended

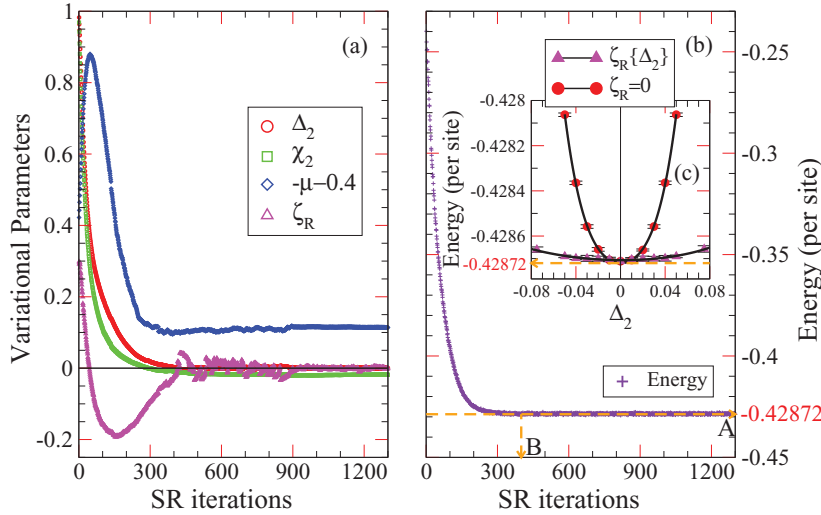


FIG. 2. (Color online) A typical variational Monte Carlo optimization run for the $\mathbb{Z}_2[0,\pi]\beta$ wave function: (a) variational parameters Δ_2 , χ_2 , μ , and ζ_R and (b) energy, as a function of SR iterations. In (a), the initialized parameter values are $\Delta_2 = \chi_2 = 1$, $\mu = -0.8$, and $\zeta_R = 0.3$. The U(1) 2nd NN $[0,\pi;0,\pi]$ Dirac SL corresponds to $\Delta_2 = 0$, $\chi_2 = -0.0186(2)$, $\zeta_R = 0$, as found in Ref. 26. The optimized parameter values are obtained by averaging over a much larger number of converged SR iterations than shown above. In (c), the variation in energy upon addition of a small Δ_2 (both for $\zeta_R = 0$, and optimized ζ_R for each value of Δ_2) upon the $[0,\pi;0,\pi]$ Dirac SL is shown, the increase in energy is apparent.

2nd NN U(1) Dirac SL, the $[0,\pi;0,\pi]$ state [see point A in Fig. 2(b)], with small but finite χ_2 [see Fig. 2(a)] previously computed by us.²⁶ For the present cluster, these values are $E/J = -0.42872(1)$ per site, and $\chi_2 = -0.0186(2)$, $\mu = -0.5124(5)$. Also, it is manifest that $(\Delta_2, \zeta_R) \rightarrow 0$, becoming exactly zero (within the error bars) after averaging over a sufficient number of converged Monte Carlo steps. Here, we bring attention to the important fact that despite the energy having converged after ≈ 400 iterations, the parameters did not converge and were still varying, converging to their final values much later than the energy (see Fig. 2). This fact is possible because, in the energy minimization, forces are calculated through the correlated sampling and not by energy differences.²⁴ Our result shows that the energy landscape along the manifold connecting the U(1) Dirac SL to the $\mathbb{Z}_2[0,\pi]\beta$ SL is *very* flat close to the U(1) Dirac SL [see Fig. 2(c) for the case $\zeta_R\{\Delta_2\}$]. Consequently, a small perturbation around the U(1) Dirac SL, e.g., by setting $\Delta_2 = 0.05$ along with the corresponding optimized value of $\zeta_R = 0.1780(2)$ will not lead to any detectable change in energy. Hence, one cannot unambiguously conclude anything about the stability of the U(1) Dirac SL by solely computing the energy of the perturbed wave function with fixed parameters, point by point locally. Only by performing an accurate SR optimization method²⁴ can one successfully optimize the parameters and transparently show that $\Delta_2 = 0$ corresponds to the actual minimum of the variational energy. This fact implies that the U(1) gauge structure is kept intact and the Dirac SL state is *locally* and *globally* stable with respect to destabilizing into the $\mathbb{Z}_2[0,\pi]\beta$ state. We verified this result by doing many optimization runs starting from different random initial values of the parameters in the four-dimensional variational space.²⁷

Regarding the remaining three gapless \mathbb{Z}_2 SLs in the neighborhood of the U(1) Dirac SL, namely, the $\mathbb{Z}_2[0,\pi]\alpha$, $\mathbb{Z}_2[0,\pi]\gamma$, and $\mathbb{Z}_2[0,\pi]\delta$ states of Ref. 21, our study reveals the same result as for the $\mathbb{Z}_2[0,\pi]\beta$ state. That is, all three of these SLs return back exactly to the gapless U(1) Dirac SL state, with the value of the parameter responsible for breaking the U(1) gauge structure down to \mathbb{Z}_2 exactly vanishing upon optimization. Thus, we can convincingly conclude that the \mathbb{Z}_2

neighborhood of the U(1) Dirac state does not contain the presumed fully gapped \mathbb{Z}_2 SL found by the DMRG study.

This conclusion forces us to shift our focus to the \mathbb{Z}_2 neighborhood of another fully symmetric (and energetically competing) gapless SL, called the uniform RVB or the $[0,0]$ SL. Despite having a slightly higher energy, it has the promising feature that all four \mathbb{Z}_2 SLs in its neighborhood are gapped, thereby opening up the possibility, albeit a slim one, that opening a gap might lead to a large gain in energy so as to make one of these four states go lower than the U(1) Dirac SL, near to the DMRG value of $E/J = -0.4379(3)$ per site. These gapped SLs are referred to in Ref. 21 as the $\mathbb{Z}_2[0,0]A$, $\mathbb{Z}_2[0,0]B$, $\mathbb{Z}_2[0,0]C$ and $\mathbb{Z}_2[0,0]D$ states; for their *Ansätze*, see Table I in Ref. 21 and also the supplementary material. Our simulations show that all four of these SLs return upon optimization to the gapless uniform RVB SL, with optimized χ_n . In particular, case by case we see that for the $\mathbb{Z}_2[0,0]A$ SL, the 2nd NN spinon pairing term goes to zero along with the on-site pairing term, thus returning back to the 2nd NN uniform RVB SL, the $[0,0;\pi,\pi]$ state given by optimized $\chi_2 = -0.032(1)$;²⁶ for the $\mathbb{Z}_2[0,0]B$ SL, the NN spinon pairing term goes to zero upon optimization, thus giving back the NN uniform RVB SL; the $\mathbb{Z}_2[0,0]C$ SL upon optimizing flows to the 3rd NN uniform RVB SL with optimized χ_2 and χ_3 's, with the spinon pairing term at 3rd NN becoming zero; and finally, the $\mathbb{Z}_2[0,0]D$ SL flows back to the 2nd NN uniform RVB SL. The results showing how the energies of these extended gapless uniform RVB SLs increase as the U(1) $\rightarrow \mathbb{Z}_2$ gauge breaking parameter is tuned on from zero to a small finite value are reported in the supplementary material (see Ref. 28).

For reasons of completeness, we mention that there are two more gapless U(1) SLs in whose neighborhoods the remaining four \mathbb{Z}_2 SLs (all gapless) lie.²¹ However, these U(1) SLs suffer from a *macroscopic* degeneracy at half-filling which leads to an open shell. This degeneracy being macroscopic cannot be removed by using any of the four real boundary condition possibilities. Hence, their energy can only be computed approximately in the limit by inserting an additional θ flux through the triangle motifs and consequently removing $\pi - 2\theta$ through hexagon motifs, and then taking the limit $\theta \rightarrow 0$. The energy of the SL- $[\pi,\pi]$ computed in

this way is $E/J \simeq -0.38372(1)$ per site, which is much higher than those of other gapless U(1) states. Hence, we did not carry out an analysis of \mathbb{Z}_2 SLs in these two neighborhoods.

Finally, we also investigated the possibility of stabilization of the $\mathbb{Z}_2[0,\pi]\beta$ state upon addition of a small 2nd NN exchange coupling (J') of both antiferromagnetic and ferromagnetic type in the NN spin-1/2 QHAF. In both cases, on optimization we found that $(\Delta_2, \zeta_R) \rightarrow 0$, becoming exactly zero (within error bars) after averaging over a sufficient number of converged Monte Carlo iterations. Thus, we recover the suitably extended, gapless 2nd NN U(1) Dirac SL. In particular, for $J'/J = 0.10$, this is the $[0,\pi;\pi,0]$ state with optimized $\chi_2 = 0.0924(2)$, and $E/J = -0.43200(2)$ per site; for $J'/J = -0.10$, this is the $[0,\pi;0,\pi]$ state with optimized $\chi_2 = -0.1066(2)$, and $E/J = -0.42898(2)$.²⁶

In summary, we investigated the possibility of stabilizing gapped \mathbb{Z}_2 SLs in the NN and next-nearest-neighbor (NNN) spin-1/2 QHAF on a kagome lattice. We found that none of the five gapped \mathbb{Z}_2 SLs [one connected to the U(1) Dirac state and the other four connected to the uniform RVB state] can occur

as ground states. In particular, the most promising gapped SL conjectured to describe the ground state, the $\mathbb{Z}_2[0,\pi]\beta$ state, is always higher in energy than the U(1) Dirac SL. Our systematic numerical results bring us to the conclusion that, at least within the Schwinger fermion approach of the spin model, the U(1) Dirac SL has the best variational energy for the NN and NNN spin-1/2 QHAF on kagome lattice. The conflict of our results, which point toward a gapless ground state, and the ones by recent DMRG calculations, which instead suggested the presence of a fully gapped spectrum, remains open and deserves further investigations. One possible direction would be to consider further improvements of our variational wave functions, based upon the application of few Lanczos steps or an approximated (fixed-node) projection technique, which, e.g., gives an energy of $E/J = -0.431453(2)$ per site for the NN U(1) Dirac SL, and $E/J = -0.431443(2)$ for the NNN $[0,\pi;0,\pi]$ state. Another possible direction would be to explore the energetics of gapped \mathbb{Z}_2 SLs which break some symmetries such as time-reversal. The possibility that the fully gapped SL found by the DMRG study possesses a different low energy gauge structure other than \mathbb{Z}_2 also remains open.

¹J. B. Marston and C. Zeng, *J. Appl. Phys.* **69**, 5962 (1991).

²M. B. Hastings, *Phys. Rev. B* **63**, 014413 (2000).

³P. Nikolic and T. Senthil, *Phys. Rev. B* **68**, 214415 (2003).

⁴R. R. P. Singh and D. A. Huse, *Phys. Rev. B* **76**, 180407(R) (2007).

⁵D. Poilblanc, M. Mambrini, and D. Schwandt, *Phys. Rev. B* **81**, 180402(R) (2010); D. Schwandt, M. Mambrini, and D. Poilblanc, *ibid.* **81**, 214413 (2010).

⁶P. W. Anderson, *Mater. Res. Bull.* **8**, 153 (1973).

⁷P. W. Anderson, *Science* **235**, 1196 (1987).

⁸S. Yan, D. A. Huse, and S. R. White, *Science* **332**, 1173 (2011).

⁹A. Olariu, P. Mendels, F. Bert, F. Duc, J. C. Trombe, M. A. de Vries, and A. Harrison, *Phys. Rev. Lett.* **100**, 087202 (2008).

¹⁰F. Bert, S. Nakamae, F. Ladieu, D. L'Hôte, P. Bonville, F. Duc, J.-C. Trombe, and P. Mendels, *Phys. Rev. B* **76**, 132411 (2007).

¹¹P. Mendels, F. Bert, M. A. de Vries, A. Olariu, A. Harrison, F. Duc, J. Trombe, J. Lord, A. Amato, and C. Baines, *Phys. Rev. Lett.* **98**, 077204 (2007).

¹²T. Imai, E. A. Nytko, B. M. Bartlett, M. P. Shores, and D. G. Nocera, *Phys. Rev. Lett.* **100**, 077203 (2008).

¹³O. Ofer, A. Keren, E. A. Nytko, M. P. Shores, B. M. Bartlett, D. G. Nocera, C. Baines, and A. Amato, e-print arXiv:cond-mat/0610540).

¹⁴J. S. Helton, K. Matan, M. P. Shores, E. A. Nytko, B. M. Bartlett, Y. Yoshida, Y. Takano, A. Suslov, Y. Qiu, J.-H. Chung, D. G. Nocera, and Y. S. Lee, *Phys. Rev. Lett.* **98**, 107204 (2007).

¹⁵S.-H. Lee, H. Kikuchi, Y. Qiu, B. Lake, Q. Huang, K. Habicht, and K. Kiefer, *Nat. Mater.* **6**, 853 (2007).

¹⁶M. A. de Vries, K. V. Kamenev, W. A. Kockelmann, J. Sanchez-Benitez, and A. Harrison, *Phys. Rev. Lett.* **100**, 157205 (2008).

¹⁷D. Wulferding, P. Lemmens, P. Scheib, J. Röder, P. Mendels, S. Chu, T. Han, and Y. S. Lee, *Phys. Rev. B* **82**, 144412 (2010).

¹⁸Y. Ran, M. Hermele, P. A. Lee, and X.-G. Wen, *Phys. Rev. Lett.* **98**, 117205 (2007).

¹⁹M. Hermele, Y. Ran, P. A. Lee, and X.-G. Wen, *Phys. Rev. B* **77**, 224413 (2008).

²⁰Xiao-Gang Wen, *Phys. Rev. B* **65**, 165113 (2002).

²¹Y.-M. Lu, Y. Ran, and P. A. Lee, *Phys. Rev. B* **83**, 224413 (2011).

²²T. Tay and O. I. Motrunich, *Phys. Rev. B* **84**, 020404(R) (2011).

²³X. G. Wen, *Phys. Rev. B* **44**, 2664 (1991).

²⁴S. Sorella, *Phys. Rev. B* **71**, 241103(R) (2005).

²⁵S. Yunoki and S. Sorella, *Phys. Rev. B* **74**, 014408 (2006).

²⁶Y. Iqbal, F. Becca, and D. Poilblanc, *Phys. Rev. B* **83**, 100404(R) (2011).

²⁷We also verified the same, by using the original non-gauge-transformed representation of the $\mathbb{Z}_2[0,\pi]\beta$ Ansatz, as given in Table I of Ref. 21.

²⁸See Supplemental Material at <http://link.aps.org/supplemental/10.1103/PhysRevB.84.020407> for more information.

Chapter 8

Finite size extrapolation of the kagomé spin-1/2 Heisenberg antiferromagnet using combined Lanczos and variational schemes

The method of application of a few Lanczos steps on a reasonably good starting trial wave function combined with variance extrapolation forms an extremely powerful method to extract the ground state energy and other observables on finite clusters. The power of the method lies in its ability to essentially reproduce the exact ground state values (if the symmetry sector of the trial state and exact state are the same) on clusters which are large enough to be currently inaccessible by exact diagonalization. After having obtained these ground state values, e.g. of energy on various cluster sizes, one can perform a finite size extrapolation to obtain the corresponding values in the thermodynamic limit.

8.1 Ground state energy on different cluster sizes

To obtain the ground state energy of the spin-1/2 Heisenberg antiferromagnet on the 48-site cluster, the smallest we considered, we took three very different starting variational wave functions, namely, (i) the U(1) Dirac spin liquid, in whose band structure the Fermi surface consists of two points where the spectrum becomes linear with Dirac conical excitations. The structure of the projected wave function is given in Fig. 8.1, as one can see about 10% of the configurations ($|x\rangle$) have zero weight ($\langle x|\Psi\rangle$) on a 48 site cluster. (ii) The uniform RVB spin liquid, which also has a U(1) low energy gauge structure and a band structure consisting of large circular spinon Fermi surfaces. The structure of the projected wave function is given in Fig. 8.1, from which we see that about 35% of the configurations have zero weight on a 48 site cluster. (iii) The $\mathbb{Z}_2[0, \pi]\beta$ spin liquid, which is fully gapped in contrast to the previous two states and the corresponding projected wave function has negligible zero-weight configurations, about 0.001% on a 48 site cluster.¹ We performed two Lanczos steps on top of these wave functions and computed their energy at every Lanczos step using variational Monte Carlo and Green function Monte Carlo techniques, subsequently we performed a zero-variance extrapolation within both these techniques to extract the ground state energy

¹The 48-site cluster is the smallest one on which one can construct a fully symmetric Gutzwiller projected wave function for the U(1) Dirac and $\mathbb{Z}_2[0, \pi]\beta$ spin liquids, using real boundary conditions, see [13].

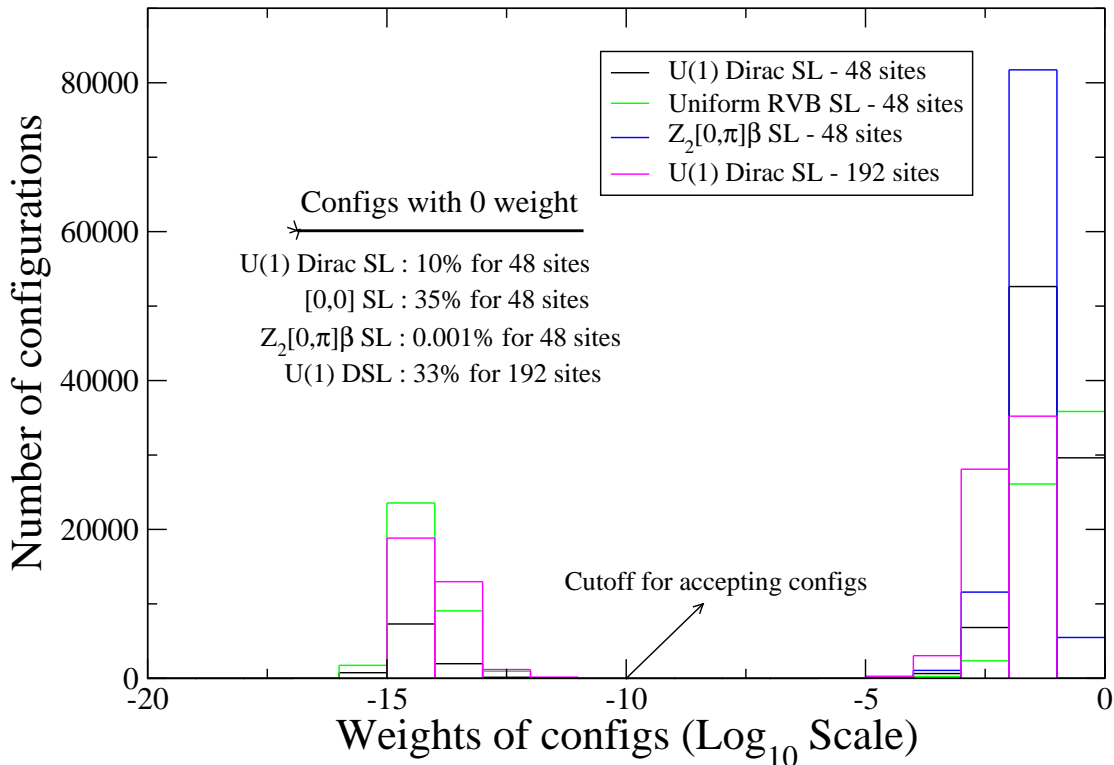


Figure 8.1: The histogram plot showing the structure of the three wave functions studied. The % of zero weight configurations (i.e. those $|x\rangle$ for which $\langle x|\Psi\rangle = 0$) for each of the wave functions are given, these are *not* visited by the random walk in our implementation of the Monte Carlo method. Despite the very different sizes of the Hilbert spaces scanned, remarkably enough, the extrapolated ground state energy estimates obtained from the three wave functions are the same within error bars, as shown in Fig. 8.2.

on the respective clusters. The results of our study on the 48 site cluster are shown in Fig. 8.2(a), all three wave functions give the same extrapolated value of the ground state energy, within error bars, showing that the extrapolation technique is indeed reliable, as we already saw before. Our estimate of the ground state energy obtained in this manner on the 48-site cluster is, energy per site $E/J = -0.437845(4)$. It is important to mention that the Monte Carlo random walk only visits those configurations for which $\langle x|\Psi\rangle \neq 0$, hence the sizes of the Hilbert spaces scanned by the Monte Carlo is very different for these three wave functions, see Fig. 8.1. Thus, despite the completely different structure of these wave functions, the extrapolated estimate of the ground state energy is the same (within error bars), which is quite remarkable.

Since, on the 48 site cluster, the extrapolations for ground state energy for the three wave functions match within error bars; for obtaining the ground state energies on larger clusters, we used only the U(1) Dirac spin liquid wave function as the starting point to perform the extrapolation. The results are given in Fig. 8.2(b). As a proof of principle, to check if the VMC estimate is exact or not, it is useful to plot the energy obtained from

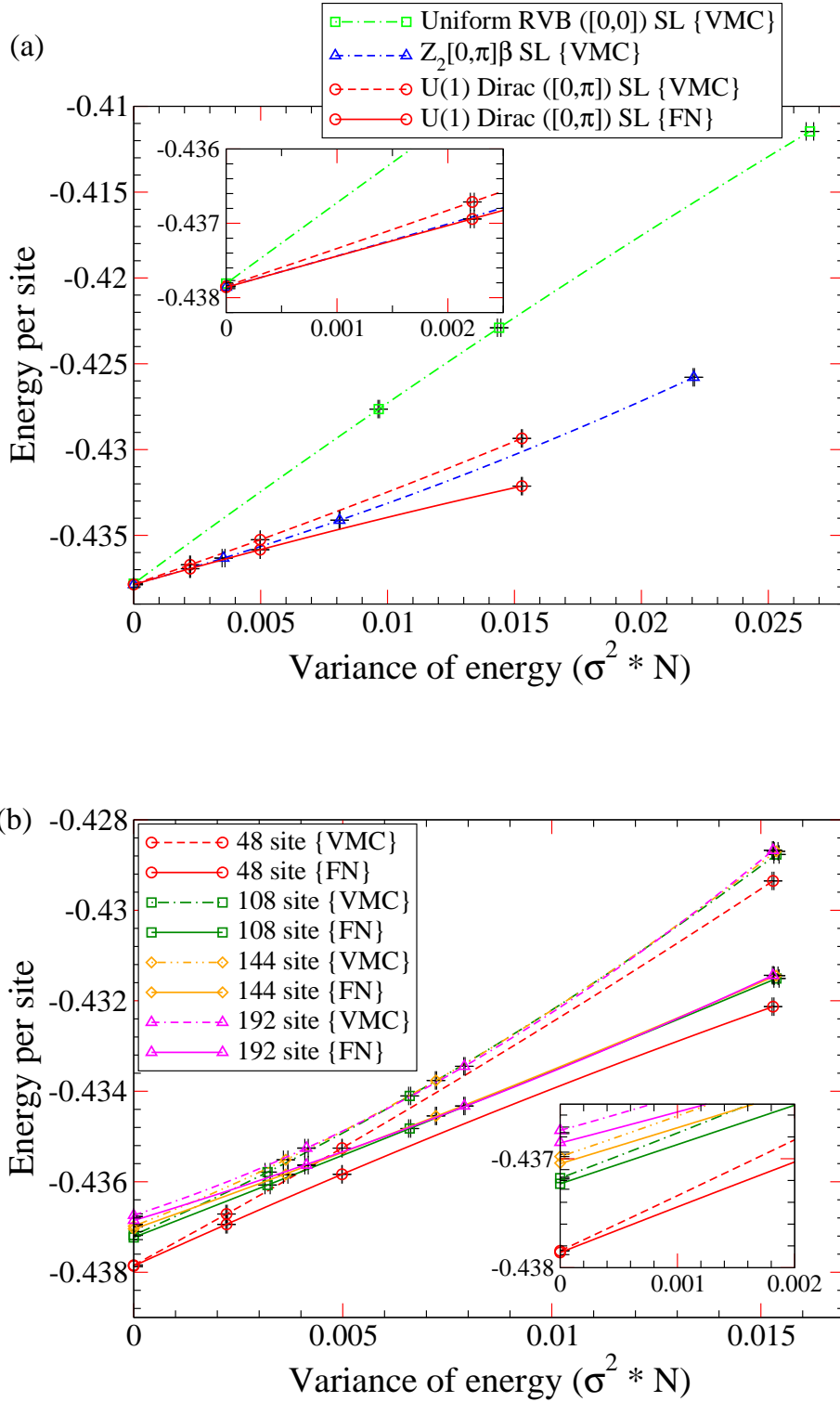


Figure 8.2: (a) On the 48 $(3 \times 4 \times 4)$ site cluster, for the spin-1/2 Heisenberg antiferromagnet, we plot the energies and variances for up to two Lanczos step wave functions for three different starting variational wave functions. These are the U(1) Dirac, the $Z_2[0,\pi]\beta$ and the uniform RVB spin liquids. The zero-variance extrapolated estimates for the ground state energies obtained from a quadratic fit for these three wave functions, all match within error bars. The U(1) Dirac spin liquid has also been analyzed using fixed node Monte Carlo, marked by {FN}, and it converges to the same value (within error bars) as the VMC value. (b) The ground state energy estimates on cluster sizes of 108-, 144- and 192-sites, from extrapolations using the U(1) Dirac spin liquid starting wave function only.

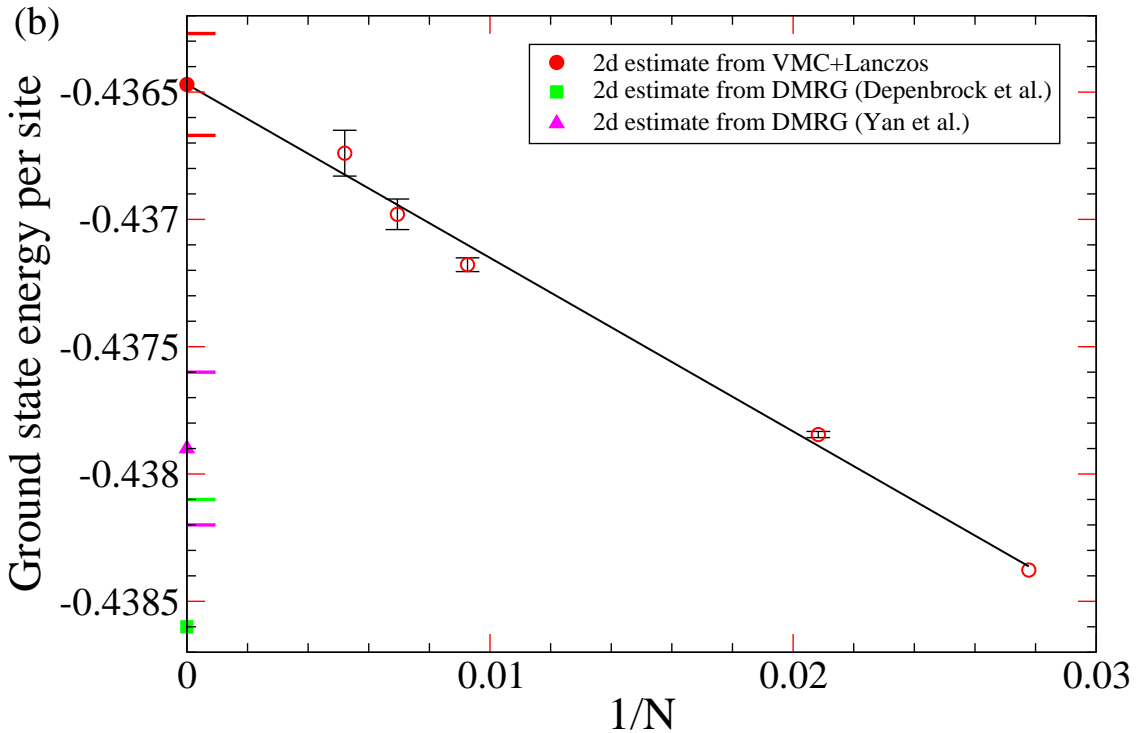
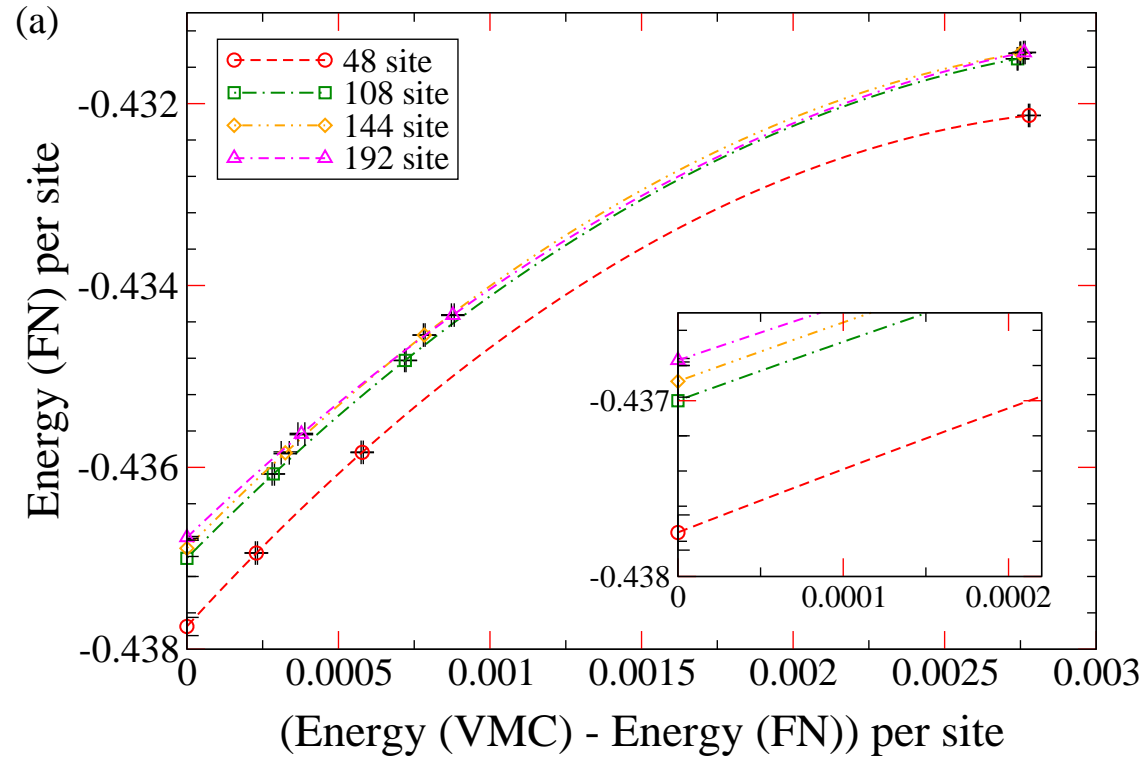


Figure 8.3: (a) On different cluster sizes, for the U(1) Dirac spin liquid the plot of E_{FN} vs $E_{\text{VMC}} - E_{\text{FN}}$ is shown. (b) Finite size extrapolation of the ground state energy. The value for the 36 site cluster is taken from exact diagonalization. The estimates from the DMRG studies are also marked.

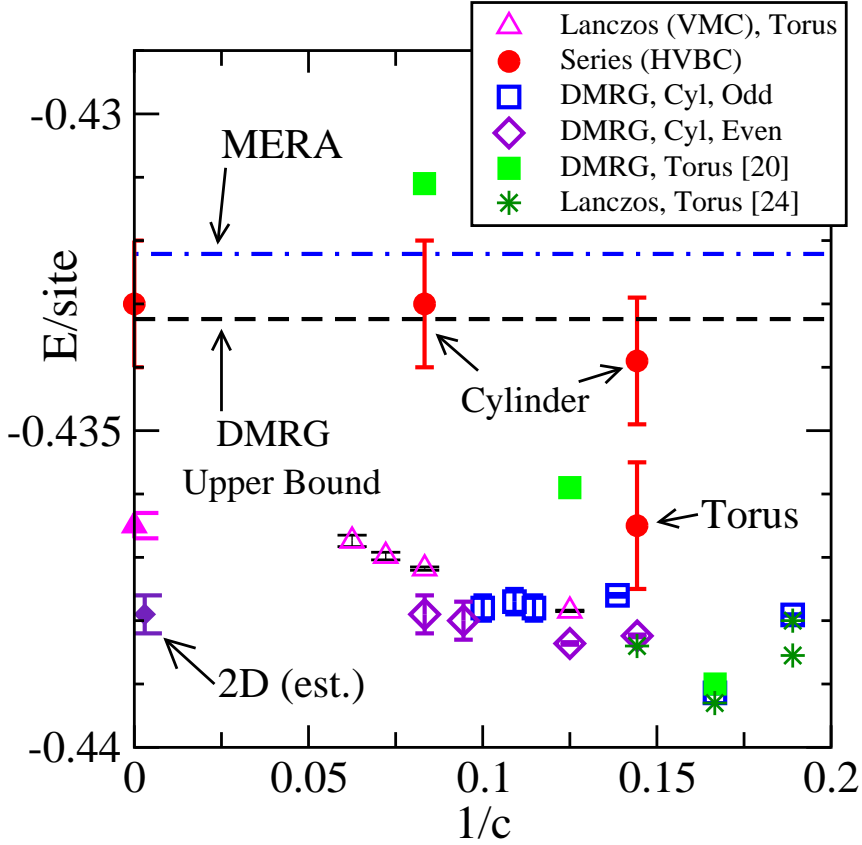


Figure 8.4: Adapted from Ref. [20] and supplemented with our results (pink up-triangles). A comparison of energies from different numerical methods for different clusters. For cylindrical geometries, the horizontal axis is the inverse circumference in units of inverse lattice spacings. For tori, it is the smallest circumference.

fixed-node Monte Carlo versus the difference of energy between VMC and fixed node Monte Carlo, i.e. E_{FN} vs $(E_{\text{VMC}} - E_{\text{FN}})$, and verify if the extrapolated value obtained in this manner matches (within error bars) to that of the VMC. This is so, because, if the VMC is exact then so is the fixed-node Monte Carlo value, and the extrapolations should give the same estimate (within error bars). We found that this is indeed the case, the corresponding results for the U(1) Dirac spin liquid on different cluster sizes are plotted in Fig. 8.3(a). After having obtained the ground state energy estimates on different cluster sizes, we performed a finite size extrapolation which is shown in Fig. 8.3(b). Our estimate of the infinite $2-d$ energy for the spin-1/2 quantum Heisenberg antiferromagnet on the kagomé lattice is $E_{\infty}^{2-d}/J = -0.4365(2)$. This estimate is slightly higher compared to similar estimates from recent DMRG studies [20, 21], see Fig. 8.3(b) and Fig. 8.4 for a global comparison with many previous results. A point of difference to be noted is that, our lattice is generated from an equal number of Bravais lattice translations in both directions on which the infinite limit is taken, whereas DMRG estimates have been obtained on cylindrical geometries in the quasi $2-d$ limit.

We would like to mention that work is in progress on the calculation of spin correlations and structure factors for the Lanczos wave functions and the ground state, so as to extract the properties of the ground state on finite clusters and also the thermodynamic limit. The results of the study will be presented in an article whose manuscript is currently in preparation.

Chapter 9

Conclusions and perspectives

In my thesis work I demonstrated that algebraic spin liquids, which are argued to be “brittle” in $2 + 1$ dimensions [15], can surprisingly enough be robust (both locally and globally) to a large class of potential instabilities on a kagomé lattice, even for spin-1/2 Heisenberg systems. Since, a particular algebraic state, the so called U(1) Dirac spin liquid has the lowest variational energy within slave particle approaches [12, 13], for the kagomé spin-1/2 Heisenberg antiferromagnetic model, we argue that it is the ground state. A gapless spin liquid behavior of the algebraic type, of the ground state is also backed up by Raman spectroscopic studies on Herbertsmithite [14], and till date no probe has detected a gap to excitations. We also found that a non-trivial 36-site VBC phase is stabilized on addition of a small ferromagnetic exchange coupling ($J_2 \approx -0.045$) to the Hamiltonian, but the U(1) Dirac spin liquid remains energetically lowest for $J_2 \gtrsim -0.045$ into the antiferromagnetic region also.

The fermionic variational quantum Monte Carlo method allowed us to access rather large system sizes. A sophisticated implementation of the stochastic reconfiguration algorithm for wave function optimization enabled us to thoroughly scan the variational landscape which can be quite non-trivial. For VBC phases, there are large number of variational parameters leading to highly complex terrains in parameter space, which can be difficult to navigate through using ordinary minimization schemes such as steepest descent method. On the other hand, when studying quantum phase transitions between U(1) and \mathbb{Z}_2 spin liquids, the energy landscape can be very flat, and ordinary optimization schemes can lead to incorrect conclusions about the nature of the energy minima. Thus, only by performing an accurate stochastic reconfiguration optimization we could transparently and unambiguously demonstrate the existence of the U(1) Dirac spin liquid as a stable phase and hence vouch for it to be the ground state. To go beyond the variational level we performed a couple of Lanczos steps on the U(1) Dirac spin liquid wave function and performed a zero-variance extrapolation of to extract the ground state energy. In this way, we gave an estimate of the ground state energy on the 48 site cluster and also larger cluster sizes, which are inaccessible to exact diagonalization. Using finite size extrapolation we then extracted the ground state energy of the infinite $2-d$ system.

I would now like to comment on the conflict of our results which point to a gapless ground state with those from recent DMRG calculations [20, 21], which instead suggested the presence of a fully gapped spectrum. This issue is open and deserves further investigations. One possible direction would be to classify and explore the energetics of gapped \mathbb{Z}_2 spin liquids which break some symmetries such as time-reversal, i.e. chiral \mathbb{Z}_2 spin liquids. In fact, such a chiral topological \mathbb{Z}_2 spin liquid has been proposed as the ground state within

the Schwinger boson mean field theory, but the energy of the corresponding projected wave function has yet to be computed so as to enable comparison with its competitors [138]. For reasons of completeness, if not for surprise the energetics of chiral gapless \mathbb{Z}_2 spin liquids would also be worth investigating. It may also be the case that the spin liquid ground state and maybe those discovered in the DMRG studies break point group symmetries, and thus the question of classification and energetics of such gapped \mathbb{Z}_2 spin liquids within slave particle approaches remains to be investigated. Another direction would be to investigate the energetics of incommensurate chiral flux phases, these class of chiral states have not been studied previously. Finally one cannot *a priori* rule out the possibility of a competing ground state possessing a different and possibly more complicated low energy gauge structure. An investigation along all these directions would be form steps towards pinning down the exact nature of this elusive ground state.

The above discussion dealt with the myriad of different spin liquid ground state possibilities that still need to be investigated. However, it must be kept in mind that a possible VBC ground state is not totally out of the game. There are again various new VBC candidates which have yet to be investigated and furthermore several improvements can be made to the simple Gutzwiller projected wave functions used here, and thus make them better in being able to capture VBC order faithfully. One possible direction would be to study the possibility that an unconventional VBC breaking time-reversal symmetry is stabilized as the ground state [145]. The possibility that a VBC with a much larger unit cell of 48 sites is stabilized, cannot be ruled out. Another direction would be to study the possible onset of VBC order via confinement transitions of \mathbb{Z}_2 spin liquids [177]. The mechanism and detailed study of confinement transitions in U(1) spin liquids using monopole PSG would be interesting and is yet to be carried out. To this effect, it may be necessary to include *vison* dynamics in the projected wave functions in order to capture topological order faithfully [176]. A further step would be to improve our variational wave functions based upon the application of a few Lanczos steps and then perform an approximated fixed-node projection technique. As mentioned before, all these investigations would form steps in the path leading towards a precise and unanimous identification of this elusive ground state.

Chapter 10

List of publications

1. Valence-bond crystal in the extended kagome spin-1/2 quantum Heisenberg antiferromagnet: A variational Monte Carlo approach.
Yasir Iqbal, Federico Becca and Didier Poilblanc, Phys. Rev. B **83**, 100404(R) (2011).
2. Projected wave function study of \mathbb{Z}_2 spin liquids on the kagome lattice for the spin-1/2 quantum Heisenberg antiferromagnet.
Yasir Iqbal, Federico Becca and Didier Poilblanc, Phys. Rev. B **84**, 020407(R) (2011). Selected as an '*Editor's suggestion*'.
3. Valence-bond crystals in the kagomé spin-1/2 Heisenberg antiferromagnet: a symmetry classification and projected wave function study.
Yasir Iqbal, Federico Becca and Didier Poilblanc.
New Journal of Physics **14**, 2012 (in press).
Invited paper for special focus issue on 'Quantum spin liquids' of New Journal of Physics. Guest editors: Steven Kivelson and Alejandro Muramatsu.
4. Finite size extrapolation of the kagome spin-1/2 Heisenberg antiferromagnet using combined Lanczos and variational schemes.
(*Manuscript in preparation*).
Yasir Iqbal, Federico Becca, Sandro Sorella and Didier Poilblanc.

Bibliography

- [1] L. D. Landau, “On the theory of phase transitions 1,” JETP **7**, pp. 1 (1937).
- [2] L. D. Landau, “On the theory of phase transitions 2,” JETP **7**, pp. 627 (1937).
- [3] L. D. Landau and E. M. Lifshitz, *Statistical Physics Part 1*, 3rd ed. (Pergamon press, Oxford, England, 1975).
- [4] L. D. Landau, “The theory of a Fermi liquid,” Soviet. Phys.-JETP **3**, pp. 920 (1957).
- [5] D. C. Tsui, H. L. Stormer, and A. C. Gossard, “Two-Dimensional Magnetotransport in the Extreme Quantum Limit,” Phys. Rev. Lett. **48**, 1559–1562 (1982).
- [6] X. G. Wen, “Mean-field theory of spin-liquid states with finite energy gap and topological orders,” Phys. Rev. B **44**, 2664–2672 (1991).
- [7] Xiao-Gang Wen, “Quantum orders and symmetric spin liquids,” Phys. Rev. B **65**, 165113 (2002).
- [8] Xiao-Gang Wen, *Quantum Field Theory of Many-Body Systems*, 1st ed. (Oxford University Press, Oxford, UK, 2004).
- [9] Xiao-Gang Wen, “Quantum order: a quantum entanglement of many particles,” Physics Letters A **300**, 175 – 181 (2002).
- [10] Matthew P. Shores, Emily A. Nytko, Bart M. Bartlett, and Daniel G. Nocera, “A Structurally Perfect $S = 1/2$ Kagomé Antiferromagnet,” Journal of the American Chemical Society **127**, 13462–13463 (2005).
- [11] E. Kermarrec, P. Mendels, F. Bert, R. H. Colman, A. S. Wills, P. Strobel, P. Bonville, A. Hillier, and A. Amato, “Spin-liquid ground state in the frustrated kagome antiferromagnet $\text{MgCu}_3(\text{OH})_6\text{Cl}_2$,” Phys. Rev. B **84**, 100401 (2011).
- [12] Ying Ran, Michael Hermele, Patrick A. Lee, and Xiao-Gang Wen, “Projected-Wave-Function Study of the Spin-1/2 Heisenberg Model on the Kagomé Lattice,” Phys. Rev. Lett. **98**, 117205 (2007).
- [13] Michael Hermele, Ying Ran, Patrick A. Lee, and Xiao-Gang Wen, “Properties of an algebraic spin liquid on the kagome lattice,” Phys. Rev. B **77**, 224413 (2008).
- [14] Dirk Wulferding, Peter Lemmens, Patric Scheib, Jens Röder, Philippe Mendels, Shaoyan Chu, Tianheng Han, and Young S. Lee, “Interplay of thermal and quantum spin fluctuations in the kagome lattice compound herbertsmithite,” Phys. Rev. B **82**, 144412 (2010).

- [15] Michael Hermele, T. Senthil, Matthew P. A. Fisher, Patrick A. Lee, Naoto Nagaosa, and Xiao-Gang Wen, “Stability of $U(1)$ spin liquids in two dimensions,” *Phys. Rev. B* **70**, 214437 (2004).
- [16] Sandro Sorella, “Wave function optimization in the variational Monte Carlo method,” *Phys. Rev. B* **71**, 241103 (2005).
- [17] Seiji Yunoki and Sandro Sorella, “Two spin liquid phases in the spatially anisotropic triangular Heisenberg model,” *Phys. Rev. B* **74**, 014408 (2006).
- [18] Sandro Sorella, “Generalized Lanczos algorithm for variational quantum Monte Carlo,” *Phys. Rev. B* **64**, 024512 (2001).
- [19] Yasir Iqbal, Federico Becca, and Didier Poilblanc, “Valence-bond crystal in the extended kagome spin- $\frac{1}{2}$ quantum Heisenberg antiferromagnet: A variational Monte Carlo approach,” *Phys. Rev. B* **83**, 100404 (2011).
- [20] Simeng Yan, David A. Huse, and Steven R. White, “Spin-Liquid Ground State of the $S = 1/2$ Kagome Heisenberg Antiferromagnet,” *Science* **332**, 1173–1176 (2011).
- [21] Stefan Depenbrock, Ian P. McCulloch, and Ulrich Schollwoeck, “Nature of the Spin Liquid Ground State of the $S=1/2$ Kagome Heisenberg Model,” *arXiv* (2012).
- [22] Yasir Iqbal, Federico Becca, and Didier Poilblanc, “Projected wave function study of Z_2 spin liquids on the kagome lattice for the spin- $\frac{1}{2}$ quantum Heisenberg antiferromagnet,” *Phys. Rev. B* **84**, 020407 (2011).
- [23] L. D. Landau and E. M. Lifshitz, *Electrodynamics of continuous media*, 2nd ed., Vol. 8 (Pergamon Press, Oxford, England, 1984).
- [24] L. Néel, “Influence des fluctuations du champ moléculaire sur les propriétés magnétiques des corps,” *Ann. de Phys.* **17**, pp. 5–105 (1932).
- [25] L. Néel, “Propriétés magnétiques de l’état magnétique et énergie d’interaction entre atomes magnétiques,” *Ann. de Phys.* **5**, pp. 232–279 (1936).
- [26] L. Néel, “Théorie du paramagnétisme constant; application au manganèse,” *C. R. Acad. Sc.* **203**, pp. 304–306 (1936).
- [27] P. Curie, “Lois expérimentales du magnétisme. Propriétés magnétiques des corps à diverses températures,” *Ann Chim Phys.* **5**, pp. 289–405 (1895).
- [28] L. D. Landau, “A possible explanation of the field dependence of the susceptibility at low temperatures,” *Phys. Z. Sowjet* **4**, pp. 675 (1933).
- [29] L. Néel, “Propriétés magnétiques des ferrites; Férrimagnétisme et antiferromagnétisme,” *Ann. Phys.* **3**, pp. 137–198 (1948).
- [30] Louis Néel, “Some theoretical aspects of rock-magnetism,” *Advances in Physics* **4**, 191–243 (1955).
- [31] W. Heisenberg, “Mehrkörperproblem und Resonanz in der Quantenmechanik,” *Zeitschrift für Physik A Hadrons and Nuclei* **38**, 411–426 (1926).

- [32] P. A. M. Dirac, “On the Theory of Quantum Mechanics,” Proceedings of the Royal Society of London. Series A, Containing Papers of a Mathematical and Physical Character **112**, pp. 661–677 (1926).
- [33] A. I. Akhiezer, V. G. Bar’yakhtar, and S. V. Peletminskii, *Spin Waves*, 1st ed. (North-Holland Publishing Company, Amsterdam, Holland, 1968).
- [34] P. A. M. Dirac, “Quantum Mechanics of Many-Electron Systems,” Proceedings of the Royal Society of London. Series A, Containing Papers of a Mathematical and Physical Character **123**, pp. 714–733 (1929).
- [35] W. Heisenberg, “Zur Theorie des Ferromagnetismus,” Zeitschrift für Physik A Hadrons and Nuclei **49**, 619–636 (1928).
- [36] J. Frenkel, “Elementare Theorie magnetischer und elektrischer Eigenschaften der Metalle beim absoluten Nullpunkt der Temperatur,” Zeitschrift für Physik A Hadrons and Nuclei **49**, 31–45 (1928).
- [37] J. Dorfman, “The Intrinsic Fields in Ferromagnetic Substances,” Nature **119**, 353 (1927).
- [38] J. H. Van Vleck, “On the Theory of Antiferromagnetism,” The Journal of Chemical Physics **9**, 85–90 (1941).
- [39] A. Z. Patashinskii and V. L. Pokrovskii, *Fluctuation theory of Phase Transitions*, 1st ed. (Pergamon Press, Oxford, England, 1979).
- [40] D. Mattis, *Theory of Magnetism*, 1st ed. (Harper-Row, New York, USA, 1965).
- [41] A. Auerbach, *Interacting Electrons and Quantum Magnetism*, 1st ed. (Springer-Verlag, Berlin/Heidelberg, Germany, 1994).
- [42] N. F. MOTT, “Metal-Insulator Transition,” Rev. Mod. Phys. **40**, 677–683 (1968).
- [43] Philip W. Anderson, *Basic Notions Of Condensed Matter Physics*, 1st ed. (Westview press, Boulder, Colorado, USA, 1997).
- [44] L. D. Landau and E. M. Lifshitz, *Statistical Physics Part 2*, 1st ed. (Pergamon press, Oxford, England, 1977).
- [45] Matthias Troyer, “Phase diagram,” (2006).
- [46] J. Villain, R. Bidaux, J.-P. Carton, and R. Conte, “Order as an effect of disorder,” J. Phys. France **41**, pp. 1263 (1980).
- [47] E. F. Shender, Soviet. Phys. JETP **56**, pp. 178 (1982).
- [48] J. T. Chalker, P. C. W. Holdsworth, and E. F. Shender, “Hidden order in a frustrated system: Properties of the Heisenberg Kagomé antiferromagnet,” Phys. Rev. Lett. **68**, 855–858 (1992).
- [49] R. Moessner and J. T. Chalker, “Properties of a Classical Spin Liquid: The Heisenberg Pyrochlore Antiferromagnet,” Phys. Rev. Lett. **80**, 2929–2932 (1998).

- [50] R. Moessner and J. T. Chalker, “Low-temperature properties of classical geometrically frustrated antiferromagnets,” *Phys. Rev. B* **58**, 12049–12062 (1998).
- [51] P. Chandra and B. Doucot, “Possible spin-liquid state at large S for the frustrated square Heisenberg lattice,” *Phys. Rev. B* **38**, 9335–9338 (1988).
- [52] P. W. Anderson, “Ordering and Antiferromagnetism in Ferrites,” *Phys. Rev.* **102**, 1008–1013 (1956).
- [53] Jacques Villain, “Insulating spin glasses,” *Zeitschrift für Physik B Condensed Matter* **33**, 31–42 (1979).
- [54] J. N. Reimers, A. J. Berlinsky, and A.-C. Shi, “Mean-field approach to magnetic ordering in highly frustrated pyrochlores,” *Phys. Rev. B* **43**, 865–878 (1991).
- [55] J. N. Reimers, J. E. Greedan, and M. Björgvinsson, “Critical properties of highly frustrated pyrochlore antiferromagnets,” *Phys. Rev. B* **45**, 7295–7306 (1992).
- [56] P. Lecheminant, B. Bernu, C. Lhuillier, L. Pierre, and P. Sindzingre, “Order versus disorder in the quantum Heisenberg antiferromagnet on the kagomé lattice using exact spectra analysis,” *Phys. Rev. B* **56**, 2521–2529 (1997).
- [57] Maged Elhajal, Benjamin Canals, Raimon Sunyer, and Claudine Lacroix, “Ordering in the pyrochlore antiferromagnet due to Dzyaloshinsky-Moriya interactions,” *Phys. Rev. B* **71**, 094420 (2005).
- [58] E. F. Shender, V. B. Cherepanov, P. C. W. Holdsworth, and A. J. Berlinsky, “Kagomé antiferromagnet with defects: Satisfaction, frustration, and spin folding in a random spin system,” *Phys. Rev. Lett.* **70**, 3812–3815 (1993).
- [59] R. Moessner and A. J. Berlinsky, “Magnetic Susceptibility of Diluted Pyrochlore and $\text{SrCr}_{9-9x}\text{Ga}_{3+9x}\text{O}_{19}$ Antiferromagnets,” *Phys. Rev. Lett.* **83**, 3293–3296 (1999).
- [60] N. P. Raju, M. Dion, M. J. P. Gingras, T. E. Mason, and J. E. Greedan, “Transition to long-range magnetic order in the highly frustrated insulating pyrochlore antiferromagnet $\text{Gd}_2\text{Ti}_2\text{O}_7$,” *Phys. Rev. B* **59**, 14489–14498 (1999).
- [61] S. E. Palmer and J. T. Chalker, “Order induced by dipolar interactions in a geometrically frustrated antiferromagnet,” *Phys. Rev. B* **62**, 488–492 (2000).
- [62] I. Pomeranchuk, *Zh. Eksp. Teor. Fiz.* **11**, pp. 226 (1941).
- [63] L. B. Ioffe and A. I. Larkin, “Gapless fermions and gauge fields in dielectrics,” *Phys. Rev. B* **39**, 8988–8999 (1989).
- [64] P.W. Anderson, “Resonating valence bonds: A new kind of insulator?” *Materials Research Bulletin* **8**, 153 – 160 (1973).
- [65] P. Fazekas and P. W. Anderson, “On the ground state properties of the anisotropic triangular antiferromagnet,” *Philosophical Magazine* **30**, 423–440 (1974).
- [66] P. W. ANDERSON, “The Resonating Valence Bond State in La_2CuO_4 and Superconductivity,” *Science* **235**, 1196–1198 (1987).

- [67] M. B. Hastings, “Lieb-Schultz-Mattis in higher dimensions,” *Phys. Rev. B* **69**, 104431 (2004).
- [68] Bruno Nachtergaele and Robert Sims, “A Multi-Dimensional Lieb-Schultz-Mattis Theorem,” *Communications in Mathematical Physics* **276**, 437–472 (2007).
- [69] Masaki Oshikawa, “Commensurability, Excitation Gap, and Topology in Quantum Many-Particle Systems on a Periodic Lattice,” *Phys. Rev. Lett.* **84**, 1535–1538 (2000).
- [70] Ian Affleck, “Spin gap and symmetry breaking in CuO_2 layers and other antiferromagnets,” *Phys. Rev. B* **37**, 5186–5192 (1988).
- [71] Leon Balents, “Spin liquids in frustrated magnets,” *Nature* **464**, 199–208 (2010).
- [72] G. Rumer, “Zur Theorie der Spinvalenz,” *Math.-Phys. Klasse* **337** (1932).
- [73] G. Rumer, E. Teller, and H. Weyl, “Eine für die Valenztheorie geeignete Basis der binären Vektorinvarianten,” *Math.-Phys. Klasse* **499** (1932).
- [74] G. Baskaran, Z. Zou, and P.W. Anderson, “The resonating valence bond state and high- t_c superconductivity - a mean field theory,” *Solid State Communications* **88**, 853 – 856 (1993), special Issue A Celebratory Issue to Commemorate 30 Years of Solid State Communications.
- [75] S E Barnes, “New method for the Anderson model,” *Journal of Physics F: Metal Physics* **6**, 1375 (1976).
- [76] S E Barnes, “New method for the Anderson model. II. The $U=0$ limit,” *Journal of Physics F: Metal Physics* **7**, 2637 (1977).
- [77] Piers Coleman, “New approach to the mixed-valence problem,” *Phys. Rev. B* **29**, 3035–3044 (1984).
- [78] G. Baskaran, Z. Zou, and P.W. Anderson, “The resonating valence bond state and high- t_c superconductivity - a mean field theory,” *Solid State Communications* **63**, 973 – 976 (1987).
- [79] G. Baskaran and P. W. Anderson, “Gauge theory of high-temperature superconductors and strongly correlated Fermi systems,” *Phys. Rev. B* **37**, 580–583 (1988).
- [80] Ian Affleck, Z. Zou, T. Hsu, and P. W. Anderson, “ $\text{SU}(2)$ gauge symmetry of the large- U limit of the Hubbard model,” *Phys. Rev. B* **38**, 745–747 (1988).
- [81] Elbio Dagotto, Eduardo Fradkin, and Adriana Moreo, “ $\text{SU}(2)$ gauge invariance and order parameters in strongly coupled electronic systems,” *Phys. Rev. B* **38**, 2926–2929 (1988).
- [82] Christopher Mudry and Eduardo Fradkin, “Separation of spin and charge quantum numbers in strongly correlated systems,” *Phys. Rev. B* **49**, 5200–5219 (1994).
- [83] Xiao-Gang Wen and Patrick A. Lee, “Theory of Underdoped Cuprates,” *Phys. Rev. Lett.* **76**, 503–506 (1996).

- [84] Patrick A. Lee, Naoto Nagaosa, and Xiao-Gang Wen, “Doping a Mott insulator: Physics of high-temperature superconductivity,” *Rev. Mod. Phys.* **78**, 17–85 (2006).
- [85] P. W. Anderson, G. Baskaran, Z. Zou, and T. Hsu, “Resonating – valence-bond theory of phase transitions and superconductivity in La_2CuO_4 -based compounds,” *Phys. Rev. Lett.* **58**, 2790–2793 (1987).
- [86] P. W. Anderson, “Comment on “Two-Dimensional Antiferromagnetic Quantum Spin-Fluid State in La_2CuO_4 ,”” *Phys. Rev. Lett.* **59**, 2497–2497 (1987).
- [87] Gang Chen, Andrew Essin, and Michael Hermele, “Majorana spin liquids and projective realization of $\text{SU}(2)$ spin symmetry,” *Phys. Rev. B* **85**, 094418 (2012).
- [88] T. Senthil and Matthew P. A. Fisher, “ \mathbb{Z}_2 gauge theory of electron fractionalization in strongly correlated systems,” *Phys. Rev. B* **62**, 7850–7881 (2000).
- [89] P Horsch and T A Kaplan, “Exact and Monte Carlo studies of Gutzwiller’s state for the localised-electron limit in one dimension,” *Journal of Physics C: Solid State Physics* **16**, L1203 (1983).
- [90] C. Gros, R. Joynt, and T. M. Rice, “Antiferromagnetic correlations in almost-localized Fermi liquids,” *Phys. Rev. B* **36**, 381–393 (1987).
- [91] Yuan-Ming Lu, Ying Ran, and Patrick A. Lee, “ \mathbb{Z}_2 spin liquids in the $S = \frac{1}{2}$ Heisenberg model on the kagome lattice: A projective symmetry-group study of Schwinger fermion mean-field states,” *Phys. Rev. B* **83**, 224413 (2011).
- [92] V L Berezinskii, *Sov. Phys.-JETP* **32**, pp. 493 (1970).
- [93] V L Berezinskii, *Sov. Phys.-JETP* **34**, pp. 610 (1971).
- [94] J M Kosterlitz and D J Thouless, “Ordering, metastability and phase transitions in two-dimensional systems,” *Journal of Physics C: Solid State Physics* **6**, 1181 (1973).
- [95] Nandini Trivedi and D. M. Ceperley, “Ground-state correlations of quantum anti-ferromagnets: A Green-function Monte Carlo study,” *Phys. Rev. B* **41**, 4552–4569 (1990).
- [96] D. M. Ceperley and M. H. Kalos, *Monte Carlo Method in Statistical Physics* (Springer-Verlag, Heidelberg, Germany, 1992).
- [97] D. F. B. ten Haaf, H. J. M. van Bemmelen, J. M. J. van Leeuwen, W. van Saarloos, and D. M. Ceperley, “Proof for an upper bound in fixed-node Monte Carlo for lattice fermions,” *Phys. Rev. B* **51**, 13039–13045 (1995).
- [98] Sandro Sorella, *Variational Monte Carlo and Markov chains for computational physics* (Lecture notes).
- [99] N. D. Mermin and H. Wagner, “Absence of Ferromagnetism or Antiferromagnetism in One- or Two-Dimensional Isotropic Heisenberg Models,” *Phys. Rev. Lett.* **17**, 1133–1136 (1966).

- [100] S. Kobe and K. Handrich, “Correlation Function and Misfit in a Computer-Simulated Two-Dimensional Amorphous Ising Antiferromagnet,” *physica status solidi (b)* **73**, K65–K67 (1976).
- [101] J Richter and S Kobe, “On the influence of competing interactions on physical properties of spin systems: numerical exact results for finite Ising and Heisenberg systems,” *Journal of Physics C: Solid State Physics* **15**, 2193 (1982).
- [102] S. Kobe and T. Klotz, “Frustration: How it can be measured,” *Phys. Rev. E* **52**, 5660–5663 (1995).
- [103] B. Bernu, C. Lhuillier, and L. Pierre, “Signature of Néel order in exact spectra of quantum antiferromagnets on finite lattices,” *Phys. Rev. Lett.* **69**, 2590–2593 (1992).
- [104] B Bernu, P Lecheminant, C Lhuillier, and L Pierre, “Néel order versus spin liquid in quantum Heisenberg antiferromagnets on triangular and Kagomé lattices,” *Physica Scripta* **1993**, 192 (1993).
- [105] B. Bernu, P. Lecheminant, C. Lhuillier, and L. Pierre, “Exact spectra, spin susceptibilities, and order parameter of the quantum Heisenberg antiferromagnet on the triangular lattice,” *Phys. Rev. B* **50**, 10048–10062 (1994).
- [106] David A. Huse and Veit Elser, “Simple Variational Wave Functions for Two-Dimensional Heisenberg Spin- $\frac{1}{2}$ Antiferromagnets,” *Phys. Rev. Lett.* **60**, 2531–2534 (1988).
- [107] Th. Jolicoeur and J. C. Le Guillou, “Spin-wave results for the triangular Heisenberg antiferromagnet,” *Phys. Rev. B* **40**, 2727–2729 (1989).
- [108] Satoru J. Miyake, “Spin-Wave Results for the Staggered Magnetization of Triangular Heisenberg Antiferromagnet,” *Journal of the Physical Society of Japan* **61**, 983–988 (1992).
- [109] R. Deutscher and H. U. Everts, “The S=1/2 Heisenberg antiferromagnet on the triangular lattice: Exact results and spin-wave theory for finite cells,” *Zeitschrift für Physik B Condensed Matter* **93**, 77–89 (1993).
- [110] Adolfo E. Trumper, “Spin-wave analysis to the spatially anisotropic Heisenberg antiferromagnet on a triangular lattice,” *Phys. Rev. B* **60**, 2987–2989 (1999).
- [111] Luca Capriotti, Adolfo E. Trumper, and Sandro Sorella, “Long-Range Néel Order in the Triangular Heisenberg Model,” *Phys. Rev. Lett.* **82**, 3899–3902 (1999).
- [112] Luca Capriotti, “Quantum effects and broken symmetries in frustrated antiferromagnets,” *Int. J. of Mod. Phys. B* **15**, 1799–1842 (2001).
- [113] D. J. J. Farnell, R. F. Bishop, and K. A. Gernoth, “Coupled cluster treatment of an interpolating triangle- *kagomé* antiferromagnet,” *Phys. Rev. B* **63**, 220402 (2001).
- [114] Ch. Waldtmann, H.-U. Everts, B. Bernu, C. Lhuillier, P. Sindzingre, P. Lecheminant, and L. Pierre, “First excitations of the spin 1/2 Heisenberg antiferromagnet on the kagomé lattice,” *Eur. Phys. J. B* **2**, 501–507 (1998).

- [115] Chen Zeng and Veit Elser, “Numerical studies of antiferromagnetism on a Kagomé net,” *Phys. Rev. B* **42**, 8436–8444 (1990).
- [116] A. B. Harris, C. Kallin, and A. J. Berlinsky, “Possible Néel orderings of the Kagomé antiferromagnet,” *Phys. Rev. B* **45**, 2899–2919 (1992).
- [117] Andrey Chubukov, “Order from disorder in a kagomé antiferromagnet,” *Phys. Rev. Lett.* **69**, 832–835 (1992).
- [118] P. W. Leung and Veit Elser, “Numerical studies of a 36-site *kagome* antiferromagnet,” *Phys. Rev. B* **47**, 5459–5462 (1993).
- [119] Kun Yang, L. K. Warman, and S. M. Girvin, “Possible spin-liquid states on the triangular and kagomé lattices,” *Phys. Rev. Lett.* **70**, 2641–2644 (1993).
- [120] F. Mila, “Low-Energy Sector of the $S = 1/2$ Kagome Antiferromagnet,” *Phys. Rev. Lett.* **81**, 2356–2359 (1998).
- [121] Ch. Waldtmann, H. Kreutzmann, U. Schollwöck, K. Maisinger, and H.-U. Everts, “Ground states and excitations of a one-dimensional *kagomé* -like antiferromagnet,” *Phys. Rev. B* **62**, 9472–9483 (2000).
- [122] Weiqiang Yu and Shiping Feng, “Spin-liquid state for two-dimensional Heisenberg antiferromagnets on a kagomé lattice,” *Eur. Phys. J. B* **13**, 265–269 (2000).
- [123] M. Mambrini and F. Mila, “RVB description of the low-energy singlets of the spin $1/2$ kagomé antiferromagnet,” *Eur. Phys. J. B* **17**, 651–659 (2000).
- [124] R. Shankar and D. Shubashree, “Hidden Goldstone mechanism in the *kagomé* lattice antiferromagnet,” *Phys. Rev. B* **61**, 12126–12133 (2000).
- [125] P. Sindzingre, G. Misguich, C. Lhuillier, B. Bernu, L. Pierre, Ch. Waldtmann, and H.-U. Everts, “Magnetothermodynamics of the Spin- $\frac{1}{2}$ Kagomé Antiferromagnet,” *Phys. Rev. Lett.* **84**, 2953–2956 (2000).
- [126] A. V. Syromyatnikov and S. V. Maleyev, “Hidden long-range order in kagomé Heisenberg antiferromagnets,” *Phys. Rev. B* **66**, 132408 (2002).
- [127] B. H. Bernhard, B. Canals, and C. Lacroix, “Green’s function approach to the magnetic properties of the kagomé antiferromagnet,” *Phys. Rev. B* **66**, 104424 (2002).
- [128] David A. Huse and Andrew D. Rutenberg, “Classical antiferromagnets on the Kagomé lattice,” *Phys. Rev. B* **45**, 7536–7539 (1992).
- [129] Jan N. Reimers and A. J. Berlinsky, “Order by disorder in the classical Heisenberg *kagomé* antiferromagnet,” *Phys. Rev. B* **48**, 9539–9554 (1993).
- [130] M. B. Hastings, “Dirac structure, RVB, and Goldstone modes in the *kagomé* antiferromagnet,” *Phys. Rev. B* **63**, 014413 (2000).
- [131] Ookie Ma and J. B. Marston, “Weak Ferromagnetic Exchange and Anomalous Specific Heat in $\text{ZnCu}_3(\text{OH})_6\text{Cl}_2$,” *Phys. Rev. Lett.* **101**, 027204 (2008).

- [132] X. G. Wen, Frank Wilczek, and A. Zee, “Chiral spin states and superconductivity,” *Phys. Rev. B* **39**, 11413–11423 (1989).
- [133] D. V. Khveshchenko and P. B. Wiegmann, “Effective action of antiferromagnetism in two dimensions: parity violating ground state and Hall effect,” *Mod. Phys. Lett B* **3**, 1383–1392 (1989).
- [134] J. B. Marston and C. Zeng, “Spin-Peierls and spin-liquid phases of Kagomé quantum antiferromagnets,” *Journal of Applied Physics* **69**, 5962–5964 (1991).
- [135] Fa Wang and Ashvin Vishwanath, “Spin-liquid states on the triangular and Kagomé lattices: A projective-symmetry-group analysis of Schwinger boson states,” *Phys. Rev. B* **74**, 174423 (2006).
- [136] Tiamhock Tay and Olexei I. Motrunich, “Variational study of J_1 - J_2 Heisenberg model on kagome lattice using projected Schwinger-boson wave functions,” *Phys. Rev. B* **84**, 020404 (2011).
- [137] Subir Sachdev, “Kagomé- and triangular-lattice Heisenberg antiferromagnets: Ordering from quantum fluctuations and quantum-disordered ground states with unconfined bosonic spinons,” *Phys. Rev. B* **45**, 12377–12396 (1992).
- [138] Laura Messio, Bernard Bernu, and Claire Lhuillier, “Kagome Antiferromagnet: A Chiral Topological Spin Liquid?” *Phys. Rev. Lett.* **108**, 207204 (2012).
- [139] H. C. Jiang, Z. Y. Weng, and D. N. Sheng, “Density Matrix Renormalization Group Numerical Study of the Kagome Antiferromagnet,” *Phys. Rev. Lett.* **101**, 117203 (2008).
- [140] G. Evenbly and G. Vidal, “Frustrated Antiferromagnets with Entanglement Renormalization: Ground State of the Spin- $\frac{1}{2}$ Heisenberg Model on a Kagome Lattice,” *Phys. Rev. Lett.* **104**, 187203 (2010).
- [141] Rajiv R. P. Singh and David A. Huse, “Ground state of the spin-1/2 kagome-lattice Heisenberg antiferromagnet,” *Phys. Rev. B* **76**, 180407 (2007).
- [142] Rajiv R. P. Singh and David A. Huse, “Triplet and singlet excitations in the valence bond crystal phase of the kagome lattice Heisenberg model,” *Phys. Rev. B* **77**, 144415 (2008).
- [143] Didier Poilblanc, Matthieu Mambrini, and David Schwandt, “Effective quantum dimer model for the kagome Heisenberg antiferromagnet: Nearby quantum critical point and hidden degeneracy,” *Phys. Rev. B* **81**, 180402 (2010).
- [144] David Schwandt, Matthieu Mambrini, and Didier Poilblanc, “Generalized hard-core dimer model approach to low-energy Heisenberg frustrated antiferromagnets: General properties and application to the kagome antiferromagnet,” *Phys. Rev. B* **81**, 214413 (2010).
- [145] Didier Poilblanc and Grégoire Misguich, “Competing valence bond crystals in the kagome quantum dimer model,” *Phys. Rev. B* **84**, 214401 (2011).

- [146] Ran Budnik and Assa Auerbach, “Low-Energy Singlets in the Heisenberg Antiferromagnet on the Kagome Lattice,” *Phys. Rev. Lett.* **93**, 187205 (2004).
- [147] Patrick A. Lee, “An End to the Drought of Quantum Spin Liquids,” *Science* **321**, 1306–1307 (2008).
- [148] Philippe Mendels and Fabrice Bert, “Quantum Kagome Antiferromagnet $\text{ZnCu}_3(\text{OH})_6\text{Cl}_2$,” *Journal of the Physical Society of Japan* **79**, 011001 (2010).
- [149] P. Mendels, F. Bert, M. A. de Vries, A. Olariu, A. Harrison, F. Duc, J. C. Trombe, J. S. Lord, A. Amato, and C. Baines, “Quantum Magnetism in the Paratacamite Family: Towards an Ideal Kagomé Lattice,” *Phys. Rev. Lett.* **98**, 077204 (2007).
- [150] J. S. Helton, K. Matan, M. P. Shores, E. A. Nytko, B. M. Bartlett, Y. Yoshida, Y. Takano, A. Suslov, Y. Qiu, J.-H. Chung, D. G. Nocera, and Y. S. Lee, “Spin Dynamics of the Spin-1/2 Kagome Lattice Antiferromagnet $\text{ZnCu}_3(\text{OH})_6\text{Cl}_2$,” *Phys. Rev. Lett.* **98**, 107204 (2007).
- [151] Philippe Mendels and Fabrice Bert, “Quantum kagome antiferromagnet: $\text{ZnCu}_3(\text{OH})_6\text{Cl}_2$,” arXiv (2011).
- [152] A. Zorko, S. Nellutla, J. van Tol, L. C. Brunel, F. Bert, F. Duc, J.-C. Trombe, M. A. de Vries, A. Harrison, and P. Mendels, “Dzyaloshinsky-Moriya Anisotropy in the Spin-1/2 Kagome Compound $\text{ZnCu}_3(\text{OH})_6\text{Cl}_2$,” *Phys. Rev. Lett.* **101**, 026405 (2008).
- [153] A Zorko, S Nellutla, J van Tol, L C Brunel, F Bert, F Duc, J-C Trombe, and P Mendels, “Electron spin resonance investigation of the spin-1/2 kagomé antiferromagnet $\text{ZnCu}_3(\text{OH})_6\text{Cl}_2$,” *Journal of Physics: Conference Series* **145**, 012014 (2009).
- [154] S. El Shawish, O. Cépas, and S. Miyashita, “Electron spin resonance in $S = \frac{1}{2}$ antiferromagnets at high temperature,” *Phys. Rev. B* **81**, 224421 (2010).
- [155] O. Cépas, C. M. Fong, P. W. Leung, and C. Lhuillier, “Quantum phase transition induced by Dzyaloshinskii-Moriya interactions in the kagome antiferromagnet,” *Phys. Rev. B* **78**, 140405 (2008).
- [156] L. Messio, O. Cépas, and C. Lhuillier, “Schwinger-boson approach to the kagome antiferromagnet with Dzyaloshinskii-Moriya interactions: Phase diagram and dynamical structure factors,” *Phys. Rev. B* **81**, 064428 (2010).
- [157] Yejin Huh, Lars Fritz, and Subir Sachdev, “Quantum criticality of the kagome antiferromagnet with Dzyaloshinskii-Moriya interactions,” *Phys. Rev. B* **81**, 144432 (2010).
- [158] M. Elhajal, B. Canals, and C. Lacroix, “Symmetry breaking due to Dzyaloshinsky-Moriya interactions in the kagomé lattice,” *Phys. Rev. B* **66**, 014422 (2002).
- [159] Danna E. Freedman, Tianheng H. Han, Andrea Prodi, Peter Müller, Qing-Zhen Huang, Yu-Sheng Chen, Samuel M. Webb, Young S. Lee, Tyrel M. McQueen, and Daniel G. Nocera, “Site Specific X-ray Anomalous Dispersion of the Geometrically Frustrated Kagomé Magnet, Herbertsmithite, $\text{ZnCu}_3(\text{OH})_6\text{Cl}_2$,” *Journal of the American Chemical Society* **132**, 16185–16190 (2010).

- [160] A. Olariu, P. Mendels, F. Bert, F. Duc, J. C. Trombe, M. A. de Vries, and A. Harrison, “ ^{17}O NMR Study of the Intrinsic Magnetic Susceptibility and Spin Dynamics of the Quantum Kagome Antiferromagnet $\text{ZnCu}_3(\text{OH})_6\text{Cl}_2$,” *Phys. Rev. Lett.* **100**, 087202 (2008).
- [161] F. Bert, A. Olariu, A. Zorko, P. Mendels, J. C. Trombe, F. Duc, M. A. de Vries, A. Harrison, A. D. Hillier, J. Lord, A. Amato, and C. Baines, “Frustrated magnetism in the quantum Kagome Herbertsmithite $\text{ZnCu}_3(\text{OH})_6\text{Cl}_2$ antiferromagnet,” *Journal of Physics: Conference Series* **145**, 012004 (2009).
- [162] T. Imai, E. A. Nytko, B. M. Bartlett, M. P. Shores, and D. G. Nocera, “ ^{63}Cu , ^{35}Cl , and ^1H NMR in the $S = \frac{1}{2}$ Kagome Lattice $\text{ZnCu}_3(\text{OH})_6\text{Cl}_2$,” *Phys. Rev. Lett.* **100**, 077203 (2008).
- [163] M. A. de Vries, K. V. Kamenev, W. A. Kockelmann, J. Sanchez-Benitez, and A. Harrison, “Magnetic Ground State of an Experimental $S = 1/2$ Kagome Antiferromagnet,” *Phys. Rev. Lett.* **100**, 157205 (2008).
- [164] Zenji Hiroi, Masafumi Hanawa, Naoya Kobayashi, Minoru Nohara, Hidenori Takagi, Yoshitomo Kato, and Masashi Takigawa, “Spin-1/2 *Kagomé*-Like Lattice in Volborthite $\text{Cu}_3\text{V}_2\text{O}_7(\text{OH})_2 \cdot 2\text{H}_2\text{O}$,” *Journal of the Physical Society of Japan* **70**, 3377–3384 (2001).
- [165] Hiroyuki Yoshida, Yoshihiko Okamoto, Takashi Tayama, Toshiro Sakakibara, Masashi Tokunaga, Akira Matsuo, Yasuo Narumi, Koichi Kindo, Makoto Yoshida, Masashi Takigawa, and Zenji Hiroi, “Magnetization “Steps” on a Kagome Lattice in Volborthite,” *Journal of the Physical Society of Japan* **78**, 043704 (2009).
- [166] M. Yoshida, M. Takigawa, H. Yoshida, Y. Okamoto, and Z. Hiroi, “Phase Diagram and Spin Dynamics in Volborthite with a Distorted Kagome Lattice,” *Phys. Rev. Lett.* **103**, 077207 (2009).
- [167] Yoshihiko Okamoto, Hiroyuki Yoshida, and Zenji Hiroi, “Vesignieite $\text{BaCu}_3\text{V}_2\text{O}_8(\text{OH})_2$ as a Candidate Spin-1/2 Kagome Antiferromagnet,” *Journal of the Physical Society of Japan* **78**, 033701 (2009).
- [168] J. A. Quilliam, F. Bert, R. H. Colman, D. Boldrin, A. S. Wills, and P. Mendels, “Ground state and intrinsic susceptibility of the kagome antiferromagnet vesignieite as seen by ^{51}V NMR,” *Phys. Rev. B* **84**, 180401 (2011).
- [169] R. H. Colman, F. Bert, D. Boldrin, A. D. Hillier, P. Manuel, P. Mendels, and A. S. Wills, “Spin dynamics in the $S = \frac{1}{2}$ quantum kagome compound vesignieite, $\text{Cu}_3\text{Ba}(\text{VO}_5\text{H})_2$,” *Phys. Rev. B* **83**, 180416 (2011).
- [170] Yoshihiko Okamoto, Masashi Tokunaga, Hiroyuki Yoshida, Akira Matsuo, Koichi Kindo, and Zenji Hiroi, “Magnetization plateaus of the spin- $\frac{1}{2}$ kagome antiferromagnets volborthite and vesignieite,” *Phys. Rev. B* **83**, 180407 (2011).
- [171] O. Janson, J. Richter, and H. Rosner, “Modified Kagome Physics in the Natural Spin-1/2 Kagome Lattice Systems: Kapellasite $\text{Cu}_3\text{Zn}(\text{OH})_6\text{Cl}_2$ and Haydeeite $\text{Cu}_3\text{Mg}(\text{OH})_6\text{Cl}_2$,” *Phys. Rev. Lett.* **101**, 106403 (2008).

- [172] R. H. Colman, C. Ritter, and A. S. Wills, “Toward Perfection: Kapellasite, $\text{Cu}_3\text{Zn}(\text{OH})_6\text{Cl}_2$, a New Model $S = 1/2$ Kagome Antiferromagnet,” *Chemistry of Materials* **20**, 6897–6899 (2008).
- [173] L. Messio B. Bernu C. Lhuillier F. Bert P. Mendels B. Koteswararao F. Bouquet J. Ollivier A. D. Hillier A. Amato R. H. Colman A. S. Wills B. Fak, E. Kermarrec, “Kapellasite: a kagome quantum spin liquid,” arXiv (2012).
- [174] P. Nikolic and T. Senthil, “Physics of low-energy singlet states of the Kagome lattice quantum Heisenberg antiferromagnet,” *Phys. Rev. B* **68**, 214415 (2003).
- [175] Didier Poilblanc and Arnaud Ralko, “Impurity-doped kagome antiferromagnet: A quantum dimer model approach,” *Phys. Rev. B* **82**, 174424 (2010).
- [176] Tiamhock Tay and Olexei I. Motrunich, “Sign structures for short-range RVB states on small kagome clusters,” *Phys. Rev. B* **84**, 193102 (2011).
- [177] Yejin Huh, Matthias Punk, and Subir Sachdev, “Vison states and confinement transitions of Z_2 spin liquids on the kagome lattice,” *Phys. Rev. B* **84**, 094419 (2011).